

MECHANISTIC REFINEMENT OF THE COMMON MARMOSSET MODEL FOR MULTIPLE SCLEROSIS

**Mechanistische verfijning van het multiple
sclerose model in de penseelaap**

Sunil Anwar Jagessar

The studies described in this thesis were performed at the Department of Immunobiology, Biomedical Primate Research Centre, Rijswijk, The Netherlands.

Printing of this thesis was financially supported by the Biomedical Primate Research Centre, JE Jurriaanse Stichting, U-CyTech, Merck Serono, Genzyme Nederland, BD Biosciences, and Radio Holland BV.

ISBN: 978-94-6182-100-3

Illustrations: Henk van Westbroek

Cover design: S.A. Jagessar, R.E. Bandhosingh & Off Page (www.offpage.nl)

Layout & printing: Off Page

© S.A. Jagessar, 2012. No parts of this thesis may be reproduced or transmitted in any form by any means without permission in writing from the author.

MECHANISTIC REFINEMENT OF THE COMMON MARMOSSET MODEL FOR MULTIPLE SCLEROSIS

Mechanistische verfijning van het multiple
sclerose model in de penseelaap

PROEFSCHRIFT

ter verkrijging van de graad van doctor
aan de Erasmus Universiteit Rotterdam
op gezag van de rector magnificus
prof. dr. H.G. Schmidt
en volgens besluit van het College voor Promoties.

De openbare verdediging zal plaatsvinden op
woensdag 23 mei 2012 om 13.30 uur

door

Sunil Anwar Jagessar

Geboren te Paramaribo, Suriname



PROMOTIECOMMISSIE

Promotoren

Prof. dr. J.D. Laman

Prof. dr. B.A. 't Hart

Overige leden

Prof. dr. R.W. Hendriks

Prof. dr. R.Q. Hintzen

Prof. dr. P.J. van den Elsen

CONTENTS

Chapter 1	General introduction	7
DISSECTION OF THE IMMUNOLOGICAL CORE EVENT IN THE MARMOSET EAE MODEL		
Chapter 2	Autoimmunity against myelin oligodendrocyte glycoprotein is dispensable for the initiation although essential for the progression of chronic encephalomyelitis in common marmosets	33
Chapter 3	Fast progression of recombinant human myelin/oligodendrocyte glycoprotein (MOG)-induced experimental autoimmune encephalomyelitis in marmosets is associated with the activation of MOG34-56-specific cytotoxic T-cells	53
Chapter 4	Induction of progressive demyelinating autoimmune encephalomyelitis in common marmoset monkeys using MOG34-56 peptide in incomplete Freund adjuvant	81
Chapter 5	Unravelling the T-cell mediated autoimmune attack on CNS myelin in a new primate EAE model induced with MOG34-56 peptide in incomplete adjuvant	103
Chapter 6	Recombinant human MOG in incomplete Freund's adjuvant induces a multiple sclerosis-like disease in the common marmoset	123
THE ROLE OF B-CELLS IN THE COMMON MARMOSET EAE MODEL		
Chapter 7	B-cell depletion abrogates T-cell mediated demyelination in an antibody non-dependent common marmoset EAE model	137
VALIDATION OF THE COMMON MARMOSET EAE MODEL AGAINST IMMUNOTHERAPIES		
Chapter 8	Antibodies against human BLYS and APRIL attenuate EAE development in marmoset monkeys	161
Chapter 9	Discrepant effects of human interferon-gamma on clinical and immunological disease parameters in a novel marmoset model for multiple sclerosis	181
Chapter 10	General discussion	201
Chapter 11	References	217
Chapter 12	English summary Nederlandse samenvatting	233
Appendices	Abbreviations	245
	Dankwoord	247
	Curriculum Vitae	249
	List of publications	250
	PhD portfolio	252

GENERAL INTRODUCTION



PREFACE

The high failure rate of immunotherapies in clinical trials of multiple sclerosis (MS) demonstrates the difficulties encountered in the translation of new therapeutic approaches from its animal model, experimental autoimmune encephalomyelitis (EAE), to the human situation. This is best explained by the fact that the current EAE models do not represent all characteristics of MS such as pathology, humoral and cellular responses in one single animal model. Other reasons are that not always a proper model is used for certain immunotherapies and that some EAE models are immunologically immature by lacking natural infections with (human) pathogens. To bridge this gap between these EAE models and MS, the common marmoset can be used as a relevant preclinical model, since it is genetically and immunologically closely related to humans. Due to its outbred nature, individual common marmosets have heterogeneous responses for neuropathological and immune parameters, which is more comparable to humans than the uniform response of rodents from a single inbred strain. Furthermore, similar to humans, common marmosets have lifelong asymptomatic infections with herpesviruses that may have a role in the etiology of MS, such as with cytomegalovirus (CMV) and CalHV-3, which is a gamma herpesvirus of common marmosets related to human Epstein-Barr virus (EBV)¹. We postulate that these herpesviruses create a repertoire of autoreactive T-cells, which may play a key role in the T-cell mediated demyelination process. To understand the contribution of these autoreactive T-cells to the pathogenesis of MS, the common marmoset EAE model has been refined to mimic the human situation as much as possible. One modification was to replace artificial requirements, such as *Mycobacteria* in complete Freund's adjuvant (CFA) with incomplete Freund's adjuvant (IFA). This will lead to better insights of the pathogenic mechanisms and the possibilities to use the refined common marmoset EAE model for therapy development.

MULTIPLE SCLEROSIS

MS is an inflammatory and demyelinating disease of the central nervous system (CNS) and is the most common disabling neurological disease in young adults. Typical symptoms of the disease are sensory disturbances, optic neuritis, limb weakness, paralysis, fatigue, and bladder dysfunction². The worldwide incidence of MS is highly variable; the highest incidence tends to be in the Northern hemisphere and increases with distance from the equator³. The global prevalence of MS is around 2.5 million individuals and in The Netherlands about 16.000⁴. The mean age of onset is between 20 and 50 years, although onset can occur before 5 years or after 60 years of age⁵. There is a gender difference, with females being more frequently affected than men. The female/male ratio has changed during the last decades, shifting from 2 to 3⁶.

Clinical features

The clinical description of MS divides the disease course into four types (Figure 1). The relapsing-remitting form of MS (RRMS) is the category with most patients (85%) and is characterized by exacerbations of the clinical symptoms alternating with recovery^{7,8}. In a major proportion of the RRMS patients, approximately 50%, the disease converts to a progressive clinical course called, secondary progressive (SPMS). SPMS is characterized by progressive worsening of clinical symptoms⁷. A small part of the MS patients (15%) is diagnosed as primary progressive

(PPMS) that is characterized by slow progression of the disease from its onset without relapses or remission^{8, 9}. The fourth type is progressive relapsing (PRMS), which is a rarer form and initially presents as PPMS. During the disease course these subjects develop neurological exacerbations¹⁰. In addition, there is also a fifth type of MS called benign MS. This type shows minimal or no disease progression and minor disabilities after the onset of disease¹¹.

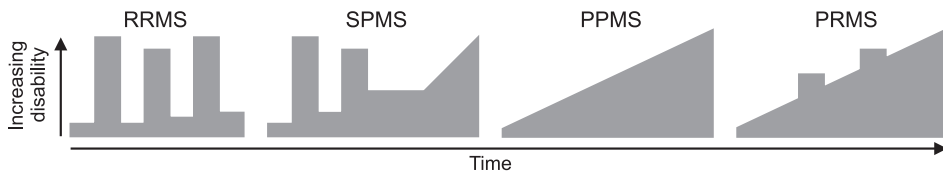


Figure 1. Clinical course of MS. The disease course of MS can be divided in four types; relapsing-remitting (RRMS), secondary progressive (SPMS), primary progressive (PPMS), and progressive relapsing (PRMS).

Etiology

Since the first description of MS by Charcot in 1868, scientists have actively searched for the cause of the disease. There are many interactions of environmental and genetic factors that are thought to play a key role in the initiation of MS. Twin and family studies have shown that the concordance rate among monozygotic twins is about 30%. In dizygotic twins the risk is about about 5%, which is two-fold higher than in siblings of different birth^{12, 13}. Family members of MS patients have a higher risk to develop the disease compared with individuals without a family history of MS^{14, 15}. Association and linkage with human leukocyte antigen (HLA) class II genes on chromosome 6 also support a genetic contribution to MS, by the *HLA-DR2* or *DRB1*15* haplotypes (*DQB1*0602*, *DQA1*0102*, *DRB1*1501*, *DRB5*0101*)^{16, 17}. The mechanisms by which the *DRB1*15* haplotype influences susceptibility to MS are unclear, but are probably related to the central function of HLA molecules in the immune responses, i.e. antigen selection and presentation, and negative selection of high-avidity autoreactive T-cells in the thymus^{18, 19}. There are also alleles with a protective function, in particular *HLA-DRB1*14* and *HLA-DRB1*11*. When *HLA-DRB1*14* and *HLA-DRB1*15* are inherited together, the risk for MS is significantly reduced²⁰. Next to HLA class II genes, there is also an association of MS risk with the HLA class I genes. Individuals with the HLA class I allele *HLA-A3*0301* have a twofold higher risk for MS, while the *HLA-A2*0201* and *HLA-C*05* alleles have a protective effect²¹⁻²³. In mouse EAE models, deficiency of the non-classical HLA class Ib molecule Qa-1, which is orthologous to human HLA-E, results in increased susceptibility to the disease²⁴. This suggests a regulatory role of Qa-1/HLA-E restricted cells, especially since higher surface expression of the inhibitory Qa-1/HLA-E-binding co-receptor CD94/NKG2A was detected during remission^{25, 26}. Non-HLA risk factors include polymorphisms in the promotor regions of two cytokine receptors genes, encoding the interleukin 7 receptor alpha chain (*IL-7RA*) and interleukin 2 receptor alpha chain (*IL-2RA*)²⁷. There are at least 50 other loci outside the HLA-region with an increased risk for MS²⁸ e.g. *STAT3*²⁹, *CD6*³⁰, *CD58* and *CLECI6A*³¹⁻³³.

Environmental factors have a strong impact on disease prevalence, such as latitude, sunlight exposure, smoking and viral infections. This is supported by observations that people migrating

before puberty from high-risk to low-risk areas, for example from the Northern continent to the equator, have a reduced risk of acquiring MS³⁴. This may be explained by higher sunlight exposure to the skin closer to the equator, which is the most important source of vitamin D. It has been shown that a high serum level of vitamin D has a protective effect in MS and has a modulatory effect on T-cell homeostasis^{35, 36}. Moreover, a diet enriched with vitamin D also has protective effects in MS³⁷. Smoking cigarettes increases the risk for MS, which is independent of latitude and ancestry³⁸. Another presumed causative environmental factor is virus infection; proposed candidates include herpesviruses such as EBV, and human herpesvirus 6 (HHV-6)³⁹. EBV has currently the strongest case since epidemiological data showed that people with a history of symptomatic EBV infection or with higher anti-EBV antibody levels have a higher risk to develop MS⁴⁰ (see also section 'Herpesviruses').

Pathology

The pathological hallmark of MS is the lesion, also known as plaque, which is the end stage of a complex pathological process involving different degrees of inflammation, demyelination, neuronal and axonal degeneration, axonal scar formation and remyelination⁵. The pathological characteristics of each lesion vary and depend on location, age and whether regeneration has occurred. Lesions are found in the CNS white and grey matter. White matter lesions are typically divided into four pathological categories; pre-active, active, chronic active and chronic inactive⁴¹. The pre-active and active lesions are defined by the presence of myelin-loaded macrophages and T-cells within the perivascular cuffs as well as in the parenchyma⁴². The major difference between these two lesion types is that the pre-active lesion contains only activated microglia cells whereas the active lesion contains T-lymphocytes, B-lymphocytes and plasma cells in the demyelinated area⁴³. Chronic active lesions are characterized as hypocellular containing few macrophages with myelin degrading products, a small number of perivascular lymphocytes and a hypercellular rim containing macrophages with phagocytized myelin debris. Chronic inactive lesions are defined as hypocellular with an increased number of astrocytes, replacing destroyed neurons and increased intracellular spaces^{44, 45}.

MS had been classically viewed as a disease with white matter lesions, but recently developed histopathological and magnetic resonance imaging (MRI) techniques reveal that lesions are also often located in the grey matter, especially in the cerebral cortex and hippocampus⁴⁵⁻⁴⁷. Histological characteristics of these cortical lesions differ considerably from lesions located in the white matter, since there is no inflammation, a low level of complement activation and absence of blood-brain barrier damage in grey matter lesions^{45, 48-50}. Furthermore, MRI studies indicate that atrophy of grey matter occurs at the earliest stages of disease, and develops faster than white matter atrophy^{51, 52}. Also, grey matter lesions seem to correlate more closely with the degree of clinical symptoms than white matter lesions⁵³. The cause of grey matter damage is unclear at this stage, it could be a consequence of tissue destruction in the subcortical white matter including axonal damage, meningeal inflammation⁴⁶, or it is more dependent on local inflammation⁵⁴.

Despite the fact that all lesions have in common inflammatory infiltrates of T-cells and macrophages, they can be distinguished into four patterns on the basis of myelin protein loss, location of the lesion, patterns of oligodendrocyte damage and deposition of complement, see Box 1^{41, 55}.

Box 1. Four different pathological features of demyelinated lesion in MS (Based on^{41, 55, 56})

- I Associated with T-lymphocyte infiltrates and macrophage-dominated inflammation without antibody or complement deposition. Demyelination surrounds small venules, and lesions appear to have the potential for remyelination.
- II Associated with T-lymphocyte and macrophage-dominated inflammation with significant antibody deposition, e.g. anti-myelin oligodendrocyte glycoprotein (MOG) and complement C9neo. Demyelination surrounds small venules, and lesions appear to have the potential for remyelination.
- III Infiltration of T-lymphocytes, activated macrophages and microglia, but complement and immunoglobulin G (IgG) deposition are absent. Lesion is marked by conservation of a rim of myelin around venules, increased damage of oligodendrocytes by apoptosis, and loss of myelin-associated glycoprotein (MAG) with preservation of other myelin proteins. The lesion has poor potential for remyelination.
- IV Infiltration of T-lymphocytes and activated macrophages, but without complement or IgG deposition, and specific loss of MAG is absent. Lesions are defined by non-apoptotic oligodendrocyte death, have poor potential for remyelination and are only detected in primary progressive MS.

Immunopathogenesis

The cause and exact mechanisms that lead to tissue damage in MS are not completely understood, but many findings point towards a central role for the immune system (Figure 2). This possibility is strongly supported by the beneficial effect of immunosuppressive and immunomodulatory therapy on the disease activity. The last decade considerable progress has been made in unravelling the immune response in MS.

According to a widely accepted concept the disease starts with activation of autoreactive CD4+ T-cells in the periphery by antigen presenting cells (APC), which present epitopes from CNS antigens or CNS molecular mimicry antigens within MHC class II molecules. T-cells are also triggered in the cervical lymph nodes (CLN) by APC presenting myelin antigens⁵⁷. These actions lead to an increased migration of T-cells into the CNS possibly through the blood-brain barrier or choroid plexus⁵⁸. In addition, next to the CD4+ T-cells also demyelinating antibodies, CD8+ T-cells⁵⁹, and Th17 cells gain access from the periphery into the CNS. CNS immigration of the T-cells is mediated by endothelial adhesion molecules such as E-selectin, intercellular adhesion molecule 1 (ICAM-1), vascular adhesion molecule 1 (VCAM-1) and $\alpha 4\beta 1$ integrin (VLA-4)⁶⁰. Further migration is promoted by proteolytic enzymes, matrix metalloproteinases (MMP), that degrade extracellular-matrix components⁶¹. In the CNS local interaction of activated autoreactive T-cells with resident APC, such as microglia cells, induces production of pro-inflammatory cytokines, e.g. interferon- γ (IFN- γ) and tumor necrosis factor- β (TNF- β) that up-regulate the expression of cell-surface molecules, such as major histocompatibility complex class II molecules (MHC class II) and costimulatory molecules (B7-1/B7-2) on APC. In addition, also monocytes and macrophages infiltrate the CNS⁶² and act as APC together with microglia

and dendritic cells. These APC present myelin proteins as MOG, myelin basic protein (MBP), proteolipid protein (PLP) and MAG to CD4+ T-cells. Depending on the type of binding with costimulatory molecules e.g. via CD28 or CTLA-4 this results in an enhanced or down regulated immune response, respectively. The consequence of the enhanced immune response is that pro-inflammatory cytokines such as IL-12, IL-17A, IL-17F, IL-23 and IFN- γ ⁶³ are released, which trigger a cascade of reactions that lead to the destruction of myelin and oligodendrocytes^{2, 4, 5, 64-66}.

Mechanisms of demyelination

Experimental studies in animal models of MS suggest that several mechanisms are involved in the immunopathogenesis of the disease (Figure 2). Besides the immunopathogenic role of CD4+ T-cells, CD8+ T-cells have also an important role in the immunopathogenesis of MS. CD8+ T-cells are prominently present in inflammatory infiltrates in the CNS, and in some cases CD8+ T-cells outnumber CD4+ T-cells⁶⁷. Moreover infiltrating CD8+ T-cells are clonally expanded and can stay for many years in the cerebrospinal fluid (CSF)⁶⁸. Adoptive transfer of activated myelin-specific CD8+ T-cell clones induced serious CNS autoimmunity in mice⁶⁹, suggesting that CD8+ T-cells function as effector cells in the disease pathogenesis. The interaction of effector CD8+ T-cells with MHC class I molecules or Fas antigens present on the myelin sheath or oligodendrocytes leads to the release of cytotoxic proteins, e.g. perforin and granzyme B⁷⁰, resulting in degradation of the myelin sheath or oligodendrocytes².

B-cells are also considered to play a key role in MS pathogenesis. The fact that B-cells function as antibody producing cells in MS, they also directly participate in the demyelination process. Antibodies secreted by B-cells against antigens located on the surface of the myelin sheath or oligodendrocytes result in activation of complement, leading to complement-mediated-cytotoxicity^{71, 72} or are recognized by the Fc receptors of macrophages inducing antibody-dependent cell-mediated cytotoxicity^{2, 73}. The pathogenic relevance of antibody-mediated injury is supported by the observation that demyelination is accelerated by providing MOG specific antibodies in EAE models⁷⁴ and by B-cell depleting therapy, e.g. rituximab, an anti-CD20 monoclonal antibody. Rituximab depletes naive and memory B-cells, which results in the reduction of active brain lesions and clinical relapses⁷⁵. However, the remarkable clinical effect of rituximab may also be explained by reduction of the antigen presentation capacity and pro-inflammatory cytokine production by B-cells (further discussed in **chapter 7**).

Therapy

Currently, therapy for MS is available for RRMS, SPMS and PRMS, but not for PPMS. Immunosuppressive drugs, such as prednisone or methylprednisone, have been used for many years to treat MS exacerbations. Both are corticosteroids which prevent the blood-brain barrier leakage and reduce the role of T-cells in the inflammatory demyelination process^{76, 77}. Novel therapies are focussing more on disease-modifying responses. Validated therapeutics used at this moment are interferon-beta (IFN- β), glatiramer acetate (GA), natalizumab, mitoxantrone and fingolimod (see Box 2)⁷⁸.

Next to these therapeutics, several potential drugs and strategies are under investigation to optimize current therapies such as statins and monoclonal antibodies against CD52 (Alemtuzumab®), CD25 (Daclizumab®). Particularly interesting are the new therapies aiming at

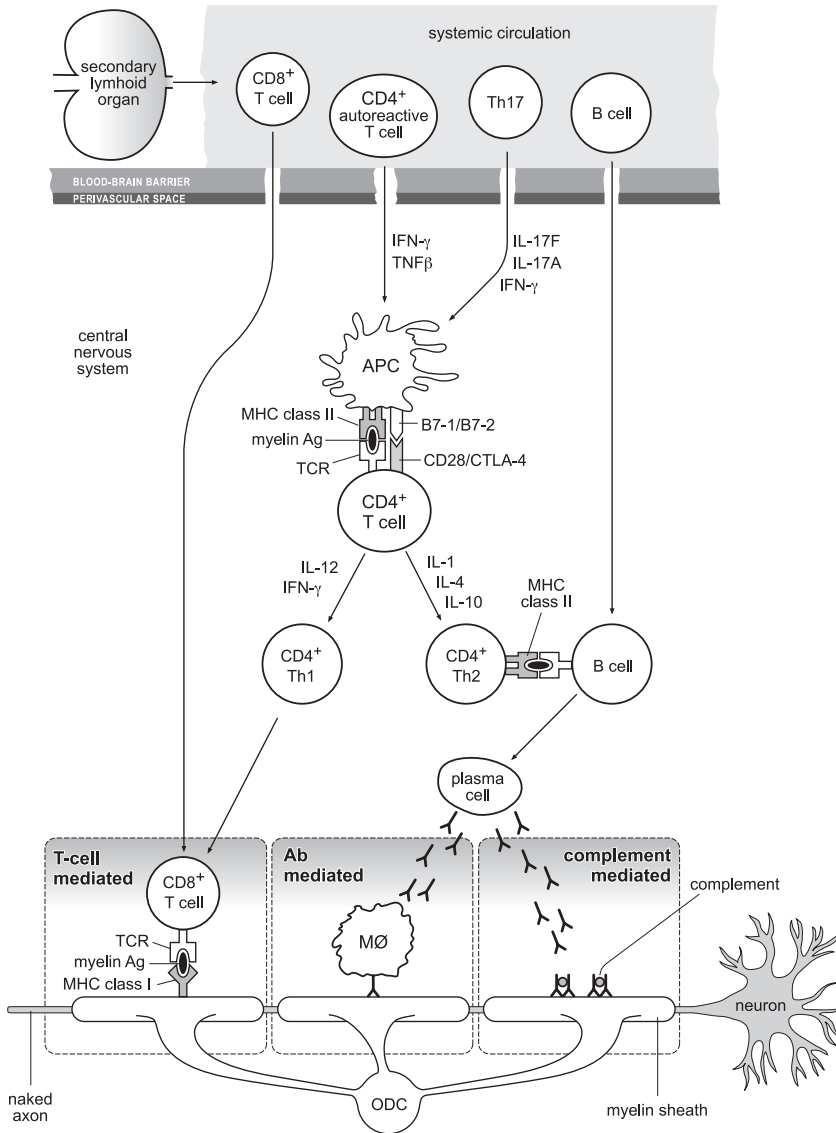


Figure 2. Schematic overview of adaptive immunopathogenic mechanisms in MS. Autoreactive CD4+ T-cells, CD8+ T-cells, B-cells, and Th17 cells from the secondary lymph nodes migrate across the blood-brain barrier into the central nervous system (CNS). CD4+ T-cells interact with antigen presenting cells (APC) via their co-stimulatory receptors (CD28/CTLA-4) with counter structures on the APC (B7-1/B7-2) and via their T-cells receptor (TCR) recognizing MHC class II molecules presenting a cognate myelin antigen (Ag). Depending on the cytokines that are produced naive CD4+ T-cells differentiate into T-helper 1 (Th1) and Th2 cells. Th2 cells activate B-cells, resulting in plasma cell activation and antibody (Ab) production against myelin antigens. Antibodies are recognized by macrophages (MØ) and complement, leading to antibody-mediated or complement-mediated myelin damage, respectively. T-cell mediated damage is triggered by CD8+ T-cells recognizing myelin antigens presented by MHC class I molecules. Furthermore, proinflammatory cytokines produced by CD4+ Th1 cells also lead to myelin destruction. Based on^{2, 65}.

B-cell depletion or B-cell inactivation using monoclonal antibodies such as anti-CD20 or anti-B-cell survival molecules e.g. anti-BLyS/BAFF. These highlight the long time neglected role of B cells in the pathogenic process.

Box 2. Validated therapies for MS

- » **IFN- β .** Four commercial preparations are available of IFN-1 β ; two of IFN- β -1b (Betaferon[®], Extavia[®]) and two of IFN- β -1a (Refib[®], Avonex[®]). IFN- β -1a and IFN- β -1b are licensed for use in RRMS. IFN- β -1a can also be used for SPMS. Treatment reduces relapse rate, occurrence of new MRI lesions and brain atrophy⁷⁹. IFN- β promotes the production of Th2 cytokines and interacts directly with the BBB, resulting in reduced migration of T-cells into the CNS⁸⁰. After several years of treatment neutralizing antibodies are formed that inhibit the beneficial action of the cytokine⁸¹. The main side-effects are flu-like symptoms and inflamed reactions at injection sites.
- » **Glatiramer acetate (GA).** GA, known as Copaxone[®], is a mixture of four synthetic polypeptides mimicking epitopes of MBP. GA blocks T-cell activation and promotes Th2 cells. Treatment is successful in about 29% of RRMS patients and has good effects on MRI lesions^{82, 83}. Adverse effects are usually mild skin reactions.
- » **Nataluzimab.** Marketed under the name Tysabri[®]. Nataluzimab is a monoclonal antibody against the $\alpha 4$ subunit of $\alpha 4\beta 1$ integrin (VLA-4). Treatment prevents lymphocyte migration across the BBB into the CNS⁸⁴ and is powerful in RRMS patients. The major adverse effect is development of progressive multifocal leukoencephalopathy (PML), a fatal neurological disease caused by the recrudescence of latent JC virus infection⁸⁵.
- » **Mitoxantrone.** Two commercial preparations are available for mitoxantrone; Ralenova[®] and Novantrone[®]. Mitoxantrone inhibits DNA and RNA synthesis, suppresses T-cell, B-cell and macrophage proliferation. Treatment promotes production of Th2 cytokines without influencing Th1 and Th17 cytokines. Mitoxantrone has a significant effect on clinical symptoms and several MRI parameters. It is only given to RRMS and SPMS patients⁸⁶. Side effects such as treatment-related leukemia are rarely observed⁸⁷.
- » **Fingolimod.** This is an antagonist of sphingosine-1-phosphate receptor and is available as Gilenya[®]. Fingolimod is the first MS oral drug and is effective in RRMS patients. Treatment prevents lymphocyte egress from lymph nodes and promotes CNS repair. Infections such as bronchitis and pneumonia occurred more frequently in fingolimod treated patients^{88, 89}.

EXPERIMENTAL AUTOIMMUNE ENCEPHALOMYELITIS

Since there are numerous restrictions to human studies, e.g. limited access to CNS tissue and ethical considerations, MS research depends strongly on animal models. Over the years various animal models have been developed for the investigation of pathogenic, clinical and therapeutic aspects of MS. The most commonly used animal model for MS is EAE⁹⁰. Virus

induced demyelination e.g. by Theiler's murine encephalomyelitis virus (TMEV)⁹¹, toxin-induced models e.g. cuprizone model⁹², spontaneous models in transgenic mice and passive transfer models are also used to study MS. A selection of these models is listed in Table 1.

EAE is a very useful experimental MS model wherein inflammatory and demyelination aspects of MS are modelled. The EAE model gives also the possibility to develop and validate new therapies. The disease is reliably generated in a number of different species by immunization with either CNS tissue or with purified components of CNS myelin, e.g. MBP, PLP and MOG. Moreover, EAE can also be induced by immunization with synthetic peptides derived from myelin proteins or by the transfer of T-cells and antibodies against myelin antigens. To enhance the response against the immunizing antigen, these components are often mixed with CFA. In mouse EAE models additional *Bordetella pertussis* particles or pertussis toxin are essential for disease induction.

Over the last three decades, well characterized EAE models have been developed in a wide range of species, e.g. mice, rats, guinea pigs, rabbits, rhesus monkeys and the common marmoset, which reproduce certain features of the immunopathology of MS.

EAE in non-human primates

Non-human primate EAE models are used in MS research because they represent specific aspects of the disease, and are immunologically and genetically closer to humans than other species.

The first EAE studies in non-human primates were conducted in the rhesus monkey (*Macaca mulatta*) and the cynomolgus monkey (*Macaca fascicularis*). Around 1930 Rivers et al. injected rhesus monkeys with rabies vaccine derived from virus grown in spinal cord of rabbits, resulting in acute disseminated encephalomyelitis (ADEM)¹²². This MS-like experimental disease was further characterized by Rivers et al. using repetitive inoculation with rabbit brain extracts¹²³. Later, single inoculations in rhesus monkeys with autologous myelin in CFA were proven to be sufficient to induce acute EAE, reflecting acute disseminated encephalomyelitis (ADEM)⁹⁹. Since then the rhesus monkey EAE model was further refined to study the immunopathogenesis of MS and for therapy development. However, disease progression was still very acute and caused death within a few days after onset. Also, post-mortem histological examination of brain and spinal cord showed highly destructive pathology, which was not comparable with MS^{101, 124, 125}. On the other hand, in cynomolgus monkeys a more chronic relapsing-remitting disease course was induced when they received a single immunization with human brain white matter in CFA¹⁰² or MBP in CFA¹⁰¹. High T-cell responses against MBP were observed and less disastrous pathology, which may have made the cynomolgus EAE model more useful for MS studies than rhesus monkeys.

The common marmoset EAE model was first developed by Massacesi and co-workers in 1995¹²⁶. EAE was induced with immunization of human myelin in CFA supplemented with intravenous injection of heat-inactivated *Bordetella pertussis* particles. The disease was very acute, resembling ADEM like disease, and animals were sacrificed within 13 weeks after immunization. Several seriously destructive large lesions in the white matter of the brain and spinal cord were detected¹²⁶. By reducing the *Mycobacterium tuberculosis* dose in the antigen-adjuvant emulsion and omitting the *Bordetella pertussis*, a milder form of EAE developed. The average day of sacrifice was delayed to 37 weeks after immunization and there were more inactive lesions than active lesions^{126,127}.

Table 1. Selection of different types of animal models for multiple sclerosis.

Type	Compound/antigen	Species/strain	Features	Ref.
Active immunization	MOG or PLP	Mouse Biozzi ABH	Chronic relapsing EAE	93, 94
	MOG35-55	Mouse C57BL/6	Chronic progressive EAE	95
	MOG	Rat Lewis	CNS pathology and paralysis	96
	SCH	Rat Dark Agouti	CNS pathology and paralysis	97
	Myelin or MOG	Rhesus monkey	Acute EAE	98, 99
	OSP	Rhesus monkey	Inflammation, optic neuritis	100
	Brain white matter or MBP	Cynomolgus monkey	Chronic EAE relapsing EAE and CNS pathology	101, 102
	rhMOG or MBP	Marmoset #	CNS pathology and paralysis	103
Passive transfer	MBP T-cell lines	Rhesus monkey, marmoset, rat	Mild inflammation, progressive EAE	104-106
Transgenic	TCR MPB 1-11	Mouse B10.PL	Spontaneous EAE	107
	TCR MOG x IgG high	Mouse C57BL/6	Spontaneous EAE	108, 109
	TCR PLP139-151	Mouse SJL/J H-2 ^s	Spontaneous EAE	110
	TCR MOG92-106	Mouse SJL/J	Spontaneous EAE	111
Toxin	Lysolecithin	Mouse, rat, rabbit	Focal areas of demyelination and remyelination, axonal loss	112
	Cuprizone	Mouse, rat	Death of ODC, axonal loss dependent on age	113, 114
	Ethidium bromide	Rat	Death of ODC, axonal loss dependent on age	115, 116
Virus	TMEV	Mouse	Flaccid paralysis and demyelination	117
Humanized	HLA-DRB1*0401 & TCR MBP11-129	Mouse C57BL/6	CNS pathology and paralysis	118
	HLA-DRB1*1502 & TCR MBP85-99	Mouse DBA/2xC57BL/6	Relapsing remitting and spontaneous EAE	119
	HLA-RB1*1501 & TCR MOG35-55	Mouse DBA/2xC57BL/6	CNS pathology and paralysis	120
	HLA-DRB1*1502 & TCR PLP95-116	Mouse C57BL/6	CNS pathology and paralysis	121

SCH, spinal cord homogenate; rhMOG, recombinant human myelin oligodendrocyte glycoprotein; OSP, oligodendrocyte-specific glycoprotein; ODC, oligodendrocyte; TMEV, Theiler's murine encephalomyelitis virus; TCR, T-cell receptor. #See also Table 1 in **chapter 10** for all marmoset EAE models that were developed during the research of this thesis.

Subsequently, common marmosets were immunized with MBP or recombinant human MOG (rhMOG) in CFA, but still without *Bordetella pertussis*. Immunization with MBP showed only mild clinical symptoms as altered walking and loss of appetite, and small CNS lesions. In contrast, immunization with rhMOG in CFA induced severe clinical symptoms such as paresis and limb paralysis. Despite the heterogeneous disease onset all rhMOG immunized monkeys developed clinically evident EAE. Lesions in the brain were detected using magnetic resonance imaging (MRI). Further neuropathological characterization showed large demyelinated areas in the white matter of both cerebral hemispheres, in the spinal cord and optic nerves¹⁰³.

Since then, we have continuously refined the EAE model to improve the similarity with MS¹²⁸, and to reduce discomfort to the animals by limiting inflammatory activity. The EAE models in the common marmoset that have been developed vary in their clinical and pathological features as described in this thesis.

Myelin oligodendrocyte glycoprotein

Myelin is the insulating material that forms a layer around axons and is necessary for saltatory conduction of electric pulses from the neuronal cell body to the innervated organ¹²⁹. The formation of myelin is dependent on the expression of various myelin proteins in large amounts e.g. MBP and PLP (Figure 3A)¹²⁹. Proteins expressed in minor quantities such as MOG (0.01% to 0.05%) have also a crucial role in the formation of the myelin sheath¹³⁰.

MOG is located on the outermost lamellae of the myelin sheath and on the surface of mature oligodendrocytes¹³¹. In its natural configuration MOG is expressed as a homodimer in a head-to-tail orientation (Figure 3)¹³². The amino acid sequence of MOG is highly conserved between species, as shown for human, mouse and marmosets in Figure 3D^{133, 134}. The non-glycosylated N-terminal domain of MOG and the linear epitopes derived from the corresponding amino acid sequence 1 to 125 are sufficient to induce EAE in mice⁹³.

MOG is an autoantigen that induces an encephalitogenic T-cell response and a demyelinating autoantibody response in susceptible species. Demyelinating anti-MOG antibodies increase disease severity and initiate extensive T-cell-mediated brain demyelination in e.g. mice, rats and non-human primates^{74, 103, 135, 136} (**chapter 3**). T-cell responses in the common marmoset EAE model are mainly directed against MOG epitopes 14-36, 34-56 and 74-96¹²⁸. In MS patients MOG1-22, MOG34-56 and MOG64-96 are the dominant T-cell epitopes^{137, 138}. IgG reactivity in common marmosets immunized with rhMOG in CFA is directed against the MOG epitopes 4-26, 14-36, 24-46, 44-66, 54-76 and rhMOG itself, but not against 34-56. IgM antibodies are directed against MOG54-76 and rhMOG¹⁰³.

HERPESVIRUSES

Herpesviruses form a large family of enveloped double-stranded DNA viruses that can cause disease in humans and animals. Infections can cause overt clinical symptoms, but more often remain latent for many years until reactivation e.g. by immune suppression. The members of this family form the taxonomic family *Herpesviridae*. Despite the fact that individual herpesviruses are widely separated based on their genomic sequence and proteins, they are similar in terms of virion structure and genome organization¹⁴¹⁻¹⁴³. Based on virion morphology and genome structure, herpesviruses are classified into three subfamilies; Alphaherpesvirinae

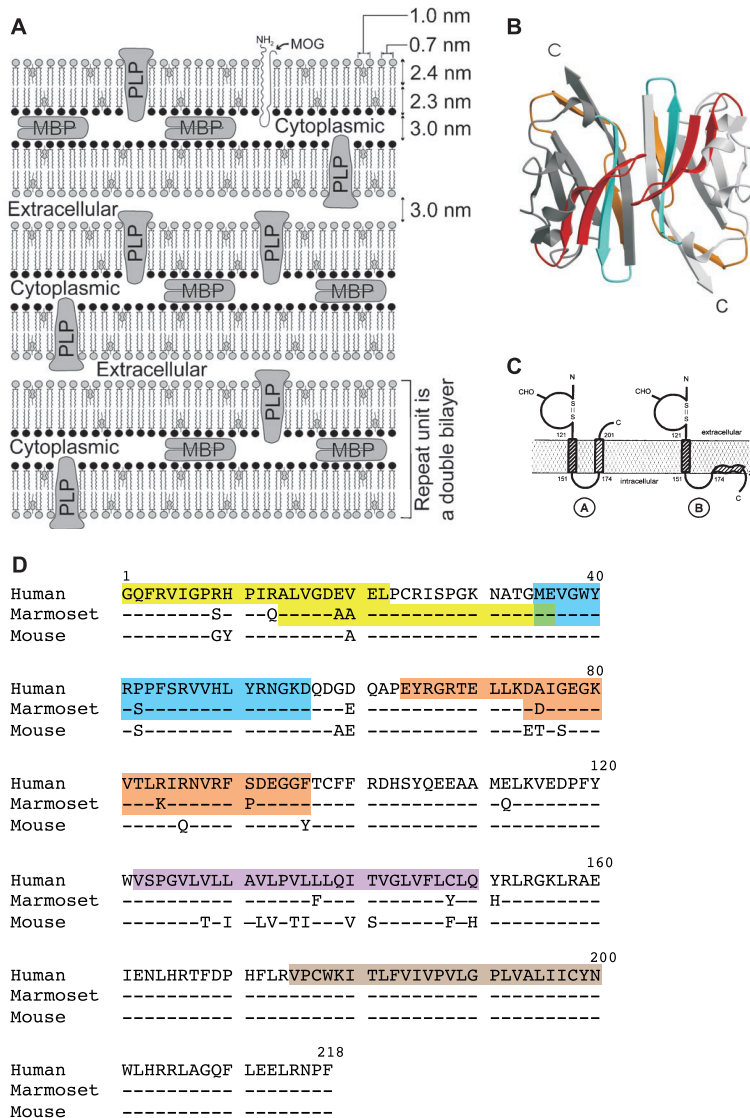


Figure 3. Structural aspects of myelin oligodendrocyte glycoprotein (MOG). **A.** Illustration shows the arrangement of lipids and proteins in myelin, adapted from¹³⁹. **B.** Crystallographic structure of the extracellular domain of MOG. Orange, red and blue parts represent encephalitogenic peptides in humans, 1-22, 35-55 and 92-106, respectively. Adapted from¹³². **C.** There are two proposed models for MOG membrane topology. The N-terminal Ig-like domain of MOG is localized on the extracellular side, corresponding the amino acid sequence 1 to 125 in humans and 1 to 121 in mouse, adapted from¹⁴⁰. Model A shows two hydrophobic domains (striped boxes) that cross the lipid bilayer with the C-terminal on the extracellular side. Model B shows that only one hydrophobic domain spans the lipid bilayer. **D.** MOG sequences are compared between human, common marmoset and mouse. Yellow, blue and orange coloured sequences indicate T-cell epitopes for MS and EAE in humans and common marmosets, respectively. Purple and beige coloured sequences indicate the N-terminal and C-terminal linked hydrophobic domains, respectively. Modified from¹³⁴.

(α), Betaherpesvirinae (β) and Gammaherpesvirinae (γ)^{144, 145}. Currently, more than 130 herpesviruses have been identified in mammals, of which eight are proven human pathogens (Table 2)^{146, 147}.

Herpesviruses infect their targets through fusion with either the host cell plasma membrane or the endocytic vesicle membrane¹⁴⁸. They are very complex and contain approximately 35 virion proteins, and have large genomes, varying from 105 to 235 Kbp. The viral genomes have unique long (UL) and unique short (US) regions, bound by inverted repeats.

Herpesviruses of non-human primates

The order of primates is subdivided into two suborders, the Prosimians and the Anthropoids. Prosimians are the earliest and most primitive primates, including lorises and lemurs. Anthropoids are divided into two geographically separated suborders, Platyrrhines and Catarrhines. Platyrrhines species, also named New World monkeys, include common marmosets and squirrel monkeys, which have their natural habitat in South and Central America. The Catarrhines comprise Apes and Old World monkeys which are found in Asia and Africa e.g. chimpanzees, macaques and baboons¹⁴⁹. Anthropoid species have been investigated extensively for their herpesviruses. A number of viruses, most of them gammaherpesvirus, were found in animals suffering from diseases, e.g. tumours, while other viruses were identified in healthy animals^{150, 151}. EBV was the first identified gammaherpesvirus, which is grouped in the lymphocryptovirus (LCV) genus of the herpesviruses¹⁵². LCV were first described in Old World monkeys, but more recently a LCV-related virus in the common marmoset, named callitrichine herpesvirus 3 (CalHV-3), has been characterized. In addition, a LCV was found in the squirrel monkey that is closely related to CalHV-3, i.e. the saimirine herpesvirus 3 (SaHV-3)^{1, 152, 153}. LCV in the common marmoset (CalHV-3) has a genetic repertoire that is highly similar to its counterparts in humans

Table 2. Overview of pathogenic human herpesviruses (HHV).

Type HHV	Common name	Abbreviation	Sub-family	Site of latency	Disease
1	Herpes simplex virus-1	HSV-1	α	Neuron	Herpes labialis
2	Herpes simplex virus-2	HSV-2	α	Neuron	Genital herpes
3	Varicella zoster	VSV	α	Neuron	Chicken pox
4	Epstein-Barr virus	EBV	γ	B-cell	Infectious mononucleosis
5	Cytomegalovirus	CMV	β	Lymphocytes, Monocytes	Retinitis
6	Herpes lymphotropic virus	HHV-6	β	T-cells	Roseola infantum
7	Human herpesvirus -7	HHV-7	β	T-cells	Roseola infantum
8	Kaposi's sarcoma-associated herpesvirus (rhadinovirus)	KSHV	γ	Unknown	Kaposi's sarcoma, Castleman's disease

Based on^{146, 147}

(EBV) and in Old World monkeys (e.g. the macaque LCV). Complete sequencing of the CalHV-3 genome showed that about one third of the genome is identical to the EBV genome e.g. to the Epstein-Barr viral nuclear antigen-1 (EBNA-1). In addition, CalHV-3 contains in total 69 open reading frames (ORF). Seven of these ORFs show homology with EBV ORF that are expressing proteins, which are involved in lytic infection at a similar position in the EBV genome (Table 3). Seven ORF in the CalHV-3 genome showed no sequence relatedness to either cellular or viral genes of EBV and are unique for the marmoset LCV. These genes are referred to as C1 to C7, and are located in different regions of the LCV genome. For example, C5 is a positional homologue of EBNA-2 and shares no relatedness at the amino acid level, and C7 is located at a position comparable to where EBV encodes a membrane protein (LMP-2)^{1, 154}.

Herpesviruses in MS

The origin of autoimmune diseases such as MS is thought to be multifactorial and highly complex. Genetic predisposition and environmental factors may play a role. These factors still are not well defined, but viral infections have been associated with MS development. Viral infections are recognized as the most critical environmental factors, and herpesviruses such as human HHV-6^{155, 156}, EBV, and to a lesser extent CMV¹⁵⁷ are prime suspects.

EBV and MS

EBV can cause acute infectious mononucleosis and lymphoproliferative diseases, such as Hodgkins lymphoma, and nasopharyngeal carcinoma⁴⁰. The prevalence of EBV infection in Western countries is very high; more than 90% of the healthy adult population is seropositive

Table 3. Comparison of CalHV-3 proteins with EBV in man.

CalHV-3	No. of aa	Homology to EBV (%)	Positional homologue in EBV	Function
ORF1	173	27.6	BALF1	Bcl-2 homologue
ORF5	1016	73.5	BALF5	DNA polymerase
ORF39	328	36.0	BKRF-1	EBNA-1 homologue
ORF42	609	39.0	BRLF1	Transcription factor
ORF43	252	29.0	BZLF1	Transcription factor
ORF64	190	20.5	BHRF1	Bcl-2 homologue
ORF65	1322	40.9	BNRF1	Tegument protein
C1	355	-	LMP-1	Transforming gene
C2	251	-	BILF2	Membrane protein
C3	825	-	EBNA-3	Unknown
C4	254	-	BHLF1	Unknown
C5	420	-	EBNA-2	Nuclear protein
C6	396	-	EBER1/2	Unknown
C7	413	-	LMP2	Membrane protein

CalHV-3, callitrichine herpesvirus 3; ORF, open reading frame; aa, amino acid; EBV, Epstein-Barr virus. Based on^{1, 154}

for EBV. Half of this population becomes EBV positive after the age of ten. Individuals who experience a primary EBV infection in adolescence 30-50% of them will develop infectious mononucleosis, due to a robust immune reaction against the virus¹⁵⁸. In developing countries most children come in contact with EBV before the age of ten and will develop an asymptomatic infection. This indicates an age-related association between primary EBV infection and infectious mononucleosis.

Over the years many studies have found an association between EBV infection and the development of MS. MS patients showed a significant increase of antibody levels to EBNA-1 compared to controls¹⁵⁹. Anti-EBV antibody levels were also found to be increased before the onset of MS¹⁶⁰. Meta-analysis of thirteen studies has found a higher risk (odds ratio of 0.06) to develop MS for EBV seropositive individuals compared to EBV seronegatives. Of all MS patients, 99.5% are seropositive compared to 94% in non-MS controls. In children with MS, 99% are positive for EBV, while only 72% of the age-matched controls are EBV positive^{161, 162}. In MS patients increased CD4+ T-cell responses against EBNA-1 are also observed compared to controls^{163, 164}. In addition, EBV can immortalize autoreactive B-cells, which can act as professional APC, leading to permanent autoimmunity¹⁶⁵.

HHV-6 and MS

HHV-6 is a beta herpesvirus with a seroprevalence of more than 95% in the human population by the age of two. There are two distinct subtypes of HHV-6, namely HHV-6A and HHV-6B¹⁶⁶. Infection is life-long and the virus stays in a latent stage until it is reactivated, especially in immunocompromised subjects. HHV-6 was originally isolated from patients with lymphoproliferative disease and co-infects human immunodeficiency virus (HIV) infected T-cells promoting the replication of HIV^{167, 168}. There is a suggestive association between HHV-6 and several neurological disorders, e.g. chronic fatigue syndrome and MS¹⁶⁹⁻¹⁷¹.

Comparing brains from MS patients to controls, a significantly higher prevalence of HHV-6 DNA in MS was found. Interestingly, higher levels of HHV-6 DNA were detected in MS lesions compared to normal appearing white matter, and HHV-6 expression was confined to oligodendrocytes^{172, 173}. In CSF and in blood of MS patients higher levels of HHV-6 viral DNA and HHV-6 antibodies were detected in RRMS^{155, 174, 175}. Association with MS is further supported by the cross-reaction of HHV-6 reactive CD4+ T-cells with MBP. T-cell lines specific for MBP (residues 93 to 105; IVTPRTPPPSQGK) generated from MS patients displayed increased reactivity against HHV-6 U24 protein (residues 1 to 13; MDRPRTPPPSYSE)^{176, 177}. Taken together, these findings suggest the possibility that HHV-6 may trigger autoimmunity against CNS auto-antigens in MS.

CMV and MS

CMV is a beta-herpesvirus and a leading cause of opportunistic infections in the human population. The prevalence of CMV infection in the human population is estimated at a range from 50% to 80%, but the infection remains asymptomatic in the vast majority of infected individuals¹⁷⁸. The prevalence is quite variable as it varies between different geographic areas, different social economic populations, and ethnic origins. CMV has been associated with several autoimmune diseases, such as systemic lupus erythematosus¹⁷⁹, diabetes mellitus type 1 and 2^{180, 181} and with Guillain-Barré syndrome, a demyelinating disorder of the peripheral nervous system¹⁸². Although there is no obvious relation with MS, a possible association with ADEM has been

found¹⁸³. ADEM is an acute neurological disease characterized by lesions in the CNS that are often indistinguishable from lesions in MS patients¹⁸⁴. CMV is also involved in acute CNS inflammatory disorders, for instance meningo-encephalitis in immunocompromised and immunocompetent individuals¹⁸⁵. Moreover, MS patients that are sufficient for vitamin D was correlated with an increased antibody level against CMV, while such a correlation was absent or in the opposite direction in controls¹⁸⁶. Furthermore, CD8+ T-cells specific against CMV could be isolated from brain lesions of MS patients¹⁸⁷.

Indirect support of a role of CMV in MS is the experimental observation that CD8+ T-cells from rhesus EAE monkeys immunized with MOG34-56 in CFA display high proliferation against a 23-mer peptide derived from the immunodominant UL86 antigen of human CMV, encoding the major capsid protein¹⁸⁸. Interestingly, peptide 986 to 993 (WLRSPFSR) of the UL86 antigen shows striking sequence similarity with the sequence 39 to 46 of mouse and marmoset MOG (WYRSPFSR) or human and rhesus monkey MOG (WYRPPFSR). T-cells from rhesus monkeys sensitized against this mimicry motif proliferated against MOG34-56, and CD3+ T-cells infiltrates were detected within the CNS parenchyma and meninges¹⁸⁹. These data suggest that anti-CMV memory T-cells may be activated by APC that present MOG34-56. It has been hypothesized that CMV does not provoke MS, but that individuals infected with CMV generate a repertoire of potentially pathogenic effector memory T-cells¹⁸⁸. In individuals genetically susceptible to MS, these memory T-cells might exacerbate CNS inflammation and demyelination upon activation with MOG34-56 presenting APC. This situation is represented in the common marmoset EAE model¹⁹⁰.



Figure 4. An adult common marmoset.

Common marmosets are characterized by a streaked grey, brown and yellow coloured pelt with white ear tufts and a long banded tail. The skin is usually pale, but darkens with exposure to sunlight. A mature monkey reaches a body length of approximately 20 cm, and the tail a size of about 30 cm.

THE COMMON MARMOSET

The common marmoset (*Callithrix jacchus*) is a small-bodied New World monkey that is native to Brazil and lives in the North-Eastern region of the country. Common marmosets have a lifespan

of 10 years in their natural habitat and both sexes are of similar size (approximately 20 cm, with a tail of 30 cm), although the males are slightly bigger (Figure 4). The body weight of adult monkeys ranges from about 250 to 350 gram, and can reach 450 gram in captivity. Common marmosets are social animals that live in groups of 3 to 15 individuals and feed themselves with e.g. gum, latex, insects, fruits, and nectar¹⁹¹. Sexual maturity is reached at 18 months and mothers give birth to twins or triplets per pregnancy, which occurs once or twice a year. Most of the offspring are bone marrow chimeras. This is explained by the fact that during pregnancy the placental blood stream is shared between fraternal siblings¹⁹². The chimeric state results in greater immunological similarity between fraternal siblings than with siblings from other births.

For decades the common marmoset has been used as experimental model in biomedical research, e.g. in neuroscience, reproductive biology, toxicology, and infectious diseases. Recently, scientific research in the common marmoset has increased since this monkey has many advantages compared to other non-human primate species, although there are also some limitations (Table 5). A benefit of using the common marmoset is that in therapeutic studies one sibling of a twin can be treated with an experimental agent and the other sibling with placebo. It is also possible to perform T-cell transfer studies between fraternal siblings of a twin, since they are immunologically compatible^{193, 194}.

Immunogenetics

HLA molecules are indicated in the common marmoset with the acronym *Caja*, and some HLA class I molecules in humans are homologous to *Caja* genes¹⁹⁵. However, the common marmoset does not express the classical MHC class Ia genes *HLA-A* and *HLA-C*, but *HLA-B* is expressed. In the *Caja-B* region nine genes have been identified (*Caja-B1–B9*), where *Caja-B2*, *-B5*, *-B8* and *-B9* are pseudogenes, because nonsense mutations and/or insertions or deletions are found in their exons. The other genes of the *Caja-B* region, *Caja-B1*, *-B3*, *-B4*, *-B6*, and *-B7* have translatable sequences¹⁹⁶. The non-classical HLA-E region is orthologous to *Caja-E*, but this is not the case for *HLA-G* with *Caja-G*¹⁹⁷. The non-classical *HLA-F* is also present in the common marmoset but it appears to be inactive. Two *Caja-E* alleles and five *Caja-G* alleles have been described so far^{195, 198}.

MHC class II loci in common marmosets have a limited polymorphism. In humans the MHC class II regions is organized into *HLA-DP*, *-DQ*, and *-DR* regions, where most nucleotide sequence variation is restricted to exon 2 of the *MHC-DPB*, *-DQA*, *-DQB*, and *-DRB* loci¹⁹⁹. The common marmoset contains also the *MHC-DR*, *-DQ* and *-DP* regions, although the *-DP* region seems to be inactivated. The *Caja-DR* region is divided into one *DRA* and three *DRB* loci *DRB1*03*, *DRB1*W12* and *DRB*W16* containing 13, 2 and 20 alleles, respectively (Table 4)^{200–205}. The polymorphic *DRB*W16* locus encodes functional MHC molecules. The two *DRB1*W12* alleles are highly similar; they differ only in two codons outside the peptide-binding cleft²⁰⁰. Most *DRB1*03* alleles are not transcribed or only at very low levels. Interestingly, by recombination of exon 2, elements of *DRB1*03* with *DRB*W16* hybrid MHC-DR molecules are produced, leading to expansion of the limited MHC class II repertoire²⁰⁶. The limited variability of *Caja* class I and II genes implies that inter-individual variation of the immune response is also limited and that common marmosets may be more susceptible to certain viral and bacterial infections than other non-human primates, such as the rhesus monkey. This limited immune genotype can be explained by the relatively recent evolution compared to e.g. Old world monkeys and humans^{195, 197}.

Table 4. Overview of the common marmoset MHC class I and II alleles.

MHC class I			
Region	Locus	Lineage	
B	1		
	2 [#]		
	3		
	4		
	5 [#]		
	6		
	7		
	8 [#]		
	9 [#]		
E		*01	
		*02	
F ^{##}			
G		*01	
		*02	
		*03	
		*04	
		*05	
MHC class II			
Region	Locus	Lineage	Allele
DP ^{##}			
DR	A		
	B1	*03	01, 02, 03, 04, 05, 06, 07 [#] , 08, 09, 10, 11, 12 [#] , 14
	B	*W12	01, 02
	B	*W16	01, 04, 05, 06, 07, 08, 09, 10, 11, 12, 13, 14, 15, 16, 17, 18, 20, 22
DQ	A1	*01	01
		*27	01
	A2 [#]		
	B1	*2201	01, 02
		*23	01, 02
B2	*01	01, 02, 03	

[#]pseudogene, ^{##}inactive

Despite the limited variation of MHC class I and II molecules in the common marmosets they have a diverse repertoire of T-cell cell receptors (TCR), which is highly comparable with the human TCR repertoire. The TCR consists of an α and β chain in 95% of mature T-cells, whereas

Table 5. Advantages and disadvantages of the common marmoset in biomedical research.

Advantage	
Proximity to humans	(Neuro)anatomy, immunology, physiology, microbiology.
Size	Relatively small (\pm 320 gram) compared to other non-human primates (e.g. macaque species), high reproductive efficiency in captivity, lower caging and feedings costs compared to macaques, socially housed.
Conventional housing	Exposure of immune-shaping pathogens from the external milieu (e.g. gut microbiota and environment) and from the internal milieu (e.g. latent infection with the herpes viruses such as the common marmoset counterparts of Epstein-Barr virus and cytomegalovirus).
Outbred nature	Comparable genetic heterogeneity as the human population. Wild populations are not endangered.
Cross-reactivity	Biological therapeutics developed for human diseases e.g. monoclonal antibodies and cytokines, can be assessed for preclinical evaluation of efficacy, safety and mechanism of action.
Bone-marrow chimeras	Twins or triplets are immunologically highly similar, and hence can be used in pairs for therapeutic studies. Twin siblings are mutually allotolerant enabling adoptive transfer of cells between siblings.
Drug development	Cheaper due to small-size, 10- to 20-fold less compound is needed compared to macaques.
Disadvantage	
High costs	Relatively high compared to rodents or other non-rodent species.
Cross-reactivity	Limited availability of diagnostic reagents such as monoclonal antibodies for flow cytometry and immunohistochemistry.
Ethical	Is closer to humans compared to rodents, limited experimental manipulations (e.g. transgenic experiments).
Size	Small size, difficult or impossible to perform certain procedures or techniques (e.g. MRI of spinal cord), small volume of blood or organs (e.g. lymph nodes) can be obtained to perform <i>ex vivo</i> experiments.

Based on^{193, 224}.

in the remaining 5% of T-cells the TCR consists of γ and δ chains. The TCR α chain is generated by recombination of the variable (V) and joining (J) segments, whereas the TCR β chain is generated by V, diversity (D) and J recombination. Combinations of these individual segments correspond to the antigen-binding domain of the T-cell, which is involved in the antigen-MHC recognition²⁰⁷. In addition, all TCR contain a constant (C) region. In the common marmoset there are two C-regions in the β chain that are similar to the human *BC1* and *BC2* genes, named *CjCB1* and *CjCB2*, respectively. There are also 36 human V-genes and 13 J-genes identified in the β chain with 91% and 16-36% similarity to the common marmoset sequences, respectively^{208, 209}. For the formation of TCR α chains one C-, 46 J- and 35 V-genes are used, which are 80%, 68-100% and 79-98% conserved compared to their human counterparts, respectively²¹⁰. The complementarity-determining region 3 (CDR3) has no conserved motifs; the average length of 10 amino acids is similar to mice and humans²⁰⁸.

At the level of immunoglobulins (Ig), the heavy chain in the common marmoset can be divided in six different types of the variable gene (IGHV1, 3, 4, 5, 6 and 7), which implies at least 80% similarity to the human IGHV. Furthermore, the IGHV2 gene is absent in the marmoset²¹¹. The Ig isotypes such as IgG and its subclasses e.g. IgG1 and IgG2 are not (yet) identified in the common marmoset. However, there are cross-reacting human monoclonal antibodies available to detect Ig isotypes as IgG, IgM and IgE²¹². This suggests that common marmosets have an Ig system similar to humans.

Immunoglobulin superfamily (IgSF) genes are a large group of proteins with sequences similar to Ig. Based on the structural characteristics, the IgSF molecules are classified in several categories. In humans there are 11 functional categories based on the Gene Ontology database. Three of the 11 functional categories - being immune system process, defence response and multi-organism process - are closely linked to the regulation of the immune system. In the common marmoset there are 11 IgSF genes that have been conserved during its evolution²¹³.

Natural killer (NK) cells are granular lymphocytes that function at the interface of adaptive and innate immunity. NK cells use cytotoxic proteins and cytokines to kill tumours or virus-infected cells. On the basis of genomic organization in the NK-complex (NKC) *CD94*, *NKG2A*, *NKG2D*, *NKG2CE* and *Ly49L* were identified for the common marmoset. The NKC region is smaller than its human counterpart due to the lack of one *NKG2* gene, but the remaining genes are highly conserved²¹⁴.

Immunological read-out parameters

The number of available reagents for immunological parameters in the common marmoset is limited. In the last decade a useful set of monoclonal antibodies was developed to phenotype leukocyte subsets and to stain lymphoid tissues for cytokines. Moreover, there is also a set of primers available for quantitative PCR to determine cytokine mRNA transcript levels in PBMC, spleen and lymph nodes²¹⁵ (also discussed in **chapter 9**).

PBMC, spleen and lymph nodes cell subsets are phenotyped by flow cytometry using an extensive panel of commercially available mAb against human cluster of differentiation (CD) markers that were selected for crossreaction with the corresponding CD markers of marmosets²¹⁶, but there are also antibodies specifically developed for the common marmoset²¹⁷⁻²¹⁹. The same principle has been used to identify cross-reacting monoclonal antibodies for immunohistochemistry²²⁰.

A standard immune parameter in common marmoset autoimmune disease models (e.g. EAE) is proliferation of PBMC against the immunized antigen and peptides of interest. Since in PBMC low proliferative responses are detected, secondary lymph nodes as spleen, axillary, inguinal and cervical lymph nodes are tested for higher proliferative responses. The most commonly used assays for lymphocyte proliferation are the tritium [³H]-thymidine incorporation assay¹⁰³ and the CFSE vital dye dilution technique²²¹.

Cytokine levels in culture supernatants of lymphocytes are routinely detected by ELISA kits developed for human cytokines such as IL-2, IL10, IL12p40, IL-13, IL-17A, TNF- α and IFN- γ .

In addition to these tests, also non-immunological assays are performed in animal disease models to characterize the pathogenesis in further detail. A crucial technique in MS research is MRI. Several MRI parameters e.g. T1, T2, lesion load and magnetization transfer ratio were implemented for visualization of abnormalities in the common marmoset brain²²². Moreover,

body weight loss and metabolic profiles in body fluids, such as change in chemical composition of urine samples at different EAE stages²²³, are measured to obtain more information during the disease progression.

AIMS AND OUTLINE OF THIS THESIS

The etiology and exact immunopathogenic mechanisms underlying MS are still unknown and no therapies without adverse effects are available. For the study of immunopathogenic mechanisms and development of novel therapeutics for MS, several EAE models can be used. In this thesis the common marmoset EAE model is used, which has high clinical and pathological similarity with MS. In conjunction with its close genetic and immunological proximity to humans, the common marmoset is a relevant animal model. The overall aim of this thesis was to model the clinical and immunological features of MS in the common marmoset, while minimizing artificial requirements that cause discomfort to the animals but are not strictly needed for disease induction. In parallel we aimed to examine the function of autoreactive T-cells during disease progression. Finally, new targets for MS therapy were assessed using novel immunotherapeutics allowing mechanistic analyses.

The principal scientific objective of the research described in this thesis was to dissect the immunological mechanisms that induce neurological dysfunction in the common marmoset EAE model. In **chapter 2** it is shown that the presence of MOG in the immunizing myelin/CFA inoculum is not required for EAE initiation, but has a critical role in the progression to clinically evident EAE. Further studies were therefore focussed on analyzing the critical autoimmune parameters. In **chapter 3** we demonstrated that immunization with rhMOG in CFA induced clinical signs in all animals, but with a variable disease onset. While the explanation for the 100% disease incidence has already been analysed by Brok et al.¹⁰³ i.e. the Caja-DRB*W1201 restricted activation of Th1 cells specific for the epitope MOG24-36, we showed that progression to overt neurological disease depends on the activation of T-cells specific for MOG34-56. Immunization with MOG34-56 in CFA led to the same clinical and pathological symptoms with a critical role of MOG34-56 autoreactive cytotoxic T-cells. In **chapter 4** we document the observation that immunization of common marmosets with MOG34-56 in IFA induces full-blown EAE. All animals showed comparable clinical symptoms and pathology to the rhMOG/CFA- and MOG34-56/CFA-induced EAE models, but with a slight delay in disease onset. In the peptide-induced models no antibody against rhMOG, residues 1-125, was formed.

This new MOG34-56/IFA EAE model challenges to establish pathogenic concepts of EAE and MS in two ways. First, ligands of innate antigen receptors, which are deemed indispensable for breaking tolerance mechanisms, were absent in the immunizing inoculum. Second, although widespread demyelination of CNS white and grey matter was observed, serum antibodies binding ELISA plate-bound rhMOG were undetectable. Taken together these findings suggest that activated T-cells induced the formation of CNS lesions and the ensuing neurological deficit.

This was further investigated in **chapter 5**. *In vivo* activated MOG34-56 T-cells are mainly CD3+CD4+CD56+ and CD3+CD4+CD8+CD56+, which have an effector memory phenotype, and display high IL-17A production as well as specific cytotoxic activity as main functional characteristics. The cytotoxic T-cells are specific for MOG40-48/Caja-E complexes. MOG40-48 is a proven mimicry epitope shared with the immunodominant UL86 antigen (major capsid

protein) of non-human primate CMV. Based on the specificity, MHC restriction and phenotype, the *in vivo* activated MOG34-56 T-cells were tentatively characterized as natural killer–cytotoxic T-lymphocytes (NK-CTL).

In a final *in vivo* experiment the immunological core event in the common marmoset EAE model was further delineated. In **chapter 6** we examined whether disease could be induced with rhMOG in IFA. So far, we concluded that all animals developed neurological deficit and T-cell responses in lymphoid organs. Remarkably, antibodies were formed against rhMOG, and the MOG peptides 14-36, 24-46 and 54-76, but not to MOG34-56. Analyses such as CNS pathology and cytokine profiling have to be performed yet.

Recent clinical trials with depleting anti-CD20 antibodies have highlighted an important pathogenic role of the antibody-independent contribution of B-cells to MS. In **chapter 7** we have assessed antibody-independent contributions of B-cells in the MOG34-56/IFA-induced EAE model. B-cells were depleted with an anti-CD20 mAb well after immunization with MOG34-56/IFA. All animals were effectively protected against EAE symptoms and lesion formation. The assumption that B-cells act as APC for pathogenic T-cells, was supported by the observation that infusion of EBV transformed B-cells pulsed with MOG34-56 induced *ex vivo* detectable IL-17A production and cytolytic activity.

Besides the anti-CD20 antibody, several new immunotherapies were tested. In **chapter 8** therapies neutralizing essential factors for B-cell survival and function level were assessed. Antibodies binding to B-cell lymphocyte stimulator/ B-cell activating factor (BLYS/BAFF) and proliferating inducing ligand (APRIL) reduced B-cell levels and antibody responses, which resulted in significant delay of EAE development in marmosets immunized with rhMOG in CFA. Experiments in **chapter 9** demonstrate that treatment with human IFN- γ in the MOG34-56/IFA model during disease initiation had modulatory effects on humoral and cellular immune parameters, but no effect on clinical symptoms.

Finally, all the three different EAE models that have now been established in the common marmoset as described in this thesis are discussed in **chapter 10** with respect to their immunization protocol and pathogenic mechanisms. Furthermore, it is discussed how these results can be translated to MS patients, and suggestions for further research are given.

**AUTOIMMUNITY AGAINST MYELIN
OLIGODENDROCYTE GLYCOPROTEIN IS
DISPENSABLE FOR THE INITIATION ALTHOUGH
ESSENTIAL FOR THE PROGRESSION OF CHRONIC
ENCEPHALOMYELITIS IN COMMON MARMOSETS**

S. Anwar Jagessar*, Paul A. Smith*, Erwin Blezer, Cecile Delarasse,
Danielle Pham-Dinh, Jon D. Laman, Jan Bauer, Sandra Amor, and Bert 't Hart

* Shared first authorship, # Shared senior authorship

J Neuropathol Exp Neurol 67, 326-340 (2008)

ABSTRACT

To elucidate the pathogenetic significance of myelin/oligodendrocyte glycoprotein (MOG)-specific autoreactivity in a genetically and immunologically heterogeneous non-human primate model of multiple sclerosis, we analyzed experimental autoimmune encephalomyelitis (EAE) in the outbred common marmoset (*Callithrix jacchus*). One sibling each of five bone marrow chimeric marmoset twins was immunized with myelin derived from wild-type (WT) C57BL/6 mice (WT myelin); the other sibling was immunized with myelin from MOG-deficient C57BL/6 mice (MOG^{-/-} myelin). One twin pair developed acute EAE simultaneously; the four remaining twin siblings immunized with WT myelin developed chronic progressive EAE, whereas siblings of these four monkeys remained free of clinical disease signs. Many EAE-related abnormalities were identified in the CNS of both groups by magnetic resonance imaging and histologic analysis, but mean percentages of spinal cord demyelination were lower in monkeys immunized with MOG^{-/-} myelin (8.2%) than in WT myelin immunized animals (40.5%). There was a strong correlation between the development of overt clinical EAE and seropositivity for anti-MOG antibodies, but blood and lymph node T-cell proliferative responses showed no relationship to disease. These results indicate that the initiation of CNS inflammation and demyelination can take place in the absence of detectable autoimmunity against MOG, but the clinical progression and histopathologic severity depends on the presence of antibodies against MOG in this multiple sclerosis model.

INTRODUCTION

Experimental autoimmune encephalomyelitis (EAE) is a widely studied model of the human neuroinflammatory disease multiple sclerosis (MS). Experimental autoimmune encephalomyelitis can be induced in a wide range of genetically susceptible laboratory animal species, including rodents and primates, by immunization with myelin or myelin components in strong adjuvants^{225, 226}. Previously, we showed that the induction of chronic EAE in Biozzi ABH mice strictly depends on the presence of myelin/oligodendrocyte glycoprotein (MOG) in the immunization inoculum. Although Biozzi ABH mice immunized with myelin from MOG deficient (MOG^{-/-}) C57BL/6 mice²²⁷ exhibited a short limited episode of neurologic deficit, they did not develop the typical relapsing/remitting disease course observed in Biozzi mice immunized with MOG containing myelin from wild-type (WT) mice⁹³. Furthermore, the addition of only a minute amount of recombinant mouse MOG (rmMOG) to the MOG^{-/-} myelin preparation used for immunization resulted in the induction of a relapsing/remitting EAE course. Whether the critical role of MOG for induction of chronic EAE is specific to the inbred Biozzi ABH mouse EAE model or if the phenomenon also holds true in a model in a more complex genetically outbred species more closely related to humans is not known. EAE in the common marmoset (*Callithrix jacchus*) provides a valid MS model of MS in which this question can be addressed²²⁸.

MOG is a highly conserved, quantitatively minor constituent of CNS myelin and is exposed on the outermost lamellae of the myelin sheath and on the surface of mature oligodendrocytes²²⁹⁻²³¹. Because of a lack of MOG expression within the thymus, autoreactive T lymphocytes likely escape negative selection and are present in the normal immune repertoire^{227, 232, 233}. After immunization of marmosets with recombinant human MOG1-125 (rhMOG) in adjuvant, MOG-specific autoreactive T cells contribute to the induction of EAE^{103, 233}. Compared with more abundant CNS myelin proteins such as myelin basic protein (MBP) and proteolipid protein (PLP), MOG is the most potent inducer of inflammatory demyelinating disease in this species. Immunization with rhMOG or synthetic MOG peptides also induces T-cell-mediated EAE in susceptible rodent strains^{93, 234-236} and in non-human primates^{98, 136, 234}. This disease model reproduces many of the clinical and histologic features of MS. Furthermore, the ability of anti-MOG antibodies to increase myelin uptake by macrophages, enhance demyelination, and augment clinical disease in rodents⁷⁴ and in nonhuman primates¹³⁶ to a greater extent than humoral responses against other myelin antigens is unique.

The aim of this study was to determine the extent to which the presence of MOG in the myelin inoculum is required for the induction of EAE in the common marmoset. This was tested in marmoset twins that, due to their natural bone marrow chimerism, are immunologically highly similar^{192, 237}. One sibling of each twin was immunized with myelin from WT C57BL/6 mice, the other was immunized with myelin from MOG^{-/-} C57BL/6 mice produced in one of our laboratories²²⁷. We found that T-cell reactivity against MOG (i.e. proliferation) was present in both siblings of each twin pair, but that anti-MOG antibodies were substantially reduced or absent in the siblings immunized with MOG^{-/-} myelin. In one twin pair, acute clinical EAE developed simultaneously in both siblings. Of the remaining four twin pairs, the siblings immunized with WT myelin developed overt chronic EAE, whereas this was observed in none of the siblings immunized with MOG^{-/-} myelin. The clinical data were confirmed using high-definition magnetic resonance brain imaging (MRI) and histopathologic analysis, showing that, although substantial abnormalities were observed in the monkeys immunized with MOG^{-/-}

myelin, CNS demyelination was less severe than in the WT myelin/immunized animals. These results indicate a strong influence of anti-MOG antibodies on the development of chronic autoimmune demyelinating disease.

MATERIALS AND METHODS

Animals

Ten healthy adult male common marmosets were purchased from the outbred colony maintained at the Biomedical Primate Research Centre (Rijswijk, The Netherlands). To reduce variation between the two experimental groups, five nonidentical twin pairs were used. Despite genetic differences inherent to the outbred nature of this species, twins are immunologically highly similar due to naturally occurring bone marrow chimerism. All animals were given a complete physical, hematologic, and biochemical health screen prior to experimental selection. During the experiments, twin siblings were pair-housed in spacious cages and were under intensive veterinary supervision. The daily diet consisted of commercial food pellets for New World monkeys (Special Diet Services, Witham, Essex, UK) supplemented with rice, raisins, peanuts, marshmallows, fresh fruit, and live insects. Drinking water was provided *ad libitum*. According to the Netherlands' law on animal experimentation, the procedures of this study have been reviewed and approved by the institute's experimental ethics committee. The housing, care, and biotechnical handlings were in conformity with guidelines of this committee.

Antigens

Myelin was purified from the spinal cords of WT and MOG^{-/-} mice as previously described⁹³. Wild-type mice were bred at the Biomedical Primate Research Centre, and MOG^{-/-} mice were obtained from Dr. D. Pham-Dinh (Université Pierre et Marie Curie, Paris, France). Protein concentrations were determined using the Bradford technique²³⁸. Synthetic 23-mer MOG peptides corresponding to the extracellular domain of human MOG were purchased from ABC Biotechnology (London, UK). Recombinant mouse MOG1-116 and rhMOG were produced, and myelin was isolated as previously described^{93, 138, 239}. Human MBP (hMBP) was a kind gift from Dr. J. M. van Noort (TNO-PG, Leiden, The Netherlands).

Induction of EAE

EAE was induced under ketamine anesthesia (40 mg/kg; AST Pharma, Oudewater, The Netherlands) by a single subcutaneous inoculation of 300 µl myelin in water (10 mg/ml) emulsified with 300 µl complete Freund's adjuvant (Difco Laboratories, Detroit, MI) into four sites of the dorsal skin¹⁰³. Animals were clinically scored twice daily by trained observers using a previously described semiquantitative scale¹²⁷. Plasma samples were collected at various post sensitization days and stored at -20°C for determination of antibody reactivity with myelin preparations by Western blotting or myelin proteins by enzyme-linked immunosorbent assay (ELISA). Animals were killed when they reached the humane end point (EAE score ≥3) or otherwise at the predetermined study end point. Humane end point criteria are discussed in detail elsewhere²⁴⁰.

Postmortem examination

At the time of necropsy, the monkeys were first deeply sedated by an injection of ketamine (50 mg/ml saline, i.m.) at a dose of 100 µl/kg body weight and subsequently euthanized by infusion of pentobarbital sodium (Euthesate; Apharmo, Duiven, The Netherlands). The brain, spinal cord, spleen, and lymph nodes from inguinal and axillary regions were aseptically removed. Spleen and lymph nodes were processed for preparation of mononuclear cell (MNC) suspensions. Representative samples of all organs were snap-frozen in liquid nitrogen or fixed with 4% buffered formalin. Frozen tissues were stored at -80°C. After at least seven days' fixation in formalin, the tissues were transferred into buffered saline containing sodium azide (Sigma-Aldrich, Gillingham, UK) for stabilization prior to MRI²⁴¹. To assess the lesion load in the brain, MRI was performed on formalin-fixed brains as described previously^{127, 241}. The frozen and fixed tissues were processed for examination with histologic and immunohistochemical techniques as described^{127, 242, 243}.

Histopathology and immunohistochemistry

After formalin fixation, samples of the brain, spinal cord, and peripheral nerves were embedded in paraffin and processed as described previously²⁴⁴. In brief, in each animal, the cerebrum and cerebellum were divided into 7 or 8 coronal sections; the spinal cord was sectioned transversely into 10 to 15 pieces. This material was embedded in three to four paraffin blocks. The extent of inflammation, demyelination, and axonal abnormalities were evaluated on 3- to 5-µm-thick sections stained with hematoxylin and eosin to visualize infiltrating cells, Luxol fast blue combined with periodic acid Schiff for myelin and myelin degradation products, and with Bielschowsky silver impregnation for axons.

For immunohistochemical staining, 3- to 5-µm-thick paraffin sections were deparaffinized in xylene and transferred to 90% ethanol. Endogenous peroxidase was blocked by 30 min incubation in methanol with 0.02% H₂O₂. Sections were then transferred to distilled water via a 90%, 70%, and 50% ethanol series. Before staining with antibodies, antigen retrieval was performed as follows: paraffin sections were pretreated in a household food steamer device (MultiGourmet FS 20; Braun, Kronberg/Taunus, Germany) by a 60 min incubation in a plastic Coplin jar filled with EDTA (0.05 mol/L) in TRIS buffer (0.01 mol/L; pH 8.5). To detect Immunoglobulin (Ig)G and IgM, antigen retrieval was performed by incubation with 0.03% protease from *Streptomyces griseus* (Sigma, St. Louis, MO) for 15 min at 37°C. After antigen retrieval, the sections were incubated with 10% fetal calf serum (FCS) in 0.1 mol/L phosphatebuffered saline (FCS/PBS). Primary antibodies for CD3 (DakoCytomation, Hamburg, Germany) and PLP (Serotec, Oxford, UK) were applied in FCS/PBS at 4°C overnight. IgG and IgM were detected by staining with biotinylated anti-human-IgG and anti-human-IgM antibodies (DakoCytomation). After washing with PBS, secondary antibodies in PBS/FCS were applied for 1 h at room temperature. Biotinylated secondary antibodies were used at a concentration of 1:200 (donkey-anti-rabbit, sheep-anti-mouse; Amersham Pharmacia Biotech, Uppsala, Sweden). As a third step, avidin peroxidase (1:100; Sigma) was used. Labeling was visualized with 3,3' diaminobenzidine-tetra-hydrochloride (Sigma).

Quantification of inflammation and demyelination

In hematoxylin-eosin-stained sections, the degree of inflammation was expressed as an index that was calculated as the average number of inflamed blood vessels per spinal cord cross

section (inflammatory index; $n = 10$ to 15 spinal cord cross sections per monkey). The degree of demyelination was quantified in Luxol fast blue/periodic acid Schiff-stained sections in each monkey on 10 to 15 spinal cord cross sections by overlay of a 100-point morphometric ocular grid and counting the amount of normal and demyelinated white matter.

Magnetic resonance imaging

High-definition T2-weighted images were made of formalin-fixed brains as previously described²⁴¹. Previous studies showed that the usually sharply demarcated hyperintense abnormalities present in the brain white matter of EAE-affected monkeys, but reference samples of non-EAE monkeys do not represent demyelinated lesions^{127, 241}. All experiments were performed on a 4.7-T horizontal bore nuclear MR spectrometer (Varian, Palo Alto, CA) equipped with a high-performance gradient insert (12-cm inner diameter; maximum gradient strength, 500 mT/m). A homebuilt solenoid coil (4 windings; \varnothing , 35 mm) was used for radiofrequency transmission and signal reception. Brain specimens were immersed in a nonmagnetic oil (Fomblin; perfluorinated polyether; Solvay Solexis, Weesp, The Netherlands) to prevent unwanted susceptibility artifacts. Forty-seven contiguous T2-weighted transversal slices of 0.75 mm were collected with the following characteristics: repetition/echo time, 3,000/15 milliseconds; field of view, 2.5 x 2.5 cm²; matrix, 128 x 128; zero-filled, 256 x 256; in-plane resolution, 195.3 x 195.3 μ m, 2 transitions.

Individual image sets were registered using the Medical Image NetCDF package (McConnell Brain Imaging Centre, Montreal Neurological Institute, McGill University, Montreal, Quebec, Canada). For quantitative analysis of the area of high signal intensity in the white matter (i.e. lesions), the free available Medical Image Processing, Analysis and Visualization (version 2.7.101; 2006; National Institutes of Health, Bethesda, MD) package was used. Regions of interest with abnormal decreased signal intensities were automatically outlined in all slices containing white matter structures using the level-set method of Medical Image Processing, Analysis and Visualization. The volumes of the region of interest were calculated.

MRI data are expressed as mean \pm SEM where appropriate. Statistical analyses were performed using the statistical software package Sigmapstat (version 3.11; 2004). Data were evaluated by 2-way repeated measures analysis of variance, followed by the Student-Newman-Keuls post hoc test. $p < 0.05$ was considered statistically significant.

T-Cell proliferative responses

According to the Institute's guidelines, the maximum blood volume that can be collected from a primate without damaging its health is 0.7% of the body weight per month for a single collection or a total of 1% when collections are spread over multiple time points. For an adult marmoset of 350 g, this represents a maximum of 3.5 ml, thereby limiting the number of tests that can be performed in this model. MNC from heparinized peripheral blood mononuclear cell (PBMC) or lymphoid organs (lymph node cell) were isolated using lymphocyte separation medium (ICN Biomedical, Inc., Costa Mesa, CA) as previously described¹⁰³. Mononuclear cells (1.10^6 cells/ml) were cultured in RPMI media supplemented with 10% fetal bovine serum, 2 mM L-glutamine, 100 IU/ml of penicillin, 100 μ g/ml of streptomycin, 5 mmol/L of 4-(2-hydroxyethyl)-1-piperazineethanesulfonic acid, and 5×10^{-5} mol/L of β -mercaptoethanol (Invitrogen, Gibco BRL, Glasgow, UK), with 10 μ g/well MOG peptides, rmMOG, rhMOG, or WT myelin for 72 h.

Proliferation was measured by the incorporation of ^3H -thymidine (Amersham Biosciences, Buckinghamshire, UK) after addition at $1\ \mu\text{Ci}/\text{well}$ during the last 18 h of culture and expressed as mean counts per minute \pm SD of triplicate cultures. Stimulation indices were calculated from measured counts per minute in cultures stimulated with antigen divided by counts per minute in cultures without antigen.

Generation of MOG-reactive T-cell lines

Lymph node MNCs were stimulated *ex vivo* with WT myelin, $\text{MOG}^{-/-}$ myelin, or rhMOG to establish T-cell lines. Briefly, lymph node cells (10^6 cells/well) were seeded onto 24-well plates (Greiner Bio-one, Frickenhausen, Germany) and stimulated with $10\ \mu\text{g}/\text{ml}$ of antigen. Every 2 to 3 days, half of the culture supernatant was removed and replaced with fresh medium containing $20\ \text{U}/\text{ml}$ of recombinant human interleukin (IL) 2 (Proleukin, Chiron Corporation, Emeryville, CA). After 14 to 21 days of culture, the T-cell lines were transferred into 96-well flat-bottom plates (Greiner Bio-one) and tested for proliferation against a panel of 23-mer overlapping peptides derived from the human MOG extracellular domain using irradiated immortalized B-cell lines as antigen-presenting cells for restimulation¹⁰³. Antigen- and peptide-reactive T-cell lines were characterized for cytokine responses by ELISA (U-Cytech, Utrecht, The Netherlands).

Western blotting

Total WT or $\text{MOG}^{-/-}$ myelin proteins were obtained by solubilization of mouse CNS samples in 80% tetrahydrofuran-20% water-0.1% trifluoroacetyl acid, and subsequent delipidation was performed by repeated ether precipitation and subjected to sodium dodecylsulfate polyacrylamide gel electrophoresis. The purified myelin protein fractions ($3\ \mu\text{g}$) or rmMOG ($4\ \mu\text{g}$) were solubilized in $15\ \mu\text{l}$ NuPAGE LDS Sample buffer containing NuPAGE Sample Reducing Agent (Invitrogen, Carlsbad, CA) was applied to a 4% to 12% gradient Bis-Tris gel (Invitrogen, CA). A semidry blotting system (Ancos, Hoejby, Denmark) was used to test reactivity of immune sera.

Samples were immunoblotted with preimmune or necropsy sera from marmosets immunized with WT or $\text{MOG}^{-/-}$ myelin. Protein bands were confirmed by monoclonal antibodies; anti-MOG Z12 (generated in our laboratory²⁴⁵), rabbit anti-myelin-associated glycoprotein (kindly provided by N. Gregson, London, UK), mouse anti-2,3-cyclic nucleotide 3-phosphodiesterase (Chemicon, Temecula, CA), mouse anti-PLP (Chemicon), mouse anti-MBP (Dako, Glostrup, Denmark), and rabbit anti-oligodendrocyte-specific protein (Abcam, Cambridge, UK). The primary antibodies were detected with the appropriate secondary antibodies, including rabbit anti-mouse Ig/horseradish peroxidase, rabbit anti-human Ig/horseradish peroxidase, or goat anti-rabbit Ig-horseradish peroxidase (all from Dako) and developed using enhanced chemiluminescence (Amersham, UK). The computerized system Chemidoc XRS and PDQuest (Bio-Rad, Hercules, CA) was used to calculate the molecular weight and density of the bands.

ELISA

Microlon plates (Greiner Bio-one) were coated overnight at $4\ ^\circ\text{C}$ with $10\ \mu\text{g}/\text{ml}$ of rmMOG, rhMOG, or hMBP in PBS. The plates were washed twice in PBS-Tween and blocked for 1 h at $37\ ^\circ\text{C}$ with 2% bovine serum albumin/PBS. After blocking, $100\ \mu\text{l}$ of diluted plasma (1:200) in 1% bovine serum albumin/PBS was added and incubated for 2 h at $37\ ^\circ\text{C}$. Individual animal pre-

immunization plasma was used as a negative control. After washing in PBS-Tween, the plates were incubated for 1 h at 37 °C with alkaline phosphatase-conjugated rabbit anti-human IgG (Abcam) or goat-anti-monkey IgM μ -chain (Rockland, Gilbertsville, PA). The reaction product was visualized using p-nitrophenyl phosphate-Tris buffer (Sigma-Aldrich, Gillingham, UK), and the absorbance read at 405 nm. Absorbances more than the mean plus 3 SD of the activity measured in pre-immune sera were interpreted as positive.

RESULTS

Clinical scores and body weights

The EAE scores and patterns of weight loss of the ten monkeys are depicted in Figure 1. All five marmosets immunized with myelin from WT mice developed overt neurologic signs of variable severity and different extents of weight loss. In one monkey (M03015), the disease remitted after a short episode of incomplete hind limb paralysis and did not exacerbate during the remainder of the 180 day observation period. We observed a similar variable disease course in our previous studies in which EAE was induced with human CNS myelin¹²⁷. By contrast, only one of the five marmosets immunized with myelin from MOG^{-/-} mice (M02115) developed an overt neurologic deficit. In the other four monkeys, there were minimal signs of EAE and moderate or no weight loss. The acute EAE course and dramatic weight loss in monkey M02115 coincided with the course of its twin sibling (M02114) that had been immunized with WT myelin. This suggests that the acute EAE in this twin was not induced by MOG and was likely caused by an immune response to other myelin components.

MRI and histology

High-definition T2-weighted postmortem images were made of the brains of each monkey to visualize white matter abnormalities. Moreover, the extent of inflammation and demyelination were quantified (Table 1). Total lesion volumes per monkey are shown in the Table 1. To demonstrate the distribution of lesions in different brain regions in the two groups of monkeys, the lesion load per slice is indicated semi-quantitatively in Figure 2, and representative slices corresponding to the arrows in Figure 2 are shown in Figure 3. The data show that MRI-detectable abnormalities were scattered throughout the brain white matter in both groups of monkeys. Quantitation of the lesion areas of twins show that with the exception of the acute EAE twins M02114/M02115, the total lesion volume of monkeys immunized with WT myelin brain lesions was larger than those induced with MOG^{-/-} myelin. The MRI findings were supported by histologic analysis of the spinal cord (Fig. 4; Table). They demonstrate that immunization with WT and MOG^{-/-} myelin induced similar amounts of inflammation (mean inflammatory index, 3.2 [range, 1.1-5.1] and 2.4 [range, 0.4-4.0], respectively). In contrast, immunization with MOG-containing myelin induced more demyelination (group mean, 40.5% [range, 14-56]) than immunization with MOG^{-/-} myelin (group mean, 8.2% [range, 0-20.3]). In two of the latter monkeys (M02115, M03006), more than 10% of the spinal cord white matter was demyelinated. Inflammation and demyelination in the spinal cord of the twin monkeys M03007 and M03006 are shown in Figure 4. Demyelination was also detectable in the optic nerves, although the extent was greatest in the monkey immunized with WT myelin (Fig. 5). The day of killing varied considerably among the individual monkeys, and long survivors have had more time to accumulate CNS lesions (Fig. 2; Table).

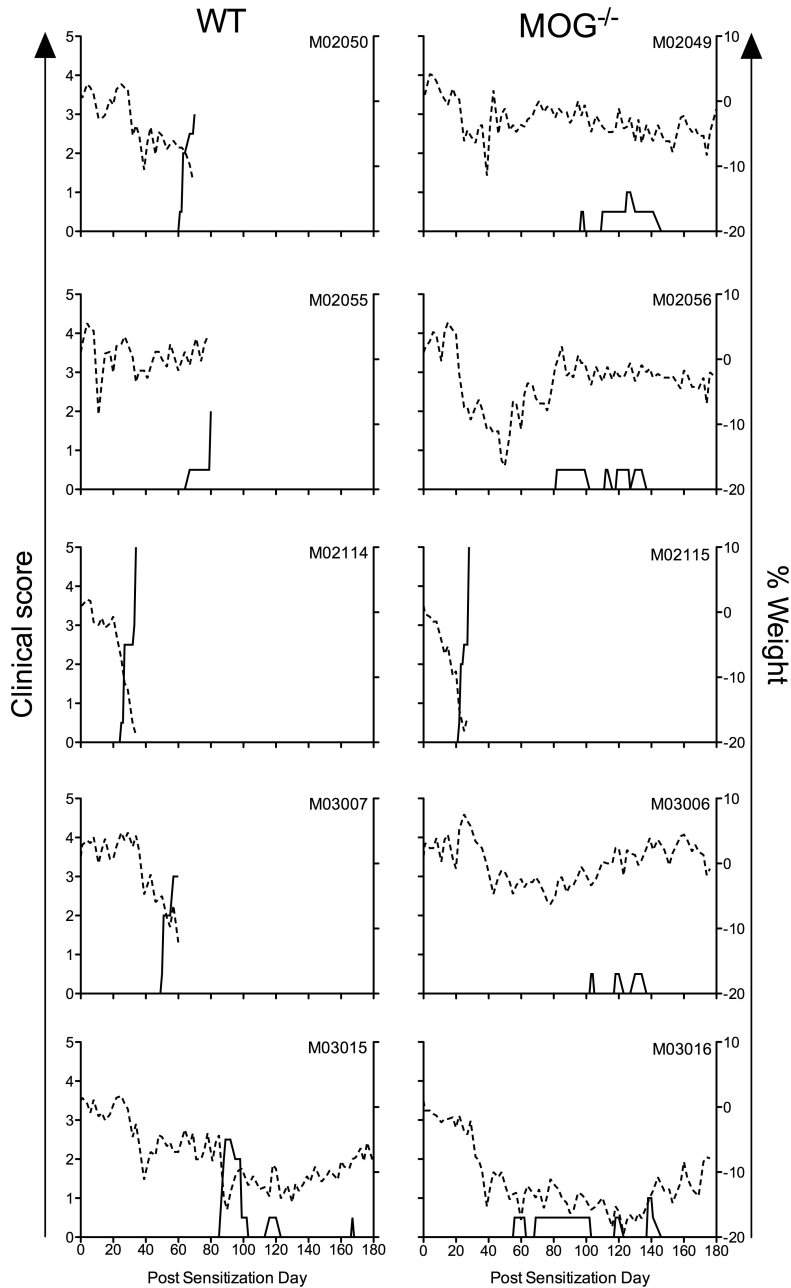


Figure 1. EAE course in marmosets immunized with myelin from WT or MOG^{-/-} mice. One twin each of five marmoset twin pairs was immunized with myelin from WT mice in CFA and the other twin with myelin from MOG^{-/-} mice in CFA. The graphs depict clinical scores of each monkey (left y-axis) and the percentage of weight loss from Day 0 weight (right y-axis) as a surrogate disease marker. The horizontal axis is days post sensitization day (PSD). The disease-free survival times between the two groups differ significantly (logrank test; $p = 0.0273$).

Table 1. Survival, MRI, and histologic summary.

	Monkey	DOK, PSD	Overt EAE Signs present	MRI-lesion Volume, mm ³	Inflammatory index	Demyelination, %	IgM Deposition	IgG Deposition
Twin 1								
WT	M02050	69	Yes	2.6	5.1	56.0	++	++
MOG ^{-/-}	M02049	180	No	0	0.4	0	+	±
Twin 2								
WT	M02055	80	Yes	61.2	2.6	36.2	++	±
MOG ^{-/-}	M02056	180	No	5.8	3.0	2.0	±	-
Twin 3								
WT	M02114	34	Yes	1.2	4.5	51.3	++	+
MOG ^{-/-}	M02115	34	Yes	289.1*	4.0	20.3	±	±
Twin 4								
WT	M03007	60	Yes	86.3	2.6	45.0	++	++
MOG ^{-/-}	M03006	180	No	1.5	3.7	15.3	+	+
Twin 5								
WT	M03015	180	Yes	2.3	1.1	14.0	++	++
MOG ^{-/-}	M03016	180	No	0	0.8	3.4	+	-
Means								
WT	Mean±SD	85±50	5/5 (100%)	30.7±36.0	3.2±1.4	40.5±14.8	NA	NA
MOG ^{-/-}		151±58	1/5 (20%)	1.8±2.4	2.4±1.5	8.2±8.1	NA	NA

Quantification of survival, MRI, and histopathology. One sibling of each of five marmoset parts was immunized with MOG-containing myelin from WT mice, whereas the other was immunized with myelin from MOG^{-/-} mice. The DOK and the Y or N at the time of necropsy are indicated. Volumes of MR abnormalities in individual monkeys were calculated from the numbers of hyperintense pixels and are given in cubic millimeters. *The outlier monkey M02115 was excluded from this calculation. The severity of CNS inflammation and demyelination was quantitated on histologic analysis by the inflammatory index, that is, the average number of inflamed blood vessels per spinal cord section and the total percentage of demyelinated white matter area. Data for individual animals and group means are given. The presence of IgM or IgG deposits in the lesions (assessed as in²³) were expressed semiquantitatively (-, absent; ±, minor staining; +, moderate staining; ++, intense staining). The disease-free survival rate of monkeys immunized with MOG^{-/-} myelin differed significantly from that of monkeys immunized with WT myelin ($p = 0.0273$; not shown). The percentage demyelination area differed significantly between the WT myelin- and MOG^{-/-} myelin-immunized animals (paired t-test; $p = 0.01$). Differences between the two test groups were not statistically significant for the other parameters. DOK, day of killing; EAE, experimental autoimmune encephalomyelitis; Ig, immunoglobulin; MOG, myelin/oligodendrocyte glycoprotein; MRI, magnetic resonance imaging; N, absence of overt signs of EAE; NA, not applicable; SD, standard deviation; Y, presence of overt signs of EAE; WT, wild type.

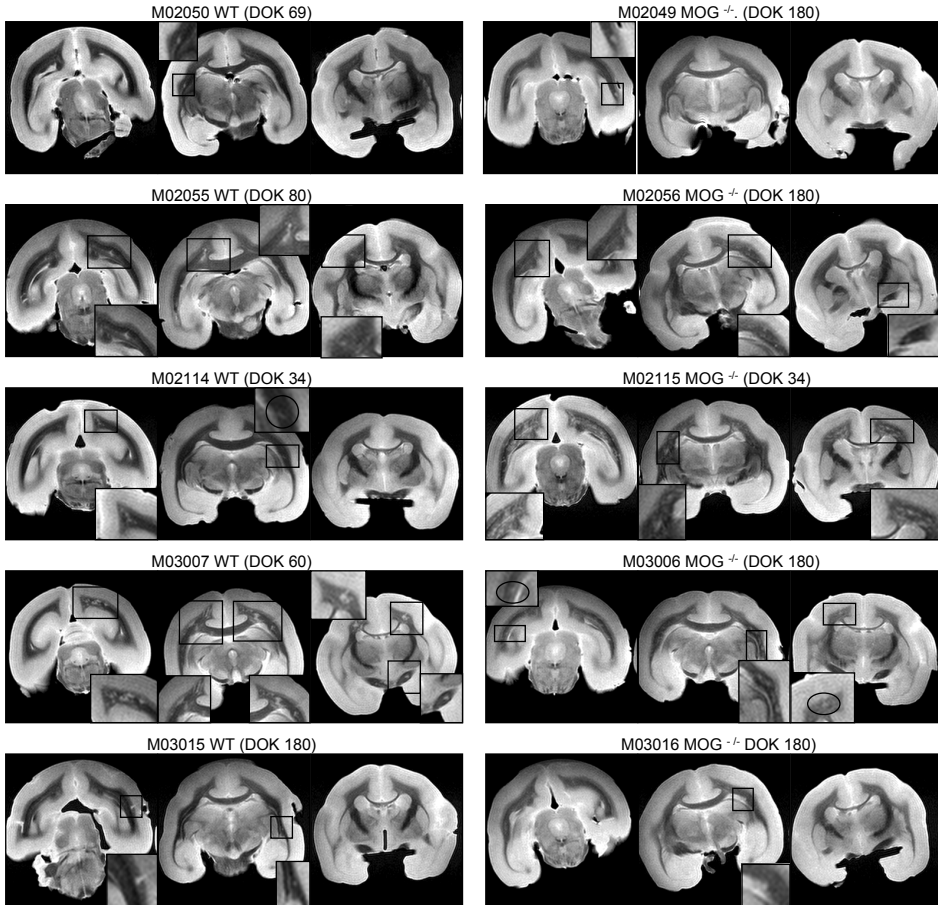


Figure 3. MRI-detectable abnormalities in formalin-fixed brains. The brains of monkeys immunized with myelin from wild type (left panels) and their twins immunized with myelin from MOG-deficient mice (right panels) were mildly fixed in buffered formalin, after which T2-weighted images were made to visualize EAE-related abnormalities. Three slices representative of the whole brain are shown for each monkey. The slices correspond to those indicated with arrows in Figure 2. The inserts are enlargements of the boxed areas.

Cellular responses

Serial venous blood samples were collected periodically for the isolation of PBMC to probe reactivity with WT and MOG^{-/-} myelin, rmMOG, rhMOG, hMBP, and the overlapping 23-mer MOG peptides. Furthermore, at necropsy, MNC suspensions were prepared from the spleen and the various lymph nodes. As observed in previous studies²⁴⁴, the distribution of autoreactive T cells within draining lymphoid tissues may vary during the progression of EAE; therefore, separate compartments were tested.

PBMC: In none of the monkeys was there significant (stimulation index >2) proliferation against the MOG peptides (not shown), but proliferation against WT myelin was present (Fig.

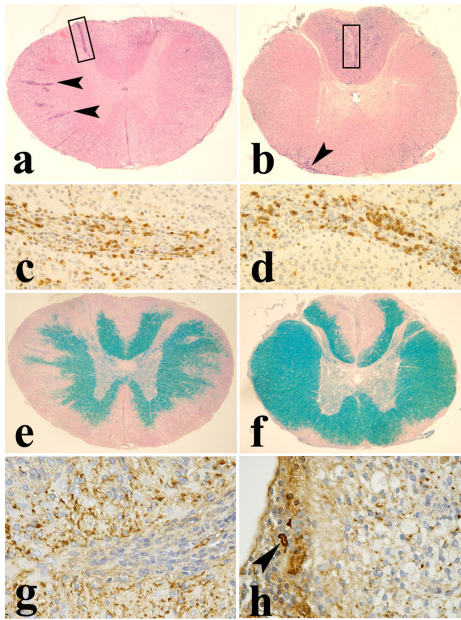
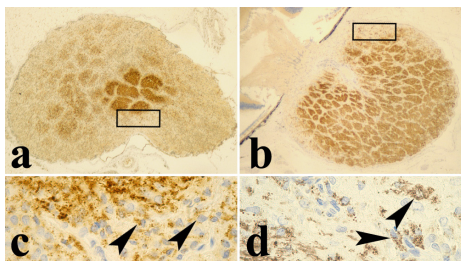


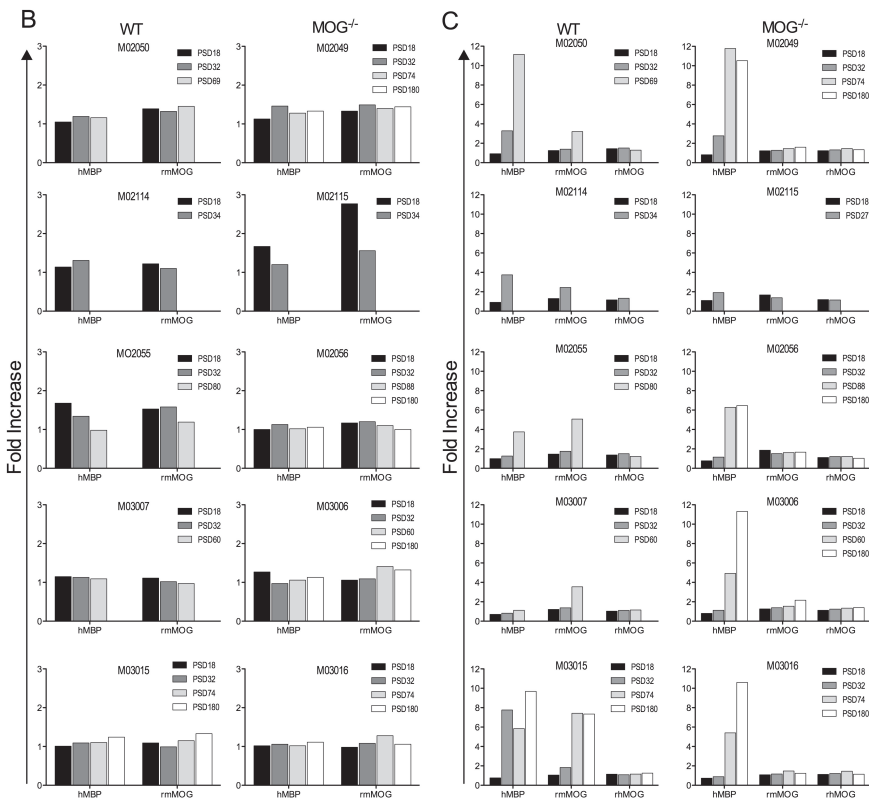
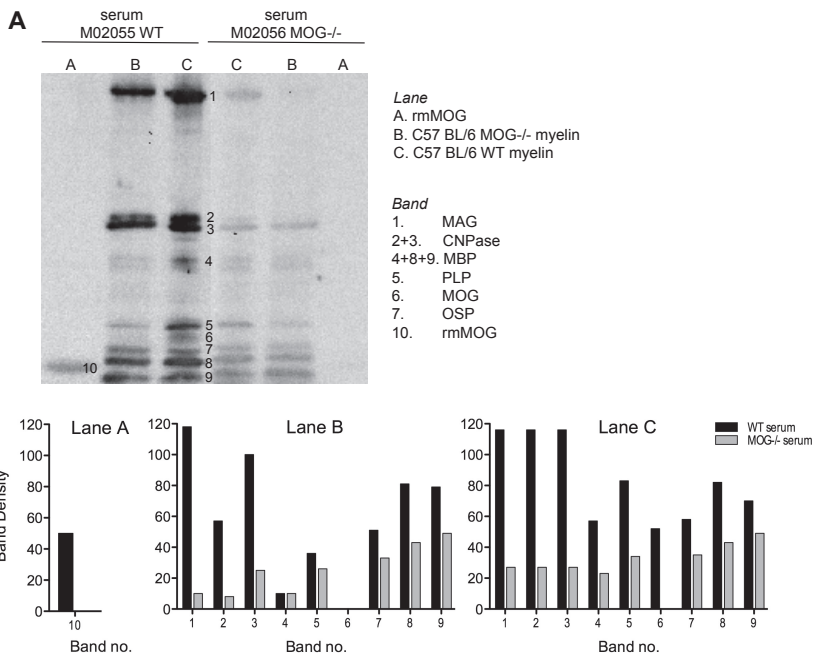
Figure 4. Inflammation, demyelination, and antibody staining in spinal cord. Spinal cord histology and immunohistochemistry of a representative twin pair of monkeys immunized for EAE with WT myelin (M03007; A, C, E, G) and MOG^{-/-} myelin (M03006; B, D, F, H; both x15), hematoxylin and eosin staining (A and B). Arrowheads indicate blood vessels with perivascular inflammation. The rectangles in (A and B) enclose the area of CD3 staining shown in (C and D), respectively. (C and D) (x120) show infiltration of CD3-positive T cells in the spinal cord in both monkeys. (E and F) (x15) show LFB/PAS stain of spinal cord sections adjacent to those in (A and B), respectively. Marked subpial demyelination affecting more than 50% of the white matter is evident in monkey M03007 (WT myelin immunized). In M03006, (MOG^{-/-} myelin immunized), demyelination is also present but is less marked. (G and H) (x210) show staining for IgM, detecting deposition of IgM antibodies in spinal cord lesions of the animals immunized with WT myelin (G) and the MOG^{-/-} myelin (H). The arrowhead in (H) indicates an IgM-positive plasma cell in the meninges.

Figure 5. Demyelination in optic nerve. Demyelination in the optic nerve of the twin pair M03007 and M03006 that had been immunized with WT myelin (A, C) or MOG^{-/-} myelin (B, D), respectively. (A and B) (x18) show PLP staining in the optic nerve close to the eye. (A) The optic nerve is almost completely demyelinated. The rectangle encloses the border of the demyelinated area that is shown enlarged in (C) (x240). (B) There is some demyelination in peripheral parts of the optic nerve, indicated by the rectangle and shown enlarged in (D) (x240). Arrowheads in (C) and (D) indicate macrophages with PLP degradation products in their cytoplasm.



7A). Proliferation levels were somewhat higher in siblings immunized with MOG^{-/-} myelin than in those immunized with WT myelin.

Lymph node and spleen MNCs: As was the case in PBMC, marked proliferative responses against the MOG peptides were not observed in spleen or lymph node MNCs (data not shown), but proliferative responses to MOG proteins, hMBP, and myelin were detected. The data in Figure 7B show that there is not a consistent and clear difference in proliferation in response to myelin or MOG between twin siblings. Remarkably, we observed in each twin similar response



levels against rmMOG and rhMOG in siblings immunized with WT or MOG^{-/-} myelin. We suspect that these responses are triggered by myelin-loaded antigen-presenting cells that drain from the CNS to the spleen²⁴⁶.

Cytokines

Various cytokines, that is, IL-2, IL-12, IL-13, tumor necrosis factor, and interferon- γ , were determined in culture supernatants of spleen and axillary lymph node cells stimulated with WT myelin or rmMOG. A high degree of variation of cytokine levels was observed, but no consistent differences were found between twin siblings immunized with WT MOG or MOG^{-/-} myelin (data not shown).

DISCUSSION

The experiments reported here were conducted in the EAE model in the common marmoset, a small neotropical primate species. EAE in the marmoset was first proposed as a non-human primate model for MS approximately a decade ago¹²⁶. In addition to its outbred nature, the marmoset has several immunologic similarities with humans. Of particular relevance to modeling of MS are similarities at the level of genes encoding the variable elements of T-cell receptors²⁰⁸ and Igs²¹¹, major histocompatibility complex class II molecules^{200, 206}, T-cell and antigen-presenting cells, costimulatory molecules, and cytokines²⁴⁷. Moreover, cross-reactivity of monoclonal antibodies against human CD markers with marmoset leukocytes has been demonstrated²¹⁶. The clinical and neuropathologic similarities between the marmoset EAE model and MS have also been previously reviewed^{228, 222}. There is an ongoing debate in the literature on the question whether patients presenting with clinically isolated symptoms, which are also seropositive for anti-MOG or anti-MBP antibodies, have an increased chance to develop clinically definite MS in later life²⁴⁸⁻²⁵⁰. The present results show that immunization of marmosets with MOG^{-/-} mouse myelin induces overt clinical EAE only in one of five monkeys. However, with MRI and with histology, abnormalities typical for EAE were detected in the brain and the spinal cord of the MOG^{-/-} immunized monkeys, in which only one monkey in this group resulted in overt clinical EAE. One abnormality observed in the one monkey that developed EAE was the presence of anti-MOG IgM antibodies, although it was immunized with MOG^{-/-} myelin. We conclude that antibodies against MOG are dispensable for the induction of early

◀ **Figure 6.** Serum antibody levels in marmosets immunized with WT myelin and MOG^{-/-} myelin. Immune sera collected at necropsy were tested for antibodies against WT myelin and MOG^{-/-} myelin by Western blotting (A). IgM and IgG antibodies against the myelin proteins rhMOG, rmMOG, and hMBP were measured with ELISA (B, C, respectively). Antibodies against whole myelin (A). Freshly isolated myelin from WT and MOG^{-/-} C57/BL6 mice (3 μ g loaded per lane) was fractionated by electrophoresis through a 4% to 12% Bis-Tris gel. In addition, rhMOG and rmMOG (both 4 μ g per lane) and molecular weight marker preparation were loaded on the gel. A gel from representative twin pair is shown in the upper portion. After fractionation, the gels were blotted with 200-fold diluted necropsy serum from all twin siblings. The densitograms show the reactivity of necropsy serum from monkeys immunized with MOG^{-/-} (gray bars) or WT myelin (black bars). IgM (B) and IgG (C) antibodies against myelin proteins. Sera were collected at the indicated time points. ELISA plates coated with rhMOG, rmMOG, or hMBP were incubated with plasma at 200-fold dilution for IgM and IgG. The results are given in arbitrary units (i.e. as fold increase compared with pre-immune sera).

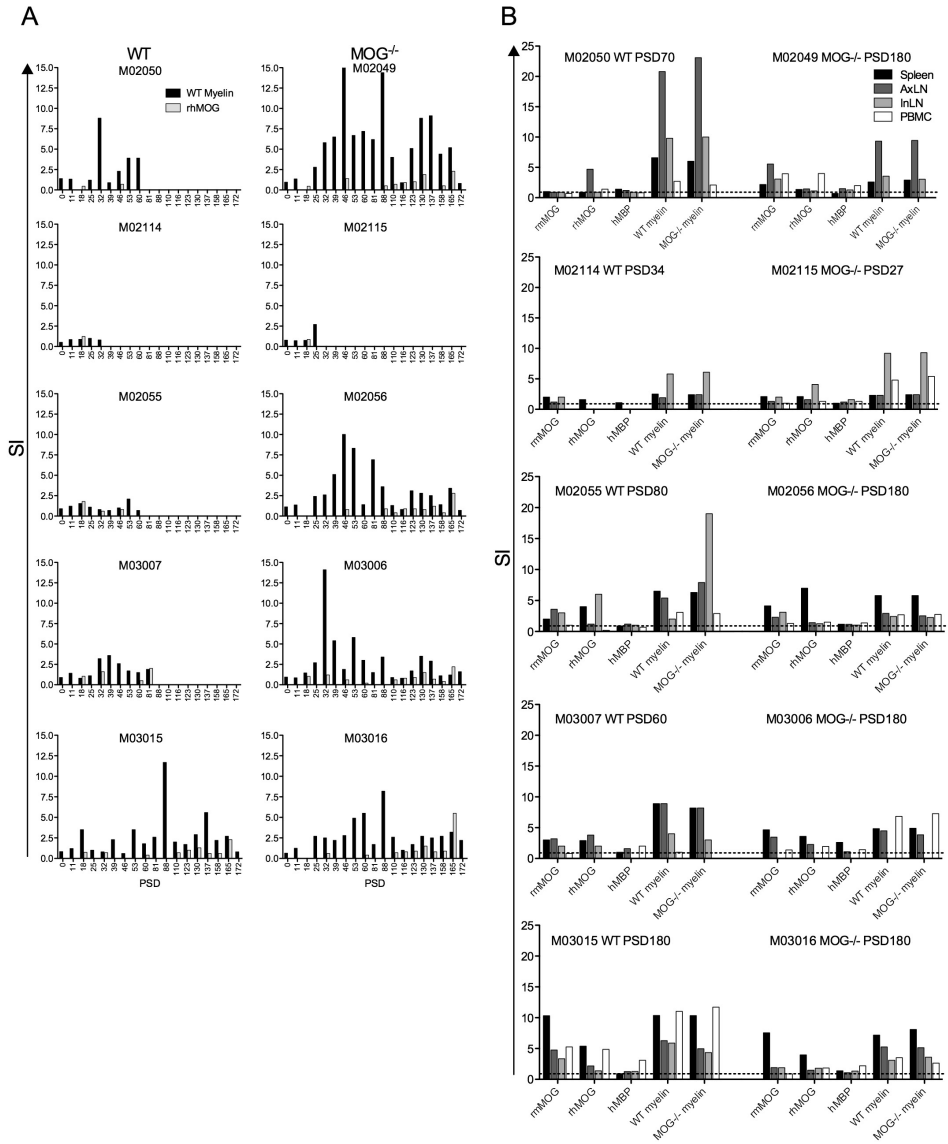


Figure 7. Proliferation of MNCs in peripheral blood and lymphoid organs. (A) Blood MNC responses to WT myelin and rhMOG. Venous blood samples of 1 ml were collected at the indicated PSDs incorporation of ³H-thymidine was determined as a measure of proliferation. Results are expressed as SI versus cultures without antigen. (B) Lymph node and spleen MNC responses against myelin and myelin proteins. At necropsy, the spleen and ALN and ILN were aseptically removed, and MNC suspensions were prepared. MNCs were cultured with WT myelin, MOG^{-/-} myelin, rhMOG, rmMOG, or hMBP, and proliferation was determined by the incorporation of ³H-thymidine during the final 18 h of 3 day cultures. Results are expressed as SI versus cultures without antigen. Only SI values above the dotted lines are considered relevant. PSD, post sensitization day; SI, stimulation index.

pathogenic mechanisms, but that they strongly impact the full development of overt clinical EAE. Essentially, similar results have been reported for the chronic relapsing EAE model in Biozzi ABH mice, that is, that mice immunized with MOG^{-/-} myelin display a short episode of neurologic deficit and CNS inflammation but lack the subsequent relapses typically found in mice immunized with WT myelin⁹³.

The maximum blood volume that can be obtained from an adult marmoset each month without harming the monkey's health is 1% of the body weight (i.e. 3.5-4 ml). Because of this, and the fact that blood samples cannot be pooled in this outbred model because each animal must be regarded as unique, extensive longitudinal immunologic testing is not feasible. We therefore tested PBMC only for reactivity with WT myelin and at some time points also against rhMOG. Comparison between PBMC of twin siblings showed that in four twin pairs (i.e. other than M03015/M03016), the proliferative responses against WT myelin were higher in siblings immunized with MOG^{-/-} myelin than in the twin immunized with WT myelin. By contrast, we observed that in most twin pairs (i.e. other than M02114/M02115), MNCs from lymphoid organs of WT myelin immunized monkeys showed a higher proliferative response against the myelin preparations and with the myelin proteins rhMOG, rmMOG, and hMBP. These data indicate that opposite results can be obtained depending on the analyzed compartment.

Mononuclear cell reactivity with MOG peptides was not observed in any monkeys, although such responses are normally present in monkeys immunized with 100 µg rhMOG¹⁰³, that is, the amount estimated to be present in 3 mg of myelin inoculum used for EAE induction⁹³. We previously proposed that the full-length MOG in its natural glycosylated conformation as present in the myelin inoculums may dampen T-cell epitope spreading²⁵¹. This yin and yang paradigm postulates that (self-)glycoproteins inhibit the capacity of dendritic cells (DC) to activate autoreactive T-cells by binding to certain C-type lectin receptors (CLRs) via their glycan epitopes. Support for this hypothesis comes from the observation that mice can be rendered tolerant to EAE by targeting of the immunizing antigen to the CLR DEC-205²⁵². Preliminary experiments show that the binding of mouse myelin to DC-SIGN, a CLR expressed on primate DC, is mediated via MOG (unpublished observation). Moreover, ligands of the CLR DC-SIGN such as ManLam from mycobacteria antagonize DC maturation and IL-12p40 production²⁵³. Thus, myelin binding to DC-SIGN may reduce the capacity of DC to induce the auto aggressive T-cells that drive the progression of EAE. The observation that B-cell activation occurs (relatively) independent of Toll-like receptor activation²⁵⁴ may explain that autoantibody production was not inhibited. Our data show that development of overt clinical EAE is associated with seropositivity for anti-MOG antibodies. The observation that demyelination is less severe in monkeys immunized with MOG^{-/-} myelin is consistent with the previous observation in the marmoset EAE model that passively transferred anti-MOG antibodies amplify demyelination¹³⁶.

Our data clearly show, however, that in monkeys immunized with MOG^{-/-} myelin, significant demyelination can take place. Therefore, we conclude that demyelination is not absolutely dependent on anti-MOG antibodies. The remarkable finding that anti-MOG IgM antibodies were present in monkey M02115, although this monkey had been immunized with MOG^{-/-} myelin, also has a precedent in the literature. McFarland et al²⁵⁵ reported that anti-MOG antibodies are occasionally induced in marmosets immunized with the MBP/PLP chimeric protein MP4, and that EAE developed only in the monkeys in which anti-MOG antibodies had been formed.

In conclusion, the current data obtained in marmosets together with previously reported data in the Biozzi ABH mouse illustrate that autoimmunity against MOG, although it is a quantitatively minor component of CNS myelin, plays a prominent role in the development of chronic EAE. These data support the concept that seropositivity for anti-MOG antibodies is a significant risk factor for chronic encephalomyelitis. We tend to agree with Gaertner et al²⁵⁶, however, that serologic assays tailored to the detection of antibodies against glycosylation variants of MOG may be more informative for MS than those detecting only the nonglycosylated (recombinant) protein.

ACKNOWLEDGEMENTS

The authors thank Fred Batenburg for superb biotechnical support, Drs. Jaco Bakker and Gerco Braskamp for veterinary care, and Dr. Rogier Hintzen (Erasmus Medical Center Rotterdam) for critical reading of the article.

**FAST PROGRESSION OF RECOMBINANT HUMAN
MYELIN/OLIGODENDROCYTE GLYCOPROTEIN
(MOG)-INDUCED EXPERIMENTAL AUTOIMMUNE
ENCEPHALOMYELITIS IN MARMOSETS IS
ASSOCIATED WITH THE ACTIVATION OF
MOG34-56-SPECIFIC CYTOTOXIC T-CELLS**

Yolanda S. Kap*, Paul Smith*, S. Anwar Jagessar*, Ed Remarque,
Erwin Blezer, Gustav J. Strijkers, Jon D. Laman, Rogier Q. Hintzen,
Jan Bauer, Herbert P.M. Brok# and Bert A. 't Hart#

* Shared first authorship, # Shared senior authorship

J Immunol 180, 1326-37 (2008)

ABSTRACT

The recombinant human (rh) myelin oligodendrocyte glycoprotein (MOG)-induced experimental autoimmune encephalomyelitis (EAE) model in the common marmoset is characterized by 100% disease incidence, a chronic disease course, and a variable time interval between immunization and neurological impairment. We investigated whether monkeys with fast and slow disease progression display different anti-MOG T- or B-cell responses and analyzed the underlying pathogenic mechanism(s). The results show that fast progressor monkeys display a significantly wider specificity diversification of anti-MOG T-cells at necropsy than slow progressors, especially against MOG34-56 and MOG74-96. MOG34-56 emerged as a critical encephalitogenic peptide, inducing severe neurological disease and multiple lesions with inflammation, demyelination, and axonal injury in the central nervous system (CNS). Although EAE was not observed in MOG74-96-immunized monkeys, weak T-cell responses against MOG34-56 and low grade CNS pathology were detected. When these cases received a booster immunization with MOG34-56 in incomplete Freund's adjuvant (IFA), full-blown EAE developed. MOG34-56-reactive T-cells expressed CD3, CD4 or CD8, and CD56, but not CD16. Moreover, MOG34-56-specific T-cell lines displayed specific cytotoxic activity against peptide-pulsed B-cell lines. The phenotype and cytotoxic activity suggest that these cells are natural killer-cytotoxic T lymphocytes (NK-CTL). These results support the concept that cytotoxic cells may play a role in the pathogenesis of multiple sclerosis.

INTRODUCTION

Multiple sclerosis (MS) is a chronic progressive inflammatory demyelinating disease of the human central nervous system (CNS). The pathological hallmark of MS is the lesion, being in the majority of cases a sharply demarcated demyelinated area in the CNS white matter (WM) that expresses a variable degree of inflammation, axonal injury, gliosis and remyelination^{2, 4}. Although the trigger of MS is not known, it is generally believed that lesion formation involves the synergistic action of cellular and humoral autoimmune reactions directed against components of the myelin sheath²⁵⁷. Anti-myelin autoimmune reactions may be induced by viruses that share cross-reactive T- and B-cell epitopes with myelin antigen (Ag), a phenomenon known as molecular mimicry²⁵⁸.

In response to the requirement for a useful preclinical model for the efficacy evaluation of new biopharmaceutical agents for the treatment of MS, we have developed a chronic progressive experimental autoimmune encephalomyelitis (EAE) model in the New World primate species, the common marmoset (*Callithrix jacchus*). This EAE model has several intriguing aspects that makes it also a highly useful disease model for basic research, including the 100% incidence despite the outbred nature, the chronic progressive course (reviewed in^{228, 259}), and the heterogeneous pathology present in white matter (WM) and grey matter (GM) that ranges from early active to chronic inactive/remyelinating lesions^{228, 260, 261}. Moreover, using serially applied magnetic resonance imaging (MRI) sequences, brain lesions can be visualized and characterized in relation to the expression of an overt neurological deficit^{222, 241, 262}.

Several lines of evidence point to a critical role of autoimmune reactions directed against myelin oligodendrocyte glycoprotein (MOG) in the induction of chronic progressive EAE. Marmosets immunized with a chimeric protein combining myelin basic protein (MBP) and proteolipid protein (PLP) developed clinical EAE only after the spreading of the autoimmune reaction to MOG has taken place²⁵⁵. Moreover, the development of chronic progressive EAE in both Biozzi ABH mice⁹³ and marmosets²⁶³ is impaired when the animals were immunized with MOG-deficient mouse myelin.

The marmoset EAE model induced with recombinant human (rh) MOG1-125 (rhMOG) is characterized by a 100% disease incidence but variable clinical course. The high susceptibility of marmosets to this model maps to an invariant major histocompatibility complex (MHC) class II molecule, Cja-DRB*W1201, which emerged as a dominant restriction element for the activation of CD4+ T-cells specific for the epitope MOG24-36¹⁰³. The monomorphic allele is present and expressed in each monkey^{200, 206}. Independently from us, Villoslada et al. showed by adoptive transfer that MOG24-36-reactive T-cells induce mild inflammatory CNS pathology²³³.

The aim of the current study was to analyze autoimmune mechanisms underlying the variable clinical course. Hence, we investigated whether the rate of disease progression in the rhMOG-induced EAE model is associated with particular anti-MOG T- or B-cell response patterns. Furthermore, we examined the phenotype and function of T-cells involved in the induction of neurological impairment. We found that fast progressor monkeys displayed a broad T-cell repertoire with responses to epitopes encompassed within MOG34-56 and/or MOG74-96. Marmosets immunized with MOG34-56 in complete Freund's adjuvant (CFA) developed CNS inflammation and widespread demyelination in the WM and GM, which may be caused by cytotoxic activity of infiltrated T-cells. In support of this, MOG34-56-specific T-cell lines (TCL) were found to express markers of natural killer-cytotoxic T lymphocytes (NK-CTL)

(CD3+, CD4+ or CD8+, CD56+, and CD16-) and to lyse peptide-pulsed, autologous as well as allogeneic EBV-transformed B-cell lines.

MATERIALS AND METHODS

Animals

All monkeys included in the current study were purchased from two purpose-bred colonies, one being kept at the Biomedical Primate Research Centre (Rijswijk, The Netherlands) and the second at the German Primate Center (Göttingen, Germany). Individual data of all monkeys used in this study are listed in Table 1. Monkeys were included in the study only after a complete physical, hematological, and biochemical check-up had been performed. The reported experiments span a period of about six years. During the experiments, the monkeys were initially housed individually in spacious cages with padded shelter provided on the floor and were under intensive veterinary care. Since 2005, pair housing became the standard within the BPRC. The daily diet during the study consisted of commercial food pellets for New World monkeys (Special Diet Services, Witham, Essex, UK), supplemented with rice, raisins, peanuts, marshmallows, biscuits, fresh fruit, grasshoppers, and maggots. Drinking water was provided ad libitum.

Ethics

In accordance with the Dutch law on animal experimentation, all study protocols and experimental procedures were reviewed and approved by the Institute's Ethics Committee before the experiments could be started.

rhMOG-induced EAE

A recombinant protein encompassing the extracellular domain of human MOG (rhMOG) was produced in *Escherichia coli* and purified as previously described¹³⁸. rhMOG-induced EAE was evoked in a total of 23 monkeys by injection into the dorsal skin of 600 µl stable emulsion containing 100 µg of rhMOG in 300 µl of buffered saline and 300 µl of CFA (Difco Laboratories, Detroit, MI) under ketamine anesthesia (40 mg/kg; AST Pharma, Oudewater, The Netherlands) as described previously¹⁰³.

MOG peptide-induced EAE

All MOG peptides for immunization and cell culture were purchased from prof. A. Ben Nun (Weizmann Institute of Sciences, Rehovot, Israel) or from ABC Biotechnology (London, UK). EAE was induced with synthetic peptides that represent amino acids 34 to 56 (MOG34-56) and 74 to 96 (MOG74-96) of the human MOG extracellular domain. The monkeys were immunized with 100 µg of MOG peptide dissolved in 300 µl of buffered saline and 300 µl of CFA as previously described¹⁰³. Monkeys that did not develop overt neurological deficit (score \geq 2.0) within 28 days received booster immunizations with the same amount of peptide in incomplete Freund's adjuvant (IFA) at time points indicated in figure 2 and 6. Ag-adjuvant emulsion was prepared by gentle stirring of the PBS/oil mixture at 4°C for at least 1 h.

Table 1. Overview of monkeys included in this study.

Monkey	Twin pair ^a	Sex ^b	Age ^c	Immunization	Experiment
KK		M	32	rhMOG	
QI		M	31	rhMOG	
QK		M	25	rhMOG	
QR		F	29	rhMOG	
QQ		M	28	rhMOG	
Mi-009		M	26	rhMOG	
Mi-010		M	26	rhMOG	
Mi-011		M	26	rhMOG	
Mi-020		M	28	rhMOG	
Mi-021		M	30	rhMOG	
Mi-022		M	48	rhMOG	
Mi-062		M	24	rhMOG	
Mi-065		M	23	rhMOG	
Mi-069		M	20	rhMOG	
9501		M	35	rhMOG	
9505		M	54	rhMOG	
9601		M	25	rhMOG	
9814		M	15	rhMOG	
9819		M	15	rhMOG	
9841		M	21	rhMOG	
9853		F	22	rhMOG	
9854		M	22	rhMOG	
M9902		M	20	rhMOG	
M0131		M	24	MOG34-56	1
M0167		M	20	MOG34-56	1
M0178		M	20	MOG34-56	1
M0182		M	19	MOG34-56	1
M02075	Twin	M	22	MOG34-56	2
M02076	Twin	M	22	MOG74-96	2,A
M02078	Twin	M	23	MOG34-56	2
M02079	Twin	M	23	MOG74-96	2,A
M02087	Twin	M	22	MOG74-96	2,A

Table 1. Overview of monkeys included in this study.

Monkey	Twin pair ^a	Sex ^b	Age ^c	Immunization	Experiment
M02088	Twin	M	22	MOG34-56	2
M02120	Twin	M	21	MOG34-56	2
M02121	Twin	M	21	MOG74-96	2,A
M03017	Twin	M	37	MOG34-56	3
M03018	Twin	M	37	MOG74-96 + MOG34-56	3,B
M03026	Twin	M	37	MOG34-56	3
M03027	Twin	M	37	MOG74-96 + MOG34-56	3,B
M03032	Twin	M	37	MOG34-56	3
M03033	Twin	M	37	MOG74-96 + MOG34-56	3,B

^aTwin pairs are indicated by 'Twin'

^bM, Male; F, Female.

^cAge in months of the monkeys at the start of the experiment

Clinical scoring

Clinical signs were scored twice daily by trained observers using a previously described semiquantitative scale²⁷. Briefly, 0 = no clinical signs; 0.5 = apathy, loss of appetite, altered walking pattern without ataxia; 1 = lethargy, anorexia, tail paralysis, tremor; 2 = ataxia, optic disease; 2.5 = para- or monoparesis, sensory loss, brain stem syndrome; 3 = para- or hemiplegia; 4 = quadriplegia; and 5 = spontaneous death attributable to EAE. A score of 2 or higher reflects an overt neurological deficit. Monkeys were sacrificed for ethical reasons once complete paralysis of hind limbs (score \geq 3.0) was observed or at the predetermined endpoint of the study. Moreover, monkeys were weighed three times per week. As in rodent EAE models, body weight serves as a reliable surrogate disease marker in the marmoset. Body weight data are depicted as a separate disease parameter above the clinical score graphs.

Ex vivo analysis of T-cell responses

The maximum blood sample that can be collected in a month from primates at the BPRC should not exceed 1% of the body weight. For an average adult marmoset weighing 350 grams, this equals a maximum monthly blood sample of 3.5 ml. Hence, volumes of up to 1.5 ml at 2-weeks interval were collected into heparinized Vacutainer tubes (Greiner, Sölingen, Germany). Peripheral blood mononuclear cells (PBMC) were isolated from heparinized venous blood using lymphocyte separation medium (LSM[®], ICN Biomedical Inc., Aurora, OH). Moreover, cell suspensions were prepared from aseptically removed axillary (ALN), inguinal (ILN), and cervical

(CLN) lymph nodes and spleen. PBMC, lymph node, and spleen cells were cultured in triplicate for the detection of proliferative responses towards rhMOG and a panel of MOG peptides as previously described¹⁰³. In some assays, PLP peptide 139-151 (PLP139-151), recombinant human MBP, and recombinant human α B-crystallin (both provided by Dr. J.M. van Noort, TNO-Preventie en Gezondheid, Leiden, The Netherlands) were included. OVA served as control Ag in all studies. All Ag were tested at 5 μ g/ml. After 48 h of culture, 0.5 μ Ci of tritiated thymidine ($[^3\text{H}]\text{Thy}$) was added per well, and incorporation of the radiolabel was determined after 18 h using a matrix 9600 beta-counter (Packard 9600; Packard Instrument Company, Meriden, CT). Results are expressed as the mean stimulation index (SI). SI values above 2.0 were considered to be relevant.

Flow cytometry and CFSE labeling

To determine the phenotype of proliferating cells, 4×10^6 viable mononuclear cells (MNC) from ALN were suspended in 1 ml PBS and incubated for 7 min at room temperature with carboxyfluorescein diacetate succinimidyl ester (CFSE, final concentration 1.5 μ M; Fluka, Deisenhofen, Germany). The labeled cells were cultured for 7 days with peptides under the standard conditions described above. For flow cytometric analysis we used the following commercially available, labeled monoclonal antibodies (mAb) directed against human CD markers: anti-CD3 with PerCP or Alexa Fluor 700 label (BD Biosciences), APC-labeled anti-CD4 (DAKO, Glostrup, Denmark), biotinylated anti-CD8 (Serotec, Düsseldorf, Germany), anti-CD56 with PE-Cy7 label, anti-CD16-PE, and streptavidin PE-Cy7 or streptavidin PerCP (BD Biosciences). Flow cytometric analysis was performed on a FACSort flow cytometer using FACSDiva software (BD Biosciences). First, viable cells were gated using the live/dead fixable violet viability stain (Invitrogen, Molecular Probes, Carlsbad, CA). Within the viable cell gate, lymphocytes/monocytes were selected using forward and side scatter. Within the lymphocyte/monocyte gate CD3⁺ cells were selected. The CD3⁺ population in the CFSE experiment consisted of CD4⁺ cells (48-70%) and CD8⁺ cells (12-18%). Within each gated subpopulation the percentage of cells with CFSE dilution was calculated.

Cytotoxicity assay

Autologous and allogeneic peptide-pulsed $^{51}\text{chromium}$ -labeled, Epstein-Barr virus (EBV)-transformed B-cell lines were used as target cells to test the cytotoxic potential of MOG peptide-specific TCL. In brief, 10^6 B-cells were incubated for 60 min at 37°C with $^{51}\text{chromium}$ and pulsed with 100 μ g MOG34-56 or MOG74-96 and subsequently washed thoroughly with PBS. Peptide pulsed B-cells were mixed with effector T-cells at 1:1, 1:4, and 1:16 ratio in U-well microtiter plates and cultured for 5 h at 37°C in culture medium, after which 100 μ l of the supernatant was collected to determine the amount of radiolabel in a gamma-counter. Controls consisted of peptide-pulsed target cells without T-cells (spontaneous release) or peptide-pulsed target cells lysed with 1% Triton X-100 (maximum release). Results are expressed as % killing using the formula: $(\text{T-cell induced} - \text{spontaneous}) / (\text{maximal} - \text{spontaneous}) \times 100$.

Generation of MOG peptide-reactive T-cell lines

At necropsy, cell suspensions were prepared from spleen, ALN, ILN, and CLN. MNC of rhMOG- or MOG peptide-immunized marmosets were stimulated *ex vivo* with rhMOG, MOG34-56, or

MOG74-96 to establish specific TCL. Briefly, MNC (10^6 /well) were seeded into 24-well plates (Greiner) and stimulated with 10 μ g/ml rhMOG, MOG34-56, or MOG74-96. Every 2 or 3 days, half of the culture supernatant was replaced with fresh medium containing 20 U/ml rh interleukin (IL)-2 (Proleukin, Chiron Corporation, Emeryville, CA) and split when needed. After 14 to 21 days of culture, part of the cells were transferred into 96-well flat-bottom plates (Greiner) and tested for reactivity with a panel of 23-mer MOG peptides¹⁰³. Lethally irradiated (50 gray) EBV-transformed marmoset B-cells from stably growing lines maintained in 75-cm² tissue culture flasks (Greiner) were used as antigen presenting cell (APC). Lines of interest were characterized by the expression of T-cell specific cell surface markers by flow cytometry using cross-reactive mAb raised against human CD markers²¹⁶. Isotype controls were kindly provided by J. Miller (Chemicon International, South Hampton, UK).

B-cell responses

Venous blood samples were centrifuged and the plasma supernatants were collected and stored frozen at -20°C until further analysis. Ab binding to myelin proteins (rhMOG, MBP, α B-crystallin, and HPLC-purified human PLP) or to a panel of overlapping 23-mer MOG peptide sequences was determined using ELISA²⁶⁴. Bound Ab was detected using polyclonal alkaline phosphatase-conjugated goat-anti-monkey IgM μ -chain (Rockland, Gilbertsville, PA) or rabbit-anti-human IgG (Abcam, Cambridge, UK). Ab specific for discontinuous MOG epitopes are considered particularly pathogenic²⁶⁵. To distinguish between Ab reactivity against discontinuous and linear epitopes, serum samples were preincubated with a mixture of all overlapping MOG peptides (10 μ g/ml for each peptide) for 1 h at 37°C before probing them for reactivity with rhMOG coated onto ELISA plates. As an internal control, the MOG54-76 peptide was left out of the peptide mix used for preincubation because in previous studies this peptide was found to contain dominant B-cell epitopes. The results of the Ab assays are expressed as the fold increase of light absorbance at 405 nm compared with the reactivity with OVA as an irrelevant antigen or compared to the reactivity in preimmune sera of the same monkeys.

Post mortem examination

Monkeys selected for necropsy were first deeply sedated by intramuscular injection of ketamine (50 mg/kg), and subsequently euthanised by the infusion of pento-barbital sodium (Euthesate®; Apharmo, Duiven, The Netherlands). Brain, spinal cord, spleen, ILN, ALN, and CLN were removed. Representative parts of all organs were snap frozen in liquid nitrogen or fixed in 4% buffered formalin. Frozen tissues were stored at -80°C. After at least 7 days of fixation in formalin, the tissues were transferred into buffered saline containing sodium azide for stabilization before MRI²⁴¹.

To assess the total lesion load in the brain, MR images were made of formalin-fixed brains as described previously^{127, 241}. Both frozen and fixed tissues were examined with histological and immunohistochemical techniques as previously described^{127, 243, 266}.

MRI procedures

Brains of MOG34-56- and MOG74-96-immunized animals were analyzed by MRI. MRI experiments were performed post mortem on a 6.3 T horizontal bore MRI scanner (Varian, Palo Alto, USA). The formalin-fixed brains were submerged in a perfluoropolyether (Fomblin, Ausimont, NJ) for

susceptibility matching. The following parameters were used in all experiments: field of view, 2.5×2.5 cm²; matrix, 128×128; slice thickness, 1 mm; number of slices, 20. T2-weighted (T2W) images were collected using a spin-echo sequence with the following parameters: repetition time, 4 s; echo time, 35 ms; number of signal averages, 8. T2-maps were recorded with a multiecho sequence using the following parameters: repetition time, 8 s; echo spacing, 20 ms; echo train length, 8; number of signal averages, 4. Diffusion tensor images were made using a pulsed field gradient spin echo sequence with the following parameters: repetition time, 4 s; echo time, 35 ms; number of signal averages, 8. Diffusion weighting was applied in 10 directions with the following pulsed field gradient parameters: Δ , 20 ms; δ , 10 ms; diffusion gradient (G_{diff}), 0; and 120 millitesla/meter (mT/m), resulting in b-value of 0 and 1717 s/mm².

Image analysis

First, WM was segmented manually. In the WM, lesions were identified as regions with a T2 value 10% above the normal appearing white matter (NAWM). Average T2, apparent diffusion coefficient, and fractional anisotropy values were determined for lesions and NAWM. Image analysis was done using Mathematica (Wolfram Research Europe Ltd, Oxfordshire, UK).

Statistics

The relation between a broad T-cell response and fast disease progression (see data in Table 2) was analyzed using Kaplan-Meier survival analysis. Statistical significance of differences between groups was calculated using the log rank test. Because four potential contrasts could be chosen for this analysis, *p* values were considered statistically significant when $< 0.05/4 = 0.0125$ (Bonferroni correction).

Results of T2 relaxation time, fractional anisotropy, and apparent diffusion coefficient were analyzed by a two population (independent) *t* test.

RESULTS

Disease course and autoimmune reactions in rhMOG-immunized monkeys

Table 2 gives a summary of data obtained from 23 rhMOG-immunized marmosets. Clinical scores are depicted in Figure 1 showing that in 100% of the monkeys clinical EAE was induced but that the time interval between EAE induction and the expression of an overt neurological deficit varied considerably. Of the 23 examined monkeys, 20 were sacrificed after they had developed an EAE score ≥ 2 . Three monkeys were withdrawn from their respective experiments without neurological impairment. One monkey (QK) had experienced serious body weight loss and was sacrificed pre-term to avoid a sudden deterioration of the clinical state, as has been observed in rhesus monkeys in which immunization with MOG34-56 induced acute onset EAE¹⁸⁹. Two monkeys (Mi020 and Mi021) were sacrificed with mild signs of EAE (score 0.5) as they reached the end of the experiment. The time interval between EAE induction and the development of hemiplegia/paraplegia (EAE score of 3) varied from 34 to 139 days (mean 73 days) (Table 2). Notably, serial MRI in selected monkeys reveals ample disease activity within the CNS WM during the asymptomatic interval, which apparently does not lead to an overt neurological deficit^{222, 267}. We have taken advantage of this unique outbred model to test whether monkeys with a fast or slow disease progression rate display different Ab and T-cell response patterns.

Table 2. T-cell and antibody responses against rhMOG and MOG peptides in rhMOG-immunized marmosets.

Monkey	Sex ^a	Sacrificed (psd)	EAE score	T-cell reactivity (MOG peptides) ^b			Ab reactivity		
							rhMOG	pMOG ^d	
QQ	M	34	3	24-36	54-76	74-96	+	0	
Mi-022	M	36	5	24-36	64-86		+	0	
KK	M	38	3	24-36	34-50	94-110	+	7	
QR	F	42	3	24-36	34-50	64-86	+	5	
M9902	M	44	3.5	24-36	94-110		+	6	
QI	M	50	2	24-36			+	6	
9601	M	58	3	24-36	4-11	12-21	24-46	+	8
Mi-011	M	62	3	24-36	4-11	34-50		+	1
9854	M	67	2.5	24-36	54-76	74-96		+	3
9853	F	67	3	24-36				+	3
Mi-069	M	67	2.5	24-36	54-76			+	7
Mi-065	M	67	2.5	24-36				+	7
9501	M	70	3	24-36				+	8
9814	M	78	2.5	24-36				+	1
9819	M	94	3	24-36				+	5
Mi-010	M	106	3	24-36				NT ^e	
Mi-009	M	112	2.5	24-36				NT ^e	
9841	M	112	2	24-36				+	1
9505	M	115	3	24-36	64-86			+	1
Mi-062	M	139	3	24-36				+	7
Mean (n=23)		73							
QK ^f	M	50	0.5	24-36				+	6
Mi-020 ^f	M	155	0	24-36				+	5
Mi-021 ^f	M	163	0.5	24-36	74-96			+	8

^a M, Male; F, Female^b MOG peptides of interest are indicated in bold^c Antibody reactivity was tested in necropsy serum^d For the serum reactivity with MOG peptides only the number of recognized peptides is given.^e NT, not tested^f Marmosets with positive MRI, no or mild clinical EAE

Antibodies

Serum reactivity with rhMOG protein was detected in all monkeys (Table 2). The anti-MOG IgG Ab reactivity was directed against linear epitopes within three main regions, namely MOG4-26, MOG24-46, and MOG54-76. Analysis of immune sera that were collected at two

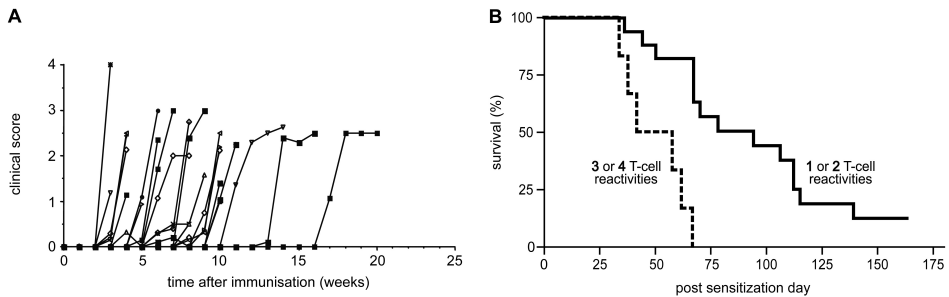


Figure 1. Association of disease progression with T-cell reactivity diversification in rhMOG-induced EAE. A, The EAE course of 23 unrelated monkeys (Table 1) that received a single immunization with 100 μ g rhMOG in CFA is shown. Note that the disease incidence is 100% but that the time interval between EAE induction and the expression of an overt neurological deficit varies clearly between individual monkeys. B, Kaplan-Meier plot shows survival curves of monkeys with a narrow (one or two peptides recognized) or broad (three or four peptides recognized) T-cell epitope diversification. The difference between both groups is highly significant ($p < 0.001$; log rank test).

week intervals during the entire disease course revealed that the first upcoming Ab reactivity was against MOG54-76. The anti-rhMOG Ab reactivity at necropsy was reduced by >95% when the immune sera were preincubated with a mix of the complete MOG peptide panel before the binding to rhMOG-coated ELISA plates was tested. However, when MOG54-76 was left out of the peptide mix the reduction of serum reactivity with rhMOG was <10% (data not shown). These data indicate that the MOG54-76 peptide contains one or more important recognition sites for rhMOG-induced Ab. Ab reactivities towards MBP and α B-crystallin were infrequently observed (data not shown). In summary, we observed no obvious association between disease progression and the number of MOG peptides recognized by IgG molecules present in necropsy sera (Table 2).

T-cell responses

rhMOG-induced TCL generated from ILN, ALN, or spleen of slow and fast disease progressors were tested for reactivity with a panel of MOG peptides. In accordance with previously published data¹⁰³ a proliferative response against the peptide MOG24-36 was found in all monkeys (Table 2). Besides this ubiquitous reactivity with MOG24-36, individual monkeys displayed a variable reactivity with other MOG peptides. When the monkeys were ranked according to the total disease duration, it was evident that fast progressor monkeys displayed a broader T-cell reactivity with the MOG peptide panel than slow progressor monkeys (Table 2). The relation between a broader T-cell response with faster disease progression is highly significant (Figure 1; $p < 0.0125$).

Characterization of potentially encephalitogenic MOG peptides

To determine the contribution of individual MOG peptide-specific T-cell reactivities to the EAE pathogenesis in marmosets, we have taken advantage of a unique biological feature of this model. Marmoset twins develop *in utero* as stable bone marrow chimeras due to the shared placental blood stream¹⁹². This implies that the T-cells of both twins are educated in the same

thymic environment and that similar mixed populations of bone marrow-derived elements are seeded into the peripheral tissues and organs of both siblings. Hence, despite the different genetic background, such nonidentical twin siblings can be regarded as immunologically similar.

Of the three peptides that were most frequently recognized by T-cells from fast progressor monkeys, MOG34-56, MOG54-76, and MOG76-96 (Table 2), we chose MOG34-56 and MOG76-96 for the immunization of chimeric twins. Because we were mainly interested in T-cell responses, MOG54-76 was not included for further analyses because this peptide is also a B-cell epitope (see above).

MOG34-56-induced EAE

A total of 11 monkeys were immunized in three separate experiments with MOG34-56/CFA followed by booster immunizations on post sensitization days (psd) 28, 56, and around 125 with MOG34-56/IFA until overt clinical signs of EAE were detectable. The individual EAE scores depicted in figure 2 show a heterogeneous clinical picture. One monkey (M0167) developed EAE associated with marked weight loss within 30 days after EAE induction. In two monkeys (M0182 and M03017) EAE developed only after psd 145 and one monkey (M02075) was sacrificed at psd 200 with only mild symptoms (score 0.5). In the remaining 7 monkeys, overt neurological deficits were first observed around psd 75. Interestingly, in three monkeys (M0178, M03026, and M03032) we observed optic neuritis, which remitted spontaneously within two weeks.

T2W MR images were made of the formalin-fixed brains of all monkeys to visualize the spatial distribution and size of lesions. Contrast in T2W images is mainly based on differences in water content caused, for example, by inflammation. Hence, altered signal intensity in the *in vivo* T2W images of a tissue mainly reflects inflammation. However, T2W images of formalin-fixed tissues, can also be used to assess the extent of myelin destruction²⁴¹. In figure 3 the post mortem brain MR images of four twins (Table 1; Experiment 2) are depicted, illustrating that significant lesion formation has taken place in the MOG34-56-immunized monkeys.

The loss of a highly organized compact myelin structure in a demyelinated lesion causes a reduction of the directional diffusivity of water, which can be visualized in diffusion tensor images (Figure 4A)²²². To obtain an overall picture of the lesion pathology, MR images of the total fixed brain were recorded. More specific, the directional diffusivity (fractional anisotropy) of water in lesions and NAWM was determined. Figure 4B and 4C depict one slice as an illustrative example that shows the disturbed organization of WM in the T2 lesion, suggesting that compact myelin has disappeared. Figure 4E shows the mean fractional anisotropy values of all T2 lesions throughout the brain of four MOG34-56-immunized marmosets; these were substantially lower in the lesions than of the perilesional NAWM, indicating the ubiquitous loss of compact WM.

Pathological changes in the brain and spinal cord were also examined by histology. Figure 5 shows dramatic demyelination in the spinal cord WM area of a MOG34-56-immunized monkey. At the time of necropsy demyelination was still taking place. The lesions were heavily infiltrated with T-cells and macrophages that contained phagocytosed myelin debris. Axonal pathology was clearly present. Significant demyelination was also observed in the spinal cord grey matter areas. Within these areas, activated microglia cells as well as infiltrating macrophages were detected.

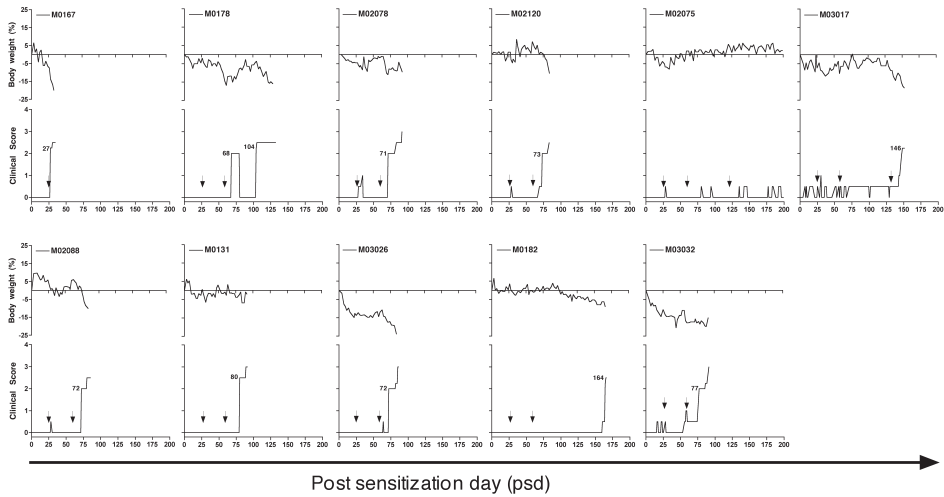


Figure 2. Clinical course of MOG34-56 induced EAE. Eleven marmosets were immunized with 100 μ g MOG34-56 in CFA. Monkeys without overt signs of EAE at the end of a pre-determined episode of \pm 28 days received one, two, or three booster immunizations with 100 μ g MOG34-56 in IFA (arrows). Clinical scores and changes in body weight (percentage compared with day 0) as a surrogate disease parameter of individual monkeys are shown. Ten of the 11 monkeys were sacrificed with a clinical score of \geq 2.5, whereas one monkey was sacrificed at the end of a 200-day observation period without neurological signs. Numbers in the figures represent the time point (psd) when overt neurological signs (score \geq 2) were first observed.

MOG74-96-induced EAE

To test the encephalitogenic potential of the MOG74-96 peptide, the twin siblings of seven of the 11 MOG34-56-immunized monkeys were immunized with MOG74-96. Two separate experiments, denoted A and B, were done comprising four and three monkeys, respectively (Table 1).

Experiment A. In the first experiment (monkeys M02121, M02076, M02079, and M02087), overt neurological disease did not develop during the 200-day observation period. However, mild signs of EAE (score 0.5) were observed (Figure 6).

To test whether monkeys immunized with MOG74-96 displayed pathological changes within the CNS WM, high definition T2W images were made of the formalin-fixed brains from all four monkeys. In three monkeys clear abnormalities, albeit of moderate severity, were detected in the brain WM, namely one large periventricular lesion in M02076, two large lesions in M02121, and several small lesions in M02087 (Figure 3).

Histological examination confirmed the presence of mild demyelination in frontal regions in the brain of two monkeys that were scored positive with MRI, i.e. M02076 and M02121. Interestingly, very little inflammatory activity was detected within these lesions (data not shown). In monkey M02087 no brain lesions were found, indicating that the abnormalities observed with MRI do not represent areas of inflammatory demyelination.

Experiment B. In the second experiment essentially the same results were obtained after the subsequent immunizations with MOG74-96, namely significant weight loss associated with

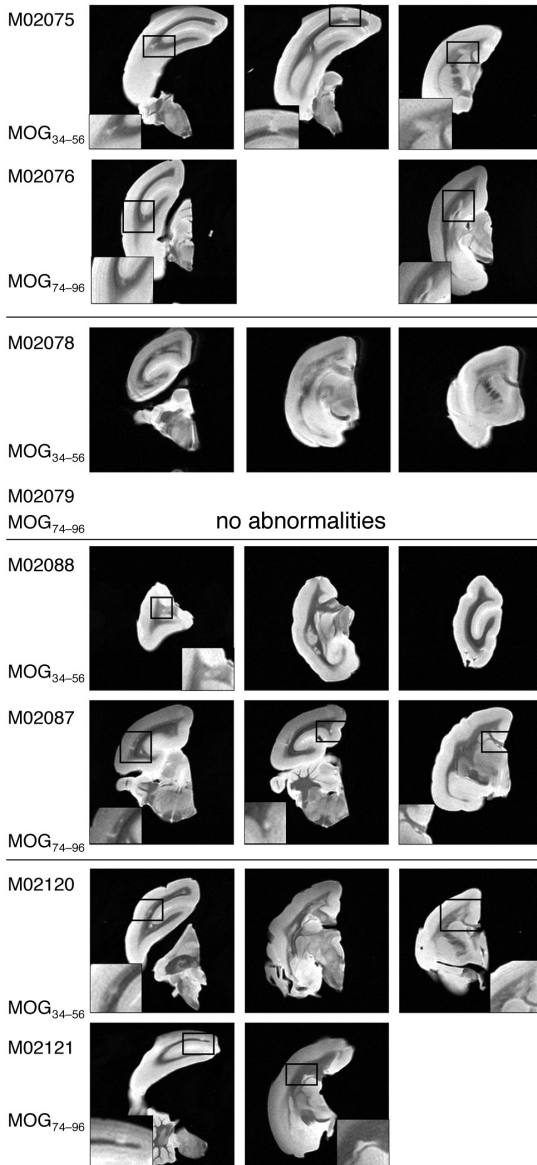


Figure 3. MRI reveals white matter pathology in MOG34-56-immunized monkeys. High contrast T2W images of formalin-fixed brains were recorded to assess the total lesion load. Corresponding slices from twins of which one sibling was immunized with MOG34-56 and the other with MOG74-96 are shown. The pictures clearly illustrate white matter pathology in MOG34-56-immunized monkeys that displayed overt neurological signs. This was negligible in the MOG34-56-immunized monkey (M02075) and in all four MOG74-96 monkeys in which overt neurological signs did not develop. Magnification of the lesions shown in the corner are indicated by boxes.

only mild clinical signs. The mild CNS pathology observed in experiment A was associated with the appearance of low-level T-cell reactivity against MOG34-56 (see next paragraph). To amplify this low-level response, all three MOG74-96-immunized monkeys were given a single booster immunization with MOG34-56 in IFA. This induced overt neurological signs in two of the three monkeys within a few weeks (Figure 6). This observation contrasts with the situation in rhesus monkeys where booster immunization with MOG34-56 in IFA did not induce EAE, although this species is much more susceptible to EAE than marmosets¹⁸⁹. In the third monkey

(M03027), EAE scores fluctuating between 0.5 and 1.0 were recorded from psd 50 onwards. After the boost with MOG34-56, the disease stabilized at EAE score of 1. The monkey was finally sacrificed at psd 168 for histological analysis of the CNS.

The T2W post mortem images showed dramatic CNS pathology. Apart from large areas with increased T2W signal intensity, likely due to demyelination, the most remarkable feature was the presence of large “black holes” in the WM (data not shown). Histological analysis demonstrated comparable pathological changes as in MOG34-56-immunized monkeys. Brain and spinal cord contained large demyelinated lesions with infiltrated T-cells and activated macrophages and microglia (Figure 7).

Autoantibodies in MOG peptide-induced EAE cases

Plasma samples prepared from venous blood collected at 7-day intervals from the first immunization and at necropsy were tested with ELISA for the presence of IgM and IgG Ab against rhMOG and MOG peptides. Only total IgG responses were tested, because IgG subclasses are not described for the marmoset. Figure 8 shows the results for IgG at necropsy, which were representative for IgM and the data of the 7-day interval plasma.

The main Ab response in MOG34-56-immunized monkeys was against MOG24-46. In some monkeys we also found antibodies against MOG34-56 and rhMOG. In two MOG34-56-immunized monkeys a diversification of the Ab response to MOG54-76 was found (Figure 8A). Because this peptide, which is a dominant B-cell epitope in rhMOG-induced EAE, has only two overlapping amino acids with the immunizing peptide, it may be that this reactivity is caused by epitope spreading.

The dominant response in MOG74-96-immunized monkeys was against the immunizing peptide; but in the monkeys from experiment B, which were boosted with MOG34-56 in IFA, low-level Ab reactivity against rhMOG and MOG24-46 was also detected (Figure 8B).

T-cell reactivity in MOG peptide-induced EAE

PBMC, isolated at 2-week intervals after immunization, and MNC from lymphoid organs were cultured with rhMOG and a MOG peptide panel to test proliferation. Moreover, cells of ALN from the twins of experiment 3 (Table 1) were CFSE labeled and subsequently stimulated for 7 days with the immunizing peptides for the phenotyping of proliferating cells, visualized by the dilution of the fluorescent dye.

Proliferative responses in MOG34-56-immunized monkeys

In all monkeys, PBMC proliferation was found against MOG34-56 (Figure 9A). The proliferative response in PBMC remained low, rarely exceeding an SI of 5.0. As expected, much higher responses were found in the lymphoid organs collected at necropsy. The highest responses were mostly found in ALN and spleen (Figure 9B), while lower proliferation was found in ILN (data not shown). Only in monkey M02088 proliferation could be detected in CLN (data not shown). Cells of ALN (Figure 9C), spleen and ILN (data not shown) also proliferated against rhMOG and peptides overlapping with MOG34-56.

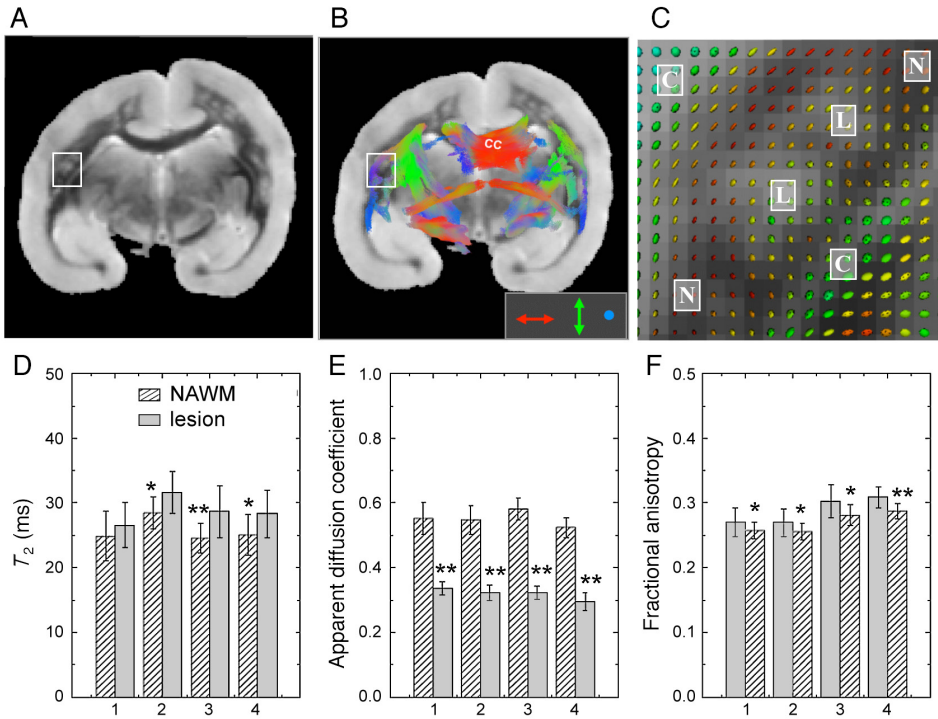


Figure 4. Diffusion tensor imaging of MOG34-56-induced brain lesions. The disruption of the normally restricted orientation (anisotropic) of water diffusion in white matter was used as an indirect MRI measure of tissue destruction in formalin-fixed brains. Brains from the four MOG34-56-immunized monkeys in experiment 1 (see Table 1) were used for this analysis. A tomographic section of the brain of monkey M0167 is depicted as a representative example. A, High contrast T2W images were made to visualize hyperintense structural abnormalities. B, The (disturbance of) fiber direction within the white matter is visualized with the standard color codes (red, left \Rightarrow right; blue, superior \Rightarrow inferior; green, anterior \Rightarrow posterior). C, The ellipsoid representation of fiber orientation within a lesion-rich area (white square) shows a round shape in the cortical (C) and lesion (L) area whereas these are more unidirectional in the compact white matter. D-F, Mean values of the total lesion (grey bars) and white matter (hatched bars) area of four monkeys (M0131, M0167, M0178, and M0182) are shown. The depicted quantitative parameters are as follows: 1) the mean of all voxels for T2 relaxation times (D), which is higher in the lesions than in the NAWM due to increased water content; 2) the degree of fractional anisotropy (E), which is decreased due to destruction of compact myelin; and 3) the apparent diffusion coefficient (F), which is slightly higher in lesions than in NAWM. Data are mean \pm SD. * $p < 0.05$, ** $p < 0.001$.

Proliferative responses in MOG74-96-immunized monkeys

In PBMC from MOG74-96-immunized monkeys proliferation against MOG74-96 was found (Figure 10A-B). In addition, from psd 104 proliferation against MOG34-56 was detectable (Figure 10A-B). The response to MOG34-56 could be amplified by a booster immunization with MOG34-56 in IFA (Figure 10B). At necropsy, MNC of MOG74-96-immunized animals proliferated against MOG74-96, but not against MOG34-56 (Figure 10C). The three monkeys challenged with MOG34-56 at the third booster displayed a reduced response against MOG74-96 and

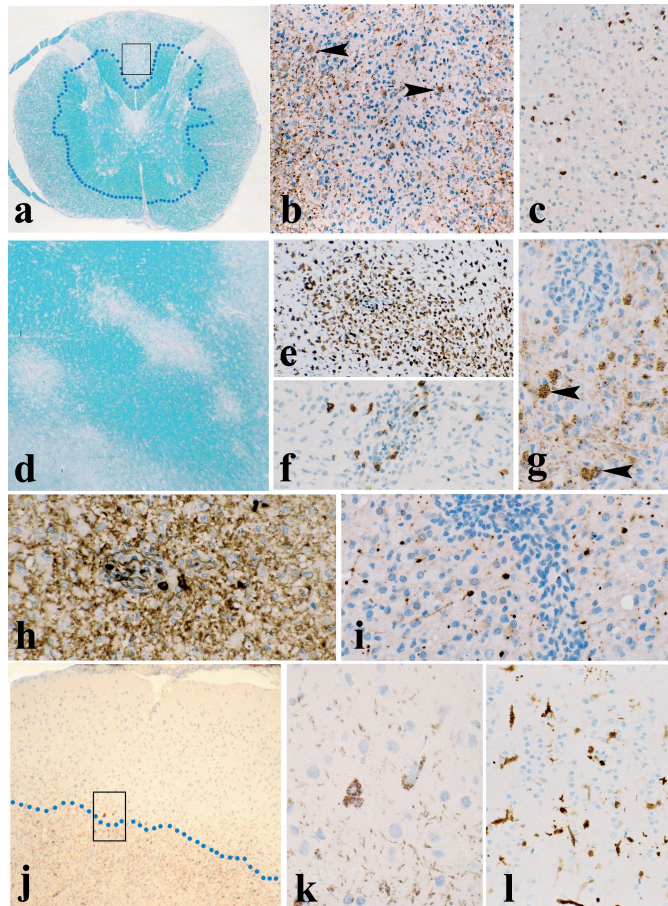


Figure 5. MOG34-56 induces inflammation and demyelination in the CNS. A, Luxol fast blue staining (original magnification x23) reveals that in this cross-section of spinal cord > 50% of the white matter has been demyelinated (blue line, border with normal white matter) and is remyelinating. Magnified views of the rectangle are shown in B and C. B, CNPase staining (original magnification x160) confirms demyelination and remyelination. Arrowheads point at oligodendrocyte cell bodies in the lesion centre. C, CD3 staining (original magnification x160) shows the presence of T lymphocytes in this area. D, Luxol fast blue staining (original magnification x38) indicates the presence of demyelinating lesions in the corpus callosum. E, MRP-14 positive macrophages are present in these lesions (E, original magnification x99) together with CD3 positive T lymphocytes (F, original magnification x200). G, PLP staining (original magnification x310) reveals PLP degradation products in macrophages (arrowheads). H, IgM staining (original magnification x290) shows plasma cells and Ig deposition on myelin. I, Axonal injury (axonal spheroids) in these white matter lesions is visualized by amyloid precursor protein staining (original magnification x275). In addition to spinal cord and brain white matter lesions, prominent cortical demyelination is also present. J, PLP staining (original magnification x50) reveals subpial demyelination. The meningeal lining is at the upper part of the figure, the blue lining marks the border of the demyelinated cortex, and a magnified view of the area inside the rectangle is shown in K. K, The area inside the rectangle in J (original magnification x990) in which microglial cells with uptake of PLP-positive myelin degradation products can be found. L, These activated microglial cells (original magnification x185) also stain positively with MRP-14, being an early activation marker of macrophages.

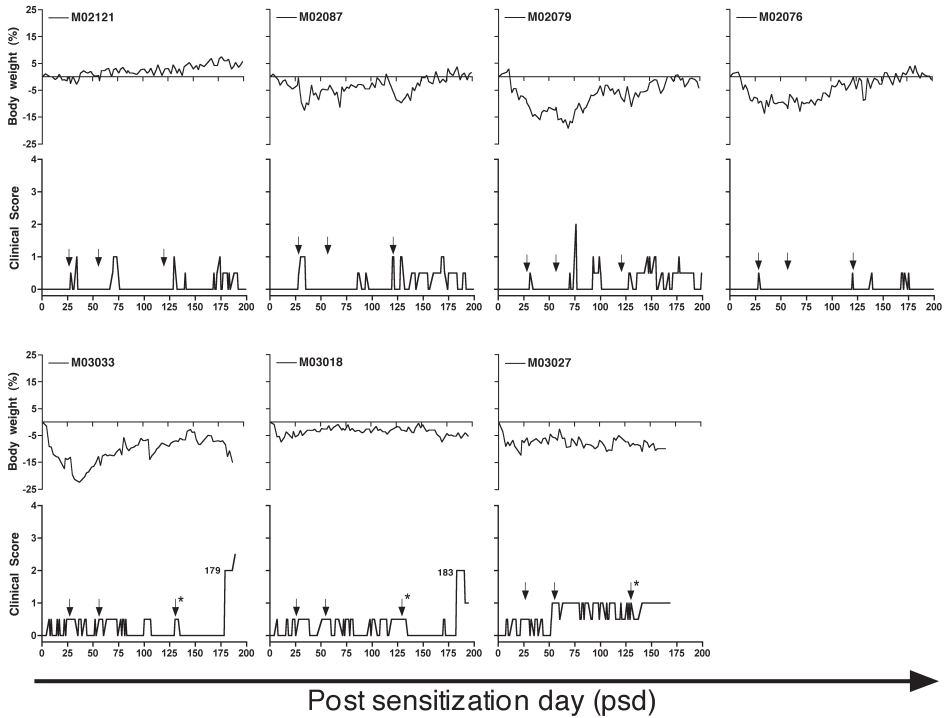


Figure 6. Immunization with MOG34-56/IFA induces full blown EAE in MOG74-96 sensitized marmosets. Seven marmosets, twin siblings of the monkeys in figure 2 (see Table 1) were immunized with 100 μ g MOG74-96 in CFA. Monkeys without overt signs of EAE (score < 2) at the end of a pre-determined episodes of \pm 28 days received three booster immunizations with 100 μ g MOG74-96 in IFA (arrows). Clinical scores and changes in body weight (percentage compared with day 0) as surrogate disease parameter of individual monkeys are shown. Because none of the monkeys developed overt neurological deficit within the pre-determined observation period of 125 days, three (M03033, M03018, and M03027) received the third booster immunization of 100 μ g MOG34-56 in IFA (arrow with an asterisk), resulting in full blown EAE in two monkeys (M03033 and M03018). Numbers in the figures represent the time point (psd) when overt neurological signs were first observed.

increased proliferation against MOG34-56 (Figure 10C). Cells of ALN collected at necropsy also proliferated against rhMOG (Figure 10D).

Phenotypic of MOG34-56- and MOG74-96-reactive T-cells

MNC from ALN, which contained the highest proliferative response, were stained with the fluorescent dye CFSE and subsequently cultured with the respective peptides. After 7 days, cells were harvested and stained with fluorescein-labeled mAb used for the phenotyping of human MNC subsets that are known to cross-react with marmoset MNC²¹⁶. Proliferating cells were identified by dilution of CFSE. MOG34-56 stimulation of MNC from MOG34-56-immunized monkeys induced CFSE dilution in both CD4⁺ and CD8⁺ T-cell subsets (Figure 11A). However, the percentage of divided CD4⁺ cells was about twice as high as that of divided CD8⁺ cells. Figure 11B shows the CFSE dilution in MNC cultures of monkeys immunized with MOG74-96 and

boosted with MOG34-56 (experiment B). Proliferation of cells stimulated with MOG34-56 or with MOG74-96 was found in both the CD4+ and the CD8+ T-cell subsets.

Cytotoxic activity of MOG34-56 and MOG74-96-specific T-cell lines

It was very difficult to generate stable TCL from the peptide-immunized monkeys from experiment 3 (Table 1), although we used the same method as successfully applied for the generation of stable TCL from rhMOG-immunized marmosets¹⁰³. Most lines collapsed after two or three rounds of restimulation with peptide-pulsed B-cell lines. Stable TCL could only be obtained of three monkeys, i.e. the twins M03017 and M03018 and the monkey M03033. Cytolytic activity towards autologous MOG peptide-pulsed APC by MOG-reactive TCL from MS patients has been described¹³⁷. Hence, we hypothesized that MOG peptide-specific T-cells from the marmoset might exert cytotoxic activity and kill the peptide-pulsed B-cell lines that were used as APC. To test this hypothesis, the phenotype and cytolytic activity of MOG peptide-specific TCL were determined.

MOG34-56- and MOG74-96-specific TCL contained a CD3+ cell population that consisted of a mixture of CD4+CD8-, CD4-CD8+, and CD4+CD8+ cells (data not shown). A significant fraction of the TCL, ranging from 14.8 to 78.9%, expressed the NK-CTL marker CD56 (Figure 11C).

Cytolytic activity of the three stable lines was tested with peptide-pulsed EBV-transformed autologous and allogeneic B-cell lines as target cells. The results in figure 11D show the peptide-specific cytotoxicity of MOG34-56 or MOG74-96 induced TCL from M03018 against autologous B-cell lines. MOG34-56-specific TCL were cytotoxic for MOG34-56-pulsed B-cells and MOG74-96-specific TCL killed MOG74-96-pulsed B-cells. MOG34-56 and MOG74-96-specific TCL of M03018 could also kill, respectively, MOG34-56 and MOG74-96-pulsed B-cell lines of M03033 (data not shown). No cytotoxicity of the MOG34-56- and MOG74-96-specific TCL against nonpulsed B-cells was observed (data not shown).

To collect phenotypical data from more monkeys, TCL that were stored frozen after three rounds of peptide stimulation and expansion on IL-2 were thawed. Reactivation was performed by a single round of peptide-specific stimulation using EBV-transformed B-cells as APC, followed by 8 days expansion on IL-2. This yielded seven MOG34-56-specific TCL derived from five monkeys (M03017, M03018, M03026, M03027, and M03033) and two MOG74-96-specific TCL derived from two monkeys (M03017 and M03027). The CD3+ population of MOG34-56-specific TCL consisted of 30.9% (range 11-58%) CD4+ cells, 11.4% (range 3-19%) CD8+ cells, and 54.2% (range 37-80%) CD4+CD8+ double positive cells. The high proportions of CD4/CD8 double positive cells is not an artifact of the freeze/thawing procedure, as this subpopulation is also found in peptide-stimulated cultures of freshly isolated lymph node and spleen cells. CD56 expression was most pronounced on single CD8+ T cells (62%; range 33-91%), followed by 45% (range 18-69%) of the double positive cells and 32% (range 9-58%) of the single CD4+ cells. In none of the subpopulations was CD16 expression observed (Figure 12). The CD3+ population of two additional MOG74-96-specific TCL consisted of 10.6% (1.8/19.4) CD4+ cells, 38.7% (63.4/13.9) CD8+ cells, and 48.3% (32.3/64.2) double positive cells. All three subpopulations expressed significant CD56 levels, respectively 50.4% (79.5/21.2) of the CD4+, 82.1% (96.9/76.3) of the CD8+, and 72.1% (93.4/50.8) of the CD4+CD8+ populations (data not shown).

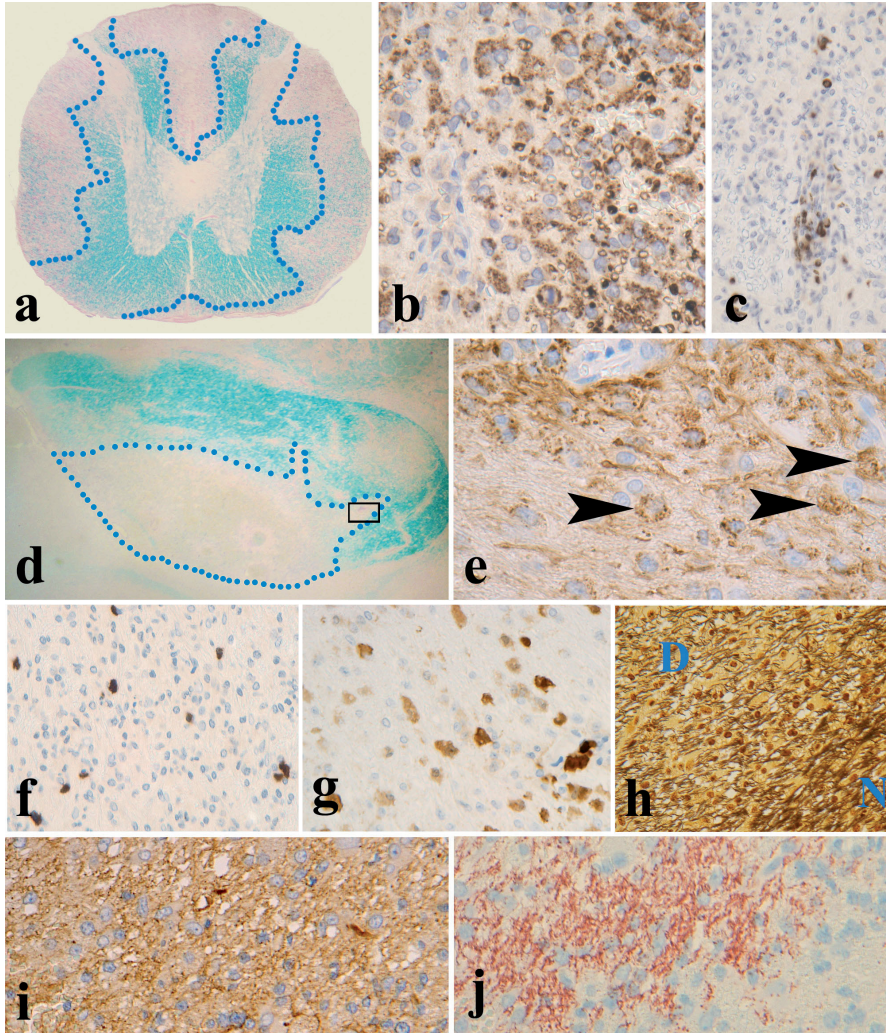


Figure 7. Pathology of MOG34-56-boosted EAE in MOG74-96-immunized monkeys. Pathology present in the spinal cord of monkey M03033 is shown in A-C; pathology in the optic tract is shown in D-J. A, Staining for luxol fast blue (original magnification x20) reveals demyelinated areas (bordered by blue dotted line) in the spinal cord white matter. B, Late active demyelination (original magnification x350) is shown by the presence of PLP-positive degradation products in macrophages. C, Besides demyelination, inflammation of the lesions is characterized by the presence of CD3+ lymphocytes (original magnification x150). D, Luxol fast blue staining (original magnification x45) shows large demyelinated lesions (borders indicated by dotted line) in the optic tract. Magnified views of the rectangular area are shown in E-J. E, Staining for PLP (original magnification x350) reveals the presence of PLP degradation products in macrophages (arrowheads). F, The optic tract lesions contained CD3+ lymphocytes (original magnification x150). G, Single macrophages are stained positively for MRP-14 (original magnification x150). H, A bielschowsky stain for axons (original magnification x150) shows a reduced density of axonal fibers in the demyelinated area (D) compared to the surrounding NAWM (N). I, Staining for IgM (original magnification x300) and complement C9 (J, original magnification x300) shows deposition in the demyelinated areas.

A

Monkey	rhMOG	hMOG peptide										
		4-26	14-36	24-46	34-56	44-66	54-76	64-86	74-96	84-106	94-116	MBP
M0167		NT	NT		NT	NT	NT	NT		NT	NT	NT
M0131		NT	NT		NT	NT	NT	NT		NT	NT	NT
M0182		NT	NT		NT	NT	NT	NT		NT	NT	NT
M0178												
M02078												NT
M02120												NT
M02088												NT
M03026		NT										
M03032		NT								NT	NT	
M03017		NT								NT	NT	
M02075												NT

B

Monkey	Exp	rhMOG	hMOG peptide										
			4-26	14-36	24-46	34-56	44-66	54-76	64-86	74-96	84-106	94-116	MBP
M02121	A											NT	
M02079												NT	
M02087												NT	
M02076												NT	
M03033	B		NT								NT	NT	
M03027			NT								NT	NT	
M03018			NT								NT	NT	

Neg.	+	++	+++

Figure 8. Diversification of antibody reactivity in MOG34-56 and MOG74-96-immunized monkeys. Plasma of MOG34-56 (A) and MOG74-96 (B) immunized monkeys were collected at necropsy and tested with ELISA for IgG reactivity with rhMOG and the panel of 23-mer peptides that covers the extracellular domain of MOG (1-125). Results are expressed as fold increase of OD relative to pre-immune marmoset serum. Neg., <2; +, 2 to <4; ++, 4 to <8; +++, ≥8. NT, not tested due to lack of material.

DISCUSSION

Several aspects of EAE in common marmosets make it a unique experimental model of MS, in particular the outbred nature, the genetic and immunological proximity to humans, and the remarkable neuropathological similarity with the disease in humans [for review²²⁸]. The disease typically follows a progressive course that can last from several weeks to more than a year¹²⁷. Of the many components of CNS myelin with proven encephalitogenic capacity in mice, MOG appeared to be the most critical for the induction of chronic progressive disease in Biozzi ABH mice and marmosets^{93, 268}. This prompted us to investigate the MOG-induced autoimmune mechanisms that drive progression of the disease using a rhMOG-induced EAE model.

We have previously shown in a relatively small group of monkeys that the 100% EAE prevalence maps to the invariant MHC class II molecule *Caja-DRB*W1201*, which is involved in the activation of MOG24-36 specific encephalitogenic T-cells¹⁰³. Although the presence of *Caja-DRB*W1201* in the MHC repertoire of each individual monkey at the genomic level was already known for several years²⁰⁰, it was only recently reported that mRNA transcripts of this allele are indeed expressed in APC of all tested monkeys²⁰⁶.

With regard to MOG-induced autoimmune mechanisms involved in the progression of rhMOG-induced EAE, we report here several novel findings that in part contrast with published data. The current results show that monkeys displaying a relatively broad reactivity of their lymph node T-cells with a MOG peptide panel developed neurological deficit significantly earlier than monkeys with a more restricted reactivity profile. By contrast, we observed no association between the reactivity profile of immune sera with the MOG peptide panel and the rate of EAE progression. Hence, we conclude that the different time spans between EAE induction and the expression of neurological signs is associated with a diversification of proliferative T-cell responses against MOG epitopes beyond MOG24-36. Our interpretation of this finding is that fast progressor monkeys may be (genetically predisposed) high responders to peptides processed from rhMOG and presented to encephalitogenic T-cells present in the

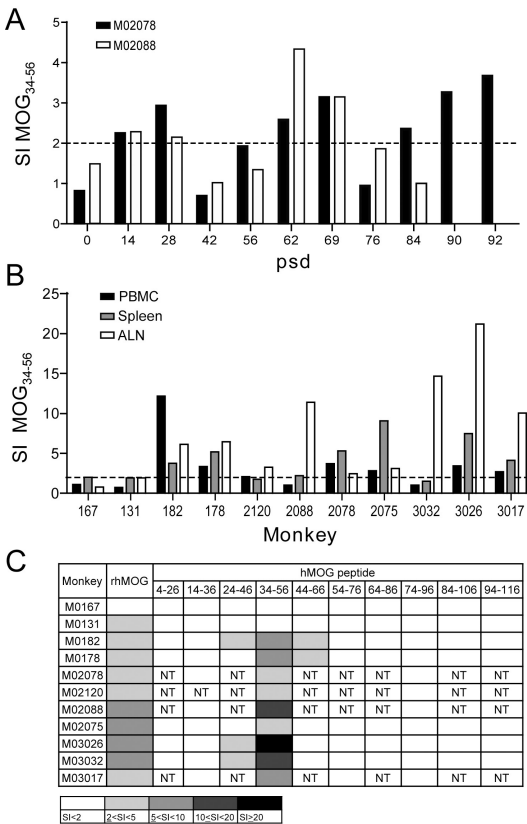
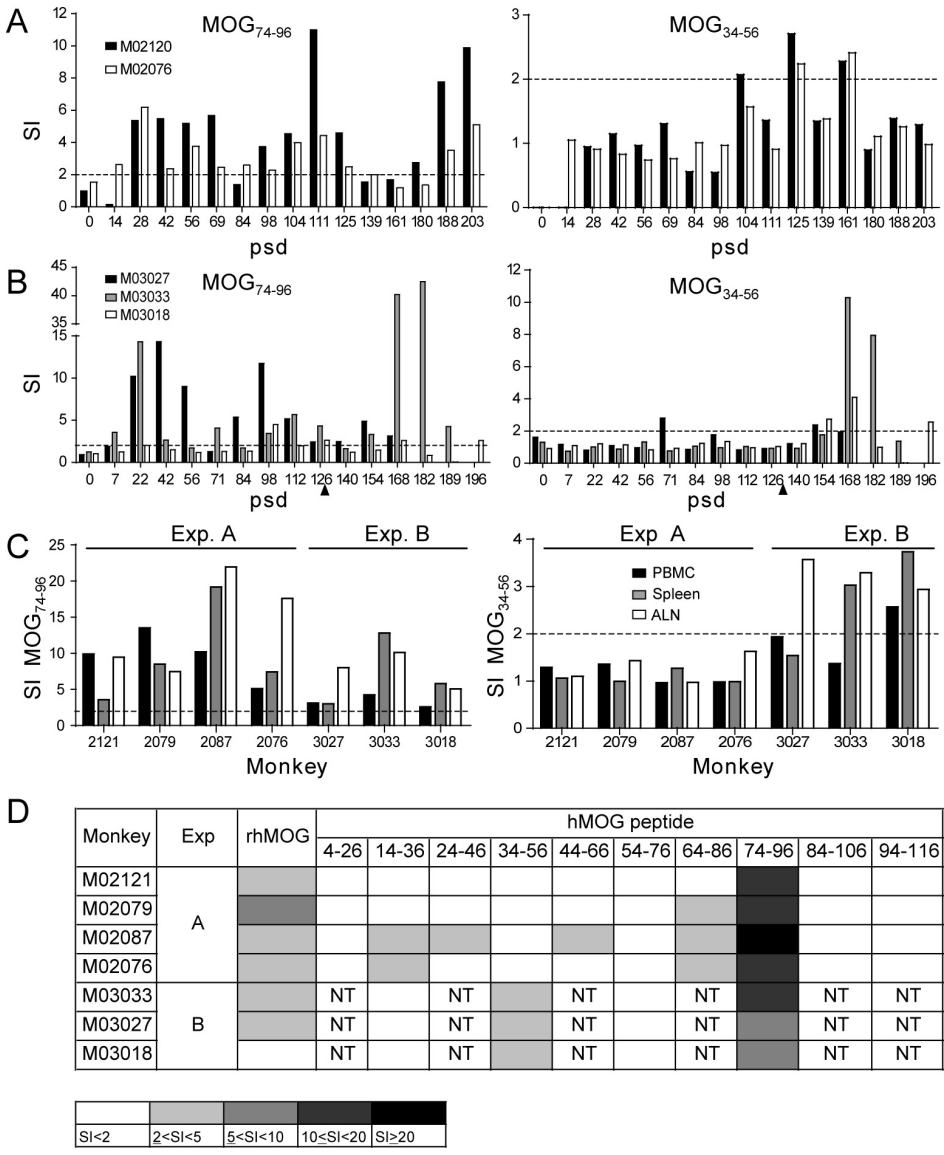


Figure 9. T-cell proliferation remains confined to the immunizing peptide MOG34-56. Eleven marmosets were immunized with MOG34-56 in CFA (psd 0) followed by booster immunizations with MOG34-56 in IFA at psd 28, 56, and ~ 125. PBMC collected at different time points and MNC of secondary lymphoid organs collected at necropsy were probed for their proliferative response against the MOG peptide panel. Only responses above an SI of 2 (dotted line) are considered positive. Proliferative responses were found against MOG34-56. A, PBMC data from two representative monkeys. B, High responses were found in ALN and spleen at necropsy. C, Summary table of proliferative responses of ALN cells from all 11 monkeys against rhMOG and the MOG peptide panel. NT, not tested.

Figure 10. Amplification of anti-MOG34-56 T-cell responses in MOG74-96-immunized animals after a booster with MOG34-56 in IFA. Four marmosets were immunized with MOG74-96 in CFA (psd 0) followed by immunizations with MOG74-96 in IFA at psd 28, 56, and 119 (experiment A). Three marmosets were immunized with MOG74-96 in CFA (psd 0) followed by two booster immunizations with MOG74-96 in IFA at psd 28 and 56. At psd 130 the monkeys received a booster with MOG34-56 ►



► in IFA (arrowhead) (experiment B). PBMC were collected at different time points and probed for their proliferative response against MOG₇₄₋₉₆ and MOG₃₄₋₅₆. Only responses above an SI of 2 (dotted line) are considered positive. A, Proliferation of PBMC of two representative monkeys of experiment A. Proliferative responses were mainly directed against MOG₇₄₋₉₆, although after psd 100 also responses above an SI of 2.0 against MOG₃₄₋₅₆ were detected. B, Proliferation of PBMC of the monkeys of experiment B. Proliferative responses were mainly directed against MOG₇₄₋₉₆, although after the booster immunization with MOG₃₄₋₅₆ in IFA proliferative responses against this peptide increased. C, Proliferation of MNC collected at necropsy. The monkey codes are given on the x-axis. The monkeys of experiment A show high responses to MOG₇₄₋₉₆, whereas the monkeys of experiment B show increased responses to MOG₃₄₋₅₆. D, Summary table of proliferative responses of ALN MNC from all 7 monkeys against rhMOG and the MOG peptide panel.

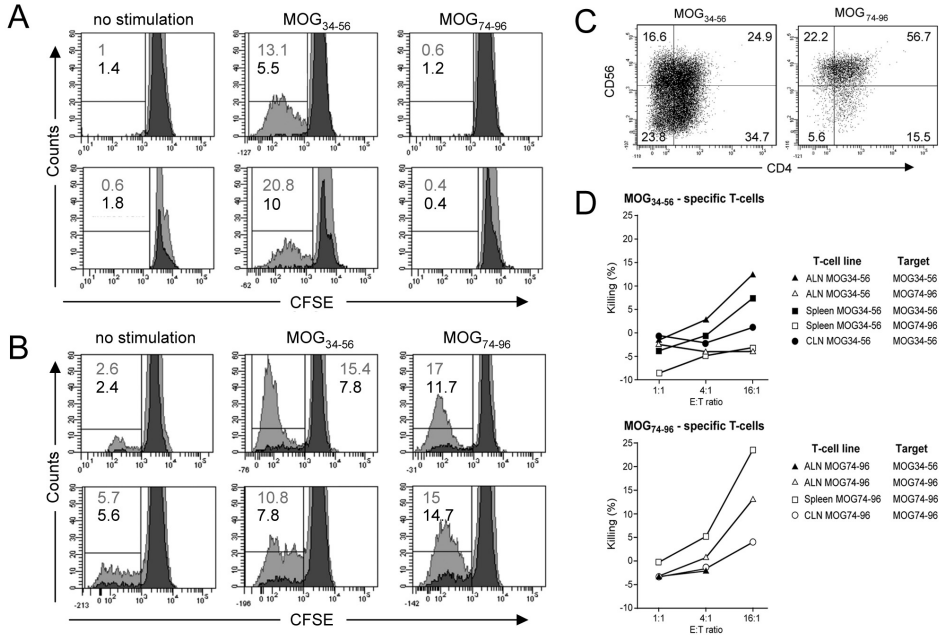


Figure 11. MOG34-56- and MOG74-96-reactive T-cells show an NK-CTL like phenotype and activity.

A-B, Freshly isolated MNC of ALN from EAE-affected marmosets were labeled with the fluorescent probe CFSE and subsequently cultured for 7 days with MOG34-56 or MOG74-96. Harvested cells were stained for CD3, CD4, and CD8 and analyzed by flow cytometry. The percentages of proliferated CD3+CD4+ (light shading) and CD3+CD8+ (dark shading) living cells under 3 stimulatory conditions are shown: without stimulant, with MOG34-56, or with MOG74-96. Data are shown for MOG34-56-immunized monkeys (M03017 and M03032) (A) and monkeys sensitized against MOG74-96 and finally boosted with MOG34-56 (M03018 and M03027) (B). C-D, Short-term T-cell lines (TCL) (effector cells) from 3 monkeys (M03017, M03018, and M03033) against MOG34-56 and MOG74-96 were established from MNC of spleen, ALN, and CLN. Shown are the data of M03018. C, Viable CD3+ cells of MOG34-56- or MOG74-96-specific TCL derived from ALN of M03018 were stained for CD4 and CD56. D, The specific cytotoxicity was tested against ⁵¹Cr labeled autologous EBV-transformed B-cell lines (target cells), which were untreated or pulsed with MOG34-56 or MOG74-96. Shown is the % killing by MOG34-56-specific TCL (top) and MOG74-96-specific TCL (bottom). TCL were cultured with MOG34-56-pulsed autologous B-cell lines (closed symbols) or MOG74-96-pulsed autologous B-cell lines (open symbols).

normal repertoire. We have chosen MOG34-56 and MOG74-96 for further examination since these peptides were detected in most fast progressor monkeys. Moreover, strong T-cell reactivity to these peptides is found in rhMOG-induced EAE models^{98,103}.

Ten of 11 monkeys immunized with MOG34-56/CFA developed overt clinical EAE, although the susceptibility of individual monkeys varied, as reflected by the number of booster immunizations needed for EAE induction. In our previous study we reported that in monkeys immunized with peptide MOG14-36, only CD4+ Th1-cells were induced together with mild inflammatory CNS pathology¹⁰³. Our current data show that in MOG34-56-immunized monkeys, CD4+ as well as CD8+ T-cells are activated and that many inflammatory/demyelinating lesions

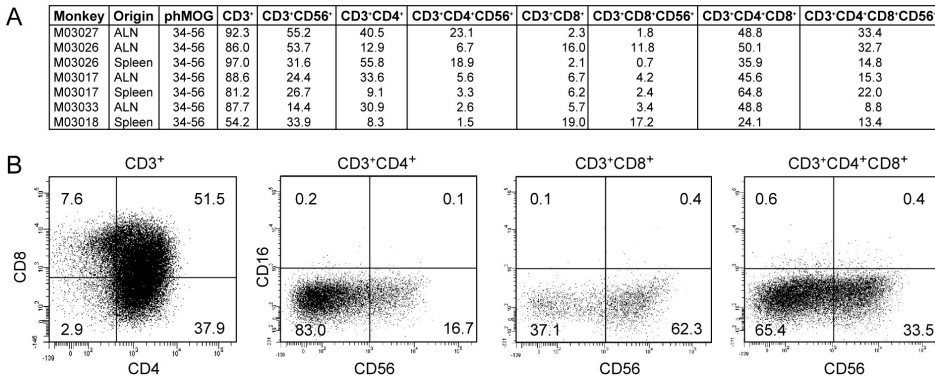


Figure 12. Phenotype of MOG34-56 specific T-cell lines. Seven T-cell lines (TCL), which were frozen after three rounds of antigenic stimulation and expansion on IL-2, were thawed and restimulated with MOG34-56 presented by autologous EBV-transformed B-cells. After 8 days expansion on IL-2, the phenotype of these lines was determined by FACS analysis. Vital CD3⁺ lymphocytes were analyzed for CD4 and CD8 expression. This resulted in CD4⁺, CD8⁺ and CD4/CD8 double positive populations. CD16 and CD56 expression was determined in these populations. The percentages of T-cell subpopulations in all 7 lines is given in table A. The dot plots in B depict a representative example, being the MOG34-56-specific TCL derived from the ALN of M03017. Numbers in the quadrants represent percentages of the subpopulation described above each dot plot.

are formed in the WM and, in some monkeys, also in the GM. Moreover, MOG34-56 induced TCL phenotypically resembled NK-CTL and displayed specific cytotoxic activity towards peptide-pulsed B-cell lines. The observation that essentially the complete clinical and pathological picture of rhMOG-induced EAE was reproduced in monkeys immunized with a single 23-mer peptide contrasts with data from Genain and colleagues showing that the development of full blown EAE depends on anti-MOG Ab recognizing discontinuous epitopes, and that full-blown EAE cannot be induced with MOG peptides²⁶⁹.

Monkeys sensitized against the peptide MOG74-96 did not show overt neurological signs, although we observed clinical EAE scores up to 1 as well as low-level CNS inflammation and demyelination by both MRI and histology. Furthermore, we detected low-level T-cell proliferation against MOG34-56. These data indicate that mild EAE may have been induced by *in vivo* activation of MOG34-56-reactive T-cells. This assumption is supported by the observation that a single booster immunization of the monkeys with MOG34-56 in IFA induced overt neurological signs within a few weeks in two out of three monkeys. This observation cannot be explained by cross-reactivity between the two peptides, as neither TCL nor immune sera from MOG34-56-immunized monkeys cross-reacted with MOG74-96 and vice versa. Hence, we conclude that in the MOG74-96-immunized monkeys MOG34-56-reactive T-cells had been recruited from the resting state, indicating that limited epitope spreading had taken place.

We like to propose as the underlying mechanism that MOG34-56-reactive (memory) T-cells present in the naive repertoire are activated by APC carrying myelin Ag from the lesions to draining lymph nodes. This concept is supported by previously reported findings. First, the ubiquitous autoreactivity against MOG14-36 induces CNS infiltration of T-cells and macrophages, which may trigger initial CNS WM damage^{103, 233}. Second, myelin-loaded APC can

be found localized in the CLN and spleen of EAE-affected monkeys²⁴⁶. We have not (yet) been able to directly demonstrate induction of autoreactive T-cells by myelin-loaded APC present within the CLN. However, the localization in T-cell areas of the lymph nodes creates the conditions needed for such a functional interaction. Third, data from the rhesus monkey EAE model show that MOG34-56-reactive T-cells present in the naive repertoire can be activated by immunization with a 23-mer peptide derived from the major capsid protein (UL86) of human cytomegalovirus (CMV; CMV UL86981-1003)¹⁸⁹. The CMV of common marmosets has not been isolated and characterized yet. However, assuming that CMV-induced memory T-cells do occur in the natural repertoire of common marmosets, as is the case in humans as well as rhesus monkeys, it is tempting to speculate that T-cells present in lymph nodes and spleen may be activated by myelin-loaded APC draining from the EAE-affected CNS²⁴⁶.

The mechanisms underlying the dramatic CNS pathology upon immunization with MOG34-56 remain to be fully elucidated. Our data demonstrate that the induction of NK-T-cell like cytotoxic activity represents at least one of the pathogenic mechanisms. The cytotoxicity assay shown in figure 11 was performed with a mixture of CD56+ cells, namely CD4+, CD8+, and CD4+CD8+. The phenotype of the cells (CD3+CD4+ and/or CD8+CD56+CD16-) as well as the capacity to lyse peptide-pulsed, autologous and allogeneic, B-cell lines are suggestive of an NK-T-cell like activity. Interestingly, a similar activity has been observed for anti-MOG T-cell-lines from MS patients¹³⁷. The possible involvement of such cells in the pathogenesis of MS has been reported by several groups^{270, 271}. We are currently exploring further the different cell subsets involved and the cytotoxic effector mechanisms, both *ex vivo* and *in situ*.

In conclusion, we report an association between disease progression in the rhMOG- induced EAE model in marmosets with the diversification of the anti-MOG T-cell response. In addition to a T-cell response against MOG24-36, which is present in all monkeys and is the presumed trigger of the disease, T-cell responses against MOG34-56 and MOG74-96 are detectable in monkeys with a rapid disease progression. MOG34-56 displays potent encephalitogenic activity leading to inflammation and tissue destruction in the CNS, most likely via the activation of cytotoxic T-cells with a NK-CTL-like phenotype. In our view the marmoset EAE model offers a unique experimental setting to further unravel the pathogenic mechanisms and to develop novel therapeutic approaches targeting these mechanisms, including the cytotoxic activity.

ACKNOWLEDGEMENTS

We thank Fred Batenburg for excellent biotechnical assistance and daily care of the monkeys; Jaco Bakker, Leo van Geest, and Gerco Braskamp for expert veterinary care; Tom Haaksma and Dr. Ivanela Kondova for autopsy of the monkeys; Boudewijn Ouwerling for laboratory work; and Henk van Westbroek for the artwork.

**INDUCTION OF PROGRESSIVE DEMYELINATING
AUTOIMMUNE ENCEPHALOMYELITIS IN COMMON
MARMOSSET MONKEYS USING MOG34-56 PEPTIDE
IN INCOMPLETE FREUND ADJUVANT**

S. Anwar Jagessar*, Yolanda S. Kap*, Nicole Heijmans, Nikki van Driel,
Linda van Straalen, Jeffrey J. Bajramovic, Herbert P.M. Brok,
Erwin L.A. Blezer, Jan Bauer, Jon D. Laman, and Bert A. 't Hart

* Shared first authorship

J Neuropathol Exp Neurol 69, 372-85 (2010)

ABSTRACT

Experimental autoimmune encephalomyelitis (EAE) in the neotropical primate common marmoset (*Callithrix jacchus*) is a relevant autoimmune animal model of multiple sclerosis. T-cells specific for peptide 34 to 56 of myelin oligodendrocyte glycoprotein (MOG34-56) have a central pathogenic role in this model. The aim of this study was to assess the requirement for innate immune stimulation for activation of this core pathogenic autoimmune mechanism. Marmoset monkeys were sensitized against synthetic MOG34-56 peptide alone or in combination with the nonencephalitogenic peptide MOG74-96 formulated in incomplete Freund's adjuvant (IFA), which lacks microbial compounds. EAE development was recorded by monitoring neurological signs, brain magnetic resonance imaging, and longitudinal profiling of cellular and humoral immune parameters. All monkeys developed autoimmune inflammatory/demyelinating central nervous system disease characterized by massive brain and spinal cord demyelinating white matter lesions with activated macrophages and CD3+ T-cells. Immune profiling *ex vivo* demonstrated the activation of mainly CD3+CD4+/8+CD56+ T-cells against MOG34-56. Upon *ex vivo* stimulation, these T-cells produced more interleukin-17A compared with Th1 cytokines (e.g. interferon- γ) and displayed peptide-specific cytolytic activity. These results indicate that the full spectrum of marmoset EAE can be induced by sensitization against a single MOG peptide in IFA lacking microbial compounds for innate immune activation and by eliciting antigen-specific T-cell cytolytic activity.

INTRODUCTION

Multiple sclerosis (MS) is a chronic neurological disease affecting the central nervous system (CNS) of 1 per 1000 young adults in the moderate climate areas of the United States and Europe⁵. During the past decades, understanding of the immunopathogenic mechanisms that drive the disease has advanced considerably, resulting in the development of several effective disease-modifying agents²⁷¹. However, the few successes are in contrast to a long list of treatments that failed to reproduce the beneficial effects in animal models of MS when tested in MS patients. The poor translation of scientific data to the clinic is in part attributed to the wide gaps between human patients and animal models^{225, 272}.

Limitations of the current MS models in inbred and specific pathogen-free laboratory rodent strains include the lack of genetic diversity and exposure to environmental pathogens, both of which have a strong influence on the developing immune system²⁷³. Moreover, persistent latent infections with herpesviruses that have a strong impact on the aging of the human immune system do not occur in rodents²⁷⁴. Finally, rodents are most often used at young adult ages (8-12 weeks). Non-human primates do not have these limitations because they are long-lived and are housed under conventional conditions in social groups where a high genetic and microbiological diversity is maintained.

The common marmoset (*Callithrix jacchus*) is a small neotropical primate that provides a valid preclinical MS model. The model reproduces the progressive clinical course and approximates the neuropathological complexity of human MS^{127, 228}. The parallel clinicopathological features of this model and the close genetic, immunological, and microbiological similarities of humans and marmosets create an attractive experimental system for the dissection of critical pathogenic mechanisms that are promising candidate targets for MS therapy²⁷⁵.

We previously demonstrated that autoimmunity against the extracellular domain of myelin oligodendrocyte glycoprotein (MOG), a quantitatively minor component of CNS myelin, is critical for the activation of the pathogenic mechanisms that drive experimental autoimmune encephalomyelitis (EAE) progression in Biozzi ABH mice⁹³ and marmosets²⁶³. The immunopathogenic mechanisms elicited by human MOG were unraveled in marmosets immunized with recombinant human MOG (rhMOG), a recombinant protein representing the extracellular domain (residues 1-125) of human MOG¹⁹⁰. Whereas the 100% incidence of EAE induction could be mapped to the activation of T helper 1 cells specific for the peptide MOG24-36¹⁰³, T-cells directed against epitopes encompassed within peptide MOG34-56 were found to play a critical role in the progression of rhMOG-induced EAE¹⁹⁰.

Having identified the activation of MOG34-56 T-cells as a core pathogenic autoimmune mechanism in the marmoset EAE model, we set out to investigate the minimum activation requirements. We report that marmosets sensitized against MOG34-56 peptide in incomplete Freund's adjuvant (IFA), a formulation that lacks microbial antigens (Ag) for innate immune activation, all developed severe clinical EAE, which is characterized by marked inflammation and primary demyelination in the CNS. Immune profiling supports a key pathogenic role for CD3+CD4+/8+CD56+ T-cells, with pro-inflammatory and cytolytic capacities. Although antibodies (Ab) against the immunizing peptides were formed, these failed to bind intact rhMOG, arguing against a direct pathogenic role. Our present results challenge the concept that innate immune mechanisms triggered by microbial compounds in the Ag inoculum are a necessary

prerequisite to break T-cell tolerance leading to EAE. The possibility of inducing EAE without the need for complete Freund's adjuvant (CFA), which induces necrotizing skin lesions that cause serious discomfort to the animals, also implies a major refinement of the model.

MATERIALS AND METHODS

Animals

The monkeys included in this study originated from purpose-bred colonies of the Biomedical Primate Research Centre (BPRC), Rijswijk, The Netherlands, and the German Primate Centre (DPZ), Göttingen, Germany. Monkeys purchased from DPZ had been housed for at least 6 months in the BPRC before use. Individual data for all monkeys are listed in Table 1. Before inclusion in the study, the monkeys received complete physical, haematological, and biochemical examination, and during the study, they remained under veterinary care. Monkeys were housed in pairs in spacious cages enriched with branches and toys and with padded shelter provided on the floor. The daily diet consisted of commercial food pellets for New World monkeys (Special Diet Services, Witham, Essex, UK), supplemented with rice, raisins, peanuts, marshmallows, biscuits, fresh fruit, grasshoppers, and maggots. Drinking water was provided ad libitum.

Ethics

In accordance with the Dutch law on animal experimentation, all study protocols and experimental procedures were reviewed and approved by the Institute's Ethics Committee before the start of experiments.

Antigens

The human MOG extracellular domain (rhMOG) was expressed as an unglycosylated recombinant protein in *Escherichia coli* and purified, as previously described¹³⁸. Synthetic MOG peptides based on the human MOG sequence used for immunization and cell culture were purchased from ABC Biotechnology (London, UK) and Cambridge Research Biochemicals (Cleveland, UK).

Induction of EAE

EAE was induced with 100 µg MOG34-56 or with the mixture of 100 µg MOG34-56 and 100 µg MOG74-96. For each immunization, the monkeys were injected into the dorsal skin with the MOG peptide dissolved in 300 µl PBS (Invitrogen, Gibco BRL, Glasgow, UK) and emulsified with 300 µl IFA (Difco Laboratories, Detroit, MI). The inoculum was injected into the inguinal and axillary regions of the dorsal skin divided over 4 spots of 150 µl each. Ag-adjuvant emulsions were prepared by gentle stirring the peptide/oil mixture at 4°C for at least 1 h. Monkeys that failed to develop serious neurological deficits (score \geq 2.0; see next paragraph) within 28 days received re-challenges at 4-weeks interval with the same dose of peptide(s) in IFA until EAE developed.

Clinical scoring

Clinical signs were scored daily by two trained independent observers, as described¹²⁷. Briefly: 0 = no clinical signs; 0.5 = apathy, loss of appetite, altered walking pattern without ataxia; 1 =

Table 1. Overview of marmosets used in this study and their response to EAE.

Experiment	Monkey	Sex ^a	Age ^b	Immunization MOG peptide	Clinical EAE signs	Lesions on MRI
1	M03138	F	36	34-56 + 74-96	Yes	Yes
	M03139	F	36	34-56 + 74-96	Yes	Yes
	M04033	F	31	34-56 + 74-96	Yes	Yes
	M04034	F	31	34-56 + 74-96	Yes	Yes
2A	M03162	M	47	34-56 + 74-96	Yes	Yes
	M05056	M	27	34-56 + 74-96	Yes	Yes
	M05082	M	25	34-56 + 74-96	Yes	Yes
	M06012	M	20	34-56 + 74-96	Yes	Yes
	M06017	M	21	34-56 + 74-96	Yes	Yes
2B	9847	M	105	34-56	Yes	Yes
	M05047	M	30	34-56	Yes	Yes
	M06006	M	29	34-56	Yes	Yes
	M06018	M	21	34-56	Yes	Yes
	M06020	M	21	34-56	Yes	Yes

^aF, female; M, male

^bAge in months at the start of the experiment

EAE; experimental autoimmune encephalomyelitis, MOG; myelin oligodendrocyte glycoprotein, MRI; magnetic resonance imaging.

lethargy, anorexia, loss of tail tonus, tremor; 2 = ataxia, optic disease; 2.5 = para- or monoparesis, sensory loss, brain stem syndrome; 3 = para- or hemiplegia; 4 = quadriplegia; 5 = spontaneous death attributable to EAE. Monkeys were sacrificed for ethical reasons once complete paralysis of one or both hindlimbs (score \geq 3.0) was observed or at a predetermined endpoint.

To obtain an objective surrogate disease marker, the monkeys were weighed three times per week. This was performed without sedation using the Perspex cylinder with which adequately trained monkeys were captured from the home cage.

Post mortem examination

At the time of necropsy, the monkeys were first deeply sedated with ketamine (50 mg/ml PBS) (Produlab Pharma, Raamsdonkveer, The Netherlands) injected intramuscularly at a dose of 100 μ l/kg body weight; they were subsequently euthanised by infusion of pentobarbital sodium (Euthesate; Apharmo, Duiven, The Netherlands). Brain, spinal cord, spleen, cervical lymph nodes (CLN), inguinal lymph nodes (ILN), and axillary lymph nodes (ALN) were aseptically removed. Small parts of all organs were snap-frozen in liquid nitrogen and stored at -80°C for immunohistochemistry. One brain hemisphere was fixed for at least 7 days in 4% buffered formalin and subsequently transferred into buffered saline with sodium azide (Sigma-Aldrich, Gillingham, UK) to allow stabilization before magnetic resonance imaging (MRI). To assess the total brain lesion load, MR images were made of formalin-fixed brains as described²⁴¹. After

MRI, the tissues were examined with histological and immunohistochemical techniques as described^{17,190}.

Magnetic resonance imaging

MR brain images were acquired from live animals and post mortem formalin-fixed brains. *In vivo* MRI experiments were performed on the two animals that had no clear overt clinical scores and were still alive at the end of the protocol (i.e. M06006 and M06012). Experiments were performed on a 4.7-T horizontal bore MRI scanner (Varian, Palo Alto, CA). T2-weighted (T2W) images (field of view, 40 x 40 mm; matrix, 128x 128; zero-filled, 256 x 256; slice thickness, 1 mm; number of experiments, 2) were collected using a spin-echo sequence with a repetition time of 2.75 s and an echo time of 30 ms. Post mortem images were obtained on a 9.4-T MRI scanner (Varian). Formalin-fixed brains were submerged in a perfluoropolyether (Fomblin, Fluortek AB, Knivsta, Sweden) for susceptibility matching. T2W images (field of view, 25 x 25 mm; matrix, 256 x 256; zero-filled, 512 x 512; slice thickness, 0.75 mm; number of experiments, 2) were collected using a spin-echo sequence with a repetition time of 2.6 s and an echo time of 20 ms.

Assays for innate immune stimulatory activity

The immunizing peptides MOG34-56 and MOG74-96 and IFA were screened for contamination with ligands of Toll-like receptors (TLR) using human endothelial kidney (HEK293) cells transfected with human TLR2, TLR3, TLR4, or TLR5 and HEK293XL cells transfected with TLR7, TLR8, TLR9, or TLR10 (all from InvivoGen, San Diego, CA). The cell lines were cotransfected using Polyfect (Qiagen Benelux, Venlo, The Netherlands) with a reporter vector expressing luciferase under the control of an NF- κ B-responsive promoter (pNifty2-luc; InvivoGen). Stably transfected clones were selected and used in bioassays. Cells were plated in flat-bottom 96-wells plates (Greiner Bio-one, Frickenhausen, Germany) at a density of 1×10^5 cells/well and were stimulated with individual MOG peptides, IFA, or a mix of MOG peptide and IFA. After 16 h incubation at 37°C, the cells were lysed in 50 μ l Steady Glo luciferase buffer (Promega Benelux, Leiden, The Netherlands) for 10 min, and bioluminescence was measured using a Packard 9600 Topcount Microplate Scintillation & Luminescence Counter (Packard Instrument Company, Meriden, CT). As a positive control for NF- κ B-mediated activation (i.e. the presence of the pNifty2-luc vector), 25 ng/ml Tumor necrosis factor (TNF)- α (PeproTech, London, UK) was used. Positive controls for TLR2 and TLR4 activation were lipopolysaccharide (100 ng/ml); TLR3, polyriboinosinic polyribocytidylic acid (Poly(I:C)) (20 μ g/ml); TLR5, flagellin (1 μ g/ml); TLR7, an adenine derivate (CL-087) (1 μ g/ml); TLR8, a thiozoloquinolone derivate (CL-075) (1 μ g/ml); TLR9, synthetic oligonucleotides that contain unmethylated CpG (ODN2006) (2 μ mol/ml). No ligands are known for TLR10, but TLR10 expression in the transfected HEK293 cell lines was confirmed with Western blot (data not shown). The TLR-specific ligands were obtained from InvivoGen.

For cytokine production assays, CD14⁺ cells isolated from buffy coats of healthy human donors with MACS beads (Miltenyi Biotech, Auburn, CA) were cultured for 7 days with 20 ng/ml macrophage colony-stimulating factor (PeproTech) to differentiate them into macrophages. Culture supernatants of macrophages and peripheral blood mononuclear cells (PBMC) also isolated from buffy coats were collected after 24 h stimulation with both immunizing MOG peptides and IFA to measure cytokine production.

Mononuclear cell and T-cell line preparation

The maximum monthly blood volume that can be collected from marmosets is 1% of the body weight, which is 3.5 ml for an average adult monkey of 350 g. Longitudinal immune monitoring was performed using 1 ml of venous blood collected at 2-weeks interval from the femoral vein into heparinized vacutainers (Greiner, Sölingen, Germany). At necropsy mononuclear cell (MNC) suspensions were also prepared from aseptically removed ALN, ILN, and spleen. MNC and PBMC were isolated using lymphocyte separation medium (LSM, ICN Biomedical Inc, Aurora, OH).

T-cell lines (TCL) were generated from MNC isolated from spleen and ALN by alternate stimulation with MOG34-56 or MOG74-96 and recombinant human IL-2 (Proleukin, Emeryville, CA), as described previously¹⁰³. Lethally irradiated (70 Gy) Epstein-Barr virus (EBV)-transformed autologous marmoset B-lymphoblastoid cells (B-LCL)²⁰⁰ from stably growing lines maintained in 75-cm² tissue culture flasks (Greiner Bio-one, Frickenhausen, Germany) were used as antigen presenting cells (APC). TCL displaying Ag specificity were characterized with cross-reactive monoclonal Ab raised against human CD markers²¹⁶.

Ex vivo analysis of T-cell responses

The PBMC and MNC suspensions were assayed in triplicate for proliferation against rhMOG (10 µg/ml) and a panel of MOG peptides (each 10 µg/ml)^{103,190}. Proliferation was assessed by the incorporation of [³H]-thymidine (0.5 µCi/well) (PerkinElmer, Boston, MA) during the final 18 h of a 64 h culture using a matrix 9600 β-counter (Packard Instrument Company). Results are expressed as stimulation index (SI), that is, the ratio of radiolabel incorporation in stimulated versus unstimulated cultures. SI values greater than 2.0 were considered positive.

Flow cytometry and carboxyfluorescein succinimidyl ester (CFSE) assay phenotyping of proliferating cells were performed as described¹⁹⁰. In brief, PBMC and MNC from ALN and spleen were suspended in 1 ml PBS and incubated for 7 min at room temperature with the fluorescent vital dye CFSE (final concentration 1.5 µM; Fluka, Deisenhofen, Germany), followed by culturing for 7 days at 37°C with or without Ag. Harvested cells were stained with labeled monoclonal Ab raised against the following human CD markers²¹⁶: anti-CD3 (BD Biosciences, San Diego, CA), anti-CD4 (DAKO, Glostrup, Denmark), anti-CD8-biotin (Serotec, Düsseldorf, Germany), anti-CD56, anti-CD16, and streptavidin PE-Cy7 or streptavidin PerCP (BD Biosciences). Viable cells were gated using violet viability stain (Invitrogen, Molecular Probes, Carlsbad, CA). Within each gated subpopulation the percentage of cells with CFSE dilution was calculated. Flow cytometric analysis was performed on a FACS LSRII flow cytometer using FACSDiva software 5.0 (BD Biosciences).

For cytokine analyses, supernatants of PBMC, ALN, and spleen cells were collected after 48 h stimulation with rhMOG or a panel of overlapping MOG peptides. Supernatants were assayed according to manufacturers' instructions with commercial ELISA kits for monkey TNF-α, monkey interferon-γ (IFN-γ) (U-Cytech, Utrecht, The Netherlands) and human cross-reactive IL-17A (eBioscience, San Diego, CA). Culture supernatants of human macrophages and PBMC stimulated with MOG34-56 and MOG74-96 peptides and IFA were assayed with human IL-6, IL-12p40+p70, TNF-α, and IL-1β (U-Cytech, Utrecht, The Netherlands) ELISA kit.

For cytotoxicity assays, autologous B-LCL labelled with ⁵¹Chromium (PerkinElmer) were pulsed with peptides of interest and used as target cells to test cytolytic activity of MOG pep-

tide-specific TCL, as described previously¹⁹⁰. Controls consisted of peptide-pulsed ⁵¹Chromium-labeled target cells without T-cells (i.e. spontaneous release) or peptide-pulsed ⁵¹Chromium-labeled target cells lysed with 1% Triton X-100 (Sigma-Aldrich, Steinheim, Germany) (maximum release). To test whether the cytolytic activity was perforin mediated, T-cells were pre-incubated with 28 nmol/l concanamycin A (Sigma-Aldrich) for 2 h at 37°C. After extensive washing, the cells were mixed with peptide-pulsed ⁵¹Chromium-labeled target cells. Results are expressed as percentage killing: (T-cell induced release – spontaneous release)/(maximal release – spontaneous release) × 100%.

Autoantibody detection

Venous blood samples were centrifuged and plasma supernatants were collected and stored at -20°C until further analysis. Ab binding to rhMOG (or to a panel of overlapping 23-mer pMOG (residues 1-125) sequences was determined using ELISA, as described²⁶⁴. Bound IgG Ab was detected using polyclonal alkaline phosphatase-conjugated rabbit-anti-human IgG (Abcam, Cambridge, UK). The results of the Ab assays are expressed as fold increase of light absorbance at 405 nm compared with the reactivity present in preimmune sera of the same monkeys.

Statistical analysis

A high variation in the disease course and associated immune parameters between individual animals is inherent to the outbred nature of this model. Statistical evaluation of data was performed using unpaired t-test when this was possible and relevant; values of $p < 0.05$ were considered significant. For the immune assays, values above the mean background ± 2 SD for T-cell proliferation ($SI \geq 2$) and Ab production (fold increase ≥ 2.0) were considered positive.

RESULTS

Lack of innate immune activation by peptide/IFA constituents

The TLR and Nodlike receptor families of pathogen recognition receptors comprise important mediators for the activation of innate immune mechanisms, which have been considered essential for EAE induction in most rodent models and are engaged by microbial compounds in CFA^{276, 277}. To determine the presence of possible innate immune stimulatory activity, the synthetic MOG peptides and IFA used for immunization were probed for stimulation of human macrophages and PBMC and TLR-transfected HEK293 cells.

Macrophages and PBMC were incubated with IFA, MOG34-56, and MOG74-96 in PBS, or MOG34-56/IFA emulsion. Culture supernatants were assayed for IL-6, IL-12p40+p70, and TNF- α . No significant levels of these cytokines were detected (Figure 1A). No IL-1 β was detected in the supernatants, indicating that this signature cytokine of the inflammasome pathway was also not activated under the conditions tested. The IFA and MOG peptides were also tested for the activation of the NF- κ B-driven luciferase reporter gene in HEK293 cells transfected with human TLR2, TLR3, TLR4, TLR5, TLR7, TLR8, TLR9, or TLR10; no cell stimulation was detected in any of these assays (Figure 1B).

Because tissue injury from skin injection of peptide/IFA emulsion may elicit danger signals that can activate APC and because skin flora microbes might infect the inoculum site despite appropriate cleaning, we also compared CFA and IFA immunization for EAE in EAE-susceptible

Biozzi ABH and C57BL/6. The mice were first immunized with human MOG34-56 in CFA or in IFA with additional intraperitoneal pertussis toxin. Booster immunizations were with MOG34-56 in IFA plus intraperitoneal pertussis toxin. Only sensitization against MOG34-56 was observed in CFA-induced (mild) EAE, whereas this was not observed in MOG34-56/IFA-immunized mice (data not shown).

Together, these data confirm that the peptides used for EAE induction are not contaminated with ligands for innate antigen receptors.

4

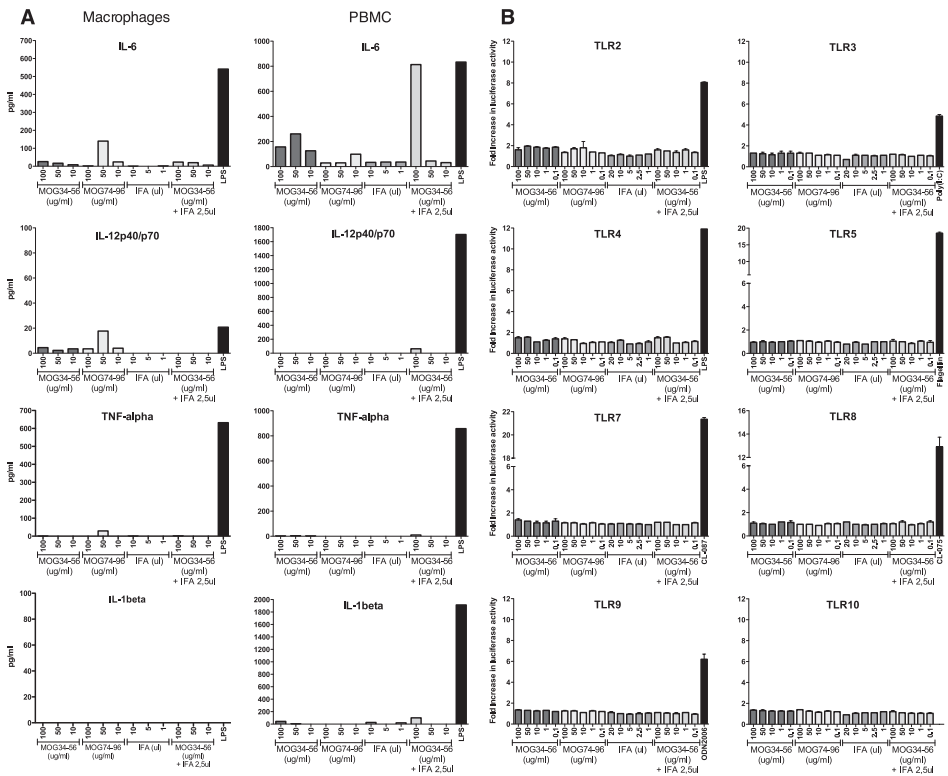


Figure 1. MOG34-56 and MOG74-96 are not contaminated with known pattern recognition receptor ligands. A. Human CD14⁺ cells were isolated and differentiated to macrophages. The macrophages (left panel) and human peripheral blood mononuclear cells (PBMC) (right panel) were incubated with MOG34-56, MOG74-96, incomplete Freund's adjuvant (IFA), or lipopolysaccharide (LPS) (500 ng/ml). The supernatants were tested for the presence of IL-6, IL-12p40/p70, TNF- α and IL-1 β by ELISA. Data are shown from 1 of 2 experiments performed. B. Toll like receptor (TLR) activity of the MOG peptides was assessed in human endothelial kidney 293 (HEK293) cell lines stably transfected with human TLR2, TLR3, TLR4, TLR5, TLR7, TLR8, TLR9, and TLR10 and the NF- κ B luciferase reporter gene. The TLR expressing cell lines were incubated with the MOG peptides, IFA, or MOG plus IFA. Responses are expressed as fold increase of luciferase activity (mean \pm SD). Peptide-stimulated HEK293 cells are compared with unstimulated cells. Fold increases greater than 2 were considered positive. In both assays, the peptides and IFA did not reveal significant stimulatory activity. Data from 2 of 6 experiments are pooled.

Clinical disease

The intracutaneous injection of the peptide/IFA emulsion elicited only moderate redness at the injection sites attributable to a moderate inflammatory reaction to local injury of the injected skin. In the first experiment, 4 female marmoset monkeys were immunized with a mixture of equal amounts of MOG34-56 and MOG74-96 in IFA. In a second experiment, the same immunization protocol was repeated in 5 males (Experiment 2A). In parallel, another 5 males were immunized with only 100 µg MOG34-56 in IFA (Experiment 2B). Figure 2 shows that the 4 monkeys in experiment 1 had onset of clinical signs almost simultaneously around psd 85, i.e. shortly after the third rechallenge immunization. Disease development in the 5 animals in experiment 2A was more heterogeneous: One monkey (M06017) developed EAE after one rechallenge; two monkeys (M05056 and M05082) needed two rechallenges; and one monkey (M03162) needed three rechallenges before clinical disease (score ≥ 2.0) developed. One monkey (M06012) recovered within a few days after a short episode of neurological signs after the second rechallenge and maintained a mild EAE score of 0.5 for the remainder of the 160-day observation period.

The 5 animals immunized only with MOG34-56 in IFA (experiment 2B) also developed heterogeneous EAE courses consisting of hind limb paralysis and ataxia along with body weight loss. Because omission of MOG74-96 did not markedly alter the courses, this is consistent with our previous observation that MOG34-56 (given in CFA) was a more relevant Ag for EAE induction and progression. One monkey in this group (M05047) developed EAE after a single immunization. M06018 and 9847 needed two immunizations, and M06020 required three immunizations for development of overt neurological disease. M06006 recovered within a few days after a short episode of neurological signs after the second immunization. Thus, EAE can be induced in marmosets with a single MOG peptide in an adjuvant formulation that does not contain microbial compounds that stimulate innate antigen immune receptors.

Brain MRI

Increased signal intensity in T2W images of an EAE-affected marmoset brain recorded *in vivo* usually reflects edema caused by inflammation, whereas a hyperintense region in post mortem T2W images usually represents a demyelinated lesion^{127,241}. *In vivo* T2W brain images confirmed the presence of brain lesions in the two monkeys (M06012 and M06006) from experiment 2 that had exhibited relapsing/remitting disease but had scores of 0.5 at the time of necropsy (Figure 3A). At the MRI level, the lesions induced with MOG34-56 in IFA do not display marked differences from those induced using CFA¹⁹⁰.

High-definition T2W post mortem brain images of all 5 EAE monkeys induced with MOG34-56 in IFA displayed variable lesion loads (Figure 3B). In particular, there were numerous large and confluent lesions in monkey M05047 and M06006. The T2 hyperintensity was not confined to the white matter because it also affected leukocortical regions.

Histology and immunohistochemistry

Representative histological and immunohistochemical findings are shown in Figure 4. The brain and spinal cord sections showed many demyelinated lesions containing infiltrating CD3+ T-cells and activated macrophages. Proteolipid protein (PLP) and MRP14 staining in lesions showed macrophages containing degraded PLP products. Spinal cord sections also showed that staining for immunoglobulin overlapped with that of complement C9neo staining, a marker

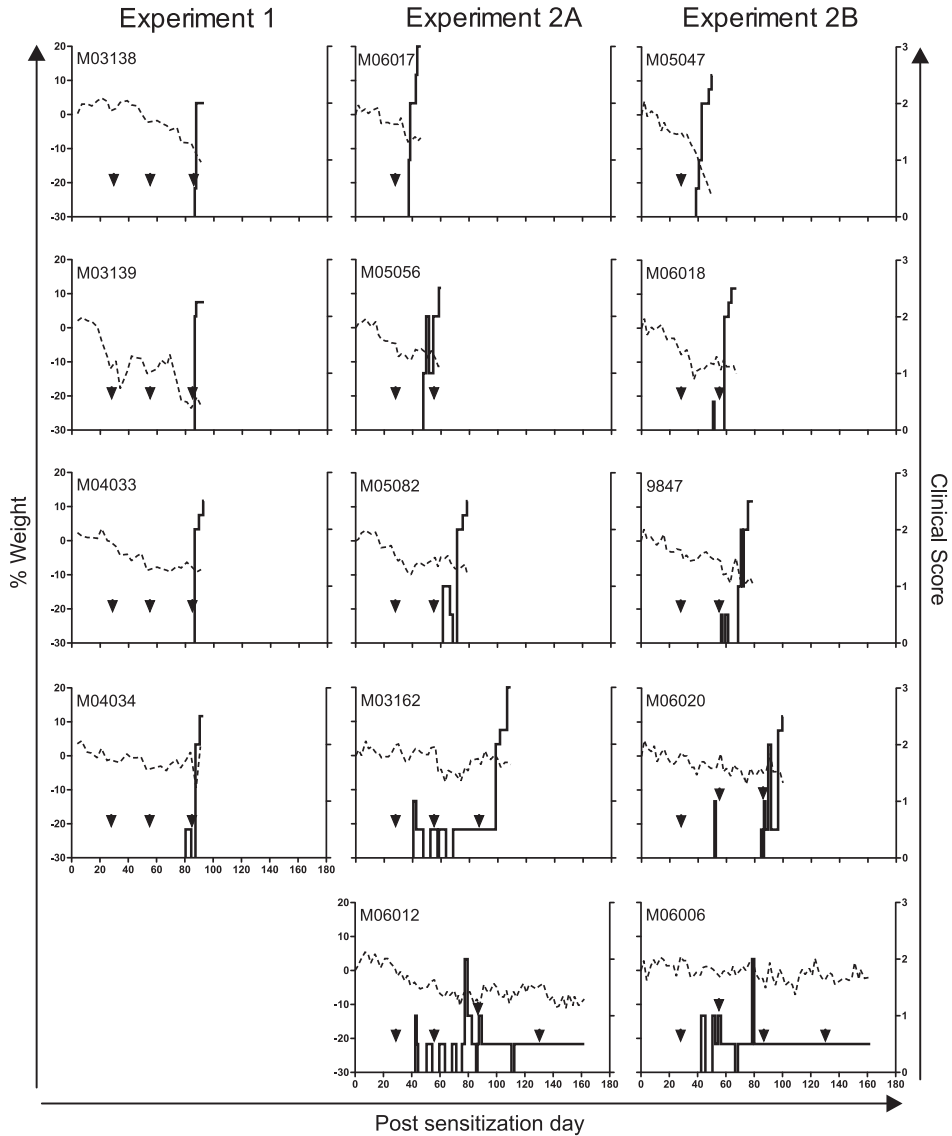


Figure 2. Monkeys immunized with MOG peptide in IFA all developed clinical EAE. In 2 experiments, 4 female (Experiment 1) and 5 male (Experiment 2A) marmosets were immunized with MOG34-56 and MOG74-96 emulsified in IFA (post sensitization day 0). A third group of 5 male monkeys was immunized with only MOG34-56 in IFA (Experiment 2B). At the indicated time points (arrows) challenges were given with the same antigen preparations. The graphs depict the clinical scores (right y-axis, solid line) and the percentage body weight loss compared with day 0 (left y-axis, dotted line).

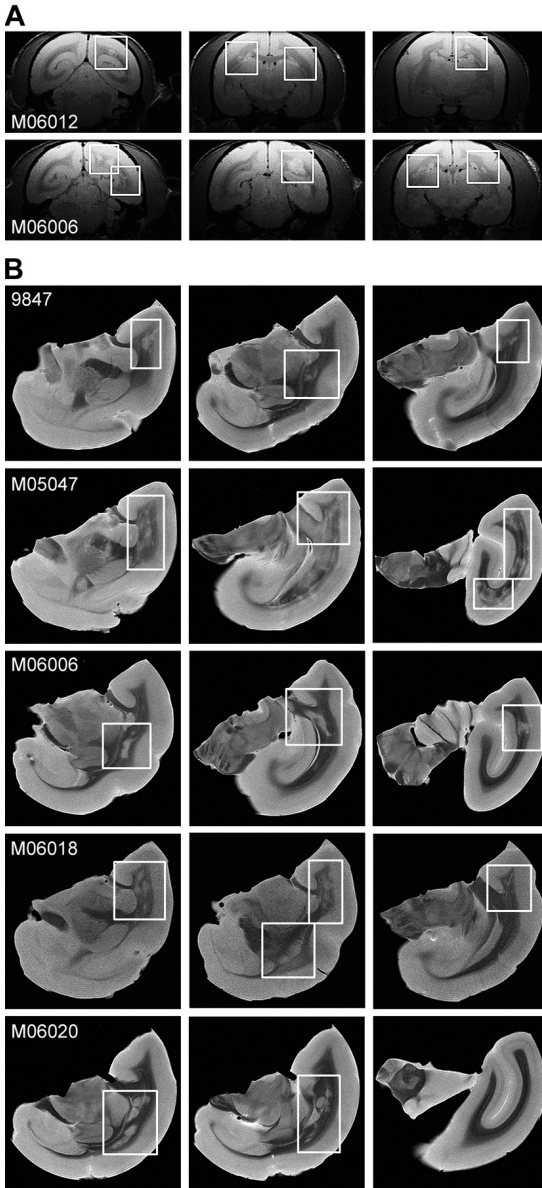


Figure 3. T2-weighted magnetic resonance brain images confirm inflammation despite clinical remission in 2 animals and show lesion load distribution in post mortem brains. Lesions framed in white lines are sharply demarcated areas of increased signal intensity. A. Brain imaging of the 2 monkeys that were in remission at the time of death (see Figure 2) demonstrated CNS white matter lesions before death. B. High-resolution T2-weighted images were made of complete formalin-fixed brains to assess the total lesion load.

of complement-mediated tissue injury. Thus, the lesions induced in monkeys immunized with MOG34-56 in IFA are highly similar to those induced by immunization with MOG34-56 in CFA¹⁹⁰.

T-cell reactivities and cytokine production

Immune parameter profiles varied among individual animals reflecting the genetic variation of this outbred model. Spleen and CLN drain the brain²⁴⁶, whereas ALN and ILN drain the peptide/

IFA inoculation sites. The MNC isolated from blood and lymphoid organs from the 4 animals in experiment 1 were tested for proliferation against MOG34-56, MOG74-96, and rhMOG (Figure 5A). In PBMC from 3 of 4 monkeys (except M03138), proliferation was detected against both MOG34-56 and MOG74-96; T-cell proliferation in PBMC against rhMOG was observed only in M04034. Spleen

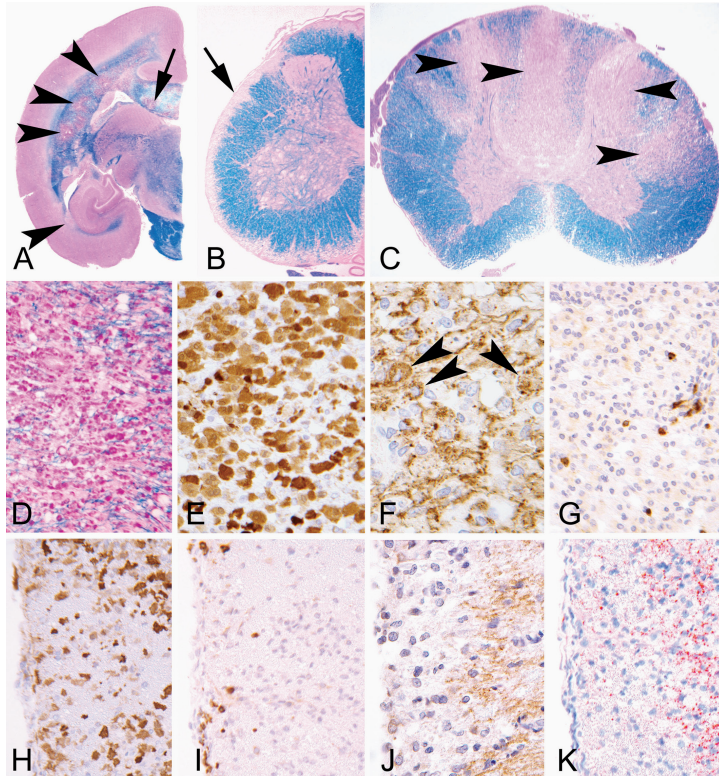


Figure 4. MOG34-56 in IFA induces demyelination and inflammation in brain and spinal cord. Hyperintense white matter areas that were detected in T2-weighted images were analyzed with histology and immunohistochemistry. Brain of M05047 (A, D-G) and spinal cord of 9847 (B,C, H-K) are shown as representatives. A. Luxol fast blue-Periodic acid-Schiff (LFB-PAS) staining (original magnification x4) shows multiple large demyelinating lesions (arrowheads). The lesion in the corpus callosum (arrow) is enlarged in figures D-G. B. Subpial demyelination in spinal cord demonstrated with LFB-PAS (original magnification x25). The arrow indicates the area enlarged in H-K. C. Multiple large focal lesions are also seen in the spinal cord (arrowheads; original magnification x25). D. Enlargement of the area indicated with arrow in panel A. LFB-PAS (original magnification x125) staining shows late active demyelination and the presence of PAS-positive macrophages. E. Macrophage immunostaining using the macrophage marker MRP14 (original magnification x400). F. Immunostaining for myelin PLP (original magnification x500) shows macrophages containing phagocytosed PLP positive fragments (arrowheads). G. Immunostaining for CD3 (original magnification x200) shows that the lesions contain few T-cells. H-K. (original magnification x200) H, Subpial spinal cord area immunostained for MRP14 shows the presence of macrophages. I, CD3 immunostaining shows some meningeal T lymphocytes. J, K, Staining for immunoglobulin (J) reveals deposition in a pattern that overlaps with that of complement factor C9neo (K).

MNC from monkey M03139 showed reactivity against the tested MOG peptides, and proliferation against rhMOG was detected only in M03139 and M04033. Proliferation responses in MNC from the pooled lymph nodes paralleled those in PBMC. In 9 of the 10 monkeys from experiment 2, proliferation against the immunizing peptide(s) was detected in at least one of the analyzed compartments, but no T-cell proliferation was detected in monkey M05056 (Figure 5A).

We next analyzed the T-cell phenotypes of the cells that displayed specific proliferation against MOG34-56. In the model induced with MOG34-56/CFA, the main proliferation response against MOG34-56 mapped to a subset of CD3+ T-cells expressing CD4 and/or CD8 in combination with CD56¹⁹⁰. Specific proliferation of T-cells in PBMC, spleen, and ALN against MOG34-56 was mainly observed in the CD4/CD8 double-positive fraction with or without CD56 expression (Figure 5B). However, ALN also showed increased proliferation of CD3+CD4+ and CD3+CD4+CD56+ cells. The highest T-cell proliferation was observed in the spleen and ALN compared with the PBMC.

Freshly isolated PBMC, spleen, and ALN cells were stimulated for 48 h with rhMOG and overlapping MOG peptides, after which culture supernatants were collected for detection of IL-17A, IFN- γ , and TNF- α cytokine levels (Figure 6). In experiment 2A, a high level of the Th17 signature cytokine IL-17A was measured in spleen cell cultures of all animals after stimulation with rhMOG

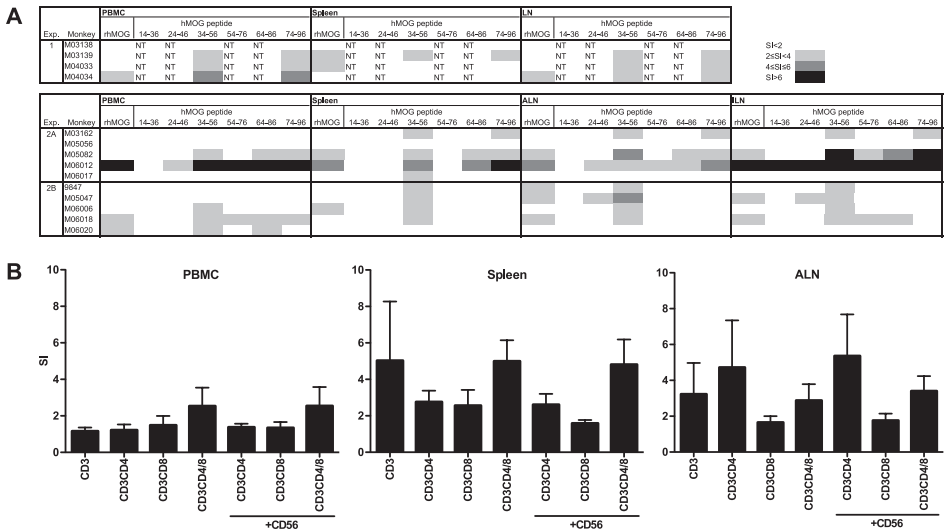


Figure 5. *Ex vivo* MOG34-56 stimulation induces proliferation in the CD3+CD4+/CD8+CD56+ fraction. Mononuclear cells (MNC) from blood, spleen, axillary lymph nodes (ALN), and inguinal lymph nodes (ILN) were collected at necropsy and tested for *ex vivo* reactivity with recombinant human MOG and the panel of 23-mer overlapping MOG peptides. A. Proliferation was determined by [³H]-thymidine incorporation and expressed as stimulation index (SI) relative to unstimulated cultures. Data are presented in graded grey scale. B. CFSE labelled MNC of animals in experiment 2 were cultured for 7 days with MOG34-56. Harvested cells were analyzed by flow cytometry to determine phenotype of MOG34-56-reactive cells. Data were pooled from monkeys that displayed clinical signs at the time of sacrifice (n=8). Mean ± SEM is given for each subset. SI greater than or equal to 2 is considered significant. NT, not tested.

or MOG34-56 and in 3 of 5 monkeys after MOG74-96 stimulation. IL-17A was produced only in PBMC cultures of M06012; in 3 monkeys, we observed production by ALN cells. In experiment 2B, there was marked IL-17A production from rhMOG-stimulated PBMC of 2 monkeys (9847, M06006), in spleen cell cultures of 3 monkeys (9847, M06018, and M06020) upon stimulation with rhMOG and MOG34-56, and in ALN cells of 2 monkeys (9847 and M06020) after stimulation with MOG34-56 and/or rhMOG. Variable profiles of IFN- γ and TNF- α production were detected in all 3 groups, i.e. they were absent in ALN cells cultures and present in PBMC and in spleen cell cultures of only some monkeys.

T-cell lines

TCL were generated from spleen and ALN against MOG34-56 and MOG74-96. There were high expansion rates of TCL specific for MOG74-96, whereas those against MOG34-56 collapsed after a few (range 4-6) restimulations. One possible explanation for this may be that MOG34-56 T-cells killed the peptide-presenting B-LCL APC; this is similar to MOG-specific T-cells from MS patients¹³⁷.

The specific cytolytic activity of MOG34-56 and MOG74-96 TCL was tested using autologous ⁵¹Chromium-labeled B-LCL presenting either peptide. The MOG34-56-induced TCL lysed target cells pulsed with MOG34-56 more effectively than they lysed target cells pulsed with MOG74-96 (Figure 7A). Conversely, MOG74-96-induced TCL lysed target cells pulsed with MOG74-96 more effectively than those pulsed with MOG34-56. Cytolysis was completely abrogated when the T-cells were preincubated with concanamycin A (Figure 7B), indicating that the cytolytic activity is largely dependent on granule exocytosis²⁷⁸.

These data show that immunization with MOG34-56 activates CD4+ and CD8+ T-cells, including CD3+CD56+ cells expressing both CD4 and CD8. Bulk cultures stimulated with MOG34-56 display specific cytolytic activity toward peptide-pulsed B-LCL and produce a higher

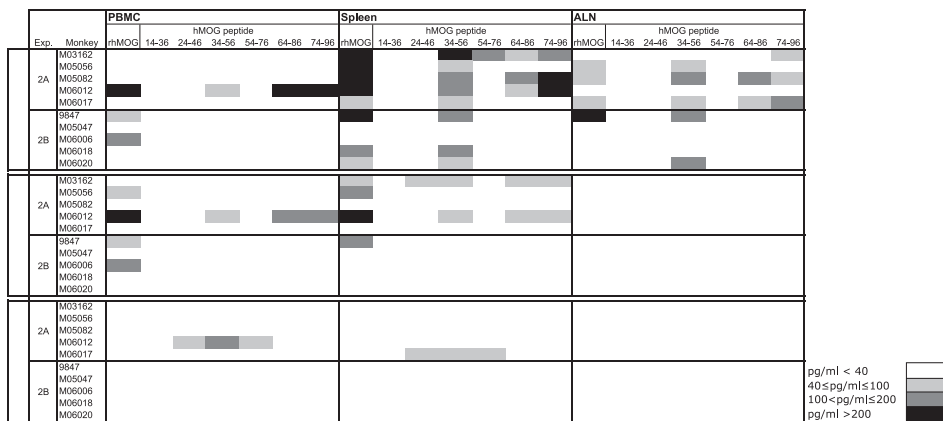


Figure 6. *Ex vivo* production of IL-17A, TNF- α , and IFN- γ by rhMOG and MOG peptide-stimulated mononuclear cells (MNC). MNC from blood, spleen, and axillary lymph nodes (ALN) from experiment 2A and 2B monkeys were cultured for 48 h with rhMOG and a panel of MOG peptides. Culture supernatants were tested for the presence of the cytokines.

level of the Th17 signature cytokine IL-17A than of the Th1 signature cytokine IFN- γ . Whether these activities are all exerted by the same subset of T-cells remains to be determined.

Autoantibody response

Plasma samples were tested for the presence of IgG binding to plate-bound rhMOG or overlapping sets of MOG peptides (Figure 8A). Figure 8B shows anti-MOG IgG levels in necropsy plasma. All monkeys in experiment 1 and 2A, immunized with MOG34-56 and

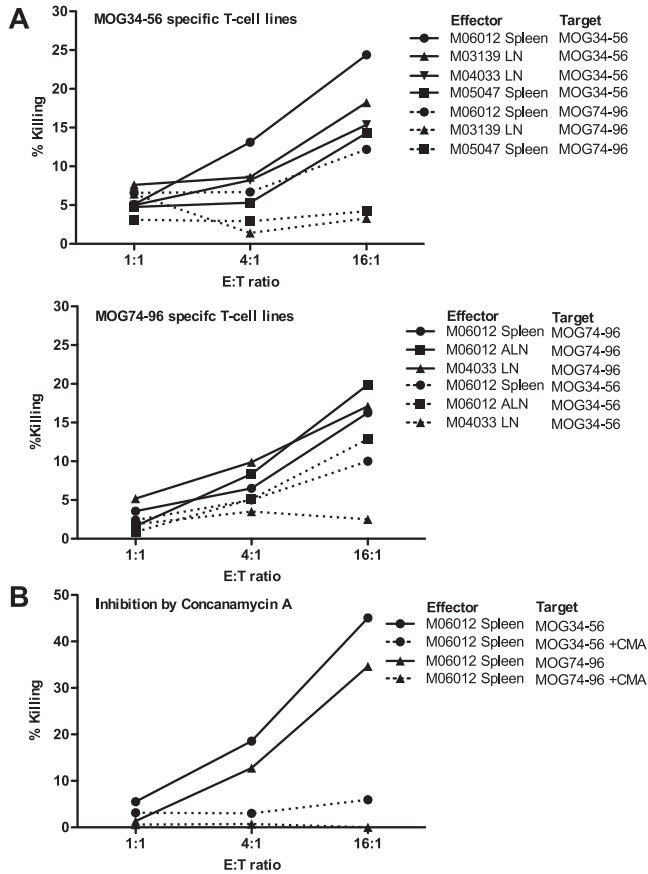


Figure 7. MOG-peptide reactive T-cell lines have cytolytic activity that can be blocked by concanamycin A. Short-term T-cell lines against MOG34-56 and MOG74-96 were obtained from spleen, axillary lymph nodes (ALN), and pooled lymph nodes (LN) by stimulation with peptide-pulsed autologous Epstein-Barr virus (EBV)-transformed B-cells. A. Cytolytic activity of specific T-cell lines (effector cells [E]) was tested using ⁵¹Chromium-labeled EBV-transformed B-cells as target cells (T) that were pulsed with MOG34-56 or MOG74-96 or without antigen. Specific lysis of target cells is expressed in percentage killing. Dotted lines indicate background killing with irrelevant peptide. The cytolytic activity of MOG34-56-induced lines is peptide-specific. B. Before cytotoxicity testing, the effector cells were incubated with concanamycin A (CMA) to inhibit cytolytic activity based on granule exocytosis²⁷⁸.

MOG74-96, showed IgG reactivity with MOG24-46, MOG34-56, and MOG64-86. In all 4 female monkeys in experiment 1, serum IgG reactivity was directed against rhMOG, but not to MOG74-96. Remarkably, sera from monkeys in experiment 2A also contained IgG against MOG74-96, but IgG binding with rhMOG was only observed in M03162 and M06012, albeit at a low levels. Interestingly, necropsy plasma of 2 monkeys from experiment 2A contained IgG against MOG54-76, a dominant B-cell epitope in the rhMOG-induced EAE model (Figure 8B)¹⁰³. Because the overlap of this peptide with MOG34-56 is only marginal (i.e. 2 amino acids), this Ab specificity was likely generated in response to demyelination. Sera from marmosets sensitized against MOG34-56 alone (Experiment 2B) only showed reactivity to the immunizing peptide and the overlapping peptide MOG24-46. There were no detectable IgG Ab levels against rhMOG, demonstrating that in monkeys immunized with MOG34-56/IFA, production of autoantibodies binding to MOG protein was not a requirement for mediating demyelination¹³³.

DISCUSSION

We report here that 14 of 14 marmosets from an outbred colony develop overt clinical EAE associated with CNS inflammation, demyelination, and axonal damage upon sensitization against MOG34-56 in IFA or MOG34-56 combined with the nonencephalitogenic peptide MOG74-96 in IFA.

Although CFA is a powerful tool for EAE induction, there are also several major disadvantages. It is notorious for the induction of granulomas at inoculation sites and in body organs (liver, lung), causing serious discomfort to immunized animals. The potent systemic stimulatory effect of CFA also causes a strong enlargement of lymphoid organs, haemopoietic dysfunction, and disruption of lymph node architecture^{279, 280}. CFA also has a strong systemic immune-stimulatory effect mediated by its component mycobacteria that may overwhelm more subtle immune regulatory mechanisms, such as causing Th1 skewing of cellular autoimmune reactions²⁷⁹. Collectively, these arguments warrant the determination of whether use of CFA is mandatory for induction of EAE in marmosets or if it can be replaced with the less noxious Ag formulation with IFA.

Immune profiling of the marmosets that were immunized with MOG peptides in IFA revealed induction of cellular and humoral autoreactivity against the sensitizing peptide as well as rhMOG protein in several cases. These results imply that EAE induction in this new EAE model relies on the activation of adaptive immune mechanisms without the need for simultaneously activating innate immune mechanisms by microbial compounds in the inoculum, as is required in rodent models. These findings suggest that the activation requirements for MOG34-56-reactive T-cells present in the mature immune repertoire of adult (2 – 5 years) marmosets living under conventional conditions differ profoundly from those for the activation of MOG34-56-reactive T-cells present in the immature repertoire of young-adult (8 – 12 weeks) specific pathogen free-laboratory mice.

Our *in vitro* experiments confirm that the components of the peptide/IFA inoculum lack innate immune stimulatory activity via receptors for pathogen-associated molecular patterns, such as TLR and Nodlike receptors, which relay danger signals to engage innate immune activation of APC. However, we cannot conclude that EAE induction in this model occurs entirely without involvement of innate immune mechanisms. Quite obviously, APC present at the

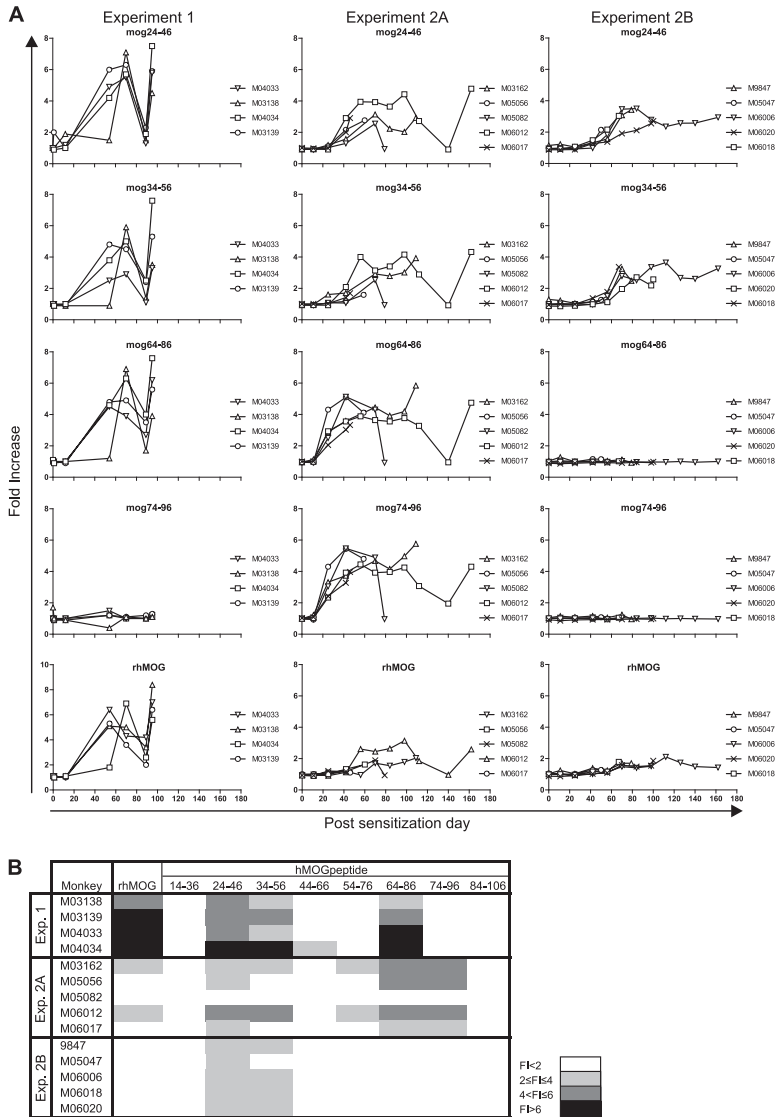


Figure 8. Plasma IgG antibody binding to MOG peptides and rhMOG. IgG antibody levels in plasma samples collected from monkeys immunized with MOG34-56 and MOG74-96 (experiment 1 and 2A) or with only MOG34-56 (experiment 2B). Antibody responses were measured by ELISA to rhMOG and a panel of overlapping MOG peptides in plasma samples collected every 4 weeks during the entire study (A) and at necropsy (B). IgG responses are expressed in fold increase; plasma levels are compared with preimmune plasma. Fold increase greater than 2 is considered positive.

injection site of the peptide/IFA emulsion can be activated by danger signals released from the injured skin and from the IFA action. Unlike the EAE model induced with CFA, however, the autoreactive T-cells would have to migrate from the lymph nodes where they are activated to the CNS in the absence of the strong systemic innate immune activation signals elicited by CFA. This might be explained by a recent report that IL-17A producing CCR6+ T-cells have the capacity to enter the resting noninflamed CNS via the choroid plexus and the cerebrospinal fluid⁵⁸. Interestingly, IL-17A producing T-cells are prominent in the MOG34-56/IFA induced EAE model but seem less prominent in the Th1-dominated models induced with CFA^{103, 268}. Our serial brain MRI studies demonstrate that the first signs of cerebral inflammation in MOG34-56/IFA immunized monkeys are often detected around the lateral ventricles is noteworthy in this context (data not shown).

The observation that autoantibodies against intact MOG are not directly involved in the generation of demyelination in monkeys immunized with only MOG34-56 in IFA is another discrepancy between the CFA-independent and CFA-dependent EAE model in marmosets and rodents. Although Ab against the immunizing peptides were consistently found in the current study, we detected Ab binding to non-glycosylated recombinant MOG1-125, a prerequisite for demyelination, only in some animals²⁶⁸. This was clearly demonstrated by von Büdingen et al^{268, 281} who reported that immunization with (pooled) MOG peptides in CFA, supported by intravenous *Bordetella pertussis* particles, incited only mild inflammatory EAE in marmosets. Induction of robust EAE associated with demyelination required supplementary infusion of Ab against conformational MOG epitopes²⁶⁸.

The close immunologic similarities between humans and marmosets suggest parallels between T-cell mediated immunopathogenic processes between MS and the MOG34-56/IFA induced EAE model. The phenotype (CD3+CD4/8+CD56+) and cytolytic activity of the MOG34-56-reactive marmoset T-cells are reminiscent of the finding of CD4+CD56+ cytolytic T-cells in MS patients, although they may use a different cytotoxic mechanism. Cytolysis of human oligodendrocytes was found to be major histocompatibility complex (MHC)-independent^{269, 270} and to involve interaction of NKG2D on CD4 cells with NKG2D ligands (MICA/B) on the target cells²⁸². By contrast, the peptide-specific and concanamycin A-sensitive cytolytic activity of the marmoset T-cells suggests that the cytolytic mechanism resembles that of classical MHC class I-restricted cytotoxic T-cells. Interestingly, another group reported that MOG-reactive T-cells cloned from blood of MS patients, but not those from the blood of healthy controls, display cytolytic activity towards autologous target cells pulsed with MOG peptides 1-22, 34-56, and 74-96¹³⁷. Although oligodendrocytes normally lack detectable MHC expression, MHC class I molecules are induced under inflammatory conditions rendering them as potential targets for killing by CD3+CD8+ cytotoxic T-lymphocytes in EAE and MS²⁸³.

In conclusion, we present a new EAE model in which MS-like clinical disease and pathological alterations are induced by immunization with a single peptide formulated with IFA. This novel model represents a major improvement for ethical, practical, and mechanistic reasons. First, the model definitively proves that the presence of microbial ligands for innate antigen receptors in the inoculum is not essential for induction of autoimmune disease in a species closely related to man. Second, replacement of CFA with IFA substantially reduces the discomfort to the animals, a central aim of biomedical research in non-human primates²⁸⁴. Third, the model is more useful for the study of the subtle regulatory networks that keep autoreactive

T- and B-cells in check and maintain homeostasis within the CNS because these are often overwhelmed by the strong systemic Th1-skewed immune stimulation by the bacterial Ag in CFA. Fourth, refinement of the model by use of IFA may reduce the attrition rate of experimental therapies by reducing the occurrence of both false-positive and false-negative studies. As an example, the disappointing effect of anti-IL-12p40 Ab (ustekinumab) therapy in MS²⁸⁵ contrasts sharply with the impressive results obtained in two marmoset EAE models^{244, 266}. In retrospect, it seems possible that these remarkably discrepant effects might be explained by the Th1-skewing effect of CFA (which is absent in MS) on the immunopathogenic process. Finally, preclinical immunotherapy studies with novel biologicals targeting immunity in EAE models induced are often hampered by the strong stimulation of neutralizing Ab formation by CFA. This complication is removed in our new model. Based on the latter two arguments, we believe that the new model is highly useful for immunotherapy development.

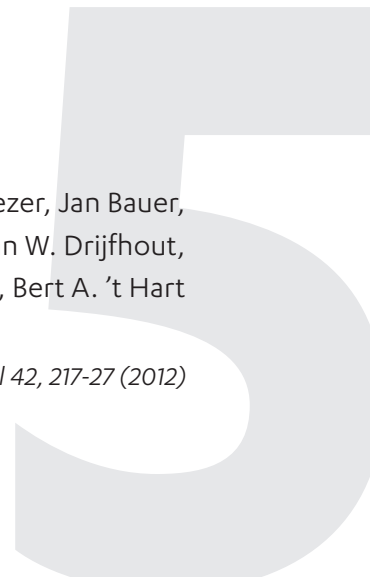
ACKNOWLEDGEMENTS

We thank Fred Batenburg Mariska van Etten and Tom Haaksma for their excellent biotechnical assistances. Prof. Rogier Q. Hintzen (MS neurologist at the Erasmus Medical Center and MS Centre ErasMS Rotterdam) is thanked for critical reading of the manuscript. The study was supported by a grant from the European Committee under framework program 6, contract number QLRI-CT-2002-02758 (EUPEAH; Glucocorticoid hormone programming in early life and its impact on adult health). The authors also acknowledge fruitful discussions within the COST Action BM0603 Inflammation in Brain Disease Neurinfnet, and networking support from COST.

**UNRAVELLING THE T-CELL MEDIATED
AUTOIMMUNE ATTACK ON CNS MYELIN IN A NEW
PRIMATE EAE MODEL INDUCED WITH MOG34-56
PEPTIDE IN INCOMPLETE ADJUVANT**

S. Anwar Jagessar, Nicole Heijmans, Erwin L. A. Blezer, Jan Bauer,
Jeroen H. Blokhuis, Jacqueline A. M. Wubben, Jan W. Drijfhout,
Peter J. van den Elsen, Jon D. Laman, Bert A. 't Hart

Eur J Immunol 42, 217-27 (2012)



ABSTRACT

Induction of experimental autoimmune encephalomyelitis (EAE) has been documented in common marmosets using peptide 34-56 from human myelin/oligodendrocyte glycoprotein (MOG34-56) in incomplete Freund's adjuvant (IFA). Here, we report that this EAE model is associated with widespread demyelination of grey and white matter. We performed an in-depth analysis of the specificity, MHC restriction and functions of the activated T cells in the model, which likely cause EAE in an autoantibody-independent manner. T-cell lines isolated from blood and lymphoid organs of animals immunized with MOG34-56 displayed high production of IL-17A and specific lysis of MOG34-56-pulsed EBV B-lymphoblastoid cells as typical hallmarks. Cytotoxicity was directed at the epitope MOG40-48 presented by the non-classical MHC class Ib allele Caja-E, which is orthologue to HLA-E and is expressed in non-inflamed brain. *In vivo* activated T cells identified by flow cytometry in cultures with MOG34-56, comprised CD4+CD56+ and CD4+CD8+CD56+ T cells. Furthermore, phenotypical analysis showed that CD4+CD8+CD56+ T cells also expressed CD27, but CD16, CD45RO, CD28 and CCR7 were absent. These results show that, in the MOG34-56/IFA marmoset EAE model, a Caja-E-restricted population of autoreactive cytotoxic T cells plays a key role in the process of demyelination in the grey and white matter.

INTRODUCTION

Multiple sclerosis (MS) is a chronic inflammatory disease of the human central nervous system (CNS) of unknown etiology. The pathological hallmark of MS is the lesion. Lesions are regions of usually focal demyelination of variable size localized in the grey and/or white matter of the brain and spinal cord, formed by a combined cellular and humoral autoimmune attack. CNS-targeting autoimmune reactions are thought to be induced as a response to infection (response-to-infection paradigm)²⁸⁶, although the pathogen(s) that elicit this pathogenic process in MS has not been identified. We have proposed a response-to-damage paradigm for MS, based on the work in a unique non-human primate model of MS, experimental autoimmune encephalomyelitis (EAE) in common marmosets (*Callithrix jacchus*)¹²⁸. The new concept postulates that autoimmunity in MS patients is caused by a genetically predisposed hyper-response to myelin antigens released from damaged white matter due to an unknown antecedent event. We showed that the most important anti-myelin reactivity for the induction of neurological deficit is mediated by antigen-experienced T-cells specific for peptide 34-56 of myelin/oligodendrocyte glycoprotein (MOG34--56)²⁸⁷. Subsequently it was demonstrated that these cells could be activated *in vivo* by immunization of marmosets with MOG34--56 in incomplete Freund's adjuvant (IFA)²⁸⁸.

A peptide in IFA emulsion is a more common formulation for the *in vivo* activation of antigen-experienced T-cells than for autoreactive T-cells as bacterial ligands of innate antigen receptors are usually required. It is noteworthy that MOG34-56-specific CD4+ T-cells identified in MS patients also display antigen-experienced characteristics²⁸⁹. The aim of the current study was therefore a more in-depth characterization of the T-cells that are activated in this new model, with a focus on specificity, MHC restriction and functional analysis.

Despite the immunological proximity of marmosets and humans, some fundamental differences exist at the level of the major histocompatibility complex, a polymorphic region encoding the molecules that present antigens to T-cell receptors. The MHC class I region of marmosets lacks the genes encoding the equivalents of the human classical MHC class I molecules HLA-A, -B and -C, but a polymorphic Caja-G (multiple alleles) and an oligomorphic Caja-E locus (two alleles) have been identified^{195, 290}. Hence, we hypothesized that peptides processed from MOG34-56 are presented by the non-classical MHC class Ib molecules Caja-G or Caja-E to antigen-specific cytotoxic T lymphocytes.

MATERIALS AND METHODS

Antigens and peptides

Synthetic MOG peptides used for immunization and for *in vitro* experiments were purchased from Cambridge Research Biochemicals Limited (Cleveland, UK) or were produced in house (JWD, Leiden University Medical Center, Leiden, The Netherlands). The amino acid sequences of all peptides used in this study are summarized in Table 1. Recombinant human myelin/oligodendrocyte glycoprotein (rhMOG), residues 1-125, purified from *E. coli* was produced in the BPRC laboratory as previously described^{93, 138}.

Induction of EAE and post-mortem examination

EAE was induced with 100 µg of MOG34-56 emulsified in IFA. As previously described the inoculum was injected into the dorsal skin at the inguinal and axillary regions²⁸⁸. All animals were daily monitored for neurological symptoms using a standard scoring system, as described before²⁸⁸. Briefly, 0 = no clinical signs; 0.5 = apathy, loss of appetite, altered walking pattern without ataxia; 1 = lethargy, anorexia, loss of tail tonus, tremor; 2 = ataxia, optic disease; 2.5 = paraparesis or monoparesis, sensory loss; 3 = paraplegia or hemiplegia; 4 = quadriplegia; 5 = spontaneous death due to EAE. The clinical endpoint for each monkey was EAE score 3. Monkeys reaching this score were first deeply sedated by intramuscular injection of Alfaxan (10 mg/kg) (Vétoquinol S.A., Magny-Vernois, France). After collection of the maximum venous blood volume, they were euthanized by infusion of sodium pentobarbital (Euthesates®; Apharmo, Duiven, The Netherlands).

At necropsy the brain and spinal cord were removed. Secondary lymphoid organs aseptically removed for preparation of mononuclear cells (MNCs) were: axillary (A), inguinal (I), lumbar (L), cervical (C) lymph nodes (LNs) and spleen.

According to the Dutch law all experimental procedures were reviewed and approved by institute's animal experiment committee.

Magnetic resonance imaging

High-contrast post-mortem magnetic resonance images (MRIs) were recorded of one cerebral hemisphere on a 9.4 T horizontal bore NMR spectrometer (Varian, Palo Alto, CA, USA), equipped with a quadrature coil (RAPID, Biomedical, Rimpf, Germany) as previously described²¹⁵. In addition, an inversion recovery experiment was performed in which the signal from the white matter was suppressed, white matter attenuated inversion recovery (WAIR), enabling the visualization of grey matter lesions (fast spin echo, echo train length = 8, echo spacing = 8.93 ms, effective TE = 17.86 ms; TR = 4050 ms; inversion time for white matter suppression was empirically determined per sample and was approximately 350-375 ms).

T-cell proliferation

MNCs were prepared every 2 wk from heparinized blood (PBMCs) or at necropsy from spleen and lymph nodes; ALNs, ILNs, LLNs and CLNs. PBMCs and MNCs were tested for proliferation against a panel of overlapping MOG peptides (10 µg/mL) and rhMOG (10 µg/mL)²⁶³. Proliferation is expressed as stimulation index (SI), being ³H-thymidine incorporation in the stimulated versus unstimulated cultures. SI values above 2.0 were considered positive.

Flow cytometry

T-cell lines against MOG34-56 were generated from spleen and ALNs as previously described¹⁹⁰. Part of the cells were phenotyped with monoclonal antibodies that were pre-selected for cross-reaction with the marmoset²¹⁶: anti-CD4 clone MT310 (Dako, Glostrup, Denmark), anti-CD8 clone LT8 (Serotec, Düsseldorf, Germany), anti-CD3 clone SP34-2, anti-CD56 clone NCAM16-2, anti-CD16 clone 3G8, CD27 clone M-T721 (BD Biosciences, San Diego, CA, USA), CD28 clone CD28.2, CD45RO clone UCHL1, CCR7 clone 150503 (R&D systems, Oxon, UK). For detection of HLA-E or Caja-E expression the anti-MHC class I antibody clone W6/32 (DAKO) was used. Flow

cytometric analysis was performed on an FACS LSRII flow cytometer using FACSDiva software 5.0 (BD Biosciences) or FACSCalibur using CellQuest.

Cytotoxicity assay

Specific T-cell lines against MOG34-56 generated from spleen and ALNs were used as effector cells in a cytotoxicity assay. Autologous or allogeneic ⁵¹Chromium-labelled EBV-transformed B-lymphoblastoid (B-LCLs) were pulsed for at least 1 h at 37°C with MOG peptides and used as target cells as previously described^{190,288}.

Cytokine profiling

Supernatants of PBMCs were collected after 48 h stimulation with rhMOG or a panel of overlapping MOG peptides. Supernatants were assayed for the presence of cytokines using commercial ELISA kits following the manufacturer's instruction or as described previously²⁸⁸.

RNA extraction and RT-PCR

Total RNA was extracted from PBMCs and snap-frozen brain material using the RNeasy mini kit from Qiagen (Hilden, Germany). Isolated RNA was used for reverse transcriptase-PCR on an aliquot (3 µL) of each sample for 25 cycles with Caja-E and Caja-G-specific primers: Caja-E; FW 5'-GCCAGGGACACCGCACAGAG-3', RV 5'-AGAAACCCAGG GCCCAGCAT-3'. Caja-G; FW 5'-GCAAGCTTATGACGGTCATGGCTCCCCGAA-3', RV 5'-CAAGCCGTGAGAGACACATCA-GAGCCCTG-3'. As an internal control the housekeeping gene G3PDH was used; FW 5'-TGAAG-GTCGGAGTCAACGGATTTGGT-3'. RV 5' CATGTGGCCATGAGGTCCACCAC-3'. See manufacture of AccesQuick™ RT-PCR System (Promega, Madison, WI, USA) for RT-PCR conditions. PCR products were analysed by electrophoresis on a 1.2% agarose gel. Bands of interest were purified according to the Qiaquick gel extraction kit (Qiagen, Hilden, Germany) and sequenced on an ABI 3130xl genetic analyser (Applied Biosystems, Foster City, CA, USA) as described²⁹¹.

Caja-E transfection into K562

K562 cells, a human erythroleukemia cell line which lacks MHC class I and II, was transfected with Caja-E*01 (FW 5'-CACCATGTAGCCCCGAAGCCTCCTCTTGCTG-3', RV 5'-TCAGACTTTACAACCTGTGAGAGACAC-3') according to the manufacturers instruction using the pcDNA™3.1 directional TOPO® expression kit (Invitrogen, Carlsbad, CA, USA). Briefly, 1 µL PCR product was blunt-end ligated into the pcDNA™3.1/V5-His-TOPO® vector and incubated for 5 min at RT. As a positive control vector pcDNA™3.1D/V5-HisD/lacZ was used. Subsequently, the construct was transduced into One Shot® TOP10 chemically competent E. coli at 42°C for 30 s. The transduced cells were plated on LB selection plates containing 50 µg/mL ampicillin and incubated overnight (o/n) at 37°C. The following day, a minimum of 24 clones were scaled up in LB+ampicillin medium o/n at 37°C. Plasmid DNA was extracted from E. coli and purified based on the alkaline lysis method (QIAprep spin miniprep kit). To confirm that Caja-E was cloned in the correct orientation, the construct was sequenced (ABI 3130xl genetic analyser). Constructs containing correctly inserted genes were scaled up to large quantity and plasmid DNA was isolated using the QIAGEN EndoFree plasmid maxi kit. Plasmids were transfected into K562 cells by electroporation using the AMAXA Nucleofector kit V for cell lines (Lonza Cologne AG, Cologne, Germany) and transfected cells were grown in IMDM medium (Gibco, Glasgow,

UK) in the presence of 200 µg/mL G418 (Gibco). After one day the cells were incubated with anti-MHC class I antibody (W6/32) conjugated to PE, and positive selection was performed with anti-PE MACS separation beads (Miltenyi Biotec, Bergisch Gladbach, Germany). Limiting dilution assay (1 cell/well in 96-well plate) was performed to select the best-transformed cells. Expression of Caja-E on the K562 cells was confirmed with anti-MHC class I antibody, (W6/32; DAKO) and anti-HLA-E clone MEM/07 (Abcam, Cambridge, UK).

K562 cells transfected with HLA-E*01033 (HLA-Eg) and the mock-transfectants, used as the negative control (pcDNA3), were kindly provided by Prof. Dr. H. Weiss (Department of Biology II, Ludwig-Maximilians-Universität München, Germany).

HLA-E/Caja-E binding assays

Direct assay K562

Caja-E or HLA-E transfectants were incubated o/n at 26°C with a selected panel of peptides (see Table 1). Then the cells were incubated for 1 h at 37°C to allow degradation of unoccupied MHC class I molecules. Residual expression of MHC class I molecules was visualized by staining with PE-labelled MHC class I antibody, clone W6/32 (DAKO). Binding of W6/32 was measured by FACS LSRII or FACSCalibur flow cytometer.

Table 1. Synthetic peptides based on the human MOG sequence.

Peptide	Amino acid sequence
MOG 13-21	ALVGDAVEL
MOG 31-39	NATGMEVGV
MOG 34-42	GMEVGWYRP
MOG 34-56	GMEVGWYRPPFSRVVHLYRNGKD
MOG 37-45	VGWYRPPFS
MOG 40-48	YRPPFSRVV
MOG 42-50	<u>S</u> PF SRV VHL ^{a)}
MOG 43-51	PFSRVVHLY
MOG 46-54	RVVHLYRNG
MOG 49-57	HLYRNGKDQ
MOG 52-60	RNGKDQDGD
MOG 75-83	DIGEGKVTL
MOG 105-113	YQEEAAMQL
HLA-G leader	VMACRTLVL ^{b)}
HCVcore34-55	LLPRRGPR ^{b)}

^{a)}In the marmoset and mouse MOG sequences, position 42 is occupied by S, whereas in human MOG this position is occupied by P.

^{b)}Peptides labelled with the fluorescent dye fluorescein

Indirect assay

K562 Caja-E or HLA-E transfectants were incubated for 4 h at 26°C with a dose range of unlabelled peptides (3 μM – 300 μM). Subsequently, a fixed concentration (5 μM) of fluorescently labelled indicator peptides with known binding capacity to HLA-E (HLA-G leader²⁹² or HCV35-44²⁹³) was added to the cells and incubated o/n at 26°C. Subsequently, cells were incubated for 1 h at 37°C to allow degradation of unoccupied MHC class I molecules. Residual expression of MHC class I molecules was tested by measuring the amount of bound fluorescently labeled peptide and with PE-labelled W6/32 staining.

Immunohistochemistry and histology

Cryosections of 6 μm thick were made from snap-frozen brains and immuno-labelled for specific markers as described previously. Slides were stained for CD3 (clone sp34-2, BD Biosciences), CD4 (home-made mix of OKT4, OKT4a, RIV6, RIV7 and MT-310), CD8-biotin (clone LT8, Serotec, Düsseldorf, Germany) and laminin (DAKO). Formalin-fixed brains were used for histological examination as described^{127, 263}.

Statistical analysis

Where possible data were analysed using the Mann–Whitney *U* test; *p*-values < 0.05 are considered to be significant.

RESULTS**Clinical and pathological aspects of EAE induced with MOG34-56/IFA**

Five unrelated marmoset monkeys were immunized with MOG34-56 in IFA at 28 day intervals until clinically evident EAE (score \geq 2.0) developed. Clinical scores (Fig. 1A) show that 4 out of 5 animals developed clinically evident EAE, whereas in one monkey (Cj1) only mild EAE symptoms were observed. Data of all animals are pooled and presented in a survival curve (Fig. 1B) showing time to EAE score 2.0 and time to necropsy. High-resolution T2-weighted and magnetization transfer ratio images showed in four monkeys the presence of white matter lesions (Fig. 1C), which were characterized with respect to the severity of inflammation and demyelination²⁴¹. A detailed histological characterization of the white matter lesions in this model has been published elsewhere²⁸⁸. While most lesions were located in the white matter, also cortical grey matter lesions were detected in Cj3 and Cj4.

T-cell localization within white matter lesion

Serum antibodies binding were detected to MOG34-56, but not to rhMOG (data not shown). Hence, we hypothesized that lesions are induced by MOG34-56-specific T-cells. To examine the presence of T cells in early brain lesion stages, these were stained for CD3, CD4, CD8 and for laminin, a component of the basal membranes lining the perivascular Virchow–Robin space (Fig. 1D). All animals displayed small to moderately sized perivascular cuffs containing CD3+, CD4+ and CD8+ T cells. CD4+ T cells were more frequently detected than CD8+ cells. Laminin staining confirmed that MNC infiltrates were largely confined to perivascular spaces whereas some cells seemed to have passed the glia limitans. Figure 1E shows a typical large sized lesion in the white matter (Fig. 1EI) and in the grey matter (Fig. 1EIII). Figure 1EII shows

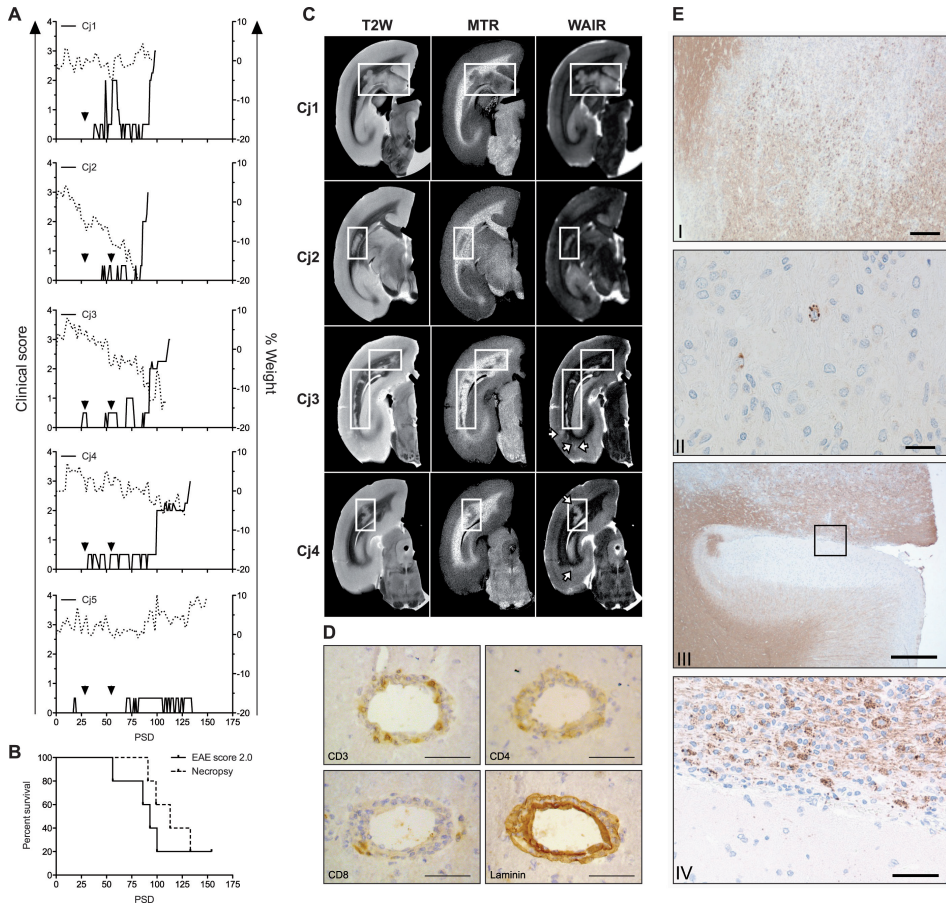


Figure 1. Clinical course and pathology of MOG34-56/IFA EAE model in marmosets. (A) Five unrelated monkeys were immunized at 28 day intervals (arrowheads) with 100 μg MOG34-56 in IFA. Monkey Cj1 was re-challenged only once because the presence of a short episode of blindness suggesting optic neuritis (EAE score 2.0) showed that the disease was already ongoing. Depicted are clinical scores (solid line, left y-axes) and % body weight loss relative to day 0 (dotted line, right y-axes). (B) Survival curves show the disease free survival (time until the animals developed EAE score 2.0) and survival time until the day of necropsy. PSD, post-sensitization day. (C) Magnetic resonance images of formalin fixed brains from 4 of the 5 monkeys. Left: T2-weighted (T2W) images; middle: magnetization transfer ratio images (MTR); right: WAIR images. White squares circumscribe the same white matter lesion in the three types of scans. White arrows in the WAIR images of Cj3 and Cj4 points to cortical grey matter lesions. (D) Snap-frozen brain sections of Cj4 were immunostained as representative example of T-cell localization within early lesions. The picture shows a small perivascular T-cell infiltrate: CD3 (upper left), CD4 (upper right) and CD8 (bottom left). Laminin (bottom right) shows that infiltrated MNCs are mainly localized in the perivascular space. (400x, bar = 50 μm). (E) Formalin-fixed brain section of Cj3 was immunostained for proteolipid protein (PLP), showing widespread demyelination in the white matter (I, 4x, bar = 200 μm) and cortical grey matter (III, 25x, bar = 500 μm). The square in (III) is enlarged in (IV, 250x, bar = 50 μm) demonstrating that activated macrophages are undetectable in grey matter, although macrophages containing degraded PLP products were detected in white matter. Few infiltrated T cells expressing Granzyme B were found in the white matter of the corpus callosum (II, 400x, bar = 20 μm). Data from monkey Cj3 is shown as a representative.

that T cells infiltrating the white matter express granzyme B, an established marker of cytotoxic T-cells. Figure 1EIV shows the absence of activated MRP-14 macrophages in grey matter lesions, although macrophages containing myelin degradation products were abundant in the white matter lesion.

Analysis of T-cell reactivity against MOG34-56

End-stage proliferation

At necropsy MNCs were isolated from blood, spleen, ALNs, ILNs, LLNs and CLNs and tested for proliferation against a panel of overlapping MOG peptides and rhMOG. Proliferation was only detected against the immunizing MOG34-56 peptide (Fig. 2A).

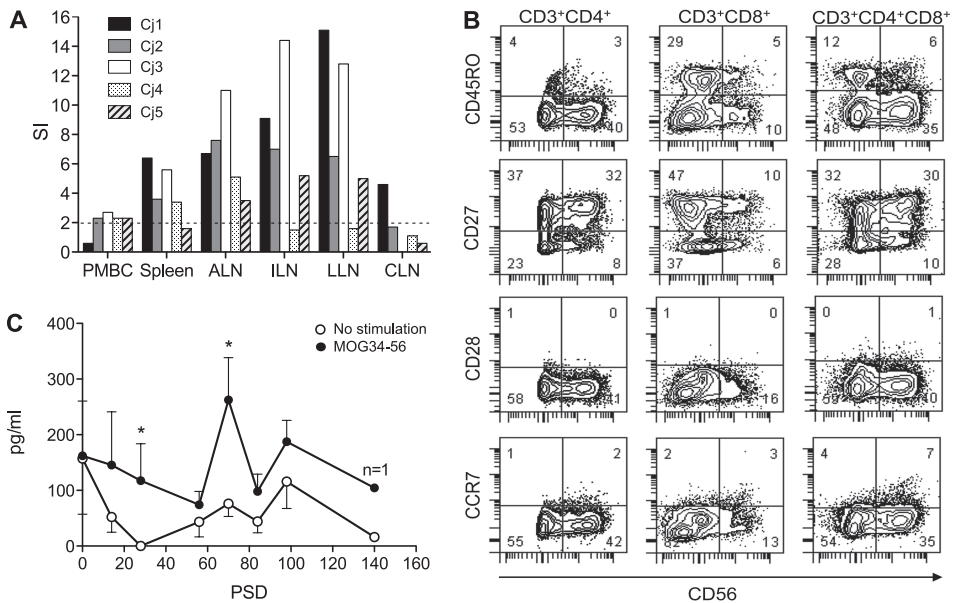


Figure 2. Analysis of T cells after *ex vivo* stimulation. MNCs were isolated from spleen, ALNs, ILNs, LLNs and CLNs. (A) Proliferation of T cells against MOG34-56 was determined by ³H-thymidine incorporation during final 18 h culture. Data are expressed as stimulation index (SI) relative to unstimulated cells. SI \geq 2.0 is considered positive. (B) T-cell lines against MOG34-56 were generated from spleen MNCs and phenotyped for CD3, CD4, CD8 and CD56 expression. The cells were further characterized on basis of CD27, CD28, CD45RO, and CCR7 expression. The T-cell lines were gated for CD3⁺ (55 \pm 17.3% of vital cells); remaining 45% were CD3 low or negative. The CD3⁺ T cells were 26 \pm 5.3% CD4⁺, 23 \pm 5.8% CD8⁺ and 36 \pm 8.2% CD4⁺CD8⁺. Percentages (mean \pm SD) are given of four pooled T-cell lines. Data from one (Cj1) out of the four T-cell lines are shown; staining patterns were analysed in two independent experiments. Numbers in each quadrant represent the percentage of each subpopulation. (C) IL-17A production was measured in PBMCs after 48 h stimulation with MOG34-56 or no antigen stimulation. Production of IFN- γ and IL-10 was below the detection level and is therefore not shown. PSD, post sensitization day. * p <0.05, Mann-Whitney U test, compared with data of not stimulated cells. The results are pooled of five animals and reported as mean \pm SEM. Experiment is performed only once since we had small volume of culture supernatant.

Cross-sectional comparison of proliferation in blood and lymphoid organs

Figure 2A summarizes the reactivity profiles against MOG34-56 of all 5 monkeys. In blood MNC proliferation against MOG34-56 was around the cut-off level of SI 2.0. Variable proliferation was observed in ALNs, ILNs and LLNs. Only in one animal, Cj1, positive response was detected in the CLN. CLN from monkey Cj3 was not tested because too few cells could be isolated.

Cell lines

T-cell lines against MOG34-56 were generated from spleen and ALN assuming that these bulk T-cells reflect the profile of *in vivo* activated T cells. These cells were phenotyped using monoclonal antibodies with confirmed cross-reactivity with marmosets. Based on CD4 and CD8 expression three subsets of CD3+ T cells were discerned: CD4 and CD8 single-positive populations and a CD4/CD8 double-positive population (Fig. 2B). The three subsets were characterized for surface expression of additional markers. The main proliferating CD3+ subset was previously found to be double positive for CD4 and CD8 and also expressed CD56, but not CD16²⁸⁸. The CD4+CD8+CD56+ subset (right column of Fig. 2B) was negative for CD45RO, CD28 and CCR7 but positive for CD27. Note that these markers are differently expressed in the CD3+CD8+ subset.

Longitudinal cytokine profiles

Blood MNCs collected at 14 days interval were cultured with or without MOG34-56. The small blood volume available per time point (1 mL) precludes large-scale analyses. We therefore chose to determine besides proliferation levels of three selected cytokines in culture supernatants: IL-17A (Th17), IFN- γ (Th1) and IL-10 (anti-inflammatory). Cytokine profile presented in Fig. 2C shows that more IL-17A was produced when MNCs were stimulated with MOG34-56 versus no antigen stimulation. Data are only shown of IL-17A as IFN- γ and IL-10 production was below the detection level (see Supporting Information Fig. 2).

Target cell specificity of the cytolytic T cells

The cytolytic activity of MOG34-56-specific T-cell lines from spleen and ALN was tested using EBV B-LCL as target cells. Figure 3A shows the results from two cell lines, which lysed autologous B-LCL pulsed with the specific peptide MOG34-56. Figure 3B shows that the peptide does not need to be presented by an autologous B-LCL as the T cells also recognized and killed MOG34-56-pulsed B-LCL from an unrelated donor (allogeneic B-LCL). This suggests that the cytotoxic T cells recognize MOG34-56-derived peptide by invariant MHC molecules. The relatively high background lysis is unexplained. We assume that this is due to background T-cell immunity against EBV-like viruses with which marmosets are naturally infected¹.

In the next experiment we determined the epitope in the MOG34-56 peptide that is presented by the B-LCL to cytotoxic T cells. To this end, ⁵¹Chromium-labelled B-LCL were pulsed with 9-mer synthetic MOG peptides overlapping by six amino acids and next exposed to autologous MOG34-56 specific effector T cells. Figure 3C shows enhanced cytotoxicity towards B-LCL pulsed with MOG40-48 and MOG46-54, indicating that these are candidate CTL epitopes in MOG34-56.

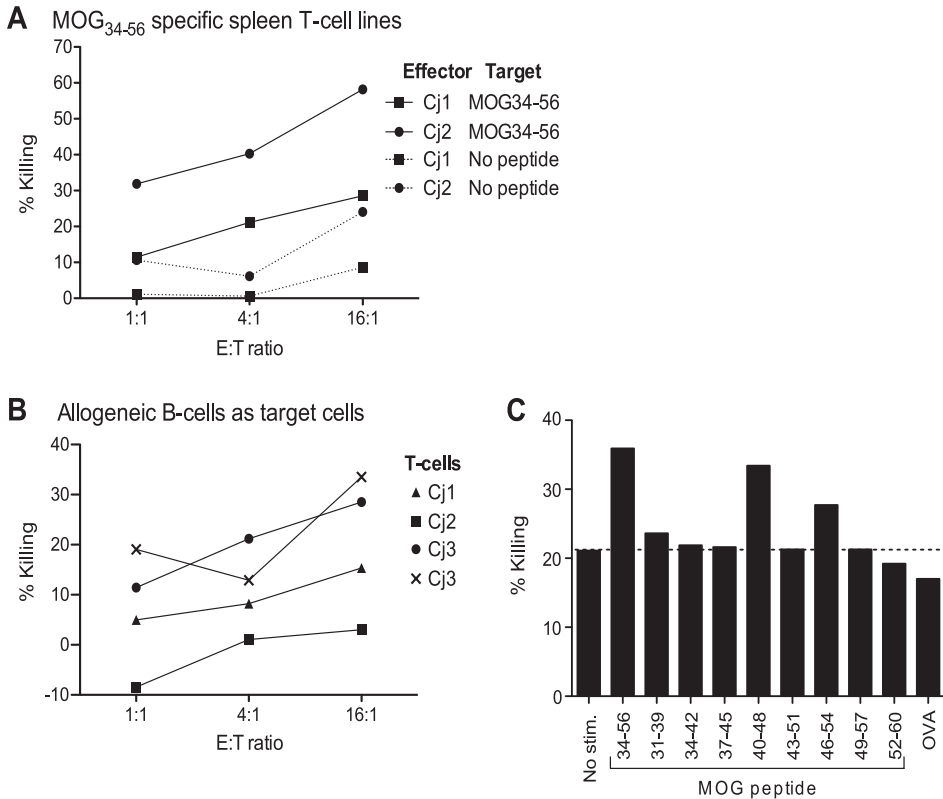


Figure 3. Specific cytotoxicity of T-cell lines. MOG34-56-specific T-cell lines (E: effector cells) isolated from the spleens of two EAE affected marmoset were tested for specific cytotoxicity against peptide-pulsed EBV B-LCLs (T: target cells) in a ⁵¹Chromium release cytotoxicity assay. (A) Autologous B-LCLs were tested without (dotted line) or with (solid lines) MOG34-56 peptide. Specific lysis of target cells is expressed as % killing. (B) Allogeneic B-LCLs pulsed with MOG34-56 were killed by MOG34-56 specific T-cell lines from unrelated marmosets. Data are expressed as % killing compared to negative control. (C) Autologous B-LCLs were pulsed with a panel of 9-mer overlapping MOG peptides derived from MOG34-56. Cytotoxicity was tested at the same three E:T ratios as in (A, B), but only data obtained at 16:1 ratio are shown. Negative control comprised non-pulsed target cells or target cells pulsed with an irrelevant protein (OVA). Baseline shows background killing (dotted line). Data shown are one representative of two independent experiments with similar results.

MHC-Caja class I expression in the marmoset brain

Classical MHC class Ia molecules equivalent to HLA-A, HLA-B and HLA-C are not encoded in the MHC genomic region of the marmoset. However, equivalents of the non-classical MHC class Ib molecules, HLA-E and HLA-G are expressed^{195, 290, 294}. According to the consensus nomenclature of primate MHC systems²⁹⁵, these are indicated with the acronym Caja i.e. *Caja-E* and *Caja-G*. Whereas *Caja-G* is polymorphic and seems to function as a classical MHC Ia molecule, *Caja-E* is oligomorphic containing only 2 alleles, differing only at amino acid position 107 outside the peptide binding cleft. Expression of transcripts for both MHC class I genes in marmoset brain has been published²⁹⁵ and is confirmed in Fig. 4. The figure showed the expression of *Caja-E* transcripts in EBV-induced

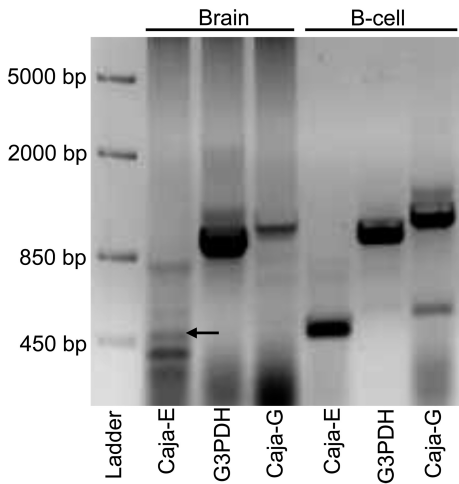


Figure 4. MHC class I gene transcripts in marmoset brain and B-LCLs. Specific primer sets for Caja-G and Caja-E (see Materials and methods section) were used to verify, using RT-PCR, that these non-classical MHC molecules are expressed in the brain and by the B-cell lines. The housekeeping gene G3PDH was used as internal control. Arrow indicates Caja-E transcript in the brain. bp, base pairs. Data shown are representative of two independent experiments.

B-LCL for comparison. Thus, we hypothesize that the cytotoxic activity of MOG34-56-induced T cells is directed against MOG34-56 epitope presented via Caja-E molecules.

Mapping of HLA-E-binding peptides on the MOG extracellular domain

We have used a published algorithm²⁹² (Fig. 5A) to identify candidate HLA-E-binding motifs within previously identified T-cell epitopes in the human and marmoset MOG extracellular domains aa1-125 (Fig. 5A)¹³³ (Fig. 5B). As can be seen in Fig. 5C the peptides MOG1-22, MOG94-116 and the overlapping peptides MOG64-86/74-96, which encompass dominant T-cell epitopes for rhMOG-immunized marmosets¹⁹⁰, contain putative HLA-E binding sequences. Remarkably, an HLA-E binding sequence was not detected in MOG34-56, although according to an algorithm published by Stevens et al.²⁹⁶ peptides 42-50 may bind to HLA-E as position 2 might be less important for binding.

The four putative HLA-E binding sequences were synthesized as 9-mer MOG peptides, 13-21, 42-50, 75-83 and 105-113 and tested for binding to HLA-E transfectants of K562 cells using thermostable expression at 37°C as read-out. In a direct binding assay (Fig. 6A) only HLA-E binding of MOG13-21 and the positive control peptide (HCV core peptides 35-44) was observed²⁹³.

We hypothesized that binding of the three other MOG peptides to HLA-E might be too weak to form thermostable complexes at 37°C. This possibility was tested in a more sensitive indirect binding assay. As a positive control we used unlabelled HCV core 35-44 peptide. Figure 6B shows that at the highest dose (300 μM), two peptides, MOG42-50 and HCV core peptide, induced increased binding of the HLA-G leader indicator peptide. Increased binding of the HCVcore35-44 detector peptide was not observed. Staining with W6/32 monoclonal antibody confirmed slightly elevated expression of HLA-E at the highest concentration of MOG42-50 (Fig. 6C). The internal control of this sensitive indirect assay showed complete blocking of binding of fluorescent HCVcore35-44 detector peptide by unlabelled HCVcore35-44, whereas binding of the HLA-G leader detector peptide was unaffected.

In conclusion, the extracellular domain of MOG contains several putative binding peptides localized within previously identified T-cell epitopes¹⁹⁰.

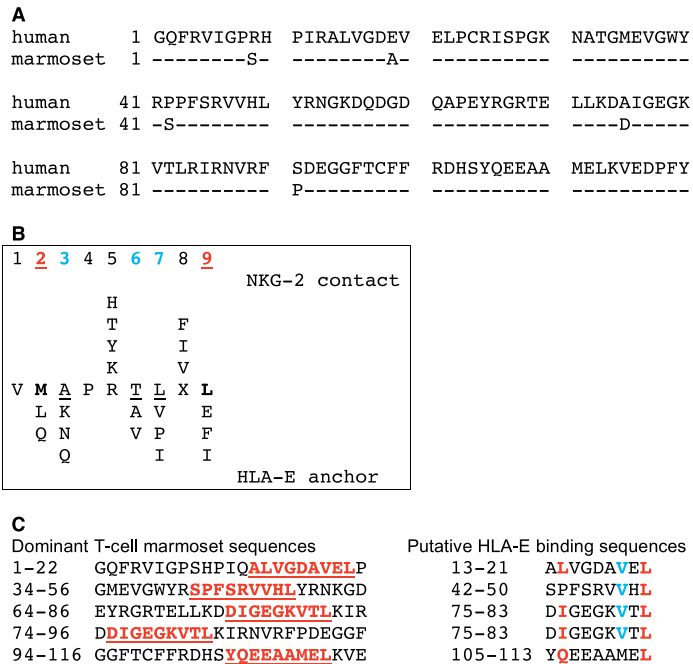


Figure 5. Delineation of putative HLA-E-binding peptides in rhMOG. (A) Extracellular domain of the human and marmoset MOG sequence, aa 1-120. (B) Algorithm for delineation of HLA-E-binding peptides in red and underlined²⁹². Position 2 and 9 are the main HLA-E contact positions. Positions 3, 6, and 7 (in blue) are minor residues. (C) Previously identified dominant T-cell epitopes (left) in the rhMOG-induced EAE model contain putative HLA-E binding sequences (right).

Caja-E binding of putative epitopes within MOG34-56

Just like HLA-E, Caja-E has two known alleles, Caja-E*01 and Caja-E*02, which differ at position 107 of the α chain by a G or T respectively, which is outside the peptide-binding cleft. Whether these two alleles have similar functional differences as their human counterparts²⁹⁷ or differ in the binding of viral peptides²⁹⁸ is not known.

Based on the encouraging HLA-E-binding data we cloned the Caja-E*01 allele from EBV-induced B-LCL for expression in K562 cells. Successful transfection was verified by PCR and surface expression of the gene product at 26°C was confirmed by staining with W6/32 mAb (Fig. 7A).

The presence of Caja-E binding epitopes in MOG34-56 was analysed using the direct binding assay of 9-mer MOG peptides overlapping by 6 (Table 1). Figure 7B shows binding of MOG40-48 being the specific epitope of the MOG34-56-induced cytotoxic T-lymphocytes.

DISCUSSION

Marmosets immunized with MOG34-56 in IFA developed EAE associated with widespread demyelination of CNS white matter²⁸⁸. Demyelination in this model seems directly induced by

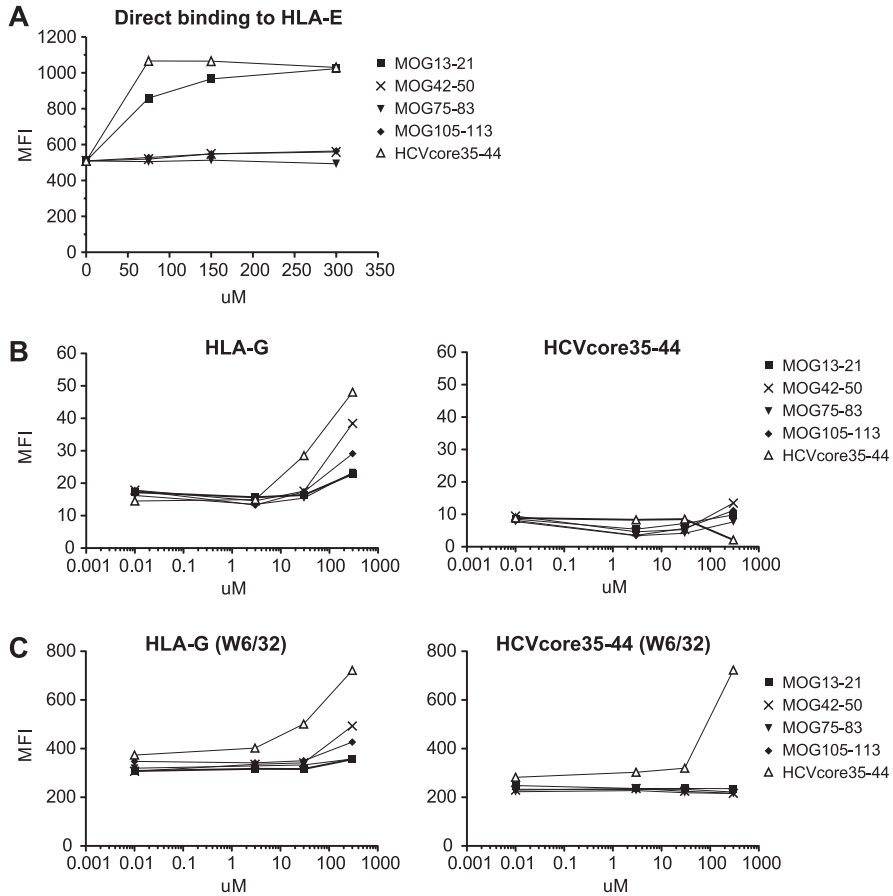


Figure 6. Binding of MOG peptides to HLA-E-expressing K562 cells. (A) K562 cells transfected with HLA-Eg were incubated o/n at 26°C with or without a dose titration of the indicated peptides. Thermostable expression of HLA-E at 37°C was visualized by anti-MHC class I antibody (W6/32) staining. Data are expressed as mean fluorescence intensity (MFI) and are corrected for background binding. Specificity controls in this assay were K562/HLA-Eg cells incubated without peptide and K562 cells transfected with mock plasmid (pCDNA3). (B) HLA-E or mock-transfected K562 cell lines were incubated for 4 h at 26°C with a dose titration of the indicated peptides. Subsequently 5 μ M of a fluorescently labelled detector peptide was added and incubated o/n at 26°C. In the left panel, HLA-G leader peptide was used as detector peptide. In the right panel, HCVcore35-44 was used as detector peptide. Binding of detector peptides was measured by flow cytometry and data are expressed in MFI. (C) From the same experiment as described in (B), MHC class I expression was measured by staining with W6/32. One representative experiment of three is shown.

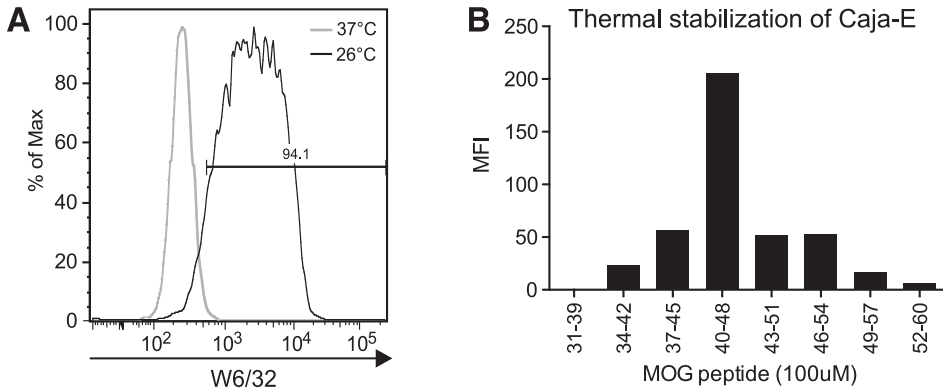


Figure 7. Binding of MOG peptides with Caja-E on K562 cells. Caja-E*01 was cloned from B-LCLs and subsequently transfected into K562 cells. (A) Transfection of Caja-E was confirmed by W6/32 staining. High expression of Caja-E molecules was observed at 26°C (black line), whereas these molecules disintegrated at 37°C (grey line). (B) Caja-E transfected K562 cells were incubated *o/n* at 26°C with a dose titration (0 – 100 μ M) of overlapping 9-mer peptides derived from the MOG34–56 sequence. Thermostable expression of Caja-E at 37°C was confirmed by W6/32 staining. One representative experiment out of 4 is shown.

MOG34-56–induced T cells independent of MOG protein-binding autoantibodies, which were undetectable in the model. To unravel the underlying mechanism, five unrelated marmosets were immunized with MOG34-56 in IFA inducing progressive EAE associated with extensive demyelination of brain white matter and cortical grey matter (Fig. 1D). This situation illustrates the pathological similarity of the marmoset EAE model with MS⁴⁹. Using immunohistochemistry CD4+ and CD8+ infiltrated T cells were detected within and around perivascular spaces of early-stage lesions. MOG34-56–specific T-cell lines generated from secondary lymphoid organs were characterized to examine their nature and possible origin (Fig. 2B).

Using flow cytometry, *in vivo* activated MOG34-56 reactive T cells were defined in three subsets, namely CD3+CD4+, CD3+CD8+ and CD3+CD4+CD8+. Of particular interest is the co-expression of CD56, which is a marker of NK cells that defines CD4+ and CD8+ T cells with cytotoxic activity towards oligodendrocytes in MS^{270,299}. The CD3+CD4+CD56+ and CD3+CD4+CD8+CD56+ populations were for a small proportion CD45RO+ and expressed CD27+, but were negative for CD28 or CCR7. The phenotype of these T cells resembles Natural Killer–Cytotoxic T-lymphocytes (NK-CTL)³⁰⁰. The CD3+CD8+CD56+ T cells had a somewhat different phenotype as only a relatively small proportion expressed CD27. It is presently unclear which of these three phenotypes mediates IL-17A production or peptide-specific cytolytic activity by the MOG34-56 reactive T cells. Attempts to elucidate this have failed thus far as the T cells kill the EBV-induced B-LCL, which were used as APC for generating lines and clones.

Next, we determined the fine-specificity and MHC restriction of the cytotoxic T cells. To distinguish between the two possible options for MHC class I restricted CTL activity, i.e. via polymorphic Caja-G or oligomorphic Caja-E molecules, we first tested whether a certain T-cell line could lyse B-LCL from unrelated monkeys. This was indeed the case indicating that MHC class I molecules presenting the peptide epitope to the CTL are shared by B-LCL from unrelated

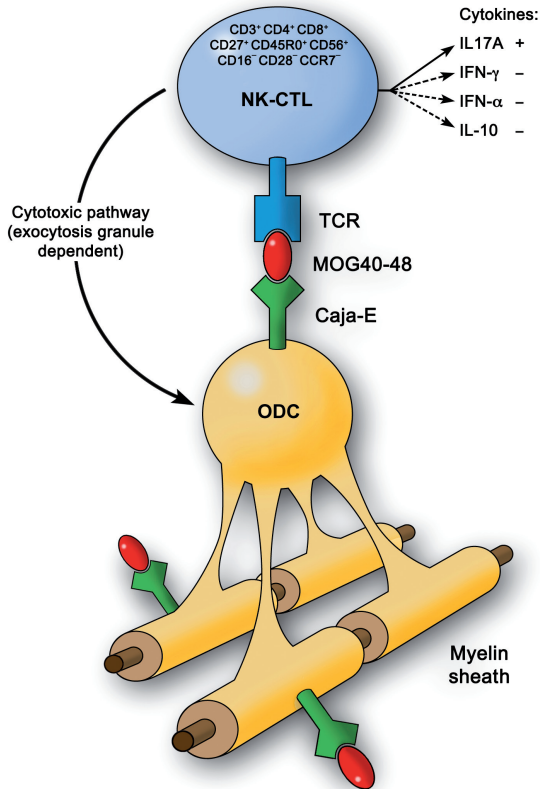


Figure 8. Proposed mechanism of demyelination in the MOG34–56/IFA marmoset EAE model. MOG40–48 peptide presented by Caja-E molecules expressed on the myelin sheath or oligodendrocyte (ODC) is recognized by cytotoxic T cells. IL-17A was the only cytokine that was produced in clearly detectable amounts. Based on various similarities with anti-CMV effector memory CTLs found in humans, we propose to call the autoreactive T cells NK-CTLs³⁰⁶. According to previously reported experiments²⁸⁸, cytotoxicity was dependent on the exocytosis of cytotoxic granules. Recognition of the MOG40–48:Caja-E complex by NKCTLs results in injury to the ODCs or myelin sheath.

monkeys, making Caja-E the most likely candidate. Further analysis supported this assumption as the 9-mer peptide, MOG40–48, which was identified as the specific epitope of the cytolytic cells, was the only MOG34–56 peptide that stably bound Caja-E. It has been shown in mice that the MOG sequence 40–48 is critical for EAE induction, and is required as the minimal epitope for stimulating MOG35–55-specific T cells³⁰¹. These findings support the conclusion that the cytotoxic activity of MOG34–56 induced T cells in the marmoset targets MOG40–48/Caja-E complexes (Fig. 8).

Several characteristics of the autoreactive T cells suspected for mediating demyelination in this new model render them capable to induce lesions. First, they share preferential production of IL-17A with Th17 cells, which infiltrate non-inflamed brain via the chorioid plexus³⁰². Indeed, the first site where in the marmoset EAE model CNS inflammation can be detected on contrast-enhanced T1-weighted magnetic resonance images is around the dorsal horns of the lateral ventricles where the chorioid plexus is located (data not shown). Second, antigen-specific cytotoxic of oligodendrocyte (ODC) by MOG34–56 activated T cells could be the cause of demyelination²⁹⁹. However, the model lacks an obvious source of IFN-γ that is needed to induce classical MHC class I molecules on ODC³⁰³. The autoreactive T-cells themselves do not produce (detectable amounts of) IFN-γ and IFA does not contain innate antigen receptor ligands that could induce this cytokine via activation of myeloid cells are absent in IFA²⁸⁸.

It has been well established that cells with low expression of classical MHC class Ia molecules, such as ODC, are exposed to cytolysis by NK cells. One of the mechanisms to avoid NK cells attack is HLA-E expression. When engaged with certain QdM peptides such as in the HLA-G leader, HLA-E relays inhibitory signals to NK cells via NKG2A/CD94. This system is used by herpesviruses, such as cytomegalovirus (CMV) for immune evasion³⁰⁴. However, HLA-E restricted CD3+CD8+CD56+CD27-CCR7- T cells are present in the human repertoire which can kill CMV-infected cells via the recognition of viral peptides (e.g. UL40) presented by HLA-E³⁰⁰.

It is unclear at this stage to which extent this situation also occurs in our marmosets. Similar to the rhesus macaque, the common marmoset is naturally infected with herpesviruses related to human CMV³⁰⁵. We observed that CD8+ T cells specific for MOG34-56 and MOG40-48 in the rhesus monkey crossreact with an almost identical peptide from the immunodominant UL86 antigen of human CMV¹⁸⁹. Both peptides bind to Caja-E. However, this could not be proven in the marmosets, as specific reagents for testing the CMV status in marmosets are not available.

In conclusion, we postulate that the T cells that induce demyelination in the MOG34-56/IFA EAE model may be recruited from the repertoire of effector memory cells that controls latent CMV infection.

ACKNOWLEDGEMENTS

The authors thank the Animal Science Department for biotechnical assistance and the Department Comparative Genetics & Refinement (BPRC) for help with molecular techniques. This work was supported by an internal grant of the Biomedical Primate Research Centre and by the Netherlands Organization for Scientific Research (NWO) funding the 9.4 T horizontal bore NMR spectrometer.

SUPPLEMENTARY FIGURES

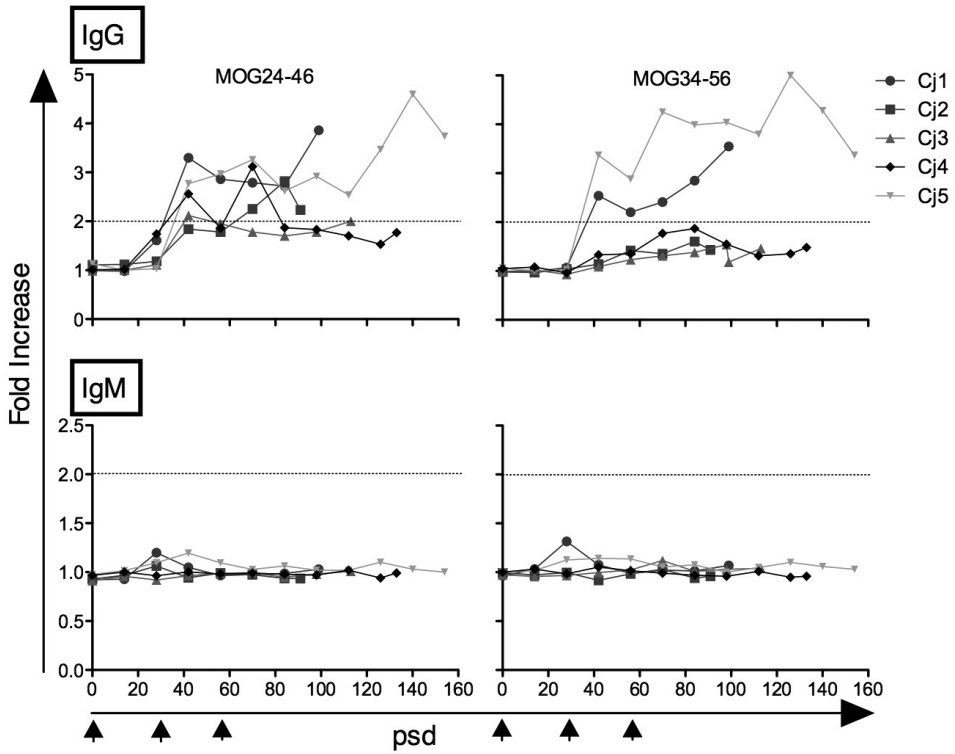


Figure S1. Antibody levels measured in plasma samples collected at 14 days interval. IgG (upper) and IgM binding to the overlapping peptides MOG24-46 (left panel) and MOG34-56 (right panel), which contain the dominant B-cell epitope was assessed. Data are expressed as fold increase relative to pre-immune sera and values greater than 2.0 were considered positive. No antibody responses were detected against rhMOG (data not shown). Arrowheads depict time points of immunizations. psd: post sensitization day.

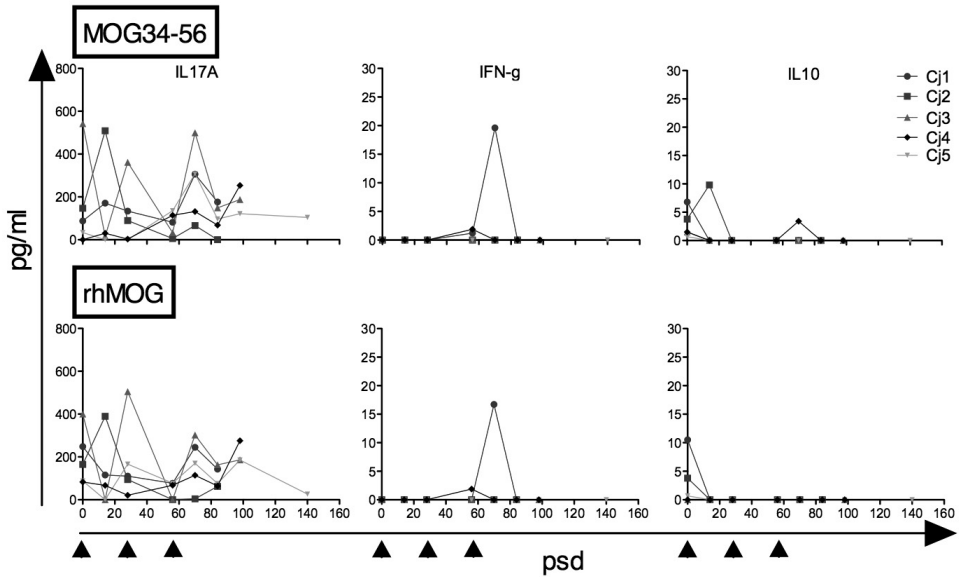


Figure S2. Cytokine profile in blood. PBMC collected every two weeks were cultured with MOG34-56 (upper) and with rhMOG. Culture supernatants were analysed for IL-17A (left), IFN- γ (middle) and IL-10 (right) production after 48 h stimulation. Arrowheads depict time points of immunizations. psd: post sensitization day.

**RECOMBINANT HUMAN MOG IN
INCOMPLETE FREUND'S ADJUVANT
INDUCES A MULTIPLE SCLEROSIS-LIKE
DISEASE IN THE COMMON MARMOSET**

S. Anwar Jagessar, Nicole Heijmans, Erwin L.A. Blezer, Jan Bauer,
Jon D. Laman, and Bert A. 't Hart

Manuscript in preparation

**B-CELL DEPLETION ABROGATES T-CELL
MEDIATED DEMYELINATION IN AN
ANTIBODY NON-DEPENDENT COMMON
MARMOSSET EAE MODEL**

S. Anwar Jagessar, Nicole Heijmans, Jan Bauer, Erwin L.A. Blezer,
Jon D. Laman, Niels Hellings* and Bert A. 't Hart*

*Shared senior authorship

Submitted

ABSTRACT

CD20+ B-cell depletion is a highly promising treatment for multiple sclerosis (MS), but the mechanisms underlying the therapeutic effect are poorly understood. B-cells are thought to contribute to the MS pathogenesis by production of autoantibodies that amplify demyelination via opsonization of myelin sheaths. To analyze autoantibody non-dependent functions of B-cells in MS, we used a novel T-cell driven experimental autoimmune encephalomyelitis (EAE) model in marmoset monkeys (*Callithrix jacchus*). In this model demyelination of brain and spinal cord white and grey matter as well as the ensuing neurological deficits are induced by immunization with peptide 34 to 56 of myelin oligodendrocyte glycoprotein (MOG34-56) in incomplete Freund's adjuvant (IFA). Although autoantibodies do not have a detectable pathogenic contribution in the model, the results show that depletion of B-cells with HuMab7D8, a human IgG1k monoclonal antibody against human CD20, suppresses clinical and pathological expression of EAE. In the CD20+ B-cell depleted monkeys, the activation of peptide-specific Th17 producing and cytotoxic T cells, which in previous studies were found to play an essential role in the induction of neurological deficits, was impaired. The assumption that the pathogenic T-cells are directly activated by B-cells is supported by the observation that infusion of autologous B-lymphoblastoid cell lines presenting MOG34-56 *in vivo* induces activation of autoreactive T-cells together with CNS inflammation. In conclusion, we demonstrate a critical antibody non-dependent role of B-cells in autoimmune encephalomyelitis, which is the activation of pathogenic T-cells.

INTRODUCTION

The canonical role of B-cells in multiple sclerosis (MS) is the production of autoantibodies, which induce and/or amplify demyelination by binding to target antigens within the CNS. The formation of antigen-antibody complexes on the surface of myelin sheaths and/or oligodendrocytes (opsonization) elicits antibody-dependent cell-mediated cytotoxicity and complement-dependent cytotoxicity². This pathogenic concept is supported by the experimental autoimmune encephalomyelitis (EAE) model and formed the basis for therapies aiming at the depletion of CD20+ B-cells using monoclonal antibodies (mAbs). Three anti-CD20 mAbs are currently evaluated for treatment of MS, i.e. the chimeric mAb rituximab and two completely human mAbs, ofatumumab and ocrelizumab³⁰⁹. Rituximab has shown long-lasting beneficial effects in a phase II clinical trial in relapsing-remitting MS⁷⁵. Ofatumumab and ocrelizumab also induced remarkable clinical improvement in a phase II clinical trial involving relapsing/remitting MS patients. Unexpectedly, the anticipated reduction of circulating antibodies by rituximab treatment was not observed, leaving the remarkable long-lasting clinical benefit of anti-CD20 mAb therapy without a mechanistic explanation.

The aim of the current study was to examine antibody non-dependent contributions of B-cells to MS-like disease in the common marmoset EAE model (*Callithrix jacchus*). Marmosets are small-bodied Neotropical primates providing several valid preclinical models for MS¹²⁸. We used a recently developed autoantibody non-dependent EAE model, which is characterized by robust clinical and pathological features of progressive MS including widespread demyelination in grey and white matter. The model is elicited by immunization with an immunodominant peptide of myelin oligodendrocyte glycoprotein (MOG34-56) formulated in IFA²⁸⁸. Evidence obtained thus far shows that the MS-like clinical and pathological features in this MOG34-56/IFA model are mediated by effector memory-like T-cells, which are present in the naive marmoset repertoire^{288, 307}. T-cells activated by immunization with MOG34-56/IFA were immunologically characterized by high production of IL-17A, low production of IFN- γ and TNF- α , and specific degranulation-dependent cytolysis of target cells presenting MOG34-56 via Caja-E molecules³⁰⁷. For effective systemic B-cell depletion we used a previously validated variant of the anti-CD20 antibody ofatumumab, HuMab 7D8, which displayed strong cross-reaction with marmoset CD20²¹⁵. The mAb suppressed EAE development in a more classical version of the model marmosets immunized with recombinant human myelin oligodendrocyte glycoprotein (rhMOG) in CFA, in which induction of pathology and neurological symptoms involves the synergy of autoreactive T helper 1 cells and autoantibodies²¹⁵.

A first set of experiments comprised five chimeric marmoset twins, which are immunologically highly comparable. In one sibling we induced profound long-lasting B-cell depletion by weekly intravenous administration of HuMab 7D8 from day 21 after the first immunization with MOG34-56/IFA. The fraternal sibling received the identical treatment, but with the solvent (PBS). The antibody treatment resulted in a sharp reduction of clinical as well as pathological features of EAE. This experiment warrants the conclusion that a critical pathogenic role of CD20+ B cells is the activation of MOG34-56 specific encephalitogenic T-cells.

The capacity of B-cells to directly activate MOG34-56 specific T-cells *in vivo* was examined in a second set of experiments involving also 5 chimeric marmoset twins. One sibling of each twin was infused with semi-autologous B-lymphoblastoid cells (BLCL; induced with EBV strain 95-8) prepulsed with MOG34-56 (BLCL_{MOG}). The fraternal sibling was infused with the identical

BLCL, which were incubated without MOG34-56 (BLCL₀). We observed a stronger capacity of BLCL_{MOG} than of BLCL₀ to induce T-cell proliferation, IL-17A production and cytotoxicity.

MATERIALS AND METHODS

Animals

Adult common marmosets were purchased from the purpose-bred colony at the Biomedical Primate Research Centre. Details of individual animals are summarized in Table 1. In accordance with the Dutch law on animal experimentation, all study protocols and experimental procedures were reviewed and approved by the Institute's Ethics Committee before the experiments were started.

Experimental outline

Experiment 1: The experiment comprised 5 female chimeric twins. EAE was induced as described elsewhere²⁸⁸. In brief, EAE was induced with 100 µg MOG34-56 dissolved in 200 µl buffered saline and emulsified in 200 µl IFA (Difco Laboratories, Detroit, MI). The inoculum was injected into the inguinal and axillary regions of the dorsal skin divided over 4 spots of 100 µl each. Antigen-adjuvant emulsion was prepared by gentle stirring at 4 °C for at least 1 h. Monkeys that failed to develop serious neurological deficit (score ≥ 2.0; see next paragraph) within 28 days received re-challenges at post sensitization days (PSD) 28 and 56 with the same peptide dose in IFA. One sibling of each twin received a single dose of 20 mg/kg (1ml/kg) of HuMab 7D8 (anti-CD20) i.v. in the saphenic or femoral vein (GenMab, Utrecht, The Netherlands) at PSD 21, subsequently treatment was continued with 5 mg/ml (i.v.) anti-CD20 every week till end of the study. HuMab 7D8 is a human IgG1κ mAb directed against human CD20^{215, 310}. As a control, the other member of the twin received 1 ml/kg buffered saline.

Experiment 2: The experiment comprised 5 male chimeric twins. For preparation of BLCL 1.5 ml venous blood sample was collected from the vena femoralis into heparinized vacutainers. Mononuclear cells (MNC) were isolated by density gradient centrifugation and infected with supernatants from the EBV-producing cell line B95-8 for immortalization²⁰⁰. Transformed B-cells were grown at least for a month to large BLCL numbers. BLCL of both twins were mixed (ratio 1:1) and subsequently divided into two equal portions, one portion (1.10⁷ cells in 1 ml) was incubated overnight at 37°C with 5 mg/ml MOG34-56, indicated henceforth as BLCL_{MOG} and the other with medium, BLCL₀. After incubation cells were washed once with buffered saline and 1.10⁷ BLCL were injected at day 0, 28 and 56. Note that the chimeric state of twin siblings implies that they are tolerant for alloantigens expressed on the mixed BLCL.

Clinical and post mortem examination

Marmosets were examined twice daily for the expression of EAE symptoms. Signs of EAE were recorded using a semi-quantitative scoring system developed for the marmoset EAE model¹²⁷. As an objective surrogate disease marker, bodyweights were measured 3 times per week. The clinical endpoint for each monkey was EAE score 3, representing complete paralysis of the hind part of the body. Monkeys reaching this score were first deeply sedated by intramuscular injection of Alfaxan (10 mg/kg) (Vétoquinol S.A., Magny-Vernois, France). After collection of the maximum venous blood volume, the monkeys were euthanized by infusion of sodium

Table 1. Overview of marmosets included in this study and their responses to clinical EAE and CNS pathology.

Exp.	Twin	Monkey	Sex	Weight (gram) ¹	Immunization	Treatment	Clinical EAE ²	Lesion on MRI WM	GM
1	1	M08031	F	374	MOG34-56/IFA	anti-CD20	-	+	+/-
		M08032	F	415	MOG34-56/IFA	placebo	+	+	-
	2	M08034	F	391	MOG34-56/IFA	anti-CD20	-	-	-
		M08035	F	370	MOG34-56/IFA	placebo	+	++	++
	3	M08088	F	385	MOG34-56/IFA	anti-CD20	-	+	-
		M08089	F	362	MOG34-56/IFA	placebo	+	-	-
	4	M08100	F	350	MOG34-56/IFA	anti-CD20	-	+/-	-
		M08101	F	396	MOG34-56/IFA	placebo	+	+	-
	5	M08106	F	396	MOG34-56/IFA	anti-CD20	-	+/-	-
		M08107	F	390	MOG34-56/IFA	placebo	+	+	-
2	6	M07022	M	359	None	BLCL ₀	-	-	-
		M07023	M	378	None	BLCL _{mog}	-	-	-
	7	M07038	M	332	None	BLCL ₀	-	-	-
		M07039	M	343	None	BLCL _{mog}	-	-	-
	8	M07043	M	389	None	BLCL ₀	-	-	-
		M07044	M	450	None	BLCL _{mog}	-	-	-
	9	M07082	M	338	None	BLCL ₀	-	-	-
		M07083	M	307	None	BLCL _{mog}	-	-	-
	10	M07105	M	410	None	BLCL ₀	-	-	-
		M07106	M	390	None	BLCL _{mog}	-	-	-

¹Weight at the start of experiment; ²EAE score ≥ 2.0 ; Exp, experiment; F, female; M, male; MOG, myelin oligodendrocyte glycoprotein; IFA, incomplete Freund's adjuvant; MRI, magnetic resonance image; WM, white matter; GM, grey matter.

pentobarbital (Euthesate[®]; Apharmo, Duiven, The Netherlands). Monkeys not reaching the clinical end-point were sacrificed at the predetermined endpoint of the study.

At necropsy brain and spinal cord were collected for immunochemistry, histology and magnetic resonance imaging (MRI). Secondary lymphoid organs including axillary (ALN), inguinal (ILN), lumbar (LLN) lymph node, spleen, and bone marrow (BM) were aseptically collected for preparation of mononuclear cells (MNC)²⁸⁸.

Blood collection

EDTA or heparinized blood was collected every two weeks from the femoral vein.

MNC and plasma were separated by density gradient centrifugation²⁶³. Plasmas were stored at -20 °C until further analysis.

Antibody detection

Antibody binding to rhMOG or to a panel of overlapping 23-mer pMOG sequences was determined in the linear range of the OD405 curve using ELISA as previously described¹²⁶⁴.

MNC phenotyping

MNC subsets were phenotyped with a pre-selected set of commercially available mAbs with proven cross-reaction with marmoset MNC subsets²¹⁶ as previously described³⁰⁷. For CD20 staining, MNC and PBMC collected at necropsy were treated with a stripping buffer (50 mM glycine-HCl, 5 mM KCl, 130 mM NaCl, pH 3.0) to remove *in vivo* bound anti-CD20 as described elsewhere²¹⁵. Phenotyping of proliferated cells for specific markers in the CFSE diluting assay was performed as previously described¹⁹⁰. Flow cytometric analysis was performed on a FACS LSRII flow cytometer using FACSDiva software 5.0 (BD Biosciences).

MNC proliferation

PBMC and MNC were tested for proliferation against a panel of overlapping MOG peptides (10 µg/ml) and rhMOG (10 µg/ml). The limited amount of available cells precludes testing of an antigen dose range. We used therefore the predetermined optimal dose (10 µg/ml) for MNC stimulation. Proliferation was quantified by the incorporation of [³H]-thymidine during the final 18 h of 3 days culture²⁶³.

Cytokine production

Supernatants of PBMC cultures were collected after 48 h stimulation with rhMOG or a panel of overlapping MOG peptides. Supernatants were assayed for the presence of cytokines using commercial ELISA kits following the manufacturer's instruction or as previously described²⁸⁸. Cytokine-specific mRNA were detected using quantitative PCR (qPCR) as described previously²¹⁵. Primer and probe combination according the Universal Probe Library set for human (Roche, Indianapolis) was used for granzyme B FW 5'-ACAGTACAGTTGAGTTGTGTGG-3', RV5'-GAGTCCCCCTTAAAGGAAGC-3', probe 64; perforin FW 5'-CCACGTGAAATCCGCTATC-3', RV 5'-AGACTCTGGCGGCATATT-3', probe 81. Transcript levels were normalized against the reference gene Abelson (ABL).

Neuropathological examination

Brains collected at necropsy were cut into two equal halves in anterior-posterior direction. One brain half was fixed in 4% buffered formalin for at least two weeks to stabilize magnetic resonance relaxation time characteristics²⁴¹. The other brain half was snap-frozen in liquid nitrogen. Spinal cord was also collected at necropsy and was only included in the histology analysis.

Formalin-fixed samples were stored in buffered saline containing sodium-azide before scanning for magnetic resonance imaging (MRI) analysis. High contrast post mortem T2-weighted (T2W), quantitative T2, magnetization transfer ratio (MTR) and white matter attenuated inversion recovery (WAIR) images were recorded on a 9.4 T horizontal bore NMR spectrometer (Varian, Palo Alto, CA), equipped with a quadrature coil (RAPID, Biomedical, Rimpf, Germany) as previously described^{215, 307, 311}. The total white and grey matter lesion volumes for each animal were determined. After completion of the MRI scanning, formalin-fixed brains were processed for (immuno)histological examination of inflammation and demyelination as described^{127, 263}.

RESULTS

HuMab7D8 depletes B-cells and prevents clinical EAE

EAE was induced in five marmoset twins by immunization with MOG34-56 in IFA. At PSD 21 one sibling of each twin was subjected to the induction of B-cell depletion by i.v. injection of HuMab 7D8 (anti-CD20 mAb). The fraternal siblings were injected with buffered saline as placebo. This procedure resulted in rapid and sustained depletion of B-cells from the circulation (Fig. 1A), whereas the control group showed an increment of circulating CD20+ B-cell numbers. MNC prepared from blood, lymphoid organs and BM at necropsy of the anti-CD20 treated group showed also a significant depletion of CD20+ cells as well as of mature CD20+CD40+ cells (Fig. 1B). In addition, we observed a significantly lower expression of CD19 mRNA transcripts in PBMC, spleen and ALN from the antibody treated group (Fig. 1C). Thus, the anti-CD20 antibody induced profound depletion of CD20+ B-cells throughout the observation period.

The clinical scores depicted in Figure 1D show that all five placebo treated siblings developed clinically evident EAE, whereas clinical signs of EAE remained mild or completely absent in the anti-CD20 mAb treated marmosets. Survival curves (Fig. 1E) showed that the time interval to clinically evident EAE (score 2.0; ataxia or blindness) as well as to the ethical end-point (score 3.0; complete paralysis of one or both hind-limbs) differed significantly between the mAb and placebo-treated groups.

In conclusion, despite the late start of treatment the anti-CD20 mAb exerted a robust effect on the EAE course.

B-cell depletion reduces MRI-detectable brain pathology.

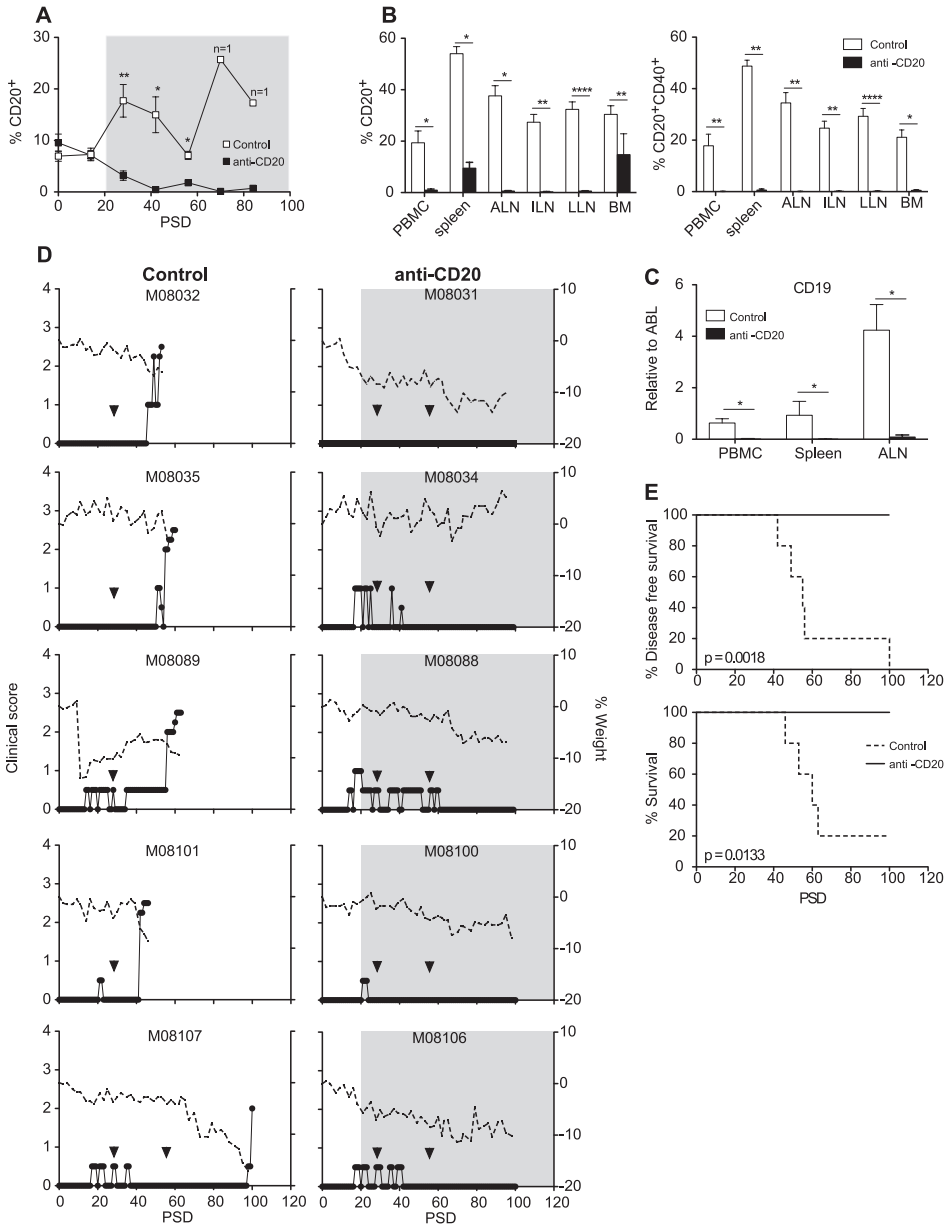
Post mortem MR images were made to assess the severity of EAE-related CNS pathology in the non-depleted and CD20+ B-cell depleted monkeys. T2, T2W, MTR and WAIR images were made of the formalin-fixed cerebral hemisphere of all five twins. Representative T2W and WAIR images are depicted in Fig. 2A, revealing in four of five control monkeys the presence of lesions in the white matter. The analyzed hemisphere of one control monkey (M08089) did not contain MRI-detectable lesions. This is not uncommon, as lesions can be diffuse and therefore invisible with the used MRI techniques or may be located in parts of the CNS that could not be analyzed with MRI, such as the contralateral hemisphere, or the spinal cord, which is too small. Moreover, lesions in the cortical grey matter are usually undetectable with routine T2W images. Monkeys in the anti-CD20 mAb treated group showed only small lesions, which were located inside or in the vicinity of the corpus callosum. This is a frequently affected region in the EAE model. WAIR images showed cortical grey matter lesions in one animal from the control group (M08035).

Quantification of the recorded MRI parameters confirmed the higher mean lesion volume in the white matter of the control animals compared to the antibody-treated monkeys. There was only one monkey in each group (M08035 and M08031) that showed presence of grey matter lesions (Fig. 2B). T2 signal intensities of white matter lesions are depicted in Figure 2C and MTR values in Figure 2D. The T2 parameter is a marker of inflammation induced tissue damage. It has been recently shown that the T2 parameter inversely correlates with myelin content in formalin fixed tissue of MS patients³¹². MTR reduction is mainly a result of demyelination but it is also sensitive for edema. The mean T2 (Fig. 2C) and MTR (Fig. 2D) values of the white matter were

somewhat higher in anti-CD20 mAb treated monkeys than in the control monkeys, although differences were not significant.

B-cell depletion prevents inflammation and demyelination in CNS

Histological analysis of the CNS showed large differences between the control and anti-CD20 treated group. In control animals inflammation and demyelination was found in spinal cord,



brain and optic nerve (Fig. 3A-C). Actively demyelinating lesions contained CD3+ T-cells, CD20+ B-cells as well as MRP14+ macrophages/microglial cells, which contained myelin degradation products suggesting active phagocytosis (Fig. 3 G-I). Animals treated with the anti-CD20 mAb contained much less inflammation in their CNS (Fig 3 J-L). Inflammatory cells were mostly found in small perivascular cuffs, while parenchymal infiltrates of T-cells and macrophages were absent. B-cells were found only sporadically, demonstrating the robust efficacy of anti-CD20 treatment. Demyelination was almost absent (Fig. 3D-F). In addition to demyelination of white matter, PBS treated animals also showed variable degrees of grey matter demyelination in subcortical, intracortical and subpial regions (Fig. 3M+O). Anti-CD20 mAb-treated animals lacked beside white matter demyelination also demyelination of cortical grey matter (Fig. 3N+P). Quantification of cell infiltration in spinal cord and of demyelinated areas in brain, optic nerve and spinal cord showed a significant decrease in the anti-CD20 mAb treated animals (Fig. 3Q). In conclusion, CD20+ B-cell depletion has a robust suppressive effect on CNS pathology.

Plasma antibodies binding rhMOG protein are undetectable

Profiles of antibodies against the immunizing MOG34-56 peptide or rhMOG in longitudinally collected immune plasmas were determined with ELISA. Figure 4A shows that the B-cell depletion had no clearly detectable effect on anti-MOG34-56 IgM plasma levels, which peak shortly after the initiation of B-cell depletion (PSD 28). The placebo group showed a somewhat lower level of anti-MOG34-56 IgM antibody compared to the anti-CD20 treated group, but the difference was not significant. Necropsy plasmas of both groups were tested against a broader range of MOG peptides, detecting low IgM plasma reactivity against MOG34-56 and the overlapping peptide MOG24-46 in the placebo group as well as in the anti-CD20 treated group. In contrast to IgM, levels of IgG antibodies against MOG34-56 in longitudinal plasmas, which peaked well after administration of the anti-CD20 mAb was started, were significantly decreased in the CD20-depleted group (Fig. 4B). In necropsy sera of control monkeys IgG antibodies were

◀ **Figure 1.** Extent of CD20+ B-cell depletion in lymphoid organs and the ensuing suppression of clinical EAE. A. CD20 expression in PBMC collected at the indicated time points was measured by flow cytometry. Grey shaded areas indicate the treatment period, which was started at post sensitization day (PSD) 21. Values on the y-axes are CD20+ cells expressed as percentage of total measured cells (mean ± SEM). No statistical analysis was performed beyond PSD 70 since there was only one animal left in the control group. B. At necropsy, MNC were prepared from PBMC, spleen, ALN, ILN, LLN and BM. After stripping *in vivo* bound anti-CD20 antibody (see Material and Methods) frequencies of viable CD20+ (left panel) and CD20+CD40+ (right panel) cells were determined by flow cytometry. Given percentages express the fraction of stained cells from the total measured cells (mean ± SEM). C. At necropsy also CD19 expression was measured by qPCR in PBMC, spleen and ALN. Data were normalized relative to the household gene ABL (mean ± SEM). D. Five twins were immunized with MOG34-56 in IFA (PSD 0). Monkeys not developing EAE score 2.0 (= ataxia/blindness) within 28 days were re-challenged with MOG34-56/IFA (▼). One sibling of each twin was injected once weekly with the anti-CD20 antibody HuMab 7D8 from PSD 21 to the end of the study (grey shaded box). The fraternal twin served as control and was injected with an equivalent volume of buffered saline (control) (left panel). Solid line indicates clinical scores (left y-axes) and dotted line body weight loss relative to PSD 0 (right y-axes). E. Survival curves show the disease free survival time (time interval to development of EAE score 2.0; upper panel) and survival (time interval to clinical endpoint; lower panel). PSD; post sensitization day. * $p < 0.05$; ** $p < 0.001$; **** $p < 0.00001$ Mann Whitney U test, treated group vs. control group. Log-rank test used for survival curves, significant when $p < 0.05$.

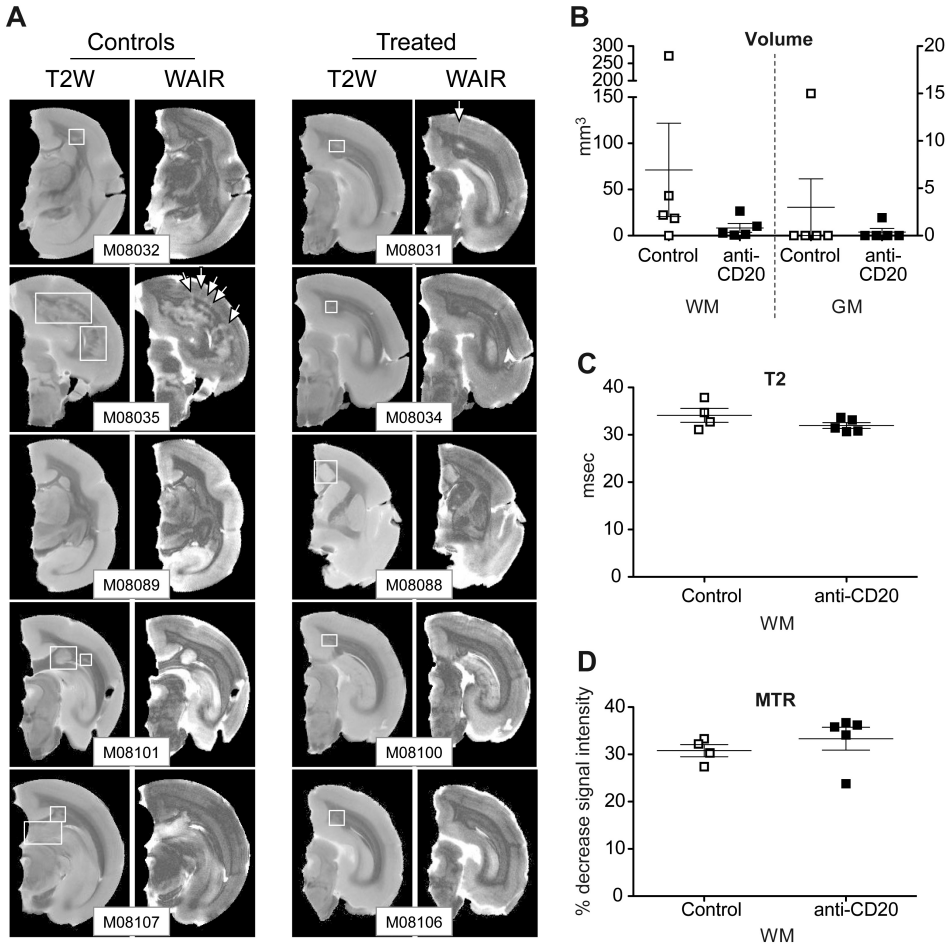


Figure 2. Post mortem MRI. MRI scans were made of the formalin-fixed brain halves of the control and CD20+ B-cell depleted monkeys to determine the number and spatial distribution of lesions in the white matter. A. High contrast T2-weighted (T2W) images were made to visualize abnormalities in white matter and white matter attenuated inversion recovery (WAIR) to visualize abnormalities in cortical grey matter. White boxes indicate lesions in the white matter, whereas the white arrows point to lesions in grey matter. B. Lesion volumes of white matter (WM) and grey matter (GM) lesion are depicted. Left y-axis indicate values of the WM and right y-axis values of the GM. T2- (C) and MTR values (D) are only shown of the WM lesions. No significant effect of anti-CD20 treatment was observed on the examined lesion parameters.

only detectable against MOG24-46 and MOG34-56, but not against intact rhMOG. The mAb treated animals showed significantly lower IgG antibodies against MOG24-46. IgM and IgG antibodies against rhMOG in longitudinal plasmas were not detected (data not shown).

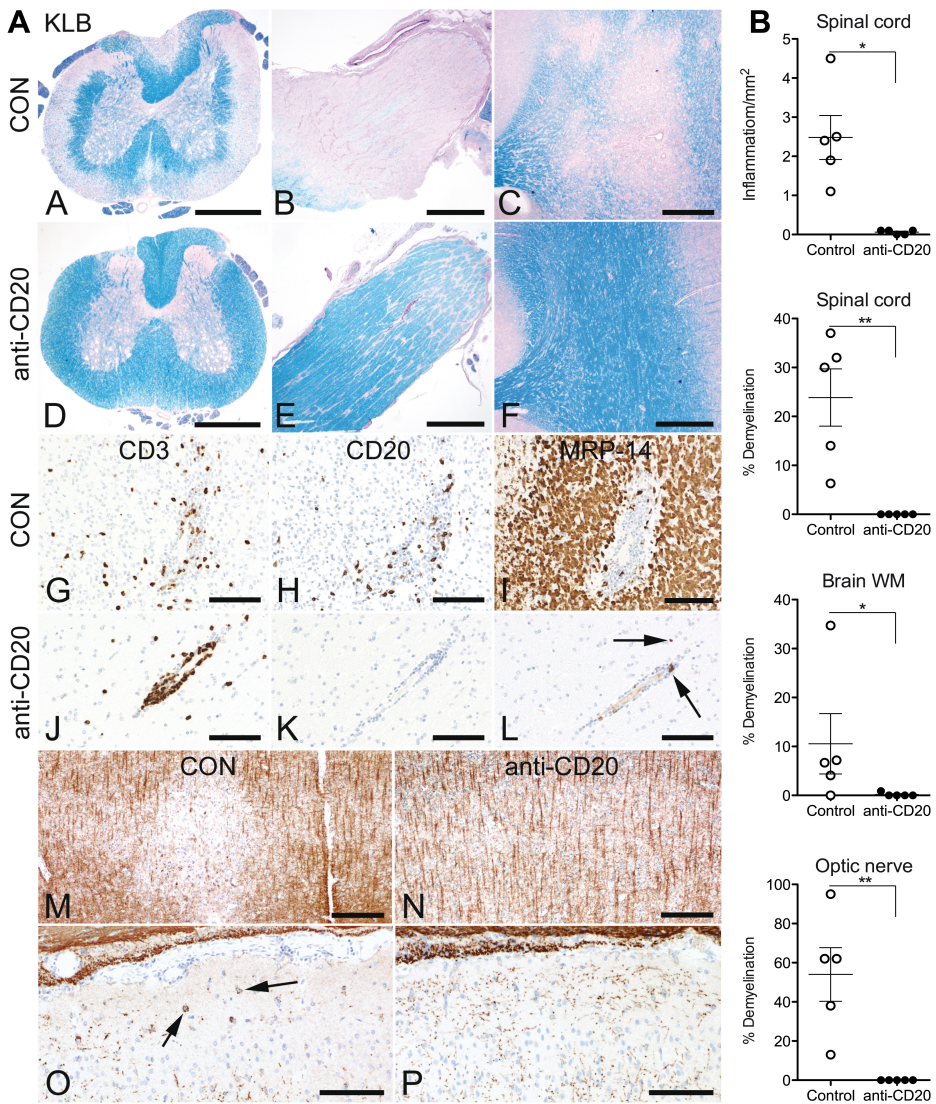


Figure 3. Histology and immunohistochemistry of spinal cord, brain and optic nerve. Formalin-fixed brain and spinal sections collected at necropsy were stained to analyze white and grey matter lesions. All animals have been evaluated, and the cases M08089 (control) (A-C) and M08088 (anti-CD20) (D-F) are depicted as representatives. Staining with Kluver-Barrera (KLB) shows extensive demyelination in the control animals, which is absent in the anti-CD20 treated animals. A+D. Spinal cord (16x, bar: 1 mm); B+E optic nerve (28x, bar: 500 μm). C+F. Corpus callosum (26x, bar: 500 μm). The cases M08035 (control) (G-I) and M08034 (anti-CD20) (J-L) are depicted as representatives for the amount of inflammation in the brain. G+J. CD3+ T-cells (130x, bar: 100 μm), H+K. CD20+ B-cells (130x, bar: 100 μm) I+L. MRP-14+ macrophages (130x, bar: 100 μm). Arrow in L depicts macrophages. M-P. Cortical demyelination was confirmed in the control group by PLP staining showing an intracortical lesion (M, M08032) (65x, bar: 200 μm) and a subpial lesion (O, M08035) (160x, bar: 100 μm) in the control case. Arrows point at PLP degradation products in phagocytizing macrophages. Anti-CD20 treated animals did not show intracortical (N, M08031) (65x, bar: 200 μm) or subpial demyelination (P, M08034) (160x, bar: 100 μm). Q. For each animal 8 brain, spinal cord or optic nerve sections were analyzed, which equals 6 cm² in total. The number of infiltrated cells per mm² is given for the spinal cord (most upper graph). The other three graphs depict the amount of demyelination in the spinal cord, brain white matter (WM) and optic nerve. Data are presented as mean ± SEM. **p*<0.05, ***p*<0.001, Mann-Whitney *U* test.

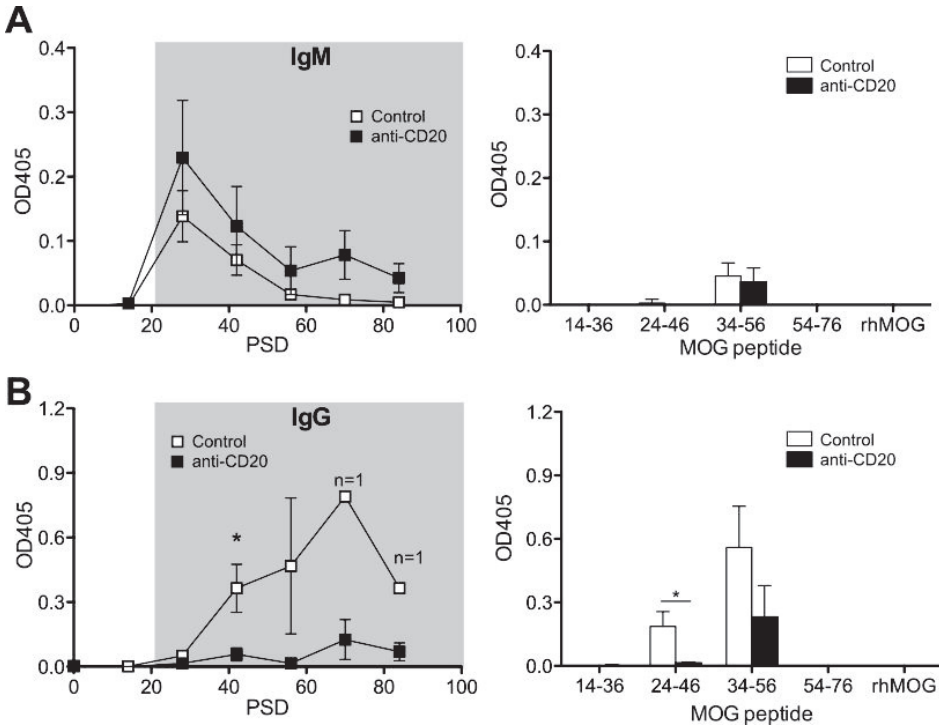


Figure 4. Anti-MOG34-56 IgG and IgM plasma levels. Plasma samples collected at 2 weeks interval and at necropsy were tested for the presence of IgM (A) and IgG (B) antibodies with ELISA. Longitudinally collected plasmas were tested for the presence of IgM and IgG against MOG34-56 (left panel), whereas necropsy samples (right panel) were tested for reactivity with a selected panel of 23-mer MOG peptides as well as rhMOG. No statistical analysis could be performed at PSD 70 and 84 since there was only one animal left in the control group. Grey shaded boxes indicate the anti-CD20 antibody treatment period. Data is expressed as light absorption at 405 nm (OD405) and is subtracted with OD405 of pre-immune plasma of the same animals (mean \pm SEM). * $p < 0.05$ Mann Whitney U test, treated group vs. control group.

Modulation of cellular responses by anti-C20 mAb treatment

MNC were isolated from blood collected from the femoral vein of control and CD20+ B-cell depleted marmosets at 14 days interval. The MNC were tested for proliferation against the immunizing MOG34-56 peptide using incorporation of [³H]-thymidine as read-out (Fig. 5A). In agreement with previous findings, proliferation responses of blood MNC (PBMC) were rather low²⁸⁸. The graph (upper panel) shows that proliferation of MNC incubated in culture medium is increased during the period of clinically active EAE (from PSD 40) and that this increase is absent in the anti-CD20 treated monkeys. However, differences were not significant. The lower panel of the picture shows that proliferation of PBMC against MOG34-56 was comparable in both groups. qPCR analysis detected somewhat reduced CD3 mRNA expression in PBMC and spleen in the antibody-treated group, while CD3 mRNA levels in ALN were higher than in control monkeys. mRNA transcripts of granzyme B and perforin, which are both markers

of cytotoxic T-cells, tended to be reduced in PBMC and ALN of the CD20-depleted monkeys. However, these differences were not significant.

Next, we determined the phenotype of the T-cells proliferating *ex vivo* in cultures stimulated with MOG34-56 or a set of 9-mer and 12-mer overlapping peptides covering MOG34-56. We assumed that these 9-mer and 12-mer MOG would delineate epitopes inducing proliferation of MHC class I restricted CD8+ and MHC class II restricted CD4+ cells, respectively. Figure 5C shows the pooled proliferation data from 4 monkeys. Proliferation of T-cells from the fifth control monkey (M08107) could not be measured due to technical failure. In all lymphoid organs and blood from control monkeys we observed increased proliferation against MOG34-56 vs. unstimulated MNC. Interestingly, in all lymphoid organs we detected increased proliferation against the 12-mer peptide MOG37-48, although this was only significant for the ALN. This test identifies MOG37-48 as a candidate epitope of MHC class II restricted CD4+ T-cells. This peptide overlaps with the previously identified 9-mer MOG40-48 epitope of the Caja-E restricted cytolytic T-cells³⁰⁷. However, it cannot be excluded that the 12-mer peptides were processed to 9-mer peptides and presented via MHC class I to CD8+ T cells.

Using CFSE vital dye dilution in combination with mAb staining, profiles of proliferating cells were measured in a 7 days culture stimulated with MOG34-56 or with the panel of 9-mer and 12-mer overlapping peptides. Reactivity in MNC isolated from ALN was only detected against MOG34-56 and the two putative epitopes MOG37-48 and MOG40-48. The graphic presentation in Figure 5D and the numerical presentation in supplementary Table 1 show that in non-stimulated cultures $\pm 45\%$ of the ALN MNC from untreated control monkeys displayed CFSE dilution as marker of proliferation. This percentage increased to $>60\%$ by the addition of MOG34-56 to the cultures and $> 50\%$ when the shorter peptides, MOG37-48 and MOG40-48, were added. Highly remarkable was the observation that $>80\%$ of the CD3+ cells in unstimulated cultures from the anti-CD20 mAb-treated monkeys displayed CFSE vital dye dilution. In these cases addition of MOG34-56, MOG37-48 or MOG40-48 exerted no detectable effect. The high percentage of CD3+ cells with CFSE dilution was for a large part attributable to CD4+ and CD4+CD56+ subpopulations. Interestingly, only in the CD4+CD8+ and CD4+CD8+CD56+ we observed the anticipated effect of the antibody-treatment, namely that the increased MNC proliferation rate in peptide-stimulated cultures from control animals, was abrogated in monkeys depleted of CD20+ B-cells.

Variable cytokine profiles in blood and lymphoid organs

MNC from blood, spleen, ALN, ILN and LLN were tested for IL-17A, IFN- γ and TNF- α production upon *ex vivo* stimulation with MOG34-56 and its overlapping 9-mer and 12-mer peptides (Fig. 6A). Increased cytokine production was only detected in cultures stimulated with MOG34-56 and MOG37-48; no detectable cytokine levels were induced by the other peptides (data not shown). IL-17A and IFN- γ were produced at a higher level than TNF- α . Cytokine responses were not only strongly variable between the groups but also between organs of individual animals. Hence, a consistent modulatory effect of the treatment on cytokine profiles could not be assessed.

The mRNA transcript levels for various cytokines in PBMC, spleen and ALN were determined by qPCR. Figure 6B shows a decreased level of IL-17A in PBMC and spleen, but a significant increase of these cytokine transcripts in ALN of CD20 treated animals. This same pattern

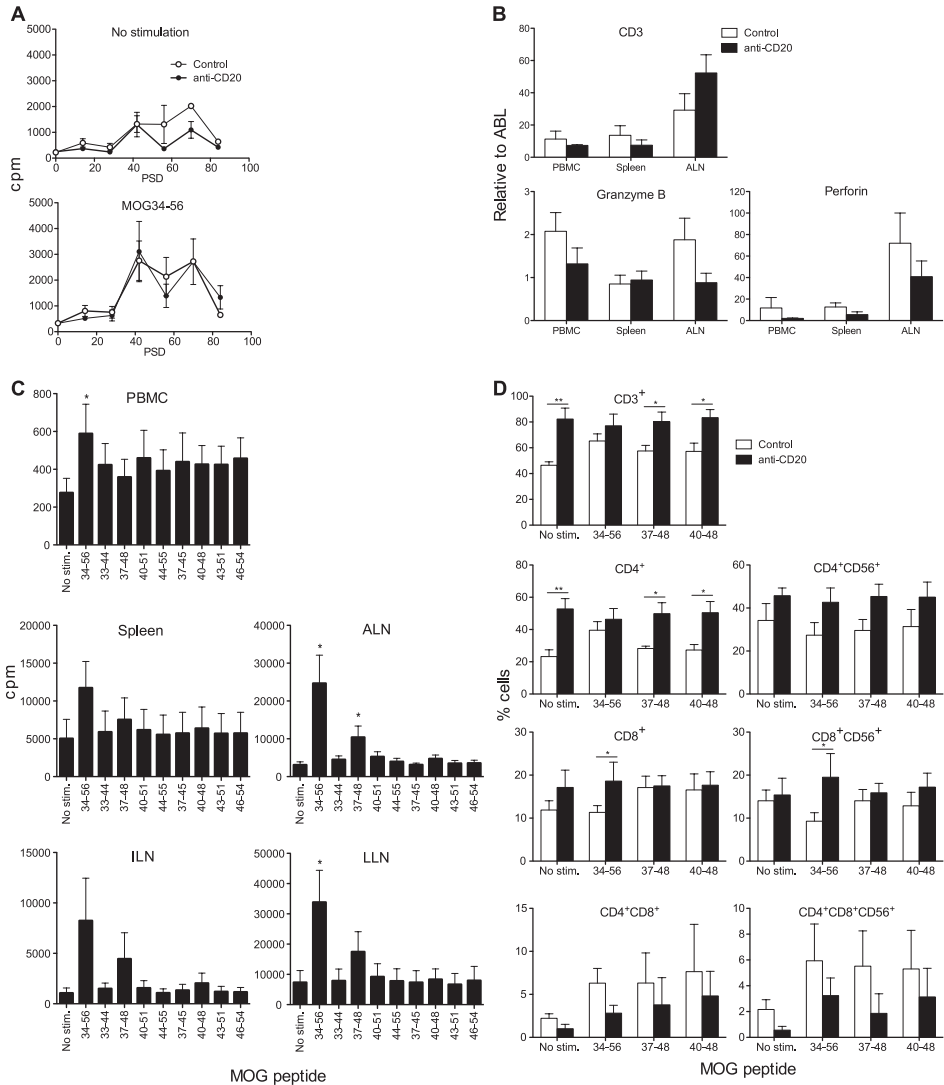


Figure 5. Analysis of proliferating T-cell subsets in *ex vivo* stimulated MNC. A. PBMC were isolated from venous blood at the indicated time points and tested for reactivity with MOG34-56 using incorporation of [³H]-thymidine as read-out. The left panel shows the background proliferation of cells without stimulation and the right panel shows cell cultures with MOG34-56 stimulation. Data presented on y-axis are in counts per minutes (cpm) (mean ± SEM). B. At necropsy CD3, granzyme B and perforin mRNA levels in PBMC, spleen and ALN were determined by qPCR. Data were normalized against the household gene ABL (mean ± SEM). C. At necropsy proliferation was measured in MNC from blood and various lymphoid organs (spleen, ALN, ILN, and LLN) against MOG34-56 and a set of 12-mer and 9-mer MOG peptides. Data from 4 control monkeys are shown as cpm (mean ± SEM). D. For phenotyping of *in vivo* activated T-cells, ALN cells were labeled with CFSE and subsequently cultured for 7 days with MOG34-56, MOG37-48 (putative CD4⁺ T-cell epitope) and MOG40-48 (proven CD8⁺ T-cell epitope)³⁰⁷. Percentages of proliferated cells (with CFSE dilution) are shown on the y-axes (mean ± SEM). Populations expressing CD4⁺, CD8⁺, and double positive for CD4 and CD8 were first gated for the CD3⁺ proliferated population and next also for CD4⁺CD56⁺, CD8⁺CD56⁺ and CD4⁺CD8⁺CD56⁺, respectively. cpm, count per minute. **p*<0.05 Mann Whitney *U* test, MNC cultures with antigen vs. MNC cultures without antigen.

was observed for TNF- α and IFN- γ mRNA transcript levels. The cytokine pattern parallels the pattern of CD3 transcript levels, suggesting that the different cytokine profiles only reflect the different distribution of CD3+ T cells (Fig.5B). We detected lower expression of IL-7 and IL-10 mRNA in all the tested organs of the CD20 group. In summary, the remarkable clinical effect of CD20+ B-cell depletion is not reflected by a clearly detectable modulatory effect on peripheral helper T-cell subsets, such as Th1 and Th17, or their signature cytokines.

Infusion of BLCL₀ or BLCL_{MOG} differently affect body weight

The experiments discussed thus far suggest that B-cells are, either directly or indirectly, involved in the activation of the autoreactive T-cells that elicit grey and white matter lesion formation and neurological deficit in the MOG34-56/IFA model. A second *in vivo* experiment was performed to examine this further. We tested whether infusion of immortalized semi-autologous B-cells presenting MOG34-56 directly activates the autoreactive T-cells. Five chimeric twins were selected and autologous B-cells were infected with EBV strain B95-8 to generate B lymphoblastoid cell lines (BLCL). One sibling of each twin was infused with BLCL pulsed with the MOG peptide (BLCL_{MOG}) and the other sibling with non-pulsed BLCL (BLCL₀). Overt neurological deficit was observed neither in the monkeys that received BLCL_{MOG} nor in those infused with BLCL₀ (data not shown). However, bodyweight measurements show a remarkably different pattern between these two groups (Fig. 7). After approximately 50 day in

7

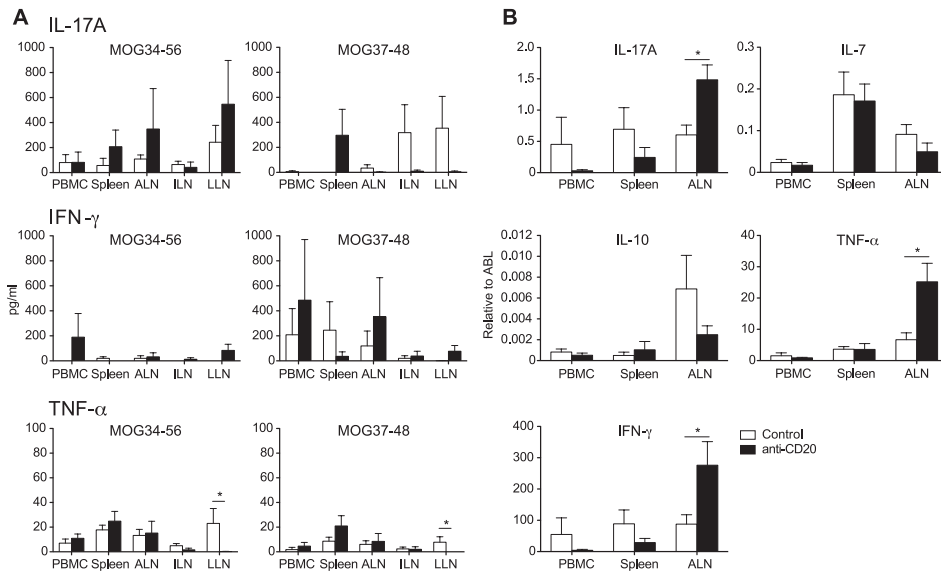


Figure 6. Cytokine expression in blood and lymphoid organs. A. At necropsy MNC were isolated from blood and lymphoid organs and cultured for 48 h with the indicated stimuli. The levels of IL-17A (upper panel), IFN- γ (middle panel) and TNF- α (lower panel) in culture supernatants were tested with ELISA. Data are shown of cultures stimulated with MOG34-56, MOG37-48 or without stimulation (mean \pm SEM). B. Cytokine mRNA transcripts of IL-17A, IL-7, IL-10, TNF- α and IFN- γ were measured in PBMC, spleen and ALN. * $p < 0.05$ Mann Whitney *U* test, antigen stimulated MNC vs. unstimulated MNC.

experiment the BLCL_{MOG} recipients showed a higher increase of bodyweight than the monkeys infused with BLCL₀, although this effect is not statistically significant. The relevance or the underlying mechanism is not understood, but the different patterns suggest a distinct systemic response against the infusion of B-LCL₀ or B-LCL_{MOG}.

Proliferation of MNC subsets in BLCL₀ and BLCL_{mog} recipients

Proliferation of venous blood MNC against BLCL₀ and BLCL_{MOG} was measured every 14 days. Proliferating cells in different T-cell subsets were visualized by CFSE vital dye dilution combined with mAb staining (Fig. 8). For normalization purposes the data of each subset are expressed as ratio (% cells with CFSE dilution against BLCL_{MOG} divided by % cells with CFSE dilution against BLCL₀). According to this definition values >1 (dotted line) represent higher proliferation against BLCL_{MOG}, where values <1 represent higher proliferation against BLCL₀. The results in Figure 8 show that after each BLCL infusion transient expansion of CD4+, CD8+ and CD4+8+ subsets in blood was observed, namely at PSD 13, 41 and 69. However, the calculated ratios for these subsets remain low, varying between 0.5 – 2.0. The high standard errors imply that the response of T-cell subsets towards the two BLCL preparations between individual animals is highly variable in this outbred model. The strongest response was observed in the CD3+CD4+CD8+CD56+ T-cells, albeit only at one time point, i.e. PSD 13. Interestingly, in previous studies in the MOG34-56/IFA model this same subset was identified as the main responding fraction against soluble MOG34-56^{288,307}.

Cytokine profiles and cytotoxic activity of MNC from BLCL₀ and BLCL_{mog} recipients

The two main immunological activities of the *in vivo* activated T-cell subsets in the MOG34-56/IFA model were production of IL-17A and specific cytolysis of BLCL_{MOG}. Hence both parameters were also analysed in this experiment.

Cytokines: MNC from blood, spleen and ALN were *ex vivo* stimulated with or without MOG34-56. In addition, the MNC were cocultured with BLCL₀ and BLCL_{MOG}. Culture supernatants were collected and tested for the presence of IL-17A, IFN- γ and TNF- α . Figure 9A shows that in MNC cultures stimulated with MOG34-56, IL-17A was the only produced cytokine. Stim-

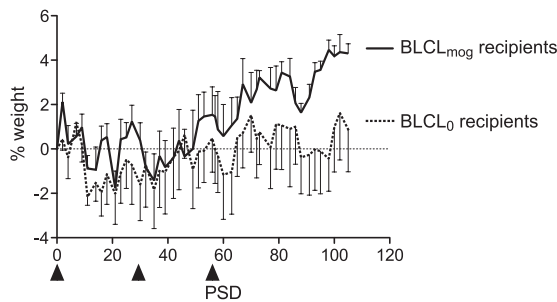


Figure 7. Body weight as a surrogate disease marker in the BLCL experiment. At the indicated time points (▲) 5 marmoset twins were infused with 1 ml PBS containing 10^7 viable BLCL. Body weights were recorded 3 times per week and are depicted as percentage weight change relative to day 0. PSD, post sensitisation day.

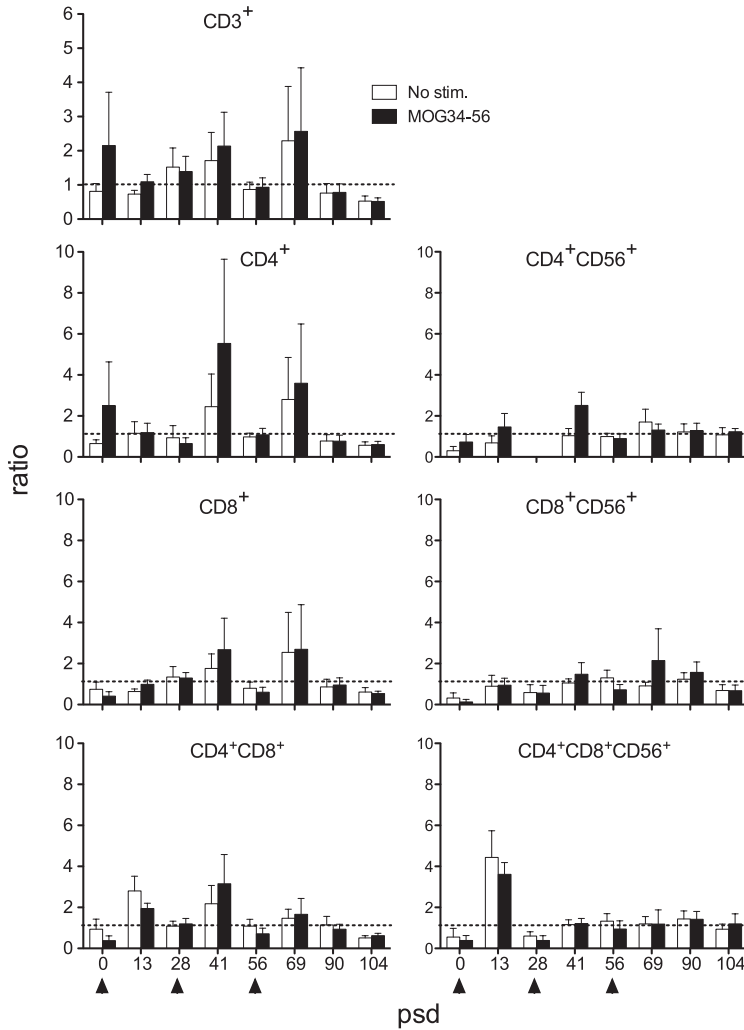


Figure 8. Differential *ex vivo* reactivity of T-cell subsets from BLCL₀ and BLCL_{MOG} recipients. Blood MNC were collected every two weeks and stained with CFSE. CFSE stained MNC were incubated for 7 days with MOG34-56 and without stimulation. Proliferation is expressed as the ratio of proliferated cells in each subset in the BLCL_{MOG} group over the proliferated cells of the corresponding subset in the BLCL₀ group. Calculations were performed for each twin. Data of all 5 twins were pooled and presented as mean ± SEM. Mann Whitney *U* test was performed, but no significant effects were obtained.

ulation of PBMC with BLCL_{MOG} or BLCL₀ induced a higher production of IL-17A in PBMC from BLCL_{MOG} recipients than PBMC from BLCL₀ recipients. Remarkably, there was a trend, albeit not statistically significant, towards lower IL-17A induction by BLCL_{MOG}. Stimulation with BLCL_{MOG} or BLCL₀ induced also a higher production of IFN- γ and TNF- α .

Cytotoxicity: We assumed that infused BLCL escaping immunity of the recipient monkey could be detected in lymph node or spleen MNC by *ex vivo* proliferation using CFSE vital dye dilution in cultures without additional antigenic stimulation. Figure 9B shows that the percentages of such spontaneously proliferating CD20+ cells were very low in blood, but can be substantial in spleen and ALN, although variation was observed between the individual animals. Interestingly, addition of MOG34-56 to the cultures led to elimination of these spontaneously proliferating CD20+ cells in 2 of 3 cases (spleen) and 1 of 3 cases in ALN. This was only observed in the recipients of BLCL_{MOG}, not in the fraternal siblings infused with BLCL₀. This finding suggests that infusion of BLCL₀ or BLCL_{MOG} led to differential induction of MOG34-56 specific cytotoxicity.

Brain inflammation in recipients of BLCL_{MOG}

At necropsy brains and spinal cord were removed and processed for examination with T2W MRI and histology. MRI scans showed no major abnormalities in the brain parenchyma (data not shown), which was confirmed by histology. Formation of perivascular cuffs in brain was also not observed. However, in two monkeys (M07023 and M07039), which were both recipients of BLCL_{MOG}, infiltrates of CD3+ and CD20+ lymphocytes were detected in meninges (Fig.10). Such infiltrates were not observed in recipients of BLCL₀.

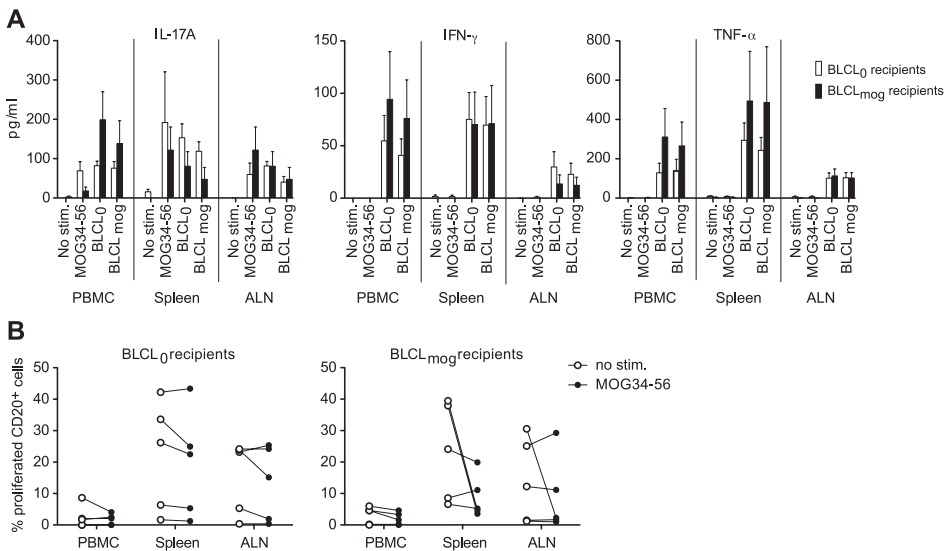


Figure 9. Cytokine profile and B-cell proliferation in MNC of the BLCL experiment. At necropsy, MNC were prepared from blood, spleen and ALN. A. Part of the MNC were cultured for 48 h without stimulation, with MOG34-56, with BLCL₀ or with BLCL_{MOG}. IL-17A (left), IFN- γ (middle) and TNF- α (right) levels in culture supernatants were measured with ELISA. B. Another part of the MNC were stained with CFSE and cultured with MOG34-56 or no antigen. After culture the cells were harvested and stained with for CD20. The figure shows the percentage CD20+ cells with CFSE dilution as a marker of proliferation. Data of individual recipients of BLCL₀ and BLCL_{MOG} are shown. Mann Whitney U test on group means was performed, but no significant effects were obtained.

DISCUSSION

The aim of the reported study was to find a mechanistic explanation for the remarkable clinical effect of CD20+ B-cell depleting mAb in MS. Previous research in a more classical variant of the marmoset EAE model, induced with rhMOG in CFA, demonstrated that the depletion of CD20+ B-cells exerts modulatory effects on the humoral as well as cellular arm of the marmoset immune system²¹⁵. Although the administration of HuMab7D8 was started after onset of autoimmunity, it induced significant suppression of lesion formation in CNS white and grey matter and to complete suppression of neurological deficits²¹⁵. This finding led us to hypothesize that B-cells may be involved in the activation of T-cell subsets associated with induction of neurological deficit²⁴¹.

According to our previous report, T-cells specific for MOG34-56 have a central role in the complex autoimmune reactions generated in marmosets immunized with human myelin that lead to the induction of neurological deficits^{288, 307}. These culprit T-cells seem to originate from a small subset of T-cells expressing CD4 and CD8 together with CD27 and CD56, but not CD28 or CD16^{288, 307}. They become engaged relatively late in the pathogenic process, hypothetically in the response against initial myelin injury caused by early acting Th1 cells specific for the epitope MOG24-36 which infiltrate the CNS white matter and cause mild inflammation^{103, 190}. The presence of CD4 and CD8 double positive T-cells with cytotoxic activity in extra-thymic immune compartments is not uncommon in primates as these were already demonstrated in Old³¹³ as well as New World³¹⁴ primate species. The pathogenic potential of the late acting T-cells was investigated in a highly refined MOG34-56/IFA EAE model showing that, besides expressing effector memory characteristics, these cells display high IL-17A production and Caja-E restricted cytotoxic activity as immunological hallmarks³⁰⁷. It is of note that Caja-E is the marmoset representative of a lineage of non-classical MHC class Ib molecules involved in NK cell regulation, comprising also HLA-E (human) and Qa-1 (mouse).

In the current study we used the MOG34-56/IFA EAE model to further examine antibody-nondependent contributions of B-cells to the development of MS-like CNS pathology. Impor-

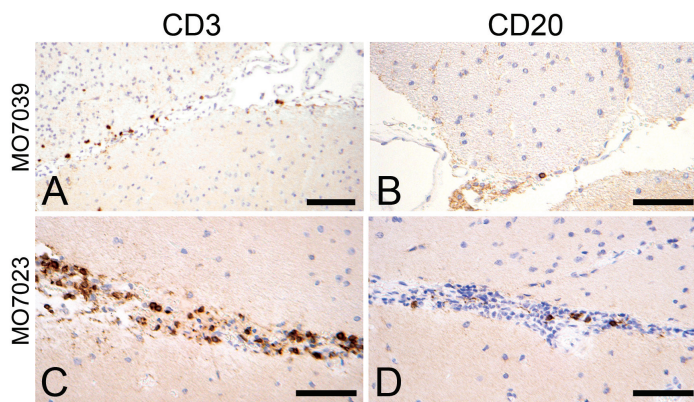


Figure 10. CNS pathology in the BLCL experiment. Immunohistochemistry was performed on formalin-fixed brain material. Only in M07023 and M07039 (both recipients of BLCL_{mog}) signs of CNS inflammation were detected, namely infiltration of CD3 (A+C) (100x, bar: 200 μ m) and CD20 cells (B+D) (40x, bar: 100 μ m).

tantly, EAE in this model develops without the deliberate TLR-mediated activation of APC and also without detectable induction of autoantibodies binding to intact rhMOG protein, which is a requirement for mediating demyelination³⁰⁸. The results reported here show a 100% clinical effect of the treatment with anti-CD20 mAb in the EAE model; all control monkeys developed clinically evident EAE but none of the anti-CD20 treated monkeys. Just like in the rhMOG/CFA EAE model, the complete protection against disease is associated with profound reduction of CNS pathology. The analyzed hemisphere of one antibody-treated monkey (M08031) contained an MRI-detectable lesion within and around the corpus callosum, but in the control group there were 4 monkeys with multiple lesions. Histology data showed a significant reduction of inflammation and demyelination in the spinal cord, brain and optic nerve of the antibody-treated monkeys. Taken together, the clinical and pathological data obtained in the marmoset MOG34-56/IFA EAE model seem to closely reproduce the clinical effects of CD20+ B-cell depletion in relapsing-remitting MS⁷⁵.

As an explanation for the therapeutic mode of action of anti-CD20 antibodies in MS, interference with several B-cell functions in the disease have been proposed³⁰⁹: 1. the production of autoantibodies that target antigens within the CNS; 2. antigen presentation to pathogenic T-cells; 3. production of cytokines that amplify rather than suppress the pathogenic process, such as lymphotoxin or TNF- α ; 4. the induction of ectopic lymphoid structures within the CNS where ongoing activation of CNS infiltrating T-cells can take place.

Option 1 is not a very likely explanation for the clinical effect of anti-CD20 antibody treatment observed in the MOG34-56/IFA marmoset EAE model. Autoantibodies binding to intact rhMOG protein, which is a requirement for their capacity to mediate demyelination³⁰⁸, were not detectable in this model. Option 4 is strongly advocated by Aloisi and co-workers³¹⁵, but could not be reproduced by other laboratories³¹⁶. Moreover, we have thus far not found ectopic lymphoid structures in the brain of EAE affected marmosets. The remaining options 2 and 3 are not mutually exclusive and both possibilities seem to be supported by our current and previous studies.

Our current data obtained in the MOG34-56/IFA model together with previously reported data in the rhMOG/CFA model²¹⁵ show that the strongest effect of B-cell depletion can be found in the activation of CD4+CD8+CD56+ T-cells specific for MOG34-56. This highly reactive subset of effector memory T-cells, characterized by IL-17A production and specific cytotoxicity, seems closely associated with the induction of CNS grey matter demyelination and neurological deficits³⁰⁷. Whether an equivalent subset of autoreactive T-cells is also present in MS patients is a subject of our current investigations. It is of note, however, that the immune repertoire of MS patients is enriched with CD4+CD56+ cytotoxic T-cells capable of inducing demyelination by killing of oligodendrocytes^{269, 270}. Moreover, we have found enrichment of these T-cells in the MS repertoire with cytotoxic activity towards cells presenting a cocktail of MOG peptides, including MOG34-56¹³⁷. Finally, Bielekova et al.³¹⁷ found increased levels of high affinity and IL-7 responsive T-cells specific for MOG34-56 in the MS repertoire. In addition, the current study shows that infusion of B-LCL_{MOG} induces MNC from blood to produce increased IL-17A levels upon *ex vivo* restimulation with BLCL_{MOG}. The current study also provides evidence that infusion of BLCL_{MOG} induces *in vivo* activation of cytotoxic T-cells that could *ex vivo* eliminate B-cells from cultures. This was not observed in MNC from the fraternal siblings, which had been infused with BLCL₀.

At this stage of the research it is unclear whether EBV infection and/or transformation is essential for their pathogenic functions of B-cells in MS as hypothesized by Pender³¹⁸. However, whereas normal B-cells are well capable to present soluble antigens via MHC class II molecules to CD4+ T-cells, their capacity to present soluble antigen via MHC class I molecules to CD8+ T-cells is limited. B-cells costimulated via TLR9 by CpG oligonucleotides are capable of presenting soluble antigen via MHC class I³¹⁹, but such TLR ligands are absent in the MOG34-56/IFA inoculum²⁸⁸. EBV infected B-cells, however, are very well capable to ingest, process and present rhMOG protein or the 23-mer MOG34-56 peptide to CD8+ T-cells (Fig. 5C).

In conclusion, we report that B-cell depletion with anti-CD20 antibody exerts an impressive clinical effect in an autoantibody non-dependent model of MS in the common marmoset. The reported data show impaired activation of the pathogenic CD3+CD4+CD8+CD56+ T-cell subset, as a possible mechanistic explanation. Positive proof that this subset of T-cells is indeed responsible for the described pathogenic features, by e.g. adoptive transfer has failed thus far. The main reason is that the EBV-transformed B-cells, which are the only available source of autologous APC in this outbred model, are killed by the T-cells when they are pulsed with MOG34-56. As an alternative we have tested T-cell transformation with Herpesvirus saimiri. However, virus-transformed T-cells produced IFN- γ but not IL-17A, and lacked cytotoxic activity suggesting that transformation had changed their function (unpublished data). We also report data supporting direct activation of these encephalitogenic T-cells by peptide presenting EBV-infected/transformed B-cells. It is tempting to speculate whether this may also occur in MS as enrichment of the T-cell repertoire of MS patients with MOG specific cytotoxic T-cells¹³⁷ as well as with IL-7 responding T-cells specific for MOG34-56²⁸⁹ has been documented. However, we are not aware that such a mechanism has been proposed as possible explanation for the well-documented, but still poorly understood association between clinical EBV infection (infectious mononucleosis) and MS³²⁰.

ACKNOWLEDGEMENTS

The anti-CD20 antibody HuMab 7D8 was a gift from GenMAB, The Netherlands. We would like to thank the biotechnical staff and veterinarians from the BPRC for the care and excellent biotechnical support during the *in vivo* phase of the experiments. Part of the reported experiments was financially supported from the EC grant EUPRIM-NET 026155.

**ANTIBODIES AGAINST HUMAN BLYS
AND APRIL ATTENUATE EAE
DEVELOPMENT IN MARMOSSET MONKEYS**

S. Anwar Jagessar, Nicole Heijmans, Jan Bauer,
Erwin L.A. Blezer, Jon D. Laman, Thi-Sau Migone,
Matt N. Devalaraja*, and Bert A. 't Hart*

* Both authors shared senior authorship

Submitted

ABSTRACT

B lymphocyte stimulator (BLyS, also indicated as BAFF (B-cell activating factor) and CD257), and A Proliferation Inducing Ligand (APRIL, CD256) are two members of the TNF superfamily with a central role in B cell survival. Antibodies against these factors have potential therapeutic relevance in autoimmune inflammatory disorders with a proven pathogenic contribution of B cells, such as multiple sclerosis MS. In the current study we performed a multi-parameter efficacy comparison of monoclonal antibodies against human anti-BLyS and anti-APRIL in the common marmoset (*Callithrix jacchus*) model of experimental autoimmune encephalomyelitis. The results show that the anti-BLyS and anti-APRIL antibody cause significant depletion of circulating CD20⁺ B cells, where levels of CD20⁺CD40⁺ B cells were unaltered. Induction of CD20⁺ B cell depletion from lymph nodes was only observed in the anti-BLyS treated monkeys. Both antibodies had a significant inhibitory effect on disease development, but all monkeys developed clinically evident experimental autoimmune encephalomyelitis (EAE). Anti-BLyS treated monkeys were sacrificed with the same clinical signs as saline-treated monkeys, but nevertheless displayed significantly reduced spinal cord demyelination. This effect was not observed in the anti-APRIL treated monkeys. The two antibodies had a different effect on T cell subset activation and the profiles of *ex vivo* released cytokines. In conclusion, treatment with anti-BLyS and anti-APRIL delays the development of neurological disease in a relevant preclinical model of MS. The two mAbs appear to achieve this effect via different mechanisms.

INTRODUCTION

Multiple sclerosis (MS) is an inflammatory demyelinating disease of the human central nervous system (CNS). The disease is pathologically characterized by the presence of demyelinated lesions within the white as well as grey matter; lesions contain a variable degree of inflammation and damage to axons and neurons³²¹. Although demyelinated lesions are likely formed by the synergy of cellular and humoral immune mechanisms, most immunotherapies developed for MS target T cells²⁷¹. The results of two recent clinical trials seem to have caused a paradigm shift in therapy development. Unexpectedly, treatment of patients with relapsing/remitting MS patients using an antibody against human anti-IL12p40 antibody, aiming at the simultaneous inhibition of Th1 and Th17 T cell responses as demonstrated in psoriasis³²², showed no detectable clinical benefit in relapsing remitting MS (RRMS)²⁸⁵. On the other hand, treatment of a similar group of patients with monoclonal antibodies against human CD20, causing profound and long lasting depletion of B cells, caused rapid and sustained suppression of neurological symptoms³⁰⁹.

Total CD20+ B cell ablation is a highly effective manner to induce robust and long-lasting disease suppression in a variety of autoimmune disorders, including rheumatoid arthritis (RA), systemic lupus erythematosus (SLE)³²³, and MS³⁰⁹. However, the treatment spares plasma cells, it causes impairment of the immune defence against new and latent infections. This warrants the search for B cell targeting treatments with less profound immunosuppressive effects.

The long-lasting depletion of B cells, being essential players in the immune defends against new and opportunistic infections, and is associated with side effects. Occasional reactivation of hepatitis B and C, and polyoma (JC) virus give rise to serious clinical complications³²⁴. This situation warrants the question whether profound systemic B cell depletion is indeed needed or whether alternative B cell targeting treatments may achieve a similar beneficial effect.

The primary aim of this study was to test the efficacy of two monoclonal antibodies, specific for B Lymphocyte Stimulator (BLYS), also known as B-cell Activating Factor (BAFF, CD257) of the TNF family, and for A Proliferation-Inducing Ligand (APRIL, CD256). Both cytokines have an important role in the differentiation of B cells³²⁵. A secondary aim was to obtain in a relevant preclinical model of MS mechanistic information on the autoimmune processes that are modulated by the two antibodies.

The efficacy of the two antibodies was tested in an experimental autoimmune encephalomyelitis (EAE) model in common marmosets (*Callithrix jacchus*), induced by immunization with recombinant human myelin/oligodendrocyte glycoprotein (rhMOG) formulated in complete Freund's adjuvant (CFA)^{103,190}. This rhMOG/CFA EAE model has been well established as a valid preclinical model of MS for translational research into immunopathogenic mechanisms and the preclinical evaluation of novel immunotherapies³²⁶.

The close immunological proximity with humans enables the efficacy testing of therapeutic antibodies developed for the treatment of MS, such as the anti-human CD20 antibody ofatumumab²¹⁵. It was shown that administration of HuMab 7D8, a novel fully human IgG that binds the same epitope on human CD20 as ofatumumab³¹⁰ suppresses cellular and humoral autoimmune mechanisms that lead to lesion formation and neurological deficit²¹⁵.

The current study shows that the anti-BLYS and anti-APRIL antibodies induce depletion of CD20+ B-cells, which is reflected by suppressed autoantibody production. However,

we observed a stronger therapeutic effect of the anti-BLyS than of the anti-APRIL antibody, associated with significant suppression of demyelination in the spinal cord.

MATERIALS AND METHODS

Animals

Eighteen adult male common marmosets (*Callithrix jacchus*) were purchased from the outbred colony maintained at the Biomedical Primate Research Centre (Rijswijk, The Netherlands). Individual data of all monkeys used in this study are listed in Table 1. Before inclusion of the animals in the study they were subjected to a complete physical, haematological and biochemical examination. Only monkeys that were declared healthy by the institute's veterinarians were used. During the study they remained under veterinary care. Monkeys were pair-housed in spacious cages enriched with branches and padded shelter on the floor. Daily diet consisted of commercial food pellets of New World monkeys (Special Diet Serviced, Witham, Essex, UK), supplemented with raisins, peanuts, marshmallows, biscuits, fresh fruit, maggots and gum. Drinking water was provided ad libitum.

According to the Netherlands' law on animal experimentation, the procedures of this study was reviewed and approved by the institute's ethics committee before initiation of the experiments.

Antigens

Human MOG extracellular domain (rhMOG) was expressed as an unglycosylated recombinant protein in *Escherichia coli* and purified in the BPRC laboratory, as previously described^{193, 138}. All synthetic peptides based on the human MOG sequence, which were used for *in vitro* assays, were purchased from Cambridge Research Biochemicals Limited (Cleveland, UK).

EAE induction and clinical scoring

EAE was induced with 100 µg of rhMOG emulsified in CFA as previously described²¹⁵. All animals were daily monitored for neurological signs using a standard scoring systems^{190, 288}. Briefly, 0 = no clinical signs; 0.5 = apathy, loss of appetite, altered walking pattern without ataxia; 1 = lethargy, anorexia, loss of tail tonus, tremor; 2 = ataxia, optic disease; 2.5 = paraparesis or monoparesis, sensory loss; 3 = paraplegia or hemiplegia; 4 = quadriplegia; 5 = spontaneous death due to EAE. The clinical end-point for each monkey was score 3 and overt neurological symptoms were observed from score 2.

Experimental design

The human anti-BLyS antibody (Benlysta; also known as belimumab) and anti-APRIL antibody were provided by Human Genome Sciences, Inc (Rockville, MD). Both antibodies bound the marmoset BLyS and APRIL with high affinity.

All monkeys were randomized to three groups of 6. Power calculations were used to assess the minimal group size for statistical evaluation. Anti-BLyS and anti-APRIL mAbs were administered intravenously at a dose of 10 mg/kg (1 ml/kg) once a week from day 21 after immunization until the end of the study. The control group received buffered saline (1 ml/kg) also once a week from day 21 after immunization.

Table 1. Overview of marmoset used in this study and the post-mortem MRI read-outs of white (WM) and grey (GM) matter lesions in one cerebral hemisphere.

Group	Animal	DOS ^a	Age ^b	MRI lesions					
				Volume (mm ³)		T ₂ (sec)		MTR (%)	
				WM	GM	WM	GM	WM	GM
Control	M02061	30	102	0	0	-	-	-	-
	M05053	57	62	540.7	34	65.9	71.7	29.3	26.5
	M07052	40	41	0	0	-	-	-	-
	M08071	50	26	0	0	-	-	-	-
	M08103	45	25	0	0	-	-	-	-
	Mi010311	55	114	1.1	0	64.9	-	31.8	-
Mean±SD		46±10	62±38	270±382	34±n/a	65±0.7	72±n/a	31±2	26±n/a
Anti-BLYS	Mi016	102	153	189.5	10.4	64.2	68	32.3	26.6
	M03163	93	82	0	0	-	-	-	-
	M05025	75	66	330.8	20.0	65.5	70.6	32.4	26.3
	M07088	79	45	0	19.6	-	70.1	-	27.6
	M08099	56	25	0	0	-	-	-	-
	M09017	52	19	398.6	54.7	68.1	75.2	30.7	25.3
Mean±SD		76±20	65±49	306±107	26±20	66±2	71±3	31±1	27±2
Anti-APRIL	M0169	64	108	170.7	13.4	68.1	73.6	30.4	24.7
	M08029	43	30	186.4	27.9	66.8	76.5	32.0	26.0
	M05049	94	62	28.7	1.1	60.7	72.5	35.0	28.8
	M07036	109	42	1.8	0	-	-	34.1	-
	M08092	52	25	0.4	0	-	-	32.3	-
	M09031	52	18	0	0	-	-	-	-
Mean±SD		69±26	48±33	78±93	14±13	62±5	74±2	33±2	27±2

All animals were males

^aDay of sacrifice

^bAge in months at the start of the experiment.

It is important to point out that the genetic heterogeneity of the marmoset implies a highly variable response of individual animals in the model at the clinical, pathological and immunological level. The inevitable consequence of the multi-factorial variation is that robust statistical data can often not be obtained. This problem in preclinical research with higher species has recently been discussed elsewhere³²⁷.

Post-mortem examination

Monkeys selected for necropsy were first deeply sedated by intramuscular injection of alfaxan (10 mg/kg) (Vétoquinol S.A., Magny-Vernois, France). After collection of the maximum venous blood (PBMC) in EDTA vacutainers, animals were euthanized by infusion of sodium pentobarbital (Euthesate®, Aphormo, Duiven, The Netherlands). At necropsy brain and spinal were removed for (immuno)histology and magnetic resonance imaging. Secondary lymphoid organs were aseptically removed for preparation of mononuclear cell (MNC) cultures; axillary (ALN), inguinal (ILN), lumbar (LLN) lymph node and spleen as previously described^{215, 263, 288, 328}. Femur was collected for isolation of bone marrow (BM) cells. Number of leukocytes, neutrophils and lymphocytes in blood was measured on an automated haematology analyzer (Sysmex XT-2000iV, Norderstedt, Germany).

T cells proliferation

Proliferation was tested on MNC derived from EDTA blood every two weeks or at necropsy from spleen and secondary lymph nodes (ALN, ILN, LLN) against a panel of overlapping MOG peptides (10 µg/ml) and rhMOG (10 µg/ml). Proliferation was expressed as stimulation index (SI), calculated as the ratio between [³H]-thymidine incorporation in the stimulated versus unstimulated cultures²⁶³. SI values above 2 were considered positive.

MNC phenotyping

MNC cells were phenotyped as previously described^{288, 307} and proliferating cells (based on CFSE vital dye dilution) were stained for specific markers¹⁹⁰. Flow cytometric analysis was performed on a FACS LSRII cytometer with the FACSDiva software 5.0 (BD Biosciences).

Cytokine profiling by ELISA

Supernatants of MNC cultures were collected after 48 h stimulation with rhMOG or a panel of overlapping MOG peptides. Supernatants were assayed according to manufacturer's instruction with commercial available ELISA kits for monkey IFN- γ , monkey TNF- α (U-Cytech, Utrecht, The Netherlands) and human IL-17A (eBioscience, San Diego, CA).

Quantitative PCR

Total RNA was extracted from PBMC, spleen and ALN. Subsequently, cDNA was synthesized for qPCR using primer and probe combination according to the Universal Probe Library (Roche, Indianapolis, In) as previously described³²⁸. Transcript levels were normalized against the reference gene Abelson (ABL).

Autoantibody detection

Immune sera were tested for the presence of IgM and IgG antibodies binding rhMOG or a panel of overlapping 23-mer pMOG sequences with ELISA as previously described²⁸⁸.

Statistical analysis

Data are presented as mean \pm sem. Statistical analysis was performed using the Mann-Whitney *U* test. Survival was evaluated using Log-Rank test. *p* values \leq 0.05 were considered significant.

RESULTS

Induction of B cell depletion by anti-BLyS and anti-APRIL antibodies

Eighteen unrelated common marmosets were randomized to 3 groups of 6 animals each (see Table 1). EAE was induced in all animals by immunization with rhMOG in CFA. Treatment with anti-BLyS and anti-APRIL was started 21 days after immunization, but prior to clinically evident EAE. Both antibodies were administered as a weekly intravenous dose of 10 mg/kg (1 ml/kg); the control group received the same volume of buffered saline. Venous blood MNC, prepared at the indicated time points, were phenotyped for CD20+ and CD20+CD40+ to visualize B cells and mature B cells, respectively. Immediately after immunization a reduction of CD20+ cells was observed in all three groups (Fig.1A). In the control group this is followed by an increase of the percentage CD20+ cells. By contrast, the percentage CD20+ cells continued to decrease in the groups treated with anti-BLyS and anti-APRIL mAb. However, the percentages CD20+CD40+ B cells did not differ between the three groups.

Data obtained at necropsy from blood, lymphoid organs and BM is shown in Figure 1C. MNC from blood, spleen, ALN and ILN showed significant reduction of CD20+ cells in the anti-BLyS treatment group. In the anti-APRIL group a significant effect on CD20+ B cells depletion was only observed in blood. In ALN and ILN the same level of CD20+ B-cells was detected with anti-APRIL compared to the control group while in spleen there was a higher percentage of CD20+. The two antibodies had no effect on the number of CD20+CD40+ cells, being mature B cells, in the tested compartments. Subsequently, mRNA transcript levels of CD19 was determined in MNC from blood, spleen and ALN, demonstrating significantly lower levels in spleen for both antibody-treated groups and in ALN only for the anti-APRIL treated group (Fig. 1D). The discrepancy between CD19 and CD20 data may be explained by the fact that CD19 is not an exclusive marker of B cells, as it is also expressed on follicular dendritic cells. In addition, at necropsy the frequency of leukocytes, neutrophils and lymphocytes was also measured in blood. Figure 1B shows that both antibody treated groups had a lower absolute number of these three cell types, in particular the neutrophils.

Taken together these data show that the anti-BLyS antibody consistently decreases B cell number in blood, spleen and lymph nodes, while a variable effect of the anti-APRIL antibody was observed in the monkeys.

Antibody levels as a surrogate marker of systemic B cell reduction

We anticipated that the effects of the anti-BLyS and anti-APRIL antibodies on B cell survival and activation are reflected by altered plasma antibody levels against the immunizing protein. Figure 2 shows the levels of IgM and IgG against rhMOG and the peptides 24-46 and 54-76, which are part of the rhMOG B cell epitopes. The figure shows the normally observed profile of IgM and IgG antibodies in the control group. However, a remarkably different profile of IgM antibodies was detected between the two antibody-treated groups (Fig. 2A). The IgM antibody levels declined with disease progression in the monkeys treated with anti-BLyS mAb, but remained at an elevated level in the group treated with anti-APRIL mAb. For IgG antibody levels this effect was less obvious (Fig. 2B).

These different effects observed of the anti-BLyS and anti-APRIL antibodies seem to be consistent with the different role of BLyS and APRIL in B cell survival, differentiation and maturation.

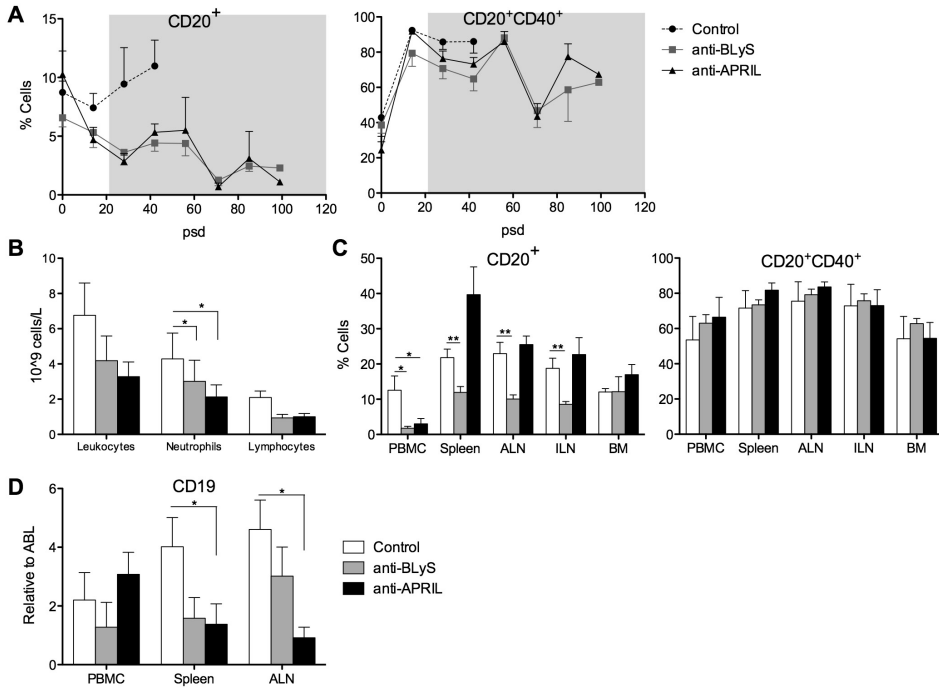


Figure 1. B cell depletion by anti-BlyS and anti-APRIL antibodies. A. CD20⁺ (left panel) and CD20⁺CD40⁺ (right panel) expression in PBMC collected at the indicated time points was measured by flow cytometry. The grey shaded area indicates the period of treatment, which was started at post sensitization day (psd) 21. Percentages on the y-axes are cell numbers expressed relative to the total analysed cell number (mean ± SEM). CD20⁺ B cells are reduced by the anti-BlyS and anti-APRIL treatment compared to untreated monkeys, but this is not the case for CD20⁺CD40⁺ mature B cells. B. At necropsy the absolute numbers of leukocytes, neutrophils and lymphocytes were determined, showing a reduction with anti-BlyS and anti-APRIL treatment. However, the decrease was only significant for neutrophils. Data on the y-axes are absolute cell numbers (mean±SEM). C. MNC were prepared from blood, spleen, ALN, ILN and BM at necropsy to measure the presence of CD20⁺ B cells (left panel) and CD20⁺CD40⁺ mature B cells (right panel). Given percentages on y-axes indicates the fraction of stained cells from the total measured cells (mean±SEM). In the anti-BlyS treated group a significant decrease of CD20⁺ B cells was detected in all tested organs except BM. Anti-APRIL treatment had only in blood a significant effect on CD20⁺ B cells. For the CD20⁺CD40⁺ cells no differences were observed between the control and antibody treated groups. D. At necropsy also the expression levels of CD19 mRNA transcripts were measured in PBMC, spleen and ALN, showing a reduction in both antibody-treated group, although the differences with anti-APRIL were only significant for spleen and ALN. Data was normalized to the household gene ABL (mean±SEM). **p*<0.05 Mann Whitney *U* test, treated group vs. control group.

Anti-BlyS and anti-APRIL delayed the development of clinical EAE

All animals in all the three groups developed clinically evident EAE and were sacrificed with a maximum score of 3, which was taken as the predefined ethical end-point. The graphs in Figure 3A depict the clinical score and body weight loss of individual monkeys relative to the day of EAE induction (psd 0). Some monkeys (Mi010311, Mi016, M03163 and M05049) went into

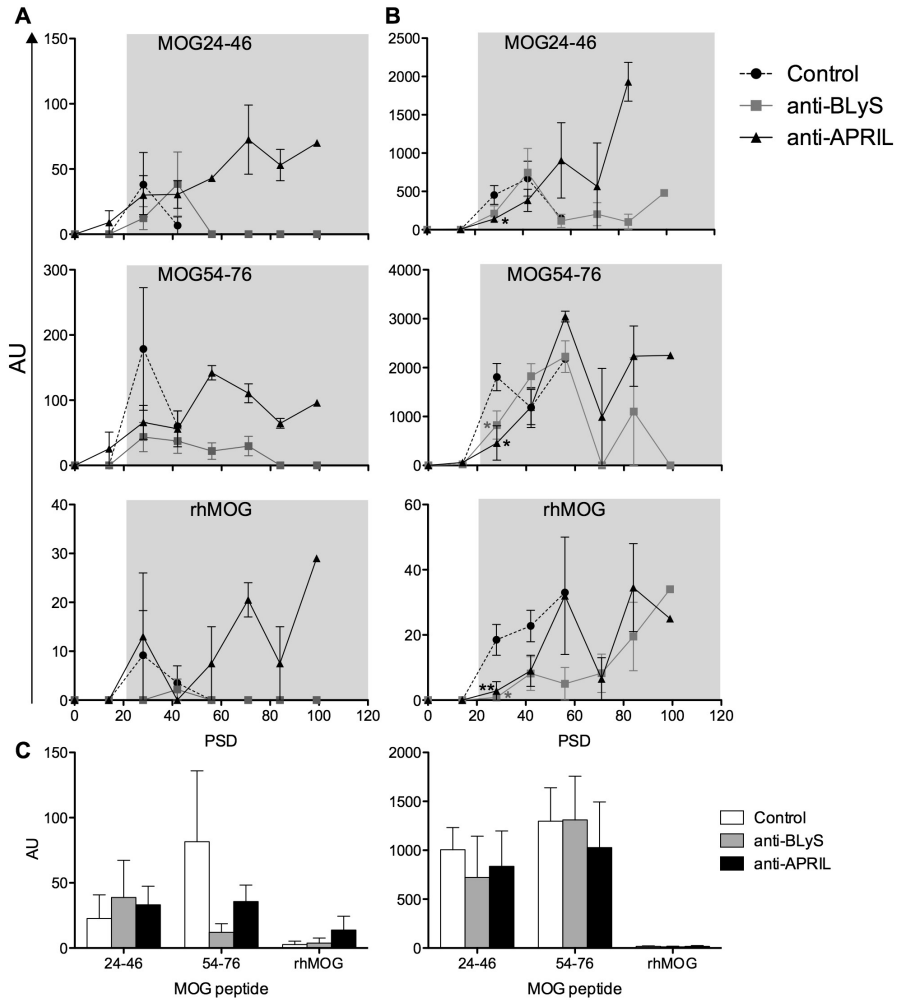


Figure 2. Anti-BLyS treatment reduced antibody production. Plasma samples collected at two weeks interval and necropsy were tested with ELISA for the presence of IgM (A) and IgG (B) antibodies against the B-cell epitopes MOG24-46 and MOG54-76, and against intact rhMOG. In the anti-BLyS treated group, reduction of IgM and IgG levels were observed during the entire study, but in the anti-APRIL treated groups IgM as well as IgG remained high. C. Plasma samples collected at the peak of the disease (necropsy samples) were analysed for binding of IgM (left panel) and IgG (right panel) to a panel of MOG peptides. * $p < 0.05$, ** $p < 0.001$ Mann Whitney *U* test, treated group vs. control group.

remission after a short period of visual problems reminiscent of optic neuritis. Two animals in the anti-APRIL group (M0169 and M05049) and one in the anti-BLyS group (Mi016) were sacrificed with an EAE score of 2 (before the ethical end-point was reached), because of the high bodyweight loss and low physical activity.

Comparison of the time interval to the onset of clinically evident EAE (score 2.0) of the anti-BLyS and anti-APRIL groups with the control group showed a significant delay in disease progression (disease-free survival curves in Fig. 3B). The subsequent disease progression to the ethical end-point (score 3.0) was also delayed in both groups. However, the delay was not significant for the group treated with anti-APRIL ($p = 0.0646$).

No effect of anti-BLyS and anti-APRIL on MRI-detectable brain lesion load

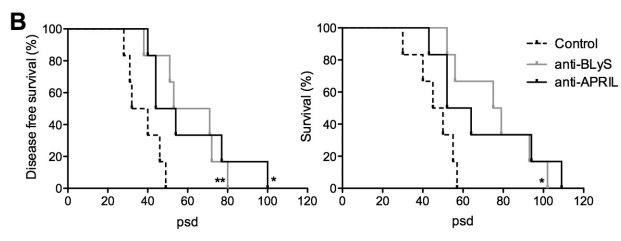
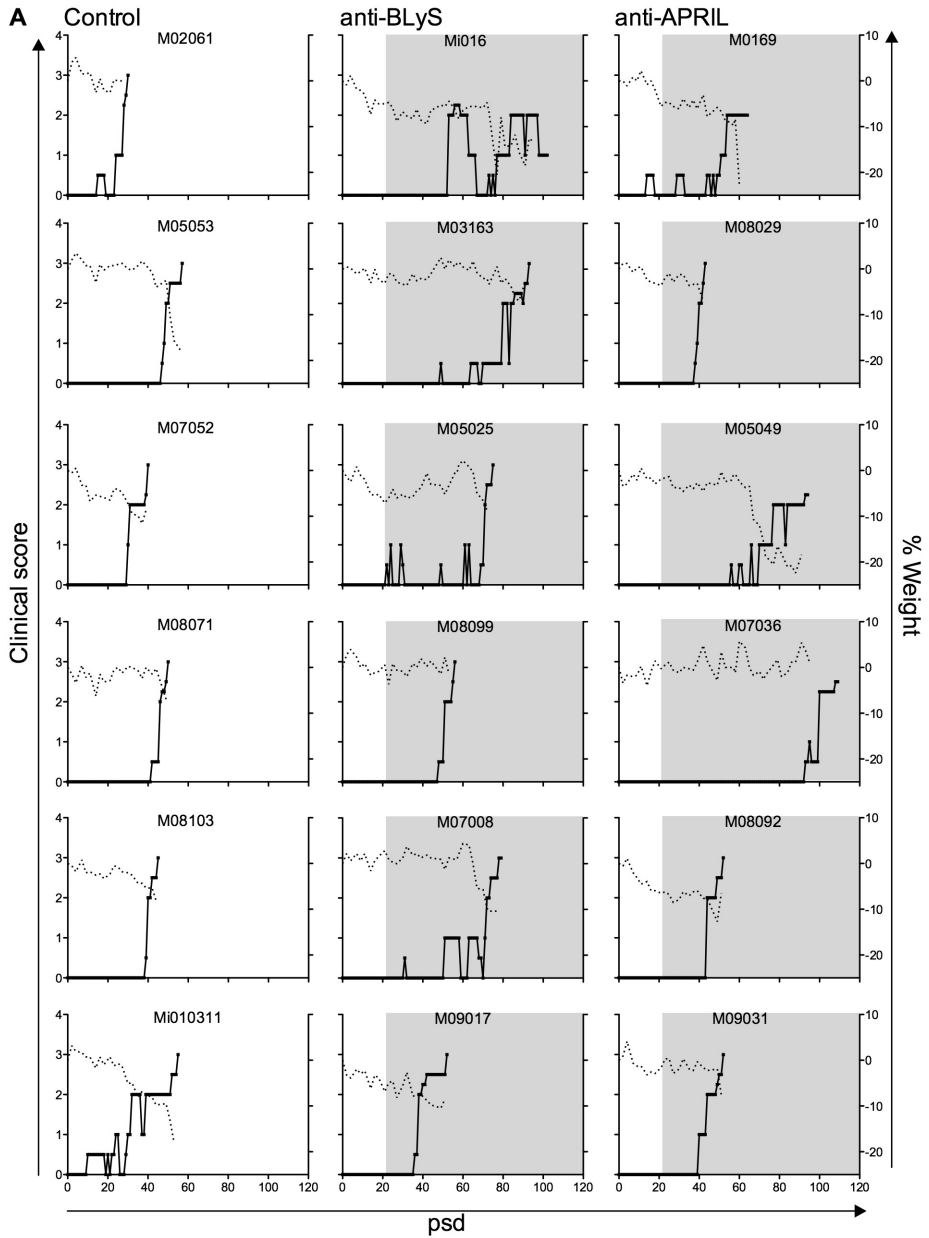
The primary end-point of the study was time to clinically evident EAE. This implies that all monkeys were sacrificed with the essentially similar symptoms of clinically evident EAE, but that this stage was reached after different disease duration. At necropsy the brains were removed and cut into two equal halves. One half was formalin-fixed and was analysed with magnetic resonance imaging (MRI). The analysed semi-quantitative parameters were lesion volume, and the T2 and MTR signal intensity (Table 1).

Lesion volume: Both antibody-treated animals showed a higher volume of grey and white matter lesion than controls. In the control group abnormality in the brain was only detected in one animal (M05053). This low brain lesion load in a monkey with severe clinical EAE is unusual for the rhMOG/CFA model as normally many T2 lesions are detected¹⁰³. A possible explanation is that lesions were located in CNS regions that were not analysed with MRI, such as the contralateral hemisphere or, more likely, in the spinal cord. The higher lesion load in the antibody-treated monkeys may be explained by the longer disease duration. In the anti-BLyS group fewer monkeys had white matter lesions than the anti-APRIL group, 3 out of 6 and 5 out of 6, respectively. The high lesion load observed in monkey (M05053) is within the normal range as such cases have also been found in earlier studies^{103, 266}.

T2 parameter: T2 values recorded in formalin fixed brain samples reflect the residual myelin-associated water fraction. A higher T2 signal implies more oedema in the brain that can be caused by inflammation. In the anti-BLyS and anti-APRIL group approximately the same mean T2 signal intensity was measured as in the control animals for white and grey matter lesion. However, in the antibody treated groups there were more animals with increased T2 signal (both $n=3$) compared to the control group ($n=2$). This is more likely a reflection of the longer disease duration than an adverse effect of the antibodies

MTR: The magnetization transfer ratio (MTR) is calculated from the ratio of protons of tissue-bound water versus free protons in tissue water. Decrease of the MTR can therefore be due to

Figure 3. Delay of EAE course by anti-BLyS and anti-APRIL treatment. A. Clinical scores are depicted of controls (left panel) and the two antibody treated groups, with anti-BLyS (middle panel) or anti-APRIL (right panel). The solid lines represent clinical scores (left y-axes) and the dotted line body weight loss relative to the immunization day, defined as post sensitization day (psd) 0. Grey shaded boxes indicate the treatment period. All animals in the experiment developed clinically evident EAE (clinical score 2.0) and most of them were sacrificed with an EAE score of 3.0. However, monkey Mi016, M0169 and M05049 had to be sacrificed at an earlier time point due to the serious body weight loss. B. Survival curves depict the disease free survival time (time interval to development of EAE score 2.0; left panel) and overall survival (time interval to clinical end point; right panel). Disease free survival times were significantly prolonged in the anti-BLyS and anti-APRIL treated monkeys. The total survival was significantly prolonged by the anti-BLyS treatment, but the delay in anti-APRIL treated monkeys was not significant ($p=0,0646$). * $p<0.05$; ** $p<0.001$ Log-rank test, treated group vs. control group.



increased tissue water (inflammation) or decrease of tissue (demyelination). The MTR value of post mortem brain images is correlated with the intensity of macrophage infiltration²⁴¹. We observed a similar effect of the antibody treatment on the MTR parameter as for the T2 parameter.

Reduced spinal cord demyelination in anti-BLyS treated animals

Histological analysis of the spinal cord shows reduced inflammation in the anti-BLyS and anti-APRIL group compared to the controls. However, these differences were not significant, probably due to the high variation between individual monkeys (Fig. 4A). The histology data also show a higher percentage demyelination of the brain in the anti-BLyS treated group, which is in accordance with the MRI data. In contrast, the anti-BLyS treated group had significantly reduced demyelination of spinal cord, which was not observed for anti-APRIL treatment (Fig. 4B). Quantification of demyelination of the optic nerve also suggested a protective effect of the anti-BLyS antibody. In this group 2/6 monkeys showed 100% demyelination of the optic nerve while in the control group there were 4 control monkeys with 100% demyelination.

In conclusion, the histology data show a highly remarkable different effect of the anti-BLyS treatment between brain and spinal cord. We have not seen this with other therapeutic antibodies tested in the model.

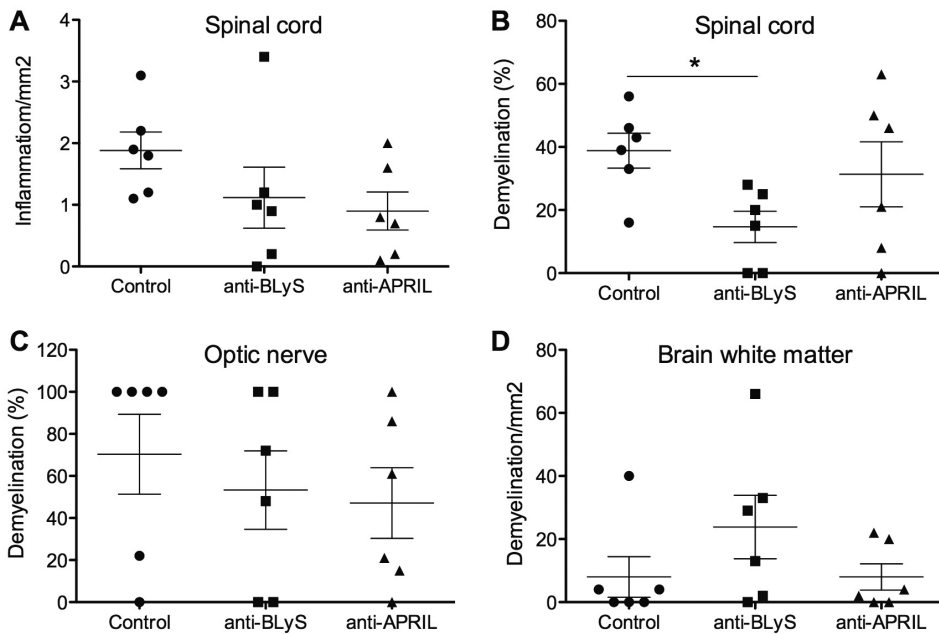


Figure 4. Reduced spinal cord demyelination in anti-BLyS treated monkeys. Formalin-fixed tissue samples were stained to analyse the intensity of inflammation and demyelination. For each animal 8 slices were examined, which equals 6 cm² in total. A. The number of infiltrated cells per mm² is given for the spinal cord. The amount of demyelination is given for the spinal cord (B), optic nerve (C) and brain white matter (D). A significant treatment effect was only observed for the spinal cord of anti-BLyS treated animals. **p*<0.05 Mann-Whitney *U* test, antibody treated group vs. control group.

Increased T cell proliferation with anti-BlyS

PBMC isolated from the femoral vein of all animals at 2 weeks interval were tested for proliferation against a panel of MOG peptide and rhMOG. As read-out for T cell proliferation we determined incorporation of [^3H]-thymidine (TCPA) and CFSE vital dye dilution (Fig. 5).

TCPA: Figure 5A shows the longitudinal proliferation of PBMC against the immunizing rhMOG protein, the peptides MOG14-36 and MOG24-46, which contain the MOG24-36 epitope of early acting Caja-DRB*W1201 restricted CD4+ Th1 cells¹⁰³ and MOG34-56, which contains the MOG40-48 epitope of late acting Caja-E restricted CD4+CD8+ cytotoxic T lymphocyte (CTL)^{190, 307}. During the initial 40 days after immunization the differences between the three groups

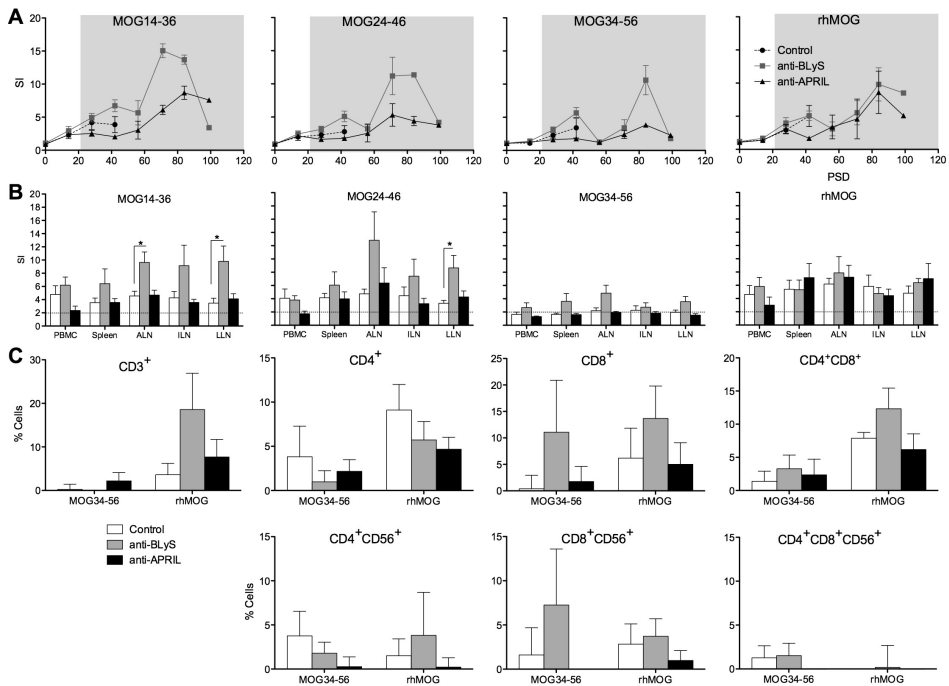


Figure 5. Modulation of T cell proliferation in anti-BlyS and anti-APRIL treated monkeys. A. PBMC were isolated at the indicated time points and assayed for the response to stimulation with rhMOG or 23-mer synthetic peptides containing previously identified dominant MOG T cell epitopes, i.e. MOG14-36, MOG24-46 and MOG34-56. The read-out was incorporation of [^3H]-thymidine during the final 18 hours of 3 days culture. Data on the left panel show the stimulation index (SI). Grey shaded boxes indicate the period of treatment. T cell proliferation increased after immunization, and was significantly enhanced during the anti-BlyS treatment, but was reduced during anti-APRIL treatment. B. At necropsy the incorporation of [^3H]-thymidine was measured as a read-out for proliferation in PBMC, spleen, ALN, ILN and LLN against the same MOG antigens as described under (A). C. Proliferated T cells in blood and lymphoid organs were phenotyped using the CFSE diluting assay. Data are shown of MNC derived from spleen, as a representative example. Stimulation with MOG34-56 and rhMOG are depicted. The y-axis indicates the percentage proliferated cells; CD4+, CD8+ and double positive for CD4 and CD8 were first gated within the CD3+ proliferated population, next for CD4+CD56+, CD8+CD56+ and CD4+CD8+CD56+, respectively. Data are presented as mean \pm SEM. * p <0.05 Mann Whitney U test, antibody treated group vs. control group.

were relatively small. However, the response of PBMC from anti-APRIL-treated monkeys was consistently lower than that of PBMC from the anti-BLyS treated group, which was significantly increased compared to the controls. The difference is very clear at the peak of disease, when all control monkeys had been sacrificed with severe clinical EAE. This was the case for the three tested peptides, but not for rhMOG.

The proliferative response of MNC from blood and lymphoid organs collected at necropsy is depicted in Figure 5B. The figure clearly shows that the MOG14-36/24-46 and MOG34-56 stimulated proliferation of spleen and lymph node MNC from the anti-BLyS treated group is consistently higher than that of the control and anti-APRIL-treated monkeys. However, no significant difference was found for the MNC proliferation against the immunizing rhMOG protein.

CFSE dilution: Flow cytometric analysis of CFSE labelled cells for dye dilution in combination with mAb staining was used to assess whether the proliferative response maps to a certain subset of T cells. We have focused on the response of spleen MNC against MOG34-56 as these contain the T cells that are the most likely culprit for the induction of neurological deficits¹⁹⁰, which are mainly found in the spleen²⁸⁸.

Freshly isolated spleen cells were stained with CFSE and subsequently cultured for 7 days culture with MOG34-56, rhMOG or without antigen. Cells harvested from the cultures were stained with monoclonal antibodies and analysed by flow cytometry. The results are given in Figure 5C. The first remarkable observation is the significantly higher CD3⁺ cells with CFSE dilution in unstimulated cultures from the anti-BLyS group. Also in the unstimulated cultures from the anti-APRIL group we observed increased background proliferation, but this was lower than that in the anti-BLyS group. This high background proliferation is mainly located in the CD4⁺CD56⁺ subset. Stimulation of the cells with MOG34-56 did not induce enhanced CFSE dilution by CD3⁺ cells in either of the groups, but the proliferation was strongly enhanced after stimulation with rhMOG. This enhancement is mainly localized in the CD8⁺ and CD4⁺CD8⁺ subsets. Interestingly, the only cells that displayed strongly elevated CFSE dilution upon stimulation with MOG34-56 were in the CD8⁺ and CD8⁺CD56⁺ subsets of the anti-BLyS group. The second remarkable observation was that the treatment with anti-APRIL had a much less outspoken modulatory effect on the analysed cellular responses than the anti-BLyS treatment. This is in accordance with the assumption that the primary focus of APRIL activity is in the humoral arm of the immune system, whereas BLyS is involved in cellular as well as humoral immune mechanisms³²⁹.

Altered cytokine levels with anti-BLyS and anti-APRIL

The immunization of marmosets with rhMOG/CFA activates both Th1 and Th17 cells, which are both pathogenically relevant in this model. We determined the levels of mRNA transcripts for several cytokines as a reflection of the frequency of functional cell subsets: Th1 (TNF- α and IFN- γ), Th17 (IL-17A), Treg (IL-10) and IL-7 (B cells). Moreover, we determined the *ex vivo* production of IL-17A, TNF- α and IFN- γ by MNC from blood, spleen and ALN after stimulation with the immunizing rhMOG antigen to test the reactivity of the autoreactive Th1 and Th17 subsets.

The profiles of secreted cytokines in the cultures were analysed with ELISA (Fig.6A). The results show a clear, albeit non-significant reduction of IL-17A in all three analysed compartments

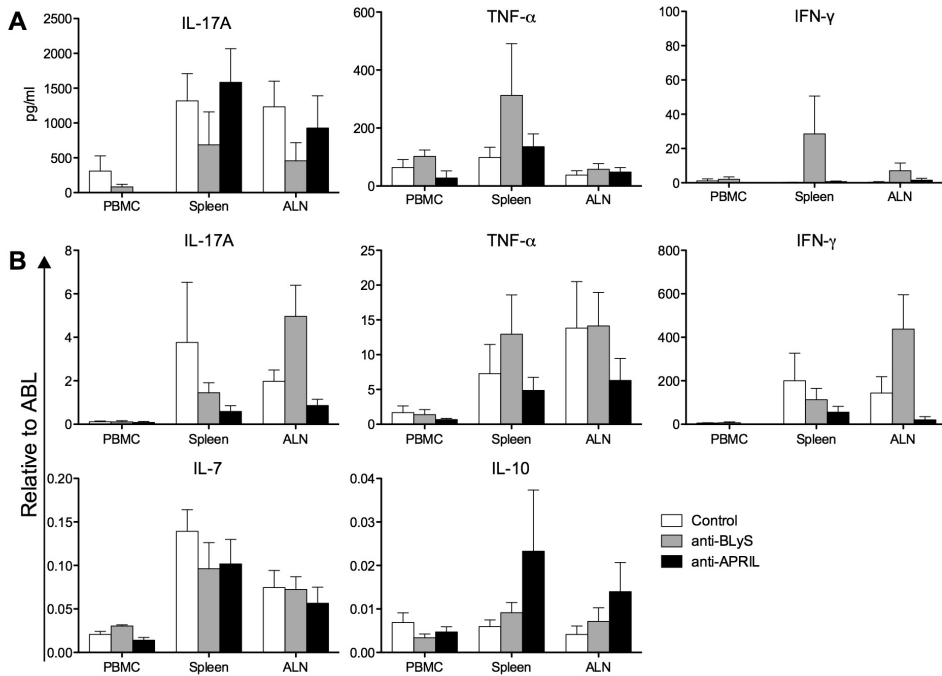


Figure 6. Altered cytokine expression with anti-BLyS and anti-APRIL. A. At necropsy MNC were collected from blood and lymphoid organs and cultured for 48 h with a panel of MOG peptides and rhMOG. Levels of IL-17A (left panel), TNF- α (middle panel) and IFN- γ (right panel) were measured in culture supernatants with ELISA (mean \pm SEM). Data is only shown of rhMOG stimulated MNC, since no high levels of cytokines were measured in the MOG peptide stimulated cells. B. Cytokine mRNA transcripts of IL-17A, TNF- α , IFN- γ , IL-7 and IL-10 were measured in PBMC, spleen and ALN. Data was normalized to the household gene ABL (mean \pm SEM). Mann Whitney *U* test was performed as statistical calculation, but no significant differences were observed.

of the anti-BLyS-treated animals, compared to both other groups, but the levels of TNF- α and IFN- γ were increased. The rhMOG stimulation of MNC from the control and anti-APRIL treated monkeys induced secretion of comparable IL-17A, TNF- α and IFN- γ profiles.

The analysis with cytokine specific qPCR of mRNA extracts from blood, spleen and ALN MNC shows inconsistent effects of the anti-BLyS and anti-APRIL treatment compared to the control monkeys (Fig.6B). Both treatments result in reduced IL-17A and IFN- γ transcript levels in spleen, whereas levels in ALN are increased by anti-BLyS treatment and decreased by anti-APRIL. Remarkably, in the anti-BLyS group increased transcript levels for TNF- α were detected in spleen, whereas these were unchanged in ALN. In the anti-APRIL group TNF- α transcripts were reduced in ALN and unaltered in spleen. We observed increased transcript levels for IL-10 in spleen and ALN in anti-APRIL treated monkeys, but the levels were unaltered in spleen and ALN from the anti-BLyS group. Finally, we observed marginally reduced IL-7 mRNA levels in spleen from the anti-BLyS and anti-APRIL treated monkeys, where these cytokines were unaltered in ALN.

In conclusion, both treatments had a modulatory effect on the cytokine profiles of rhMOG-reactive T cells, although the direction of the effect is opposite for several cytokines.

DISCUSSION

The rhMOG/CFA induced EAE model in marmosets is a useful preclinical model for translational research into MS³²⁶. On the one hand the model shares well-documented features with the equivalent EAE model in mice and rats. On the other hand the model shares clinical and pathological features with MS, in particular the progressive course and the prominent involvement of grey matter demyelination.

The pathogenesis of the model is not only variable, which is inherent to the genetic heterogeneity of this outbred model, but also highly complex. As discussed elsewhere³²⁶, the induction of inflammation and demyelination, which affects the white as well as grey matter of the CNS, and the induction of neurological deficits involves at least two pathways. The “canonical” pathway I, which seems to be primarily active in the initiation phase of the disease, involves the concerted action of MHC class II-restricted Th1 cells and autoantibodies^{103, 244, 264}. The “non-canonical” pathway II likely becomes engaged later in the pathogenic process, involves MHC class I-restricted effector memory natural killer-like cytotoxic T cells (NK-CTL) and likely Th17 cells^{190, 288, 307}. The MHC-class II (*Caja-DRB*W1201*) and MHC class I (*Caja-E*) restriction elements are both monomorphic in the common marmoset, explaining why they are active in all animals. Pathway I is not strictly dependent of MOG, as it can be induced with MOG-deficient myelin, but for the activation of pathway II, MOG seems indispensable²⁶³.

B cells have an important role in both pathways. The main role of B cells in the canonical pathway I is the production of autoantibodies against myelin, which elicit cellular and/or complement dependent cytotoxicity reactions. The primary role in the non-canonical pathway II, which is independent of autoantibodies is antigen presentation to the NK-CTL. The latter role was shown in two independent experiments. One set of experiments demonstrated that depletion of CD20+ B cells from marmosets at 21 days after the immunization with rhMOG/CFA abrogates the development of EAE symptoms²¹⁵ as well as of EAE pathology in the grey and white matter of the brain and spinal cord³¹¹. The mechanistic explanation for this highly robust effect is that activation of the cellular autoimmune mechanisms that mediate disease progression is impaired. A second set of experiments was performed in the MOG34-56/IFA EAE model in which white and grey matter demyelination is induced by peptide-specific NK-CTL without a detectable influence of autoantibodies^{288, 307}. In the same MOG34-56/IFA EAE model it was observed that depletion of CD20+ B cells from 21 days after the immunization abrogates the development of EAE symptoms and pathology (submitted for publication).

We report here the effect on the rhMOG/CFA EAE model of two monoclonal antibodies against essential factors for B cell survival and differentiation. BlyS and APRIL have partially overlapping roles in B cell survival and differentiation involving at least 3 receptors, i.e. BCMA, TACI and BR3, which recognize homo-trimeric forms of BlyS and APRIL³³⁰. BlyS binds to all three receptors, but with highest affinity for BR3. APRIL does not bind BR3 and has about 100-fold higher affinity for BCMA than BlyS. TACI binds both factors with comparable affinity. The expression of these receptors on B cell subsets or stages of B cell differentiation varies.

The results of the current study show that anti-BlyS and anti-APRIL administration to rhMOG/CFA immunized marmosets exerted similar hematological changes, i.e. reduction of

neutrophil and lymphocyte numbers, and induced a similar rate and depth of CD20+ B cell depletion from blood. However, only anti-BLyS treatment induced CD20+ B cell reduction in spleen and lymph nodes. With qPCR analysis it was shown that CD19 transcript levels were reduced in spleen and ALN of anti-APRIL treated monkeys. It is difficult to explain these discrepancies although it should be noted that CD20 is an exclusive marker of the B cell lineage, whereas CD19 is also expressed by follicular dendritic cells. Remarkably, we observed no effect of anti-BLyS or anti-APRIL mAb on the levels of CD20+CD40+ cells. The relevance of this subset in the EAE pathogenesis is illustrated by the finding that administration of an antagonist mAb against human CD40 results in impairment, and does not completely suppress the disease in the rhMOG/CFA model²⁶⁴. This is a remarkable difference with the effect of anti-CD20 mAb treatment in the rhMOG/CFA model, where complete depletion of the CD20+CD40+ subset of B cells was observed²¹⁵.

The separate inhibition of BLyS and APRIL exerted comparable clinical effects in the EAE model, although differences at the immunological and pathological level were observed. Neutralization of BLyS and APRIL caused a significantly delayed onset of overt clinical EAE (EAE score 2.0, ataxia). However, the effect on the time to the study end-point (EAE score 3.0, hemi-/paraplegia) was statistically significant only for the group treated with anti-BLyS antibody. Second, in the monkeys treated with anti-BLyS, but not in those treated with anti-APRIL, we observed a significant suppressive effect on the demyelination of spinal cord. The discrepant effect may be explained by the fact that the anti-BLyS antibody targets processes in the periphery, i.e. B cell survival, and in the CNS, i.e. neuronal outgrowth. BLyS is produced within the CNS by reactive astrocytes and exerts via NgR1 similar effects on neurons as the natural ligand Nogo66³³¹.

The two mAbs modulated EAE-associated cellular autoimmune reactions in different ways. This was observed in regular proliferation assays using MNC isolated from different immune compartments; response patterns of T cell subsets assessed by CFSE vital dye dilution and the cytokine profiles. We observed in the anti-BLyS-treated group enhanced proliferation of MNC from blood and lymphoid organs against MOG peptides 14-36 and 24-46, which both contain the epitope MOG24-36, which is presented by ubiquitously expressed monomorphic Cja-DRB*W1201 molecules to Th1 cells^{103, 206}. These cells are engaged in the initiation of EAE, as was confirmed by adoptive transfer between fraternal siblings²³³. The higher production of TNF- α and IFN- γ by the rhMOG-stimulated splenocytes supports this conclusion. At the cytokine level we observed lower production of IL-17A than in the other two groups i.e. anti-APRIL and the controls. Phenotyping of proliferating cells via CFSE vital dye dilution and monoclonal antibody staining shows that CD3+ T cells from anti-BLyS treated monkeys have a higher proliferative reactivity than those from the other two groups, which are localized mostly within the CD4+CD56+ subset. However, the rhMOG and MOG34-56-stimulated proliferation are localized mainly in the CD8+, CD4+CD8+, CD8+CD56+ subsets. Importantly, the reactivity of the CD4+CD8+CD56+ subset to antigenic stimulation, which is the main source of the autoreactive T cells cytotoxic activity in the marmoset EAE model^{288, 307}, is not increased by the treatment.

In the monkeys treated with the anti-APRIL mAb we did not observe marked differences with the control monkeys at the level of the proliferative response of MNC from blood, spleen or lymph nodes, neither in the TCPA test, nor with CFSE vital dye dilution. However, the cytokine

analyses showed the lowest expression of IL-17A, IFN- γ and TNF- α mRNA with concomitant increased expression of IL-10 mRNA in this group.

In conclusion, the treatment with anti-BLyS and anti-APRIL antibody, which was started at a relatively late stage (day 21 post immunization), results in a significant delay of EAE onset and progression. Due to the heterogeneity between individual monkeys, which is inherent to this outbred model, differences between investigated variables in the three groups often did not reach statistical significance. This implies that they should be interpreted with caution as only trends can be indicated. The clinical effect of the therapeutic antibodies seems to be based on different mechanisms. The anti-BLyS treated group displays reduced antibody levels against rhMOG and MOG peptides, together with reduced Th17 and increased Th1 activation. Besides this immunomodulatory effect, the depletion of BLyS could also have consequences inside the CNS, such as removal of axonal outgrowth inhibition. For the anti-APRIL antibody such central effects are not known, which may explain why the disease progression after initiation (score 2.0 to 3.0) is not significantly affected. However, the antibody has modulatory effects on the autoimmune reaction, most notably a reduction of Th1 and Th17 signature cytokine transcripts and an increase of IL-10 mRNA. This may suggest that the inhibitory activity of the anti-APRIL mAb is based on skewing from a pro- to anti-inflammatory T cell profile. Further research should demonstrate whether this is indeed the case.

ACKNOWLEDGEMENT

The authors thank the Animal Science Department for biotechnical assistance, in particular Jeroen Sollie, Mariska van Etten and Tom Haaksma. This work was supported by Human Genome Sciences.

**DISCREPANT EFFECTS OF HUMAN
INTERFERON-GAMMA ON CLINICAL AND
IMMUNOLOGICAL DISEASE PARAMETERS
IN A NOVEL MARMOSSET MODEL FOR
MULTIPLE SCLEROSIS**

S. Anwar Jagessar, Bruno Gran, Nicole Heijmans, Jan Bauer, Jon D
Laman, Bert A. 't Hart and Cris S. Constantinescu

J Neuroimmune Pharmacol 7, 253-65 (2012)



ABSTRACT

The core pathogenic process in the common marmoset model of multiple sclerosis (MS) is the activation of memory-like T cells specific for peptide 34 to 56 derived from the extracellular domain of myelin/oligodendrocyte glycoprotein (MOG34-56). Immunization with MOG34-56 in incomplete Freund's adjuvant is a sufficient stimulus for *in vivo* activation of these T cells, together with the induction of MS-like disease and CNS pathology. *Ex vivo* functional characteristics of MOG34-56 specific T cells are specific cytolysis of peptide pulsed target cells and high IL-17A production. To identify possible functions in this new model of T helper 1 cells, which play a central pathogenic role in MS models induced with complete Freund's adjuvant, we tested the effect of human interferon- γ (IFN- γ) administration during disease initiation of the disease (day 0-25) and around the time of disease expression (psd 56-81). The results show a clear modulatory effect of early IFN- γ treatment on humoral and cellular autoimmune parameters, but no generalized mitigating effect on the disease course. These results argue against a prominent pathogenic role of T helper 1 cells in this new marmoset EAE model.

INTRODUCTION

Experimental autoimmune encephalomyelitis (EAE) is a well-established animal model of the human central nervous system (CNS) targeting neuroinflammatory disease multiple sclerosis (MS). Various versions of the model are being used to investigate immunopathogenic mechanisms in MS and to develop new therapies. In response to the need of an EAE model with high relevance to MS in which biological therapeutics can be tested, we have set up an EAE model in the Neotropical primate “common marmoset” (*Callithrix jacchus*). The model that was induced by sensitization against human myelin or the immunodominant component myelin/oligodendrocyte glycoprotein (MOG) and its advantage over equivalent models in rodents has been discussed elsewhere, most recently in¹²⁸.

Analogous to EAE models in lower species, such as mice and rats, T helper 1 (Th1) cells have a central pathogenic role in marmoset EAE models induced with recombinant human myelin/oligodendrocyte glycoprotein (rhMOG) in complete Freund’s adjuvant (CFA)¹⁰³. Accordingly, antibodies against human CD40, a co-stimulatory molecule of antigen presenting cells involved in the induction of IL-12, or against IL-12p40 subunit displayed strong suppressive activity, both in a prophylactic^{243, 244, 264} and in a therapeutic experimental setting^{266, 332}. However, the recent failure of the anti-IL-12p40 antibody (Ustekinumab) in a phase II clinical trial in relapsing-remitting MS points at an important discrepancy with MS²⁸⁵. The question is therefore warranted whether the pathogenic role of Th1 cells in MS is comparable to that in EAE models.

We hypothesize that the dominant pathogenic role of Th1 cells in EAE models can be attributed to the use of CFA²⁷⁹. This would imply that EAE models induced without use of CFA are less sensitive to reagents that modulate Th1 functions. Interferon-gamma (IFN- γ) is the principal Th1 cytokine induced by IL-12 and has consistently been found to be protective in mouse models of EAE³³³. In a mouse model, we showed that IL-12 suppressed disease when administered systemically during the early phase of EAE induction³³⁴. The suppressive effect was dependent on IFN- γ , as it was not observed in IFN- γ deficient mice. Moreover, genetic deficiency or antibody neutralization of IFN- γ consistently exacerbates EAE³³⁵. On the other hand, in another mouse model, IL-12 given during the remission phase after the first attack induced more severe relapses, and restored EAE susceptibility in mice in which CD40-CD40 ligand interaction had been blocked. However, it is not known whether these effects are mediated by IFN- γ ³³⁶.

The aim of the current study was to test the activity of human IFN- γ in a recently developed marmoset EAE model that is induced without usage of CFA, namely by immunization with a synthetic peptide representing the sequence 34 to 56 of human MOG (MOG34-56) formulated in incomplete Freund’s adjuvant (IFA)²⁸⁸. The development of characteristic MS-like clinical and pathological features in this model is driven by CD3⁺CD4⁺/CD8⁺CD56⁺CD16⁻ T cells that display high IL-17A production and antigen-specific cytotoxicity as activities potentially contributing to EAE development²⁸⁸. We have examined the effect of human IFN- γ administration during two periods, namely an early treatment period from the time of immunization to post sensitization day (psd) 25 and a late treatment period from psd 56 to 81. The primary outcome measures were the susceptibility to, and the severity of clinical EAE. Secondary and exploratory outcome measures included immunological parameters and histological evidence of disease activity.

The data show a modulatory effect of early IFN- γ treatment on cellular as well as humoral autoimmune parameters, yet with only a marginal effect on the disease course. This finding

argues against a generalised pathogenic role of the IL-12/IFN- γ axis in the marmoset EAE model induced with MOG34-56/IFA.

MATERIALS AND METHODS

Animals

Fifteen healthy marmoset monkeys (*Callithrix jacchus*) were included in this study originated from purpose-bred colonies of the Biomedical Primate Research Centre (BPRC), Rijswijk, The Netherlands, and the German Primate Centre (DPZ), Göttingen, Germany. Monkeys purchased from DPZ had been housed for at least 6 months in the BPRC before use. Individual data of the monkeys used in this study are listed in Table 1. Before inclusion in the study, the monkeys were subjected to a complete physical, hematological and biochemical examination. During the study they remained under veterinary care. Monkeys were pair-housed in spacious cages enriched with branches and toys and with padded shelter provided on the floor. The daily diet consisted of commercial food pellets for New World monkeys (Special Diet Services, Witham, Essex, UK), supplemented with rice, raisins, peanuts, marshmallows, biscuits, fresh fruit, grasshoppers, and maggots. Drinking water was provided ad libitum.

Ethics

In accordance with the Netherland's law on animal experimentation, all study protocols and experimental procedures were reviewed and approved by the Institute's Ethics Committee before the start of experiments.

EAE induction

Synthetic MOG peptides based on the human MOG extracellular sequence, which were used for immunization and cell culture, were purchased from Cambridge Research Biochemicals (Cleveland, UK).

The monkeys were sedated with Alfaxan (10mg/kg) (Vétoquinol S.A., Magny-Vernois, France) and were immunized with an emulsion of 100 μ g MOG34-56 dissolved in 300 μ l buffered saline with 300 μ l IFA (Difco Laboratories, Detroit, MI). The inoculum was injected into the inguinal and axillary regions of the dorsal skin divided over 4 spots of 150 μ l each. Antigen-adjuvant emulsions were prepared by gentle stirring the peptide/oil mixture at 4 °C for at least 1 h. Monkeys that failed to develop serious neurological deficit (EAE score \geq 2.0) were again immunized at psd 28 and 56 with the same dose of peptide in IFA.

Treatment schedule

Clinical grade recombinant human IFN- γ (Immukin[®]) was purchased from Boehringer Ingelheim, Vienna, Austria. Biological activity in the marmoset system was confirmed by increase of MHC class II expression on marmoset PBMC (Fig. S1).

Three groups of 5 animals each were randomly created and as outlined in Fig. 1. Power calculation was used to calculate the minimal group size for statistical evaluation (Mann-Whitney *U* test). Based on historical data we assumed a 100% disease incidence. To achieve a statistical power of 80% the group size should be 5. The control group received 3 subcutaneous injections per week (Mon, Wed, Fri) of buffered saline (1.0 ml/kg) during two treatment episodes

Table 1. Overview of marmosets used in this study.

Group	Name	Sex	Age*	Sacrificed (psd)	Score 2.0	Score 2.25
Control	M06054	F	32	99	56	95
	M07009	M	28	91	86	90
	M07034	F	25	113	93	101
	M07076	F	22	154	>154	>154
	Mi12699	M	59	133	100	108
Mean \pm SD				118 \pm 26	98 \pm 36	110 \pm 26
rhIFN- γ	M04014	F	64	154	>154	>154
Day0-25	M06036	M	35	133	127	128
	M07062	F	23	57	51	54
	M07101	F	20	135	119	120
	Mi13264	M	41	144	138	143
Mean \pm SD				125 \pm 39	118 \pm 40	120 \pm 39
rhIFN- γ	M06063	M	32	127	100	110
Day56-81	M07016	F	26	81	72	77
	M07035	F	25	155	>155	>155
	M07047	F	24	57	44	55
	Mi12700	M	59	155	>155	>155
Mean \pm SD				115 \pm 44	105 \pm 50	110 \pm 45

*Age in months at the start of the experiment; F, female; M, male; psd, post sensitization day
Score 2.0 = ataxia; score 2.25 = incomplete paralysis of hind limbs

from psd 0-25 and psd 56-81. The early IFN- γ treatment (prophylactic group) and the late IFN- γ treatment (therapeutic group) received 3 subcutaneous test substance injections at a dose of 1.5 μ g/kg (1.0 ml/kg) per week during psd 0-25 and psd 56-81, respectively.

Clinical scoring

Clinical signs were scored daily by two independent observers as described¹²⁷. Briefly: 0 = no clinical signs; 0.5 = apathy, loss of appetite, altered walking pattern without ataxia; 1 = lethargy, anorexia, loss of tail tonus, tremor; 2 = ataxia, optic disease; 2.5 = para- or monoparesis, sensory loss, brain stem syndrome; 3 = para- or hemiplegia; 4 = quadriplegia; 5 = spontaneous death attributable to EAE. Monkeys were sacrificed for ethical reasons once complete paralysis of one or both hind limbs (score \geq 3.0) was observed, or at a pre-determined endpoint.

Body weight, measured three times per week, served as an objective surrogate disease marker. Weighing was performed without sedation using the perspex cylinder: adequately trained monkeys were captured from the home cage.

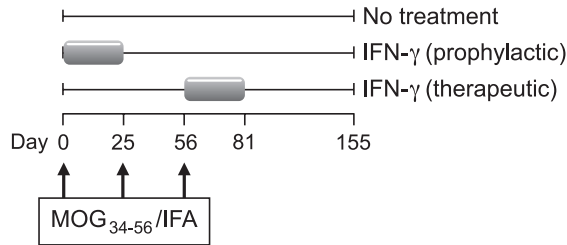


Figure 1. Design of experiment. Fifteen marmosets of either sex were randomly divided over 3 groups, 5 animals in each group (see table 1). All marmosets were immunized with MOG₃₄₋₅₆ in IFA and were re-challenged at days 25 and 56. The first group (control) received only solvent of the drug recombinant human IFN- γ between post sensitization day (psd) 0-25 and psd 56-81. The second group (prophylactic treatment) received three subcutaneous injections of human IFN- γ (1.5 μ g/kg) per week (Mon-Wed-Fri) between psd 0-25; the third group (therapeutic treatment) received the same injection schedule between psd 56-81.

Necropsy

Monkeys selected for necropsy were first deeply sedated by intramuscular injection of alfaxan (10 mg/kg). Maximum blood volume was collected into heparinized vacutainers and subsequently the marmoset was euthanized by infusion of pentobarbital sodium (Euthesate[®]; Apharmo, Duiven, The Netherlands).

Spleen and several lymph nodes were collected aseptically and cut into four pieces, which were used for cell culture or stored in 4% formalin, -80°C, and RNeasy (Sigma, St. Louis, MO). Half of the brain and spinal cord were stored in 4% formalin and the other half were snap-frozen in liquid nitrogen.

Cell preparation

The maximum monthly blood volume that can be collected from marmosets is 1% of the body weight, which is 3.5 – 4.0 ml for an average adult monkey of 350 - 400 grams. Longitudinal immune monitoring was performed using 1.5 ml venous blood collected at 2 weeks interval from the femoral vein into heparinized vacutainers (Greiner, Sölingen, Germany).

At necropsy mononuclear cell (MNC) suspensions were prepared from aseptically removed spleen and axillary (ALN), inguinal (ILN), cervical (CLN) and lumbar (LLN) lymph nodes. MNC and PBMC were isolated using lymphocyte separation medium (LSM[®], ICN Biomedical Inc., Aurora, OH).

Proliferation of T cells

PBMC and lymphoid organ MNC suspensions were assayed in triplicate for proliferation against rhMOG (10 μ g/ml) and a panel of MOG peptides (each 10 μ g/ml)²⁸⁸. Proliferation was assessed by the incorporation of [³H]-thymidine (0.5 μ Ci/well) during the final 18 h of 64 h culture using a matrix 9600 β -counter (Packard 9600; Packard Instrument Company, Meriden, CT). Results are expressed as stimulation index (SI), being the ratio of radiolabel incorporation in stimulated versus unstimulated cultures. SI values above 2.0 were considered positive.

Flow cytometry

Cells were phenotyped as described previously²⁸⁸. Flow cytometric analysis was performed on a FACS LSRII flow cytometer using FACSDiva software 5.0 (BD Biosciences).

Cytokines

Supernatants of PBMC, ALN, and spleen MNC were collected after 48 h stimulation with rhMOG or a panel of overlapping MOG peptides. Supernatants were assayed according to manufacturers instructions with commercial ELISA kits for monkey IL-10, monkey IFN- γ (U-Cytech, Utrecht, The Netherlands) and human IL-17A (eBioscience, San Diego, CA).

Quantitative PCR

Total RNA was extracted from PBMC, spleen and ALN using RNeasy minikit (Qiagen, Hilden, Germany) and subsequently cDNA was synthesized using RevertAid First Strand cDNA Synthesis Kit (Fermentas, St. Leon-Rot, Germany) according to the manufacturer's instructions. Random hexamer primers were used for cDNA synthesis. Quantitative PCR was performed in duplicate using a iTaq supermix with ROX and CFX96 Real-Time System (both from Bio-Rad, Hercules, CA). The primers (Invitrogen) and probes (purchased from the Universal Probe Library set for human, Roche, Indianapolis, In) used are listed in Table 2. mRNA expression of tested primers was related to mRNA expression of the reference gene ABL ($2^{Ct_{reference} - Ct_{target}}$).

Autoantibody detection

Plasma samples were analyzed for IgG and IgM antibody binding to rhMOG or to a panel of overlapping 23-mer pMOG sequences using ELISA as described^{264, 263}. Bound IgG and IgM were detected using polyclonal alkaline phosphatase-conjugated rabbit-anti-human IgG (Abcam, Cambridge, UK) or goat-anti-monkey IgM (Rockland, Gilbertsville, PA). Antibody binding was measured at 405 nm and results are expressed in arbitrary units (AU) using the software ADAMSEL (developed by Dr. E. Remarque, Biomedical Primate Research Centre, Rijswijk, The Netherlands).

Table 2. Primers with corresponding probes used for quantitative PCR.

Gene	Forward primer (5'-3')	Reverse primer (3'-5')	Probe
ABL	CAGAGAAGGTCTATGAACTCATGC	GGTGGATTCAGCAAAGGAG	86
IL-1 β	TGGTCCTAAACAGATGAAGTGC	GTAGTGCTGGCGGGAGAGT	85
IL-2	AAGTTTTACATGCCCAAGAAGG	AAGTGAAAGTTTTTGCTTTGAGCTA	65
IL-10	GTTGCCTTCAGCAGAGTGAA	GCAACCCAGGTAACCCCTTAA	67
IL-17A	CCTCATTGGTGTCACTGCTG	TGCAATTCCTGCCTTCACTA	146
IFN γ	GGAGAGAGGAGGGTGACAGA	TTGGATGCTCTGGTTGTCTTTA	21
TNF α	GGACGAGCTCTCCAAGGACT	GTCACCTCGGGATTCGAGAAG	81
CD3	AGGCAAGAGTGTGTGAGAACTG	GATGCAGATGTCCACTATGACAA	10
CD4	TCTGTGAAGTGAGAGCAAAAA	TGACAGTCAATCCGAACACC	10
CD8	TCATGTACTTCAGCAGCTTCC	GCTCTGGTGTGGGTGGTC	4

Histology

Formalin-fixed brain sections were used for histological examination as described previously^{127, 263, 288}. For quantification of demyelination 8 brain sections, in total 6 cm², were stained with Luxol fast blue – periodic acid Schiff (LFB-PAS). The Scion Image Program (NIH, USA) was used to calculate the amount of demyelination per mm² as total of the white and grey matter. Another set of 8 brain sections was stained with hematoxylin and eosin and CD3 to determine the amount of inflammation.

Statistical analysis

A high variation of the disease course and associated immune parameters between individual animals is inherent to the outbred nature of this model. Where possible data were analyzed using the Mann-Whitney *U* test; *p* values < 0.05 are considered to be significant.

RESULTS

Human IFN- γ has a variable effect on the disease course in MOG34-56 induced EAE

Fifteen unrelated marmosets from an outbred colony were randomized over three experimental groups of 5 monkeys each (see Table 1), the group size was determined by power calculation (see Materials and Methods)³²⁷. EAE was induced by immunization with human MOG34-56 in IFA. Despite the absence of ligands of innate receptors for antigen presenting cell activation this procedure has induce clinically evident EAE in almost all tested monkeys. Sometimes a case is found without evident neurological signs within the predetermined observation period, but such cases do display the characteristic CNS pathology. Human IFN- γ was administered during 25 days between the first and second immunization (psd 0-25), modeling a prophylactic treatment regimen, or for 25 days after psd 56 (psd 56-81), modeling therapeutic treatment (Fig.1).

The results are expressed as clinical course of individual animals, demonstrating that in each group 1 monkey did not display evident neurological deficit (Fig. 2). Besides, a second monkey in the therapeutic group (Mi12700) did not show neurological symptoms but suffered from weight loss. The actual survival times of individual animals depicted in Table 1 show that the time interval to the first symptom of overt neurological disease (ataxia; score 2.0) was delayed from 98 to 118 days by early treatment with IFN- γ and from 98 to 105 days in monkeys receiving late treatment with IFN- γ . Two parameters were statistically analyzed, namely disease-free survival (time to EAE score 2.0) and overall survival (time to the ethical end-point: score 3.0) (Fig. 2B). The survival curves show that neither the prophylactic, nor the therapeutic treatment with IFN- γ had a consistent positive effect on the disease course.

Demyelination and inflammation in brain

Pathological differences between the three groups were examined by histology and immunohistochemistry. As representative example of the control group and IFN- γ treated group, respectively, M07034 and M07035 are shown in Figure 3. Brain sections in both animals showed demyelinated areas populated by activated macrophages that contain degraded myelin products and by infiltrated CD3⁺ T cells. Demyelinated lesions were also observed in the optic tract and in the corpus callosum. Interestingly, Granzyme B staining detected some

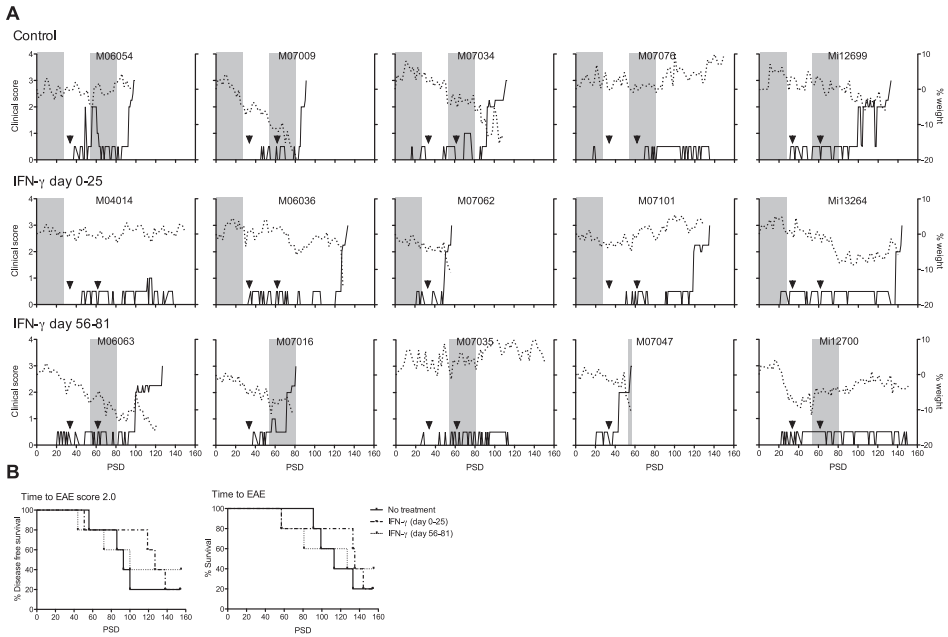


Figure 2. Clinical scores and body weights of all animals. Marmoset monkeys (n=15) were immunized with MOG34-56 in IFA and subsequently treated for a period of 25 days with recombinant human interferon- γ by intravenous injection at a frequency of 3 times per week (see Fig.1). A. The period of IFN- γ treatment is shown as grey shaded areas. The control group received only the solvent of IFN- γ . Left y-axis (solid line) indicates clinical scores and right y-axis (dotted line) the percentage body weight loss relative to day 0 as a surrogate disease marker. On the x-axis time after immunization is plotted as post sensitization day. Arrowheads indicate day of booster-immunizations with MOG34-56 in IFA. M07062, M06054 and M07016 were boosted only once. PSD; post sensitization day. B. Survival curves are shown where the control group is compared to the IFN- γ treatment groups. In the left panel time to EAE score 2.0 and in the right panel time to the ethical end-point (EAE score 3.0) is depicted.

cytotoxic T cells. Quantification of the amount of inflammation and demyelination in brain for each animal (Fig. 3N), revealed no differences in the intensity of demyelination between the control and IFN- γ treated groups. However, inflammation tended to be less intensive in the late treatment group (psd 56-81) although differences were not statistically significant.

Modulation of humoral immunity by IFN- γ

Immunization with MOG34-56 in CFA or IFA induces IgM and IgG antibodies binding to ELISA-plate bound overlapping peptides, i.e. MOG24-46 and MOG34-56, but not to rhMOG protein^{263, 288}. Results of the analysis of serial immune sera from the current experiment are depicted in Fig. S2. The data from individual monkeys and the mean areas under the curve (AUC) show that the highest IgM antibody levels against both peptides were measured in the early (psd 0-25) IFN- γ treated animals, although differences between the groups were not statistically significant. Fig. 4A shows that IgG antibody levels against both peptides were significantly reduced in early

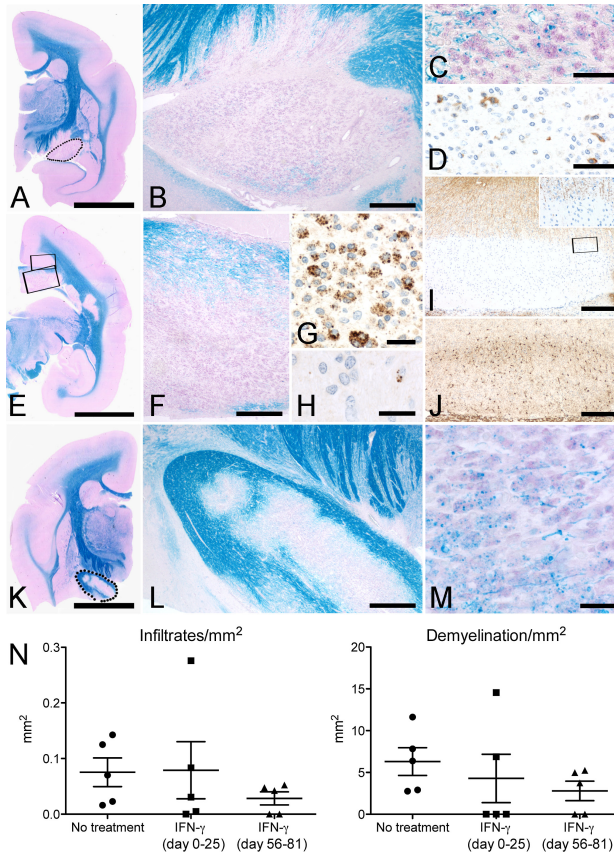


Figure 3. Inflammation and demyelination in the brain characterized by histology and immunohistochemistry. A-J Brain of M07034 as a representative of the control group. A. A low magnification scan from a Kluver-Barrera (KLB) stained section (bar: 5 mm). The encircled area represents the demyelinated optic tract, which is depicted enlarged in B (bar: 500 μ m). C. Luxol fast blue - periodic acid Schiff (LFB-PAS) staining shows in the optic tract the presence of macrophages with intracellular myelin degradation products (bar: 50 μ m). D. Immunostaining for CD3 reveals the presence of some single T cells in the optic tract (bar: 50 μ m). E. Another brain slice of M07034 stained for KLB (bar: 5 mm) is shown. The lower rectangle shows demyelination in the corpus callosum that is enlarged in F and contains LFB-PAS positive macrophages (bar: 500 μ m). G. Immunostaining for myelin proteolipid protein (PLP) shows macrophages containing PLP degraded products (bar: 25 μ m). H. A single Granzyme B positive cytotoxic T cell is shown in the corpus callosum (bar: 20 μ m). The upper rectangle in E shows a cortical area that is shown enlarged in I (bar: 250 μ m) and in a PLP staining reveals subpial demyelination. The rectangle in I shows the edge of the lesion, which is enlarged in the insert. J. Although no PLP positive degradation products are present, staining for macrophage/microglia marker Iba-1 identifies increase of microglial cells at the border of the subpial lesion (bar: 250 μ m). K. A low magnification scan of a KLB stained section from M07035 as representative of the late IFN- γ treated group. The encircled area again shows the optic tract, which is only partially demyelinated and enlarged in L (bar: 500 μ m). M. Further enlargement of L reveals the presence of macrophages with myelin degraded products (bar: 25 μ m). N. For each animal in the three groups 8 brain sections were analysed, which is comparable with 6cm² in total. The amount of infiltrated cells per mm² in the brain is given. Same quantification is done for the amount demyelination in the brain. A detailed description of the calculation is given in 'Material and methods'.

treated monkeys. Bar diagrams show mean antibody concentrations, which were calculated for the four time blocks, i.e. the no-treatment interval (psd 28-56). Summarizing, early treatment with IFN- γ resulted in suppressed IgG antibody production, whereas IgM antibody levels were not affected by the treatment.

Modulation of cellular immunity by IFN- γ

The modulation of cellular immunity in the model was examined with two *ex vivo* assays, namely antigen-induced proliferation and cytokine induction.

Proliferation of PBMC during the EAE course: Every 14 days PBMC were collected and tested for proliferation against MOG34-56 or rhMOG. As shown in Figure 5A responses against MOG34-56 were much stronger than against rhMOG and the highest responses were measured in the control monkeys from group 1. SI values > 2.0 were regarded as positive. Interestingly, Figure 5B shows that early treatment with IFN- γ significantly prolonged the time to reach SI values of 3.0, whereas this was not observed for the late treatment group.

Proliferation of PBMC and lymphoid organ MNC at necropsy: Our previous study demonstrated that only a minor quantity of the T cells proliferating against anti-MOG34-56 is

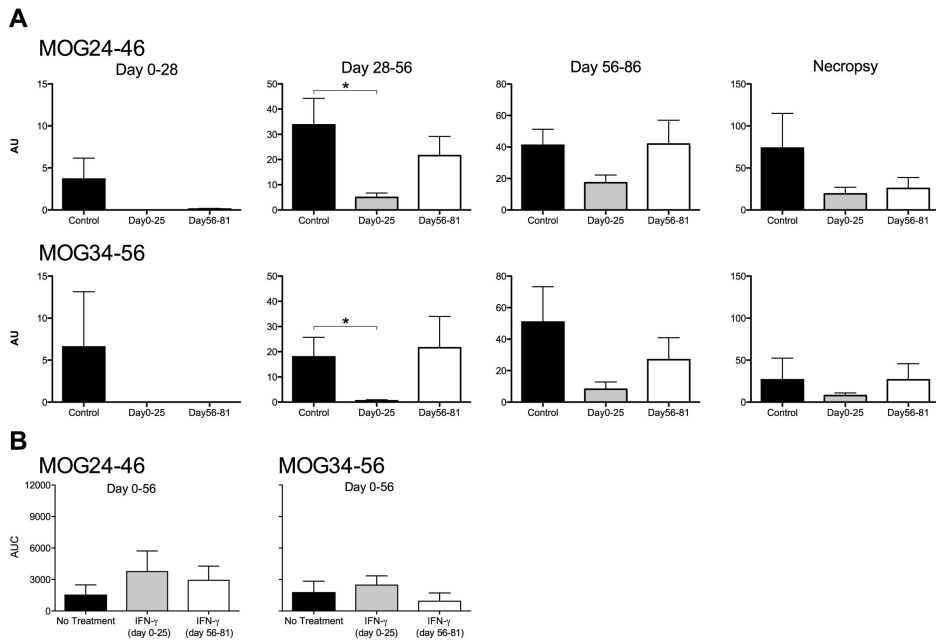


Figure 4. Plasma IgG and IgM antibody binding to MOG peptides. Longitudinally collected plasma samples (2 weeks interval and at necropsy) were tested for the presence of IgG and IgM binding to ELISA plates coated with a panel of overlapping MOG peptides. Only antibodies binding to MOG24-46 and MOG34-56 were detected. A. IgG plasma levels were compared during and after the treatment periods to assess whether there is a significant difference in antigen binding. Data are processed with ADAMSEL and expressed in arbitrary units (AU). B. IgM antibody responses were only compared from day 0-56. Data are expressed in area under curve (AUC), which is calculated from data of Fig. S2. * $p < 0.05$, Mann-Whitney U test was used as statistical calculation. Data are presented as mean \pm SEM.

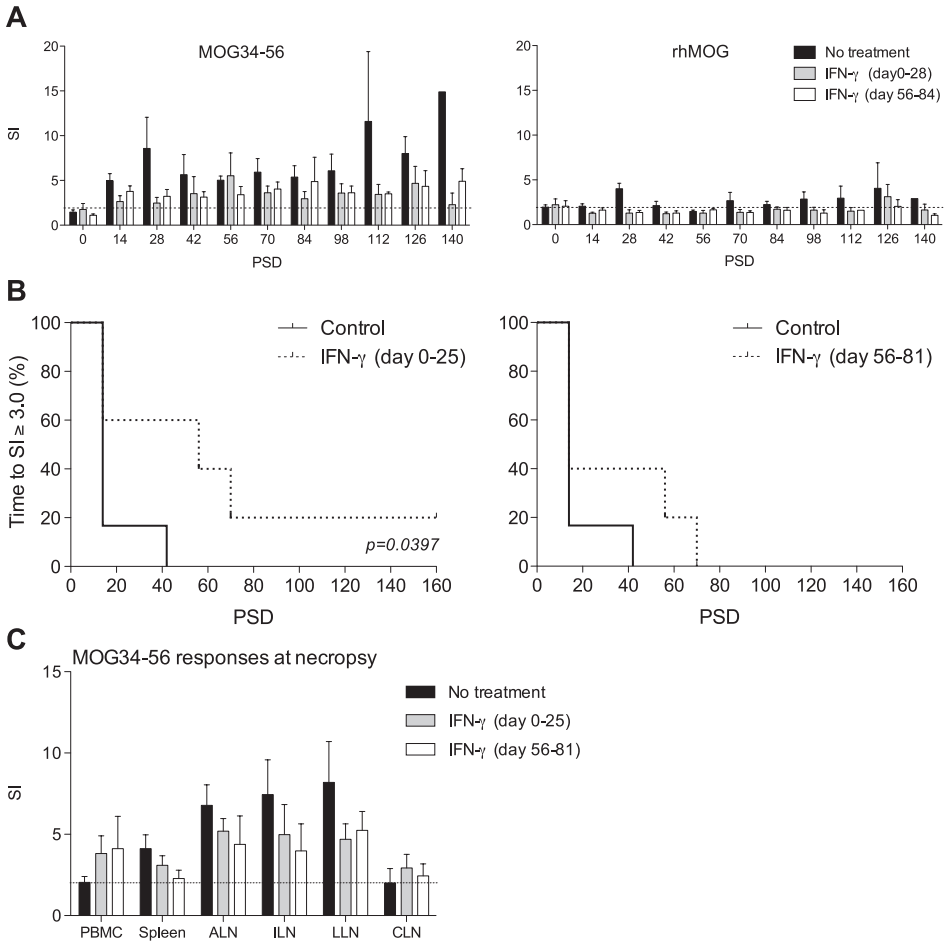


Figure 5. T-cell proliferation against MOG34-56 and rhMOG. Mononuclear cells (MNC) isolated from venous blood (PBMC) or various lymphoid organs were probed for their proliferative response against MOG34-56 and rhMOG. Proliferation was quantified as the incorporation of [3 H]-thymidine in the final 18 h of 3 days culture. All data are expressed as stimulation index (SI) relative to unstimulated cultures. SI above 2 (dotted line) is considered positive. **A.** Longitudinal reactivity of PBMC to MOG34-56 (left panel) and rhMOG (right panel) is shown. **B.** Time to a stimulation index (SI) of 3.0 against MOG34-56 in blood was compared between the control group and IFN- γ treated groups. Log-rank was used to calculate p -value. **C.** At necropsy MNC were prepared from blood, spleen, axillary (ALN), inguinal (ILN), lumbar (LLN), and cervical (CLN) lymph nodes. Only proliferation data from cultures stimulated with MOG34-56 are shown. Mann-Whitney U test was used as statistical calculation. Data are presented as mean \pm SEM.

present in blood, and that the vast majority can be found in the lymphoid organs. Hence we also tested the antigen reactivity of several secondary lymphoid organs collected at necropsy, namely spleen, the ALN and ILN that drain the immunization sites, and the LLN and CLN that respectively drain the spinal cord and brain.

It is of note that the proliferation data at necropsy did not provide an explanation for the absence of neurological signs in the EAE affected control monkey M07076. This monkey's proliferation profile was similar to that of control monkey M112699, which did develop clinical EAE. By contrast, the proliferation was markedly suppressed in monkeys from both IFN- γ -treated groups that did not develop overt neurological disease, i.e. M04014 and M07035. Overall the results show that the proliferation profiles of individual monkeys differ markedly within each group (data not shown), but that there are no obvious differences between the three groups (Fig. 5C). These data suggest that IFN- γ treatment did not exert a consistent positive or negative effect on T cell responses.

Cytokines

The main induced cytokine by *ex vivo* stimulation of PBMC with MOG34-56 or rhMOG was IL-17A, as measured by ELISA based on cross-reactive reagents. This was confirmed in the current study (Fig. S3). Expression profiles of IL-17A, IFN- γ or IL-10 did not differ significantly between the three groups, although IL-17A production after the first (psd 0) and third immunization (psd 56) was consistently observed in the monkeys that received IFN- γ treatment. To investigate this further we performed qPCR analysis of mRNA transcripts extracted from PBMC, spleen and ALN for a broader range of cytokines (Fig. 6A). The qPCR analysis showed no differences in cytokine

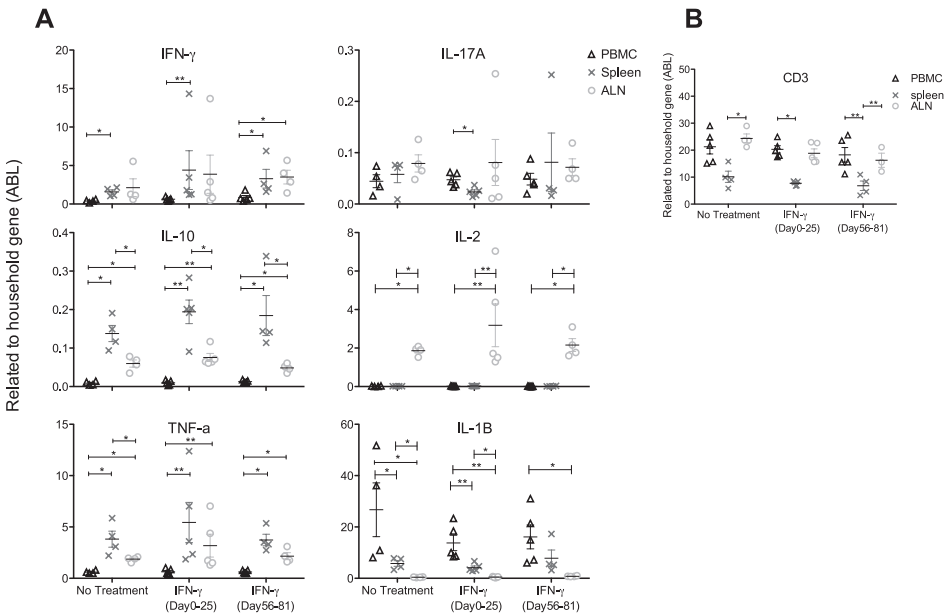


Figure 6. Cytokine expression measured by qPCR. mRNA was extracted from PBMC, spleen and ALN that were aseptically collected at necropsy and from PBMC collected at 2 weeks interval during the disease course. Primers with the corresponding probes as detailed in Table 2 were used for qPCR. A. IFN- γ , IL-17, IL10, IL-1 β , TNF- α and IL-2 mRNA level in PBMC, spleen and ALN were determined in all three groups. Data depicted in the graph were expressed relative to the household gene ABL (see Materials & Methods). B. CD3 (epsilon) expression was also determined in PBMC, spleen and ALN. Mann-Whitney *U* test: **p*<0.05; ***p*<0.001

expression between IFN- γ -treated groups and the control group. However, transcript levels differed statistically between the organs (PBMC, spleen and ALN), mainly for IL-10, IL-1 β , TNF- α and IL-2. A higher expression of IL-10 and TNF- α was detected in spleen and ALN compared to PBMC in all three groups. The opposite effect was observed for IL-1 β , i.e. a higher expression in PBMC than in ALN or spleen. Level of expression of IL-2 was only higher in ALN compared to PBMC and spleen. Differences for the other two tested cytokines, IFN- γ and IL-17A, were less explicit.

DISCUSSION

The optimal immunotherapy for MS selectively targets only the immune processes that cause the progressive accumulation of neurological deficit, while sparing immune functions protecting against infections or tumorigenesis²⁷⁵. In the past years we have dissected the core pathogenic autoimmune factor against human CNS myelin in a unique EAE model in marmosets. The well-documented clinical and pathological similarity with MS is particularly relevant for translational research into pathogenic mechanisms as well as for therapy development^{222, 272}.

The original model was induced by immunization with CNS myelin from human MS patient emulsified in CFA¹²⁷. The discovery that autoimmunity against MOG is essential for the induction of clinically evident EAE¹²⁷ led us to develop a reproducible disease model induced with rhMOG protein in CFA. Subsequent fine-specificity analysis revealed that the progression rate to full-blown clinical disease was associated with the activation of CD3+CD4+/8+CD56+ cytotoxic T cells specific for MOG34-56¹⁹⁰. The strong clinical effect of antibodies against human CD40 and against the shared p40 subunit of IL-12 and IL-23 underlined the important role of the CD40/IL-12/23 axis in the rhMOG-induced EAE model in marmosets^{264, 266, 332}. Up to that point, the marmoset EAE model reproduced the essential pathogenic features of rodent EAE models.

However, further research led to the unexpected finding that immunization with MOG34-56 in IFA could also induce full-blown clinical EAE²⁸⁸. The immunopathogenic mechanism of this new model was found to be driven by T cells that are activated without involvement of the otherwise required Toll-like receptor ligands and which induce widespread CNS demyelination in the absence of antibodies binding MOG protein. Fine-specificity analysis of this model revealed a central role of T cells specific for MOG peptide 40-48 with a remarkable phenotype, namely CD3+CD4+CD8+CD16-CD27+CD28-CD45RO-. The MOG34-56 specific T cell lines generated from this model shows two immunological hallmarks i.e. high IL-17A production and specific cytolytic activity towards peptide presented via Caja-E molecules expressed by EBV-transformed autologous B-lymphoblastoid cells³⁰⁷.

These features clearly distinguish the new model from the MHC class II-restricted Th1 dominated classical EAE models in rodents and marmosets induced with CFA. To analyze this in further detail we have tested to what extent modulation of Th1-mediated pathogenic mechanisms by treatment with human IFN- γ modulates the disease course in this new model. Our prior expectation was analogous to the situation in mouse models of EAE³³⁵ or of collagen-induced arthritis³³⁷, presence of high IFN- γ levels during disease induction stimulated the disease, whereas late administration is suppressive. An explanation for the early stimulation is a general-

ized immune stimulatory effect, whereas the late suppressive effect might be that injection of IFN- γ suppresses production of IFN- γ at the tissue level³³⁸.

In the marmoset EAE model, administration of IFN- γ between psd 0 and 25 exerted modulatory effects on several immunological parameters demonstrating *in vivo* biological activity, but had no systemic effect on the time of onset or the clinical course of the EAE model. Importantly, different from the observation in MS patients³³⁹, administration of IFN- γ did not aggravate clinical signs.

The body weight loss is a useful objective disease parameter, which is usually attributed to a systemic metabolic effect of inflammatory mediators such as TNF- α , IL-6 or IFN- γ , the cachectic syndrome³⁴⁰. The body weight loss in the MOG34-56/IFA model is less serious than in the EAE models induced with CFA and shows a high interindividual variability that is inherent to the outbred nature of the marmoset EAE model. Mean body weight measurements of the early IFN- γ -treated animals remained stable between psd 0 and 56, whereas a decrease was observed in the control and late treated animals, which were untreated during this time period. Late treatment with IFN- γ during the episode psd 56 to 81 had no clear effect on the mean weight loss. It is tempting to speculate that the variable clinical effect of IFN- γ may be due to a similar variation in immunopathogenic profile as observed in MS patients³⁴¹.

Another level of modulation by IFN- γ was the skewing of the IgM or IgG ratio of anti-MOG peptide antibodies, i.e. the increase of IgM and decrease of IgG. This was less evident in the late treatment group. Although proliferation of PBMC remained relatively low, it was affected by the IFN- γ treatment. The time to exceed the SI threshold 3 was delayed in the early treatment group. Moreover, PBMC from IFN- γ treated monkeys proliferated less against MOG34-56 and rhMOG than PBMC from control monkeys during late stage disease, i.e. after psd 100. However, the reactivity profiles of MNC from the lymphoid organs were largely comparable between the three groups. At the level of cytokine production no effect of IFN- γ treatment was observed, only the lymphocytes from the various organs within each group showed significant differences. Differences between PBMC, spleen and ALN were mainly found in the expression of IL-10, IL-1 β , TNF- α and IL-2.

Treatment with human IFN- γ exerts several modulatory effects on immune parameters in the new EAE model, in particular when the cytokine is administered during the induction of the pathogenic process. These effects are more subtle than those observed in regular EAE models induced with CFA. Despite these immunomodulatory effects, IFN- γ treatment had no clear effect on the severity nor the course of neurological disease. We would like to propose as explanation that the IL-17A producing cytotoxic CD3+CD4+/CD8+CD56+CD16- T cells that form the core pathogenic factor in the MOG34-56/IFA EAE model are not affected by IFN- γ treatment.

In conclusion, human IFN- γ is biologically active on several immune parameters in the marmoset EAE model. Nevertheless, we observed neither of the early nor the late treatment a detectable effect on the severity or course of EAE. This marks a clear difference with rodent EAE models. We also did not observe aggravation of clinical signs as was observed in relapsing remitting MS patients. Our interpretation of this discrepancy is that the T cells that cause pathology and neurological deficit in this model are committed effector memory cells³⁰⁷, which exert their activity in the late progressive phase of the disease¹⁹⁰. Taken together the conclusion is warranted that Th1 cells do not have a detectable role in the new model.

ACKNOWLEDGEMENTS

The authors would like to acknowledge Fred Batenburg, Mariska van Etten and Tom Haaksma for experimental assistance and Dr Angela Fahey for the experiments validating the human IFN- γ effects on marmoset immune cells. This work was supported by PRIMOCID, which is part of the European Union–funded project EUPRIM-NET. The funding source had no part in the design, interpretation or preparation of the data for publication.

SUPPLEMENTARY FIGURES

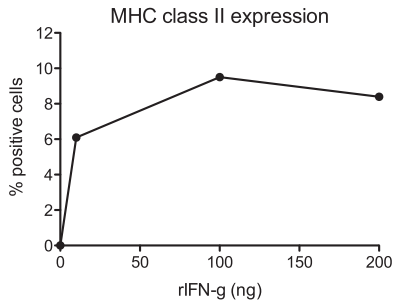


Figure S1. Cross-reactivity of rhIFN- γ on marmoset cells. Marmoset PBMC were stimulated with a dose titration of rhIFN- γ and MHC class II expression was determined by flow cytometry. Percentages positive cells were corrected with background staining. Data is shown from one marmoset as representative of three.

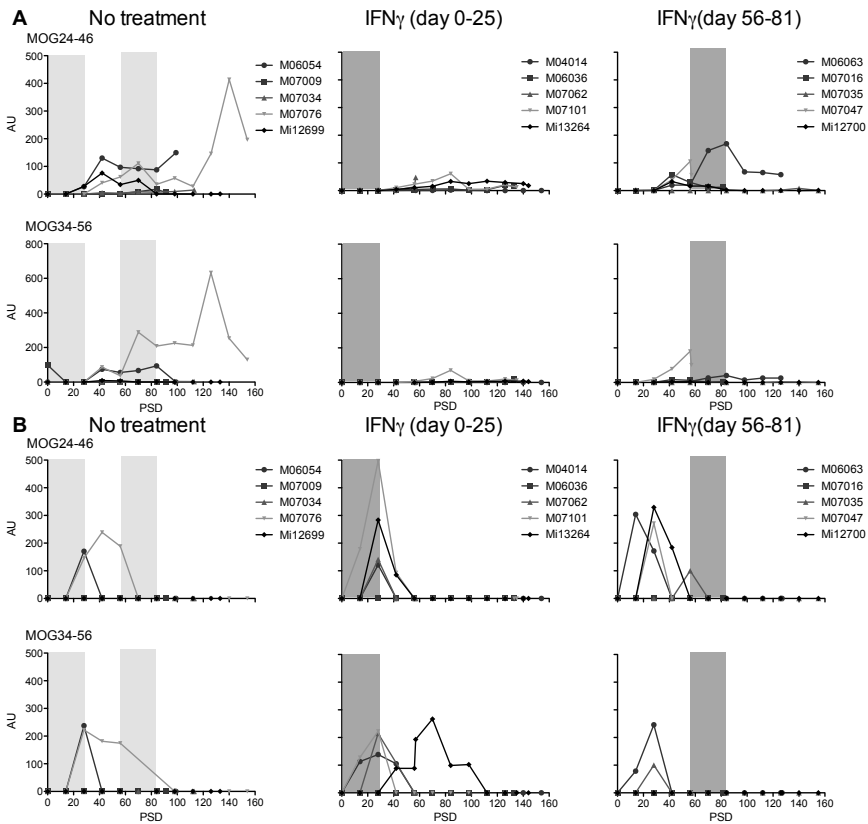


Figure S2. IgG and IgM levels of individual animals. Longitudinally collected plasma samples (2 weeks interval and at necropsy) were tested for the presence of IgG antibody binding to a panel of overlapping MOG peptides and rhMOG. IgG (A) and IgM (B) responses only to MOG24-46 and MOG34-56 are shown. No antibody binding to other overlapping MOG peptides or rhMOG was detected. Data is expressed in arbitrary units (AU). 1000 AU are equivalent to an OD of $\pm 0,7$. The treatment period is indicated as a grey shaded area in the graphs.

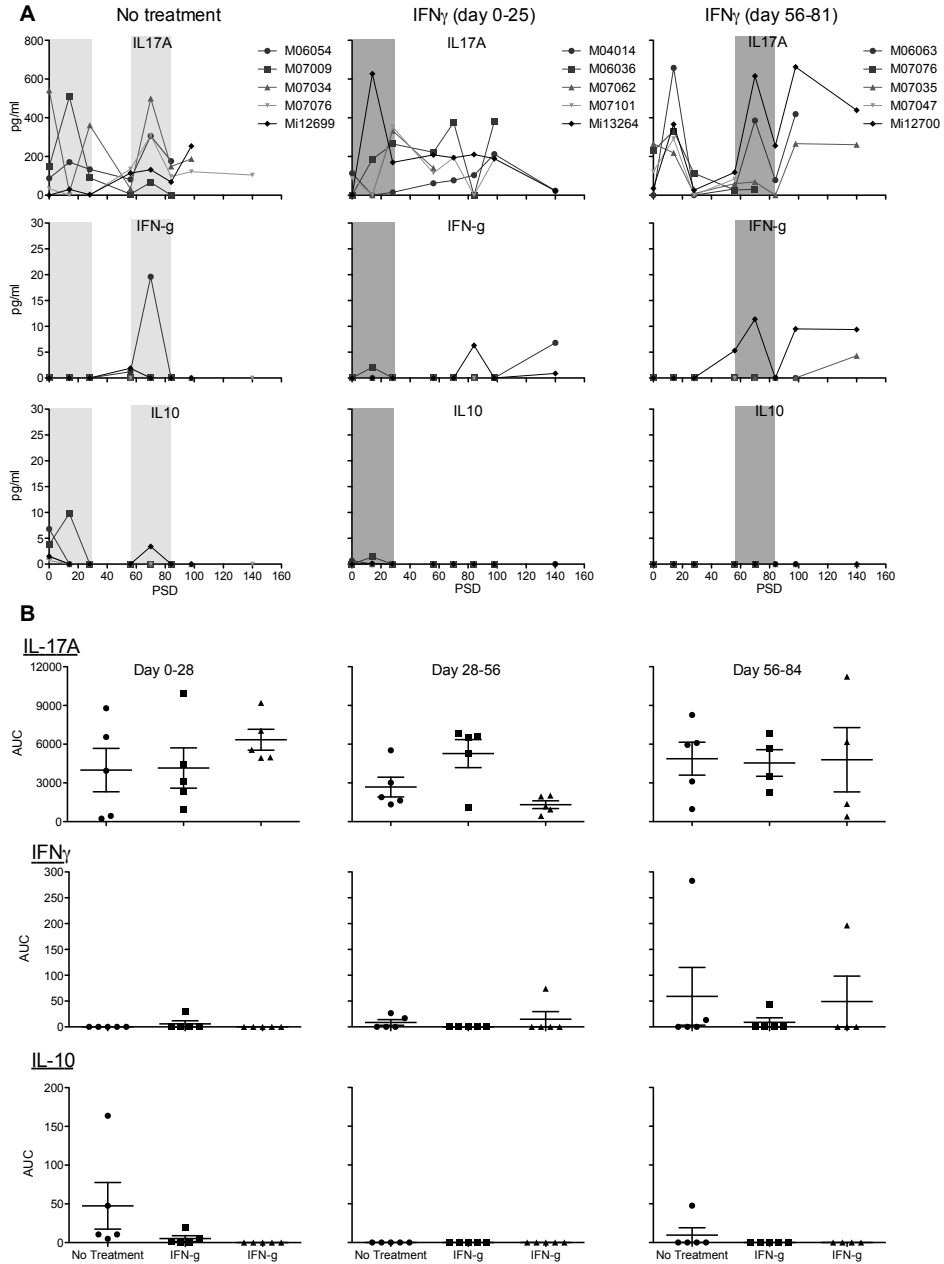


Figure S3. Production of IL17A, IFN- γ and IL10 by MOG34-56 stimulated PBMC. Blood MNC were stimulated for 48 hours with MOG34-56 and rhMOG. Culture supernatants were tested for the presence of IL17A, IFN- γ and IL10 protein with ELISA. A. MNC stimulated with MOG34-56. Grey shaded areas in the graphs indicate the period of treatment with rhIFN- γ ; control (left), early treatment (middle), late treatment (right) B. Three periods (before, during and after IFN- γ treatment) were compared between the control and IFN- γ treated groups. Data is expressed is in area under curve (AUC).

GENERAL DISCUSSION

10

PREFACE

The exact immunopathogenic mechanisms and causes behind MS are still unrevealed. Although immunotherapy for MS is continuously improving, MS progression is not stopped, and side effects related to immune suppression are sometimes severe. For unraveling the immunological pathways and developing novel therapeutics, the common marmoset EAE model was used as a relevant animal model for MS. When the EAE research in the common marmosets was started at the Biomedical Primate Research Centre, little was known about the critical immunological pathways in this monkey model. The then available common marmoset EAE model, namely active induction with rhMOG or MBP in CFA supplemented with or without *Bordetella* particles, gave an acute disease, which resembled acute disseminated encephalomyelitis (ADEM)¹²⁶. The characteristic clinical presentation of MS, such as chronic progression of the clinical symptoms, was not observed.

The main objective of this project was a mechanistic refinement of the common marmoset EAE model. This was achieved by systematic dissection of the immunological reactions against the myelin/CFA inoculum, which induce neurological dysfunction in the common marmoset EAE model. The reduction of artificial requirements led to an important improvement of the welfare of the animals, also in conceptual terms, with regard to the immunization protocols. The most important improvement was that CFA could be replaced with IFA, meaning that microbial ligands for innate immune activation were eliminated from the inoculum.

Simultaneously, we investigated the role of autoreactive T-cells and B-cells in respect to the development of CNS pathology and clinical symptoms. Finally, we tested the validity of new targets for MS therapy using novel immunotherapeutics to elucidate mechanistic pathways.

10

THE COMMON MARMOSET EAE MODELS

Different EAE models in the common marmoset have been developed and described in this thesis, which mainly vary in their induction requirements, disease progression, T- and B-cell activation and pathology in brain and spinal cord. The developed EAE models are myelin in CFA, rhMOG in CFA, rhMOG in IFA, MOG34-56 in CFA and MOG34-56 in IFA. These are discussed below and summarized in Table 1.

At the onset of the current project (this thesis), immunization with rhMOG in CFA without *Bordetella pertussis* was the latest developed common marmoset EAE model at the Biomedical Primate Research Centre in 2000 by Brok et al¹⁰³. The immunological parameters were not studied in detail, and monkeys had a heterogeneous disease onset (four to ten weeks after immunization) and severe clinical symptoms as paresis and paralysis of the limbs. Since the pathology and clinical symptoms were highly comparable with MS patients, this was a major step forward in modelling of MS in non-human primates. To understand the immunopathogenic mechanisms in more detail, the common marmoset EAE model was further refined.

Myelin-induced EAE

The first aim was to verify the pathogenic significance of MOG (**chapter 2**). To this end, one sibling of five marmoset twins was sensitized against myelin derived from wild-type C57BL/6 mice and the other sibling with myelin derived from MOG deficient C57BL/6 mice, a mutant strain developed by Pham-Dinh et al.²²⁷.

Table 1. Comparison of various common marmoset EAE models.

Antigen	Adjuvant	Disease type	Demyelination		T cells	IgG to rhMOG	Ref.
			Grey matter	White matter			
Human myelin	CFA+ <i>B. pertussis</i>	Acute	ND	+	ND	ND	126
Human myelin	CFA	Acute	ND	+	ND	ND	127
Mouse myelin	CFA	Acute	ND	+	ND	ND	Ch.2
MBP	CFA	Mild	ND	+/-	ND	-	103
MOG ^{-/-} mouse myelin	CFA	Mild	ND	+/-	ND	-	Ch.2
rhMOG	CFA	Chronic	+	+	Th1/Th17	+	Ch.3
rhMOG	IFA	Chronic	ND	ND	ND	+	Ch.6
MOG14-36	CFA	Chronic	ND	+	ND	+	103
MOG34-56	CFA	Chronic	+	+	Th1/Th17	+	Ch.3
MOG34-56	IFA	Chronic	+	+	Th17	-	Ch.4

ND, not determined

Both groups had inflammation and lesion formation in the white matter, which were highly comparable with the rhMOG/CFA common marmoset EAE model. However, the progression to clinical EAE was disturbed in 4 out of 5 monkeys immunized with MOG deficient myelin. The cause of the clinical EAE signs in the one monkey immunized with MOG deficient myelin can probably be attributed to autoimmune reactions against other myelin proteins such as MBP and PLP.

The same principle was observed in the chronic relapsing EAE model in Biozzi ABH mice. In that model we found that adding a physiological dose of rhMOG to mice immunized with MOG deficient myelin restored the induction of chronic relapsing EAE⁹³. From these experiments we concluded that the quantitatively minor component of CNS myelin, MOG, plays a prominent role in the hierarchy of CNS antigens with encephalitogenic potential in chronic EAE.

rhMOG-induced EAE

The immunodominance of MOG was investigated in greater detail in common marmoset monkeys immunized with rhMOG in CFA (**chapter 3**), a formulation that has previously been used for immunization of common marmoset monkeys. This rhMOG/CFA formulation induced a more chronic disease in all animals. The 100% EAE incidence was found to map to the monomorphic MHC class II allele *Caja-DRB*W1201*, which is expressed in all common marmoset monkeys^{200,206}. In addition, all animals had a typical MS-like pathology, which was characterized as early-active lesions with transient axonal pathology³⁴² and deposition of complexes with antibody and complement components. The first pathological change in the CNS was formation of vesicles (vesicularization) in the white matter containing myelin products probably due to redistribution of the myelin lipids¹³⁹. Antibodies were formed against rhMOG and several MOG peptides, such as MOG14-36, MOG34-56 and MOG54-76. We assumed that these anti-MOG

antibodies played a crucial role in the cause of the disease progression, especially since it was shown by others that anti-MOG antibodies are associated with disintegration of myelin in the common marmoset EAE model and in MS patients³⁴³. At the T-cell level, a high proliferation against several MOG peptides was observed at the peak of disease, in particular to MOG34-56 and the overlapping peptides MOG64-86 and MOG74-96. Interestingly, monkeys with a rapid disease progression displayed T-cell proliferative responses against a broader range of MOG peptides than monkeys with a longer disease duration. Immunization led to the activation of Th1 and Th17 cells, producing e.g. IFN- γ and IL-17A, respectively. Neutralization of IL-17A with a candidate therapeutic antibody in this model had marginal effect on the late disease course³⁴⁴, whereas neutralization of IL-12/-23 was highly effective²⁴⁴ suggesting that Th1 cells are more important in the rhMOG/CFA model than the single cytokine IL-17A.

From this experiment we conclude that the pathogenic mechanism and histological aspects of the lesions were reminiscent of the secondary progressive form of MS, which resembled the presumed pattern II lesion pathology⁵⁵.

MOG peptide induced EAE with CFA

The MOG peptides 34-56 and 74-96 were immunized separately to test their encephalitogenicity (**chapter 3**). It was observed that only monkeys immunized with MOG34-56 in CFA developed clinical EAE. The patterns of CNS inflammation and demyelination were very similar to the rhMOG/CFA EAE model. Also activation of autoreactive T-cells was observed, which were phenotypically characterized as CD3+CD4+, CD3+CD8+, or CD3+CD4/CD8 double positive, co-expressing CD56 but not CD16. Interestingly, T-cells with a similar phenotype and cytotoxic activity against MOG were found in MS patients¹³⁷, and were associated with demyelination in MS^{270, 269}. This phenotype was found also to be similar to natural killer–cytotoxic T- lymphocytes (NK-CTL) like cells^{300, 345} (see Table 2), which displayed a cytolytic activity to EBV-transformed B-cells. In addition, antibodies were formed against rhMOG, MOG34-56 and the partly overlapping peptides MOG14-36 and 24-46.

In contrast to the immunization with MOG34-56 in CFA, monkeys immunized with MOG74-96 in CFA remained asymptomatic, although small abnormalities were detected on post-mortem T2W images suggestive of inflammatory lesions. But after a single booster immunization with MOG34-56 in IFA, all MOG74-96/CFA immunized monkeys developed neurological deficits and CNS pathology within a few weeks.

These results led to the conclusion that anti-MOG74-96 T-cells were not or mildly encephalitogenic unlike anti-MOG34-56 T-cells that were able to induce typical EAE symptoms as CNS white matter pathology and clinical symptoms.

MOG peptide induced EAE with IFA

A single immunization with MOG34-56 in IFA was sufficient to induce MS-like features in MOG74-96/CFA sensitized animals. This warranted the question whether it is possible to induce EAE in naive common marmoset monkeys just with MOG34-56 in IFA (**chapter 4**). Also for ethical reasons replacing CFA with IFA would be a major advancement. CFA is a major cause of serious discomfort such as granuloma formation at the injection sites, and it is very artificial since it is involved in the activation of a broad range of cytokines. All these reasons prompted us to assess if EAE could be induced using an immunization-booster protocol solely with MOG34-56 in IFA.

More than 90% of the immunized animals developed EAE symptoms and in all animals the white and/or grey matter were affected by widespread demyelination. Interestingly, animals developed only IgG antibody responses to MOG24-46 and MOG34-56, but not to rhMOG, and disease occurred in the absence of microbial innate immune receptor antigens engaging for instance Toll-like receptors. From these results we concluded, first that activation of APC via microbial antigens driving innate immune activation via the inoculum is not required for the induction of clinically evident EAE, and second that disease progression take place in the absence of autoantibodies against rhMOG mediating demyelination. Thus we conclude that pathological and clinical features in the MOG34-56/IFA EAE model, which were highly comparable with MS, were caused most likely by autoreactive T-cells.

To investigate the mechanism and nature of these autoreactive T-cells in the MOG34-56/IFA EAE model in more depth, several immunological assays were used (**chapter 5**). With CFSE vital dye dilution assay it was found that the highest T-proliferation was directed against the MOG34-56, and that responding T cells were mainly located in the secondary lymph nodes (ALN, ILN, LLN and spleen), but not in blood. The phenotype of these T-cells was defined in three subsets, CD3+CD4+, CD3+CD8+ and CD3+CD4+CD8+. The three subsets were CD56 positive and

Table 2. NK-CTL features of humans compared with the common marmoset.

Characteristics	Human	Marmoset
HLA-E restricted cytotoxicity	+	+
Reactive to allogeneic cells	+	+
CD8	+	+
CD4CD8	-	+
CD27	-	+
CD28	-	-
CD45RO	+	+
CD56	+	+
CCR7	+	+
TCRV β 16	+	+
TCR $\alpha\beta$	+	ND ^a
CD94/NKG2A	-	ND
NKp46	-	ND
NKp44	-	ND
NKp30	-	ND
NKG2D	+	ND
NK2B4	+	ND
iNKR receptors	+	ND

iNKR, inhibitory natural-killer receptors; ND, not determined; NK, Natural-killer cells; TCR, T-cell receptor. ^aNot tested for these markers due to lack of crossreactive antibodies for common marmosets. Based on^{269, 270, 300, 345}

CD16 negative. The CD3+CD4+CD56+ and CD3+CD4+CD8+CD56+ populations were CD45RO+, CD27+, CD28- and CCR7-, which resembles the phenotype of NK-CTLs (see Table 2). Functional characterization with respect to the pathogenic role of the T-cells, demonstrated that *ex vivo* stimulation with MOG34-56 induced high levels of IL-17A, and low levels of IFN- γ and TNF- α , along with specific cytolytic activity to autologous as well as allogeneic EBV-transformed B-cells presenting MOG34-56. Fine-specificity analysis revealed that the autoreactive T-cells recognized a 9-mer MOG epitope within the MOG34-56 sequence, namely MOG40-48, presented by monomorphic Caja-E molecules. Caja-E is a representative of the non-classical MHC class 1b lineage in the common marmoset, and is the equivalent of human HLA-E. HLA-E lineage members have a regulatory role for NK-cells via NKG2A/CD94³⁴⁶.

All together these results reveal that the phenotype and function of the T-cells resemble effector memory NK-CTL; these are present in the human repertoire and can kill CMV-infected cells via the recognition of viral peptides presented by HLA-E molecules³⁰⁰. Herpesviruses such as CMV use the inhibitory signals of HLA-E molecules for immune evasion from NK cells³⁰⁴. In addition, the amino acid sequence of MOG34-56 and MOG40-48 are highly similar to the immunodominant UL86 antigen of human CMV. Rhesus monkeys immunized with this cross-reactive peptide displayed small infiltrations in the perivascular space and meninges¹⁸⁹. These data suggest that the pathogenic T-cells in the MOG34-56/IFA model may originate from the repertoire of effector memory cells that regulate latent CMV infection³⁰⁰.

10

rhMOG in IFA

As a final experiment of the dissection of the immunological core event in common marmoset, monkeys were immunized with rhMOG in IFA (**chapter 6**). The aim of this study was to compare the clinical and pathological features of the rhMOG/IFA model with other common marmoset EAE models, especially with the rhMOG/CFA model. The questions that we would like to answer were: 1. is the disease course of the rhMOG/IFA EAE model less acute compared to the rhMOG/CFA model, 2. do these monkeys display IgG antibody responses against rhMOG, 3. do it contribute to therapy development and 4. is CNS pathology comparable to other common marmoset EAE models?

Since not all data are analysed yet, so far we can say that all immunized monkeys developed neurological symptoms and that IgG antibodies were formed against rhMOG, and the MOG peptides 14-36, 24-46 and 54-76 but not to 34-56. The remaining parameters such as CNS pathology and cytokine profile need to be examined.

THE ROLE OF B-CELLS IN EAE PATHOGENESIS

We observed no clear association between the diversity of the antibody response and the rate of disease progression in our common marmoset EAE models (**chapter 3**). The role of anti-MOG antibodies in the induction of CNS demyelination in common marmoset has been demonstrated by Genain et al^{343, 136}. The main pathogenic antibody reactivity was directed against conformational epitopes²⁶⁸. Nevertheless, we were able to induce full-blown EAE in the absence of anti-rhMOG antibody formation (**chapter 4**). This raises the question whether and how B-cells contribute to the development of disease in the MOG34-56/IFA EAE model and how the pathogenic autoreactive T-cells are activated.

To investigate this, one sibling of five common marmoset twins was treated with the crossreactive anti-human CD20 IgG1κ antibody (HuMab7D8)²¹⁵ (**chapter 7**), see Figure 1. The treatment resulted in almost 100% depletion of mature B-cells in blood and lymphoid organs, and suppression of clinical and pathological EAE signs in all treated monkeys. Essentially the same data was found in the rhMOG/CFA common marmoset EAE model, where treatment with the same anti-CD20 resulted in radical reduction of CNS pathology and complete disease protection^{215, 311}. Also our results reproduced the beneficial clinical effect of B-cell depletion in RRMS patients⁷⁵.

However, the CD20+ B-cell depletion therapy in the MOG34-56/IFA common marmoset EAE model is in contradiction with the work of Weber et al.³⁴⁷. They describe that in the MOG35-55/CFA mouse EAE model, also a setting in which B-cells are not required or involved in the disease progression, CD20-treatment exacerbates EAE symptoms. In addition, CD20-treatment had no influence on the development of Th1 or Th17 cells, and reduced the frequency of regulatory T-cells. The authors suggest that EAE aggravation in this B-cell independent mouse model is associated with an increased production of the pro-inflammatory cytokine TNF- α ³⁴⁸. In the MOG34-56/IFA common marmoset EAE model no increased production of pro-inflammatory cytokines was detected compared to the untreated monkeys, which might explain why common marmosets are protected from EAE symptoms with the anti-CD20 treatment in a B-cell independent mediated immune response.

Another explanation for the success of the B-cell depletion therapy in MS and in the MOG34-56/IFA common marmoset EAE model is that antigen presentation to the pathogenic T-cells and the ability to induce cytokines, such as lymphotoxin, are abrogated. An additional mechanism could be that lymphoid structures of B-cells in the meninges are not formed, which may imply that infiltrated T-cells from the periphery cannot be activated²¹⁵.

Furthermore, the assumption that the NK-CTL like cells are activated by B-cells was supported by the finding that infusion of one sibling of a common marmoset twin with MOG34-56 pulsed EBV-transformed B-cells activated autoreactive T-cells together with mild CNS pathology. Also, we observed *in vivo* activation of cytotoxic T-cells that most likely killed *ex vivo* B-cells from cultures. The other sibling that was infused with the EBV-transformed B-cells not loaded with the MOG peptide lacked these effects.

These results led to the interpretation that in our MOG34-56/IFA EAE model 1. disease progression takes place in an antibody independent way as formation of anti-rhMOG antibodies is absent, and 2. B-cells are involved in the activation of pathogenic T-cells.

UNRAVELLING THE CORE PATHOGENIC PROCESS WITH IMMUNOTHERAPIES

A mechanistic explanation of B-cell depleting therapies

In common marmoset monkeys immunized with rhMOG in CFA and in MS patients, treatment with anti-CD20 antibody caused a significant depletion of B-cells. This resulted in rapid and prolonged suppression of neurological symptoms and reduction of the volume lesion in the CNS^{75, 215}. However, long-lasting depletion of B-cells in humans is associated with side effects, such as activation of the polyoma JC virus that causes the serious clinical problem progressive multifocal leukoencephalopathy (PML)³⁴⁹. Complications like these warrant the question

whether extensive B-cell depletion for a long term is sensible. To get an answer to this question, we have used an alternative approach for B-cell depletion. Monoclonal antibodies were used to inactivate or block factors required for the survival and differentiation of B-cells, namely the cytokines B Lymphocyte Stimulator (BLYS) and A Proliferation-Inducing Ligand (APRIL) (**chapter 8**), see Figure 1. The two antibodies were tested in the rhMOG/CFA common marmoset EAE model in which a marked clinical effect of the anti-CD20 had been observed²¹⁵.

Treatment with anti-BLYS and anti-APRIL monoclonal antibodies significantly delayed the disease onset compared to the control monkeys, but a significant rescue from severe motor defects was only observed for the anti-BLYS group. Both groups displayed an increase of the total lesion load in the brain, but there was a notable decrease of demyelination and inflammation in the spinal cord. This suggests that development of neurological defects in the antibody treated groups could be attributed to the abnormalities in the spinal cord and not to the brain lesions.

At the immunological level the anti-BLYS monoclonal antibody displayed another mechanism of action than anti-APRIL. Anti-BLYS treatment reduced antibody levels against rhMOG and MOG peptides, along with a reduced activation of Th1 (IFN- γ) and Th17 (IL-17A) cytokines. In addition, it has been shown that anti-BLYS treatment in mice activated neuronal outgrowth and axonal regeneration in the CNS³³¹. Such effects are not described for anti-APRIL, which may explain the shorter survival period compared to the anti-BLYS group. Nevertheless, anti-APRIL affected immunological parameters such as reduction of mRNA transcript levels of Th1 and Th17 related cytokines, but it increased IL-10 mRNA levels. From these results we propose that anti-APRIL treatment shifted the T-cell profile from a pro- to an anti-inflammatory response, whereas anti-BLYS had a beneficial effect on the disease progression. Further research is needed to understand the exact mechanisms underlying the outcome of treatment with these two antibodies and whether they can be used as a replacement for the anti-CD20 treatment.

Atacicept (TACI-Ig), a human recombinant fusion protein that binds BLYS and APRIL, was found to be effective in clinical trials and in animal models of autoimmune diseases such as systemic lupus erythematosus (SLE) and rheumatoid arthritis (RA)³⁵⁰⁻³⁵². Circulating immunoglobulin levels, mature and total B-cells numbers were reduced by the treatment. For this reason clinical studies were started to examine the safety, tolerability, and efficacy of atacicept in MS patients. However, initiation of atacicept treatment in MS patients led to an increase of inflammatory disease activity, and the trial was terminated early³⁵³. So far, it is not understood why this fusion protein exacerbated the disease activity in MS and not in other autoimmune diseases. An explanation could be that targeting B-cells and its function in MS is more complex compared to SLE and RA, and that regulatory B-cells in MS may be depleted.

The role of Th1 cells in the MOG34-56/IFA EAE model

As described before, the core pathogenic role in the common marmoset MOG34-56/IFA EAE model was attributed to the activation of NK-CTL like cells, together with the activation of Th17 cells, but not Th1 cells. This pathogenic mechanism differs markedly from common marmoset EAE models induced with antigen/CFA. To investigate a possible role of Th1 cells in this Th17 mediated common marmoset EAE model, monkeys were treated with recombinant human IFN- γ (rhIFN- γ) around disease initiation (day 0-25) and around the start of disease expression (day 56-81) (**chapter 9**).

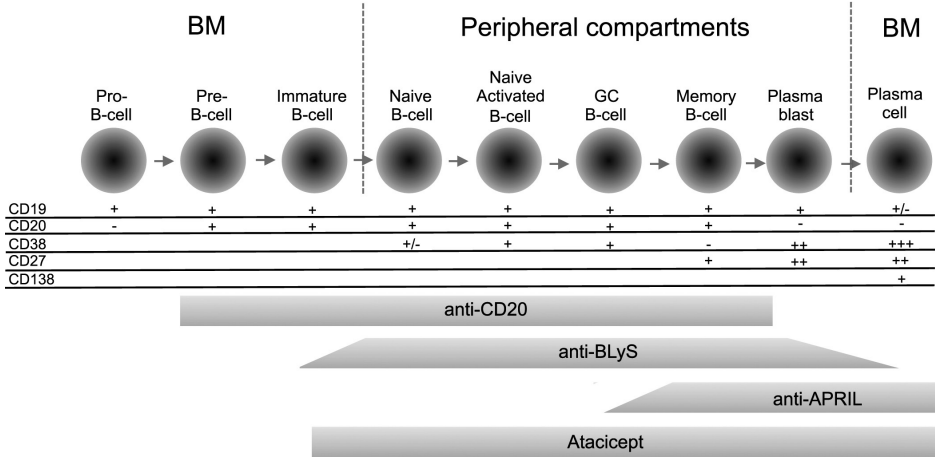


Figure 1. B-cell targeting therapies in the B-cell developmental pathway. B-cell differentiation and maturation is initiated in the bone marrow (BM) from a stem cell into a pro-B-cell and an immature B-cell. Immature B-cells egress the BM to peripheral compartments such as the spleen and lymph nodes. When these cells are activated, they migrate to the germinal center (GC), and differentiate into memory B-cells and antibody producing plasma B-cells. Several B-cell depleting therapies for autoimmune diseases have developed to target specific B-cell subsets. Depleting anti-CD20 therapy affects pre- to memory B-cells; anti-BLyS affects naïve to memory B-cells and a small part of the immature and plasma blasts; anti-APRIL affects mainly memory B-cells and plasma cells; Atacicept affects immature B-cells to plasma cells. Based on^{354, 355}.

The treatment had no effect on the disease course, but altered humoral and cellular autoimmune parameters, e.g. decrease of antibody levels and T-cell proliferation, especially when rhIFN- γ was administered around disease induction. At the level of cytokine production there was no detectable effect of rhIFN- γ .

These data led to the assumption that the effects of IFN- γ in the MOG34-56/IFA EAE model are less prominent compared to the classical CFA induced EAE models in rodents^{333, 279}. It also feeds the speculation that the IL-17A producing effector memory T-cells in this model are not affected by rhIFN- γ , and exert their pathogenic activity mainly in the late phase of the disease. Furthermore, a prominent pathogenic role of Th1 cells in this EAE model seems unlikely.

A 5R CONCEPT FOR THE USAGE OF COMMON MARMOSETS IN BIOMEDICAL RESEARCH

The popularity of the common marmoset in the biomedical research has significantly increased over last decades due to the distinct advantages compared to other non-human primate species. Within the area of autoimmune-mediated inflammatory disorders (AIMID) common marmosets are a relevant model for translational research into pathogenic mechanism and validation of novel immunotherapies, in particular those based on monoclonal antibodies³⁵⁶ that often not crossreact with rodents.

The considerate usage of animal disease models require investments into the welfare of animals in experiments, as stipulated in the 3R (Replacement, Reduction and Refinement) concept of Russell & Burch³⁵⁷. The principles of the 3R are already widely accepted as an ethical basis for animal experimentation. It has been proposed that a fourth R should be added, i.e. for Responsibility. Here we like to introduce an additional R, namely Relevance.

Replacement

The first R is assigned to Replacement. For ethical reasons non-human primates such as the common marmoset should not be used for experimental procedures when the same quality of information can be obtained in lower species (e.g. mice and rats) or the human itself. For this reason a clear explanation is required from the investigators to the ethical committee why the proposed experiments cannot be performed in lower species. Moreover, the proposed protocols are reviewed by independent academics for scientific significance and quality. Currently, humanized mouse models and cell/tissue cultures provide the possibility to study certain pathogenic aspects for some diseases. MS and EAE models represent the end-result of a highly complex network of autoreactive cells and molecules operating in different compartments, including the CNS and secondary lymph nodes. As long as the pathogenic complexity of MS or EAE cannot be modelled in an *in vitro* system, MS research is still dependent on the use of animals.

Reduction

To perform an experiment with the minimal number animals and obtaining meaningful data, power analysis is performed to calculate the group size. For this statistical calculation the power is usually set at $\geq 80\%$. Since the $\geq 80\%$ power is arbitrary, it has been suggested for studies assessing novel concepts to start with smaller sample sizes³²⁷. Recently it has been shown that new clinical studies with small groups can produce more value for the money spent than studies with larger sample sizes³²⁷. In addition, the study value will not increase as rapidly as the sample size, if the study value is assumed to be proportional to the power calculation³⁵⁸. Another way to reduce the number of animals is by genetic typing. For example, the common marmoset has been genotyped for certain study designs, because due to its outbred system individuals can be selected for the presence or resistance of susceptibility alleles within the MHC, e.g. presence of the *Caja-DRB*W1201* molecule for EAE induction. This will give more homogeneous data, translating into smaller group sizes.

Refinement

Another point that warrants attention is reduction of discomfort to the animals, and that maximum information is obtained from each animal with minimal inconvenience. In the common marmoset this is achieved by using non-invasive techniques, such as MRI, telemetry, and urine and faeces sampling for biomarker analysis. There is also the possibility to use micro-methods for small-volume blood sampling (100 μ l) without sedation for immune monitoring³⁵⁹. Another important aspect for refinement is environmental enrichment. It has been shown that habitat enrichment influences the animal in a positive way; reduction of the stress hormone cortisol^{360, 361}, increase of brain cell density, enhancement of memory, improvement of speed and other cognitions. Furthermore, enrichment also has a positive impact on behavior and improves the immune response³⁶².

Responsibility

Recently Ronald Banks introduced a 4th R, because in some cases animal life is still required for biomedical research, e.g. MS research³⁶³. Generally the 4th R covers the other 3Rs, but here the responsibility for scientific correctness, integrity and reasonable use of animals are emphasized. Furthermore, the 4th R highlights that investigators are responsible for social housing of laboratory animals in spacious accommodations that mimics their natural habitat, and that inconveniences such as stress or pain are reduced.

Relevance

The 5th R that we like to introduce is for Relevance. The 3R principles provide guidelines for the reduction of discomfort for animals in experiment. However, they do not address the consideration that when answers for biomedical questions are sought in animals, the conducted experiments should also be highly relevant and translatable to humans. Frequently, in pharmaceutical studies a major challenge is the choice of species for preclinical safety evaluations. Due to the high specificity of e.g. monoclonal antibodies for humans, the use of rodents is often irrelevant and is therefore usually excluded, and in some cases there are no suitable species to select. To respond to such limitations and to obtain relevant information, non-human primates such as the common marmoset or rhesus macaque can be considered. Generally, non-human primates have an equivalent mechanism of therapeutic action, and a comparable binding affinity or avidity to antibodies as humans.

Since our research concentrates on MS it raises in particular the questions 1. which immune process cause the neurological problems and 2. can the immune process be targeted by therapeutic interventions. It is therefore highly important that the chosen animal model approximates the pathological and clinical features of MS as closely as possible. Thus, we propose that the relevance of the animal model to the human disease has to be an essential criterion in the ethical review.

CONCLUDING REMARKS

The research described in this thesis has led to several common marmoset EAE models, which gave more insights into the immunopathogenic mechanism of MS (see also Box 1). In summary, it has been found that the quantitatively minor myelin protein MOG plays a crucial role in the EAE progression, but it is dispensable for disease initiation. Investigating the immunogenicity of MOG in greater detail showed that several B-cell and T-cell epitopes within the extracellular domain of MOG contribute to the disease progression. At the T-cell level the dominant epitopes were mapped to MOG24-36 and MOG34-56, inducing Th1, Th17 and CTL responses. Furthermore, antibodies were generated against MOG24-46, MOG54-76, and rhMOG. Dissection of the immunizing antigen/adjuvant formulations showed that immunization with the single peptide MOG34-56 in CFA or IFA also induced full-blown EAE. However, replacing CFA with IFA resulted in a more Th17 instead of a Th1 mediated disease, and antibodies binding to rhMOG protein, which can mediate demyelination³⁰⁸, were not formed. This strongly suggests a T-cell mediated disease. Since IFA lacks pathogen-associated molecular patterns (PAMPs) we could conclude that our immunization protocol did not deliberately activate innate immune receptors. It is of note, however, that damage-associated molecular patterns (DAMPs) could have been

Box 1. Major conclusions of the experiments described this thesis

- » MOG is the immunodominant antigen of myelin in the common marmosets EAE model.
- » Expression of clinically evident EAE is associated with the activation of MOG34-56 specific T-cells.
- » MOG34-56 reactive T-cells with an effector memory phenotype can be activated *in vivo* by immunization with MOG34-56 in IFA.
- » The cytolytic activity of MOG34-56 induced T-cell is directed against the epitope MOG40-48 presented by Caja-E molecules.
- » B-cells are most likely the preferential APC for the MOG34-56 specific T-cells.
- » Common marmosets immunized with the full-length rhMOG protein in IFA develop clinically evident EAE.
- » Replacement of CFA by IFA in the rhMOG and MOG34-56 induced EAE models has major ethical, conceptual, and mechanistic implications for modelling of MS in the common marmoset.

10

released from the injected skin tissue, although a control experiment in two EAE susceptible mouse strains demonstrated this was an insufficient trigger of EAE (own unpublished data). In addition, using IFA in the inoculum improved the welfare of the animals, since no granulomas were formed at the immunization sites.

By refining the immunization protocol, various common marmoset EAE models were created, which mainly differ in their clinical disease progression, CNS pathology, antibody response to rhMOG, and T-cell profile. In Figure 2 the onset of disease (EAE score at least of 2.0 indicating for blindness and/or ataxia) is compared between all the developed common

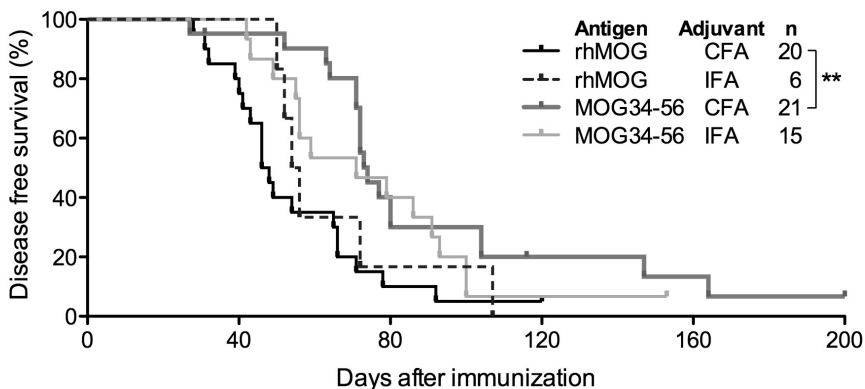


Figure 2. Disease-free survival curves of the common marmoset EAE models. Time to disease onset (EAE score 2.0, blindness and/or ataxia) is compared of four common marmoset EAE models. A significant difference is only observed between the rhMOG/CFA and MOG34-56/CFA immunized animals. The trend is that disease progression of rhMOG/CFA EAE immunized animals is more acute compared to the other models. ** p -value ≤ 0.001 , the Log-rank test was performed as statistical calculation.

marmoset EAE models. The figure shows that the only significant difference was between the rhMOG/CFA and the MOG34-56/CFA EAE model. Moreover, disease progression seems most acute in the rhMOG/CFA immunized monkeys compared to all other EAE models. Comparing the MOG34-56/CFA and MOG34/IFA EAE model, it appeared to be that EAE induced with MOG34-56 in CFA is slightly delayed in the initiation of the disease, but both curves overlapped around day 70 after immunization. This indicates that they have a comparable disease course, although as discussed before, EAE progression in these models is likely based on different mechanisms.

In conclusion, the common marmoset EAE model resembles MS closely and is a valid system for fundamental and applied research, despite the high costs and ethical constraints. However, further research is needed to find the exact immunopathogenic mechanisms, which will improve the understanding and treatment of MS.

FUTURE DIRECTIONS

As stated before the EAE model described in this thesis needs more exploration to translate the key findings to MS. Some central questions for future directions are listed below and summarized in Box 2.

Box 2. Outstanding questions

- » Do MOG34-56 reactive T-cells induce MS-like symptoms?
- » Are the MOG34-56 reactive T-cells found in MS patients related to anti-CMV effector memory T-cells?
- » Is MOG40-48 sufficient to induce EAE in the common marmoset?
- » What are the major differences related to CNS pathology in the distinct common marmoset EAE models?
- » What is the role of herpesviruses in the common marmoset EAE model?
- » How are environmental factors, in particular the gut microbiota, involved in the pathogenesis of EAE in the common marmoset?

Do MOG34-56 reactive T-cells induce MS-like symptoms?

In this thesis we demonstrated that MOG34-56 reactive T-cells play a key role in the pathogenic process, which seems to be mediated by their cytolytic activity. This warrants the question whether these cells are able to directly induce CNS demyelination and clinical symptoms or whether the effect is indirect, e.g. involving the activation of microglia cells. One of the possibilities to assess this is by adoptive transfer. To prevent allograft rejections common marmoset twins can be used. One sibling will be immunized with MOG34-56 in IFA, and MOG34-56 specific T-cell lines will be generated. The T-cell lines will be infused in the other sibling. Since it is not easy to maintain MOG34-56 specific T-cell lines in culture and to scale up into large quantities, T-cells lines can be transformed with Herpesvirus saimiri or Herpesvirus Ateles³⁶⁴⁻³⁶⁶. However, characteristics of the T-cells such as phenotype and cytokine production have to be assessed whether they are the

same as untransformed T-cells. Furthermore, to prove the cytolytic activity of the transformed and untransformed T-cells, next to the EBV transformed B-cells, marmoset oligodendrocyte cultures can be used as target cells, and as a final experiment human oligodendrocytes can be used.

Are the MOG34-56 reactive T-cells found in MS patients related to anti-CMV effector memory T-cells?

Since the MOG34-56 reactive T-cells play a key role in the common marmoset EAE model and that the amino acid sequence of MOG34-56 reacts with an almost identical peptide from the immunodominant UL86 antigen of human CMV, the question remains whether these cells also can be observed in MS patients. In particular, the antigen experienced T-cells that resemble the phenotype of NK-CTLs (CD3+CD4/CD8+CD16-CD27+CD28-CD45RO+CD56+)³⁰⁰, and originate from the CMV effector memory T-cell pool. This can be done by isolating MOG34-56 reactive T-cells from MS patients and expand these cells with certain stimuli as IL-7²⁸⁹ and MOG34-56 peptide. After generating T-cell lines and phenotyping, their reactivity can be tested against the CMV major capsid protein.

Is MOG40-48 sufficient to induce EAE in the common marmoset?

In **chapter 5** it is demonstrated that in the MOG34-56/IFA EAE model, T-cells are directed against a dominant 9-mer MOG peptide within the MOG34-56 sequence, namely MOG40-48. Also cytotoxicity was directed against this 9-mer MOG peptide. Since MOG40-48 shares 90% sequence identity with the major capsid protein UL86 of human CMV, the question that arises is whether it is also possible to induce full-blown EAE in common marmoset monkeys with MOG40-48 in IFA. This immunization protocol will give more insight into the role of CD4+ or CD8+ T-cells in the disease mechanism.

What are the major differences related to CNS pathology of the distinct common marmoset EAE models?

Since we have developed various common marmoset EAE models and all of them showed pathology in the CNS, the challenge is to define the crucial differences between these EAE models. So far, lesions in the white and grey matter are well defined with MRI, but the identity and specificity of the infiltrated cells needs more research. A possibility to characterize these infiltrates is by laser capture microdissection technique. This method provides the opportunity to distinguish the cells at the molecular level, and generating information in detail will give more insights to optimize existing therapies and to develop new ones.

What is the role of herpesviruses in the common marmoset EAE model?

Accumulating evidence suggests that exacerbations in MS are linked to several human herpesviruses such as EBV and HHV-6. To understand their pathogenic role or how they are activated can be extensively investigated in the common marmoset, since these monkeys are naturally infected with related viruses. First, these viruses have to be characterized in detail, which can be done by developing techniques such as quantitative PCR to investigate how the virus-infected cells are distributed in the monkey or in the organs. Furthermore, common marmoset EAE samples can be tested for crossreactivity to the human herpesviruses, and subsequently it can be determined whether there is a correlation between prevalence of virus infection and onset of disease.

REFERENCES



REFERENCES

1. Cho, Y. et al. An Epstein-Barr-related herpesvirus from marmoset lymphomas. *Proc Natl Acad Sci USA* 98, 1224-9 (2001)
2. Noseworthy, J.H. et al. Multiple sclerosis. *N Engl J Med* 343, 938-52 (2000)
3. Kurtzke, J.F. Multiple sclerosis: changing times. *Neuroepidemiology* 10, 1-8 (1991)
4. Compston, A. et al. Multiple sclerosis. *Lancet* 359, 1221-31 (2002)
5. Compston, A. et al. Multiple sclerosis. *Lancet* 372, 1502-17 (2008)
6. Orton, S.M. et al. Sex ratio of multiple sclerosis in Canada: a longitudinal study. *Lancet Neurol* 5, 932-6 (2006)
7. Keegan, B.M. et al. Multiple sclerosis. *Annu Rev Med* 53, 285-302 (2002)
8. Lublin, F.D. et al. Guidelines for clinical trials of new therapeutic agents in multiple sclerosis: relations between study investigators, advisors, and sponsors. National Multiple Sclerosis Society (USA) Advisory Committee on Clinical Trials of New Agents in Multiple Sclerosis. *Neurology* 48, 572-4 (1997)
9. Thompson, A.J. et al. Primary progressive multiple sclerosis. *Brain* 120, 1085-96 (1997)
10. Lublin, F.D. et al. Defining the clinical course of multiple sclerosis: results of an international survey. National multiple sclerosis society (USA) advisory committee on clinical trials of new agents in multiple sclerosis. *Neurology* 46, 907-11 (1996)
11. Ramsaransing, G.S. et al. Benign course in multiple sclerosis: a review. *Acta Neurol Scand* 113, 359-69 (2006)
12. Ebers, G.C. et al. A population-based study of multiple sclerosis in twins. *N Engl J Med* 315, 1638-42 (1986)
13. Dyment, D.A. et al. Genetics of multiple sclerosis. *Lancet Neurol* 3, 104-10 (2004)
14. Sadovnick, A.D. et al. Multiple sclerosis: updated risks for relatives. *Am J Med Genet* 29, 533-41 (1988)
15. Sadovnick, A.D. et al. Parent-child concordance in multiple sclerosis. *Ann Neurol* 29, 252-5 (1991)
16. Oksenberg, J.R. et al. Multiple sclerosis genetics: leaving no stone unturned. *Genes Immun* 6, 375-87 (2005)
17. Barcellos, L.F. et al. Heterogeneity at the HLA-DRB1 locus and risk for multiple sclerosis. *Hum Mol Genet* 15, 2813-24 (2006)
18. Stratmann, T. et al. Susceptible MHC alleles, not background genes, select an autoimmune T cell reactivity. *J Clin Invest* 112, 902-14 (2003)
19. Wucherpfennig, K.W. The structural interactions between T cell receptors and MHC-peptide complexes place physical limits on self-nonsel discrimination. *Curr Top Microbiol Immunol* 296, 19-37 (2005)
20. Ramagopalan, S.V. et al. The inheritance of resistance alleles in multiple sclerosis. *PLoS Genet* 3, 1607-13 (2007)
21. Fogdell-Hahn, A. et al. Multiple sclerosis: a modifying influence of HLA class I genes in an HLA class II associated autoimmune disease. *Tissue Antigens* 55, 140-8 (2000)
22. Harbo, H.F. et al. Genes in the HLA class I region may contribute to the HLA class II-associated genetic susceptibility to multiple sclerosis. *Tissue Antigens* 63, 237-47 (2004)
23. Burfoot, R.K. et al. SNP mapping and candidate gene sequencing in the class I region of the HLA complex: searching for multiple sclerosis susceptibility genes in Tasmanians. *Tissue Antigens* 71, 42-50 (2008)
24. Lu, L. et al. Regulation of CD8+ regulatory T cells: Interruption of the NKG2A-Qa-1 interaction allows robust suppressive activity and resolution of autoimmune disease. *Proc Natl Acad Sci USA* 105, 19420-5 (2008)
25. Hu, D. et al. Analysis of regulatory CD8 T cells in Qa-1-deficient mice. *Nat Immunol* 5, 516-23 (2004)
26. Sarantopoulos, S. et al. Qa-1 restriction of CD8+ suppressor T cells. *J Clin Invest* 114, 1218-21 (2004)
27. Hafler, D.A. et al. Risk alleles for multiple sclerosis identified by a genomewide study. *N Engl J Med* 357, 851-62 (2007)
28. Bahreini, S.A. et al. The role of non-HLA single nucleotide polymorphisms in multiple sclerosis susceptibility. *J Neuroimmunol* 229, 5-15 (2010)
29. Jakkula, E. et al. Genome-wide association study in a high-risk isolate for multiple sclerosis reveals associated variants in STAT3 gene. *Am J Hum Genet* 86, 285-91 (2010)
30. De Jager, P.L. et al. Meta-analysis of genome scans and replication identify CD6, IRF8 and TNFRSF1A as new multiple sclerosis susceptibility loci. *Nat Genet* 41, 776-82 (2009)
31. Zoledziewska, M. et al. Variation within the CLEC16A gene shows consistent disease association with both multiple sclerosis and type 1 diabetes in Sardinia. *Genes Immun* 10, 15-7 (2009)
32. Hoppenbrouwers, I.A. et al. Replication of CD58 and CLEC16A as genome-wide significant risk genes for multiple sclerosis. *J Hum Genet* 54, 676-80 (2009)
33. Sawcer, S. et al. Genetic risk and a primary role for cell-mediated immune mechanisms in multiple sclerosis. *Nature* 476, 214-9 (2011)

34. Kurtzke, J.F. Epidemiologic evidence for multiple sclerosis as an infection. *Clin Microbiol Rev* 6, 382-427 (1993)
35. Munger, K.L. et al. Serum 25-hydroxyvitamin D levels and risk of multiple sclerosis. *JAMA* 296, 2832-8 (2006)
36. Correale, J. et al. Immunomodulatory effects of vitamin D in multiple sclerosis. *Brain* 132, 1146-60 (2009)
37. Goldberg, P. et al. Multiple sclerosis: decreased relapse rate through dietary supplementation with calcium, magnesium and vitamin D. *Med Hypotheses* 21, 193-200 (1986)
38. Riise, T. et al. Smoking is a risk factor for multiple sclerosis. *Neurology* 61, 1122-4 (2003)
39. Hauser, S.L. et al. The neurobiology of multiple sclerosis: genes, inflammation, and neurodegeneration. *Neuron* 52, 61-76 (2006)
40. Levin, L.I. et al. Multiple sclerosis and Epstein-Barr virus. *JAMA* 289, 1533-6 (2003)
41. Lassmann, H. et al. Immunopathology of multiple sclerosis: report on an international meeting held at the Institute of Neurology of the University of Vienna. *J Neuroimmunol* 86, 213-7 (1998)
42. Barnett, M.H. et al. The pathology of multiple sclerosis: a paradigm shift. *Curr Opin Neurol* 19, 242-7 (2006)
43. van der Valk, P. et al. Preactive lesions in multiple sclerosis. *Curr Opin Neurol* 22, 207-13 (2009)
44. van der Valk, P. et al. Staging of multiple sclerosis (MS) lesions: pathology of the time frame of MS. *Neuropathol Appl Neurobiol* 26, 2-10 (2000)
45. Calabrese, M. et al. Cortical lesions in multiple sclerosis. *Nat Rev Neurol* 6, 438-44 (2010)
46. Lucchinetti, C.F. et al. Inflammatory cortical demyelination in early multiple sclerosis. *N Engl J Med* 365, 2188-97 (2011)
47. Kangarlu, A. et al. Cerebral cortical lesions in multiple sclerosis detected by MR imaging at 8 Tesla. *AJNR Am J Neuroradiol* 28, 262-6 (2007)
48. Bo, L. et al. Grey matter pathology in multiple sclerosis. *Acta Neurol Scand Suppl* 183, 48-50 (2006)
49. Geurts, J.J. et al. Grey matter pathology in multiple sclerosis. *Lancet Neurol* 7, 841-51 (2008)
50. Brink, B.P. et al. The pathology of multiple sclerosis is location-dependent: no significant complement activation is detected in purely cortical lesions. *J Neuropathol Exp Neurol* 64, 147-55 (2005)
51. Dalton, C.M. et al. Early development of multiple sclerosis is associated with progressive grey matter atrophy in patients presenting with clinically isolated syndromes. *Brain* 127, 1101-7 (2004)
52. Chard, D.T. et al. Progressive grey matter atrophy in clinically early relapsing-remitting multiple sclerosis. *Mult Scler* 10, 387-91 (2004)
53. Magliozzi, R. et al. Meningeal B-cell follicles in secondary progressive multiple sclerosis associate with early onset of disease and severe cortical pathology. *Brain* 130, 1089-104 (2007)
54. Evangelou, N. et al. Regional axonal loss in the corpus callosum correlates with cerebral white matter lesion volume and distribution in multiple sclerosis. *Brain* 123, 1845-9 (2000)
55. Lucchinetti, C. et al. Heterogeneity of multiple sclerosis lesions: implications for the pathogenesis of demyelination. *Ann Neurol* 47, 707-17 (2000)
56. Lassmann, H. et al. Heterogeneity of multiple sclerosis pathogenesis: implications for diagnosis and therapy. *Trends Mol Med* 7, 115-21 (2001)
57. Furtado, G.C. et al. Swift entry of myelin-specific T lymphocytes into the central nervous system in spontaneous autoimmune encephalomyelitis. *J Immunol* 181, 4648-55 (2008)
58. Reboldi, A. et al. C-C chemokine receptor 6-regulated entry of TH-17 cells into the CNS through the choroid plexus is required for the initiation of EAE. *Nat Immunol* 10, 514-23 (2009)
59. Galea, I. et al. An antigen-specific pathway for CD8 T cells across the blood-brain barrier. *J Exp Med* 204, 2023-30 (2007)
60. Polman, C.H. et al. A randomized, placebo-controlled trial of natalizumab for relapsing multiple sclerosis. *N Engl J Med* 354, 899-910 (2006)
61. Waubant, E. et al. Serum MMP-9 and TIMP-1 levels are related to MRI activity in relapsing multiple sclerosis. *Neurology* 53, 1397-401 (1999)
62. Engberink, R.D. et al. Magnetic resonance imaging of monocytes labeled with ultrasmall superparamagnetic particles of iron oxide using magnetoelectroporation in an animal model of multiple sclerosis. *Mol Imaging* 9, 268-77 (2010)
63. Korn, T. et al. IL-17 and Th17 cells. *Annu Rev Immunol* 27, 485-517 (2009)
64. Hemmer, B. et al. Immunopathogenesis and immunotherapy of multiple sclerosis. *Nat Clin Pract Neurol* 2, 201-11 (2006)
65. Holmøy, T. Immunopathogenesis of multiple sclerosis: concepts and controversies. *Acta Neurol Scand Suppl* 187, 39-45 (2007)
66. Comabella, M. et al. Immunopathogenesis of multiple sclerosis. *Clin Immunol* (2011)

67. Babbe, H. et al. Clonal expansions of CD8(+) T cells dominate the T cell infiltrate in active multiple sclerosis lesions as shown by micromanipulation and single cell polymerase chain reaction. *J Exp Med* 192, 393-404 (2000)
68. Skulina, C. et al. Multiple sclerosis: brain-infiltrating CD8+ T cells persist as clonal expansions in the cerebrospinal fluid and blood. *Proc Natl Acad Sci USA* 101, 2428-33 (2004)
69. Huseby, E.S. et al. A pathogenic role for myelin-specific CD8(+) T cells in a model for multiple sclerosis. *J Exp Med* 194, 669-76 (2001)
70. Barry, M. et al. Cytotoxic T lymphocytes: all roads lead to death. *Nat Rev Immunol* 2, 401-9 (2002)
71. O'Connor, K.C. et al. Antibodies from inflamed central nervous system tissue recognize myelin oligodendrocyte glycoprotein. *J Immunol* 175, 1974-82 (2005)
72. Piddlesden, S.J. et al. The demyelinating potential of antibodies to myelin oligodendrocyte glycoprotein is related to their ability to fix complement. *Am J Pathol* 143, 555-64 (1993)
73. Pouly, S. et al. Multiple sclerosis and central nervous system demyelination. *J Autoimmun* 13, 297-306 (1999)
74. Linington, C. et al. Augmentation of demyelination in rat acute allergic encephalomyelitis by circulating mouse monoclonal antibodies directed against a myelin/oligodendrocyte glycoprotein. *Am J Pathol* 130, 443-54 (1988)
75. Hauser, S.L. et al. B-cell depletion with rituximab in relapsing-remitting multiple sclerosis. *N Engl J Med* 358, 676-88 (2008)
76. Miller, D.M. et al. A meta-analysis of methylprednisolone in recovery from multiple sclerosis exacerbations. *Mult Scler* 6, 267-73 (2000)
77. Sloka, J.S. et al. The mechanism of action of methylprednisolone in the treatment of multiple sclerosis. *Mult Scler* 11, 425-32 (2005)
78. Derwenskus, J. Current disease-modifying treatment of multiple sclerosis. *Mt Sinai J Med* 78, 161-75 (2011)
79. Rudick, R.A. et al. Beta-interferon for multiple sclerosis. *Exp Cell Res* 317, 1301-11 (2011)
80. Floris, S. et al. Interferon-beta directly influences monocyte infiltration into the central nervous system. *J Neuroimmunol* 127, 69-79 (2002)
81. Hartung, H.P. et al. Interferon {beta}-1b-neutralizing antibodies 5 years after clinically isolated syndrome. *Neurology* 77, 835-843 (2011)
82. Johnson, K.P. et al. Copolymer 1 reduces relapse rate and improves disability in relapsing-remitting multiple sclerosis: results of a phase III multicenter, double-blind placebo-controlled trial. The Copolymer 1 Multiple Sclerosis Study Group. *Neurology* 45, 1268-76 (1995)
83. Comi, G. et al. European/Canadian multicenter, double-blind, randomized, placebo-controlled study of the effects of glatiramer acetate on magnetic resonance imaging-measured disease activity and burden in patients with relapsing multiple sclerosis. European/Canadian Glatiramer Acetate Study Group. *Ann Neurol* 49, 290-7 (2001)
84. Ransohoff, R.M. Natalizumab for multiple sclerosis. *N Engl J Med* 356, 2622-9 (2007)
85. Schwab, N. et al. Immunological and clinical consequences of treating a patient with natalizumab. *Mult Scler* (2011)
86. Vogelgesang, A. et al. Mitoxantrone treatment in multiple sclerosis induces TH2-type cytokines. *Acta Neurol Scand* 122, 237-43 (2010)
87. Hasan, S.K. et al. Risk of acute promyelocytic leukemia in multiple sclerosis: coding variants of DNA repair genes. *Neurology* 76, 1059-65 (2011)
88. Horga, A. et al. Fingolimod for relapsing multiple sclerosis: an update. *Expert Opin Pharmacother* 11, 1183-96 (2010)
89. Kappos, L. et al. A placebo-controlled trial of oral fingolimod in relapsing multiple sclerosis. *N Engl J Med* 362, 387-401 (2010)
90. Munoz, J.J. et al. Elicitation of experimental allergic encephalomyelitis (EAE) in mice with the aid of pertussigen. *Cell Immunol* 83, 92-100 (1984)
91. Tsunoda, I. et al. Two models for multiple sclerosis: experimental allergic encephalomyelitis and Theiler's murine encephalomyelitis virus. *J Neuropathol Exp Neurol* 55, 673-86 (1996)
92. Irvine, K.A. et al. Age increases axon loss associated with primary demyelination in cuprizone-induced demyelination in C57BL/6 mice. *J Neuroimmunol* 175, 69-76 (2006)
93. Smith, P.A. et al. Native myelin oligodendrocyte glycoprotein promotes severe chronic neurological disease and demyelination in Biozzi ABH mice. *Eur J Immunol* 35, 1311-9 (2005)
94. Heijmans, N. et al. Encephalitogenic and tolerogenic potential of altered peptide ligands of MOG and PLP in Biozzi ABH mice. *J Neuroimmunol* 167, 23-33 (2005)
95. Slavin, A. et al. Induction of a multiple sclerosis-like disease in mice with an immunodominant epitope of myelin oligodendrocyte glycoprotein. *Autoimmunity* 28, 109-20 (1998)
96. Sasaki, M. et al. Focal experimental autoimmune encephalomyelitis in the Lewis rat induced by immunization with myelin

- oligodendrocyte glycoprotein and intraspinal injection of vascular endothelial growth factor. *Glia* 58, 1523-31 (2010)
97. Stosic-Grujicic, S. et al. Induction of experimental autoimmune encephalomyelitis in Dark Agouti rats without adjuvant. *Clin Exp Immunol* 136, 49-55 (2004)
 98. Kerlero de Rosbo, N. et al. Rhesus monkeys are highly susceptible to experimental autoimmune encephalomyelitis induced by myelin oligodendrocyte glycoprotein: characterisation of immunodominant T- and B-cell epitopes. *J Neuroimmunol* 110, 83-96 (2000)
 99. Kabat, E.A. et al. Studies on acute disseminated encephalomyelitis produced experimentally in rhesus monkeys; disseminated encephalomyelitis produced in monkeys with their own brain tissue. *J Exp Med* 89, 395-8 (1949)
 100. Bajramovic, J.J. et al. Oligodendrocyte-specific protein is encephalitogenic in rhesus macaques and induces specific demyelination of the optic nerve. *Eur J Immunol* 38, 1452-64 (2008)
 101. Shaw, C.M. et al. Chronic remitting-relapsing experimental allergic encephalomyelitis induced in monkeys with homologous myelin basic protein. *Ann Neurol* 24, 738-48 (1988)
 102. Massacesi, L. et al. Experimental allergic encephalomyelitis in cynomolgus monkeys. Quantitation of T cell responses in peripheral blood. *J Clin Invest* 90, 399-404 (1992)
 103. Brok, H.P. et al. Myelin/oligodendrocyte glycoprotein-induced autoimmune encephalomyelitis in common marmosets: the encephalitogenic T cell epitope pMOG24-36 is presented by a monomorphic MHC class II molecule. *J Immunol* 165, 1093-101 (2000)
 104. Mein, L.E. et al. Encephalitogenic potential of myelin basic protein-specific T cells isolated from normal rhesus macaques. *Am J Pathol* 150, 445-53 (1997)
 105. Genain, C.P. et al. In healthy primates, circulating autoreactive T cells mediate autoimmune disease. *J Clin Invest* 94, 1339-45 (1994)
 106. Paterson, P.Y. Transfer of allergic encephalomyelitis in rats by means of lymph node cells. *J Exp Med* 111, 119-36 (1960)
 107. Goverman, J. et al. Transgenic mice that express a myelin basic protein-specific T cell receptor develop spontaneous autoimmunity. *Cell* 72, 551-60 (1993)
 108. Krishnamoorthy, G. et al. Spontaneous optico-spinal encephalomyelitis in a double-transgenic mouse model of autoimmune T cell/B cell cooperation. *J Clin Invest* 116, 2385-92 (2006)
 109. Bettelli, E. et al. Myelin oligodendrocyte glycoprotein-specific T and B cells cooperate to induce a Devic-like disease in mice. *J Clin Invest* 116, 2393-402 (2006)
 110. Waldner, H. et al. Fulminant spontaneous autoimmunity of the central nervous system in mice transgenic for the myelin proteolipid protein-specific T cell receptor. *Proc Natl Acad Sci USA* 97, 3412-7 (2000)
 111. Berer, K. et al. Commensal microbiota and myelin autoantigen cooperate to trigger autoimmune demyelination. *Nature* 479, 538-41 (2011)
 112. Hall, S.M. The effect of injections of lysophosphatidyl choline into white matter of the adult mouse spinal cord. *J Cell Sci* 10, 535-46 (1972)
 113. Suzuki, K. et al. Status spongiosus of CNS and hepatic changes induced by cuprizone (biscyclohexanone oxalylidihydrazone). *Am J Pathol* 54, 307-25 (1969)
 114. Carlton, W.W. Spongiform encephalopathy induced in rats and guinea pigs by cuprizone. *Exp Mol Pathol* 10, 274-87 (1969)
 115. Reynolds, R. et al. Cellular reaction to an acute demyelinating/remyelinating lesion of the rat brain stem: localisation of GD3 ganglioside immunoreactivity. *J Neurosci Res* 36, 405-22 (1993)
 116. Yajima, K. et al. Demyelination and remyelination in the rat central nervous system following ethidium bromide injection. *Lab Invest* 41, 385-92 (1979)
 117. Theiler, M. Spontaneous encephalomyelitis of mice - a new virus disease. *Science* 80, 122 (1934)
 118. Quandt, J.A. et al. Unique clinical and pathological features in HLA-DRB1*0401-restricted MBP111-129-specific humanized TCR transgenic mice. *J Exp Med* 200, 223-34 (2004)
 119. Madsen, L.S. et al. A humanized model for multiple sclerosis using HLA-DR2 and a human T-cell receptor. *Nat Genet* 23, 343-7 (1999)
 120. Vandenberg, A.A. et al. Recombinant TCR ligand induces tolerance to myelin oligodendrocyte glycoprotein 35-55 peptide and reverses clinical and histological signs of chronic experimental autoimmune encephalomyelitis in HLA-DR2 transgenic mice. *J Immunol* 171, 127-33 (2003)
 121. Kawamura, K. et al. HLA-DR2-restricted responses to proteolipid protein 95-116 peptide cause autoimmune encephalitis in transgenic mice. *J Clin Invest* 105, 977-84 (2000)
 122. Rivers, T.M. et al. Observations on Attempts to Produce Acute Disseminated Encephalomyelitis in Monkeys. *J Exp Med* 58, 39-53 (1933)

123. Rivers, T.M. et al. Encephalomyelitis accompanied by myelin destruction experimentally produced in monkeys. *J Exp Med* 61, 689-702 (1935)
124. Rose, L.M. et al. Remitting-relapsing EAE in nonhuman primates: a valid model of multiple sclerosis. *Clin Immunol Immunopathol* 59, 1-15 (1991)
125. Kabat, E.A. et al. Studies on acute disseminated encephalomyelitis produced experimentally in rhesus monkeys. *J Exp Med* 93, 615-33 (1951)
126. Massacesi, L. et al. Active and passively induced experimental autoimmune encephalomyelitis in common marmosets: a new model for multiple sclerosis. *Ann Neurol* 37, 519-30 (1995)
127. 't Hart, B.A. et al. Histopathological characterization of magnetic resonance imaging-detectable brain white matter lesions in a primate model of multiple sclerosis: a correlative study in the experimental autoimmune encephalomyelitis model in common marmosets (*Callithrix jacchus*). *Am J Pathol* 153, 649-63 (1998)
128. 't Hart, B.A. et al. Clinical, pathological, and immunologic aspects of the multiple sclerosis model in common marmosets (*Callithrix jacchus*). *J Neuropathol Exp Neurol* 68, 341-55 (2009)
129. Dubois-Dalcq, M. et al. The cellular and molecular events of central nervous system remyelination. *Bioessays* 12, 569-76 (1990)
130. Amiguet, P. et al. Purification and partial structural and functional characterization of mouse myelin/oligodendrocyte glycoprotein. *J Neurochem* 58, 1676-82 (1992)
131. Scolding, N.J. et al. Myelin/oligodendrocyte glycoprotein (MOG) is a surface marker of oligodendrocyte maturation. *J Neuroimmunol* 22, 169-76 (1989)
132. Clements, C.S. et al. The crystal structure of myelin oligodendrocyte glycoprotein, a key autoantigen in multiple sclerosis. *Proc Natl Acad Sci USA* 100, 11059-64 (2003)
133. Mesleh, M.F. et al. Marmoset fine B cell and T cell epitope specificities mapped onto a homology model of the extracellular domain of human myelin oligodendrocyte glycoprotein. *Neurobiol Dis* 9, 160-72 (2002)
134. Delarasse, C. et al. Complex alternative splicing of the myelin oligodendrocyte glycoprotein gene is unique to human and non-human primates. *J Neurochem* 98, 1707-17 (2006)
135. Schluesener, H.J. et al. A monoclonal antibody against a myelin oligodendrocyte glycoprotein induces relapses and demyelination in central nervous system autoimmune disease. *J Immunol* 139, 4016-21 (1987)
136. Genain, C.P. et al. Antibody facilitation of multiple sclerosis-like lesions in a nonhuman primate. *J Clin Invest* 96, 2966-74 (1995)
137. Van der Aa, A. et al. Functional properties of myelin oligodendrocyte glycoprotein-reactive T cells in multiple sclerosis patients and controls. *J Neuroimmunol* 137, 164-76 (2003)
138. Kerlero de Rosbo, N. et al. Predominance of the autoimmune response to myelin oligodendrocyte glycoprotein (MOG) in multiple sclerosis: reactivity to the extracellular domain of MOG is directed against three main regions. *Eur J Immunol* 27, 3059-69 (1997)
139. Ohler, B. et al. Role of lipid interactions in autoimmune demyelination. *Biochim Biophys Acta* 1688, 10-7 (2004)
140. Kroepfl, J.F. et al. Investigation of myelin/oligodendrocyte glycoprotein membrane topology. *J Neurochem* 67, 2219-22 (1996)
141. Guo, H. et al. Role of tegument proteins in herpesvirus assembly and egress. *Protein Cell* 1, 987-98 (2010)
142. McGeoch, D.J. et al. Molecular phylogeny of the alphaherpesvirinae subfamily and a proposed evolutionary timescale. *J Mol Biol* 238, 9-22 (1994)
143. McGeoch, D.J. et al. Molecular phylogeny and evolutionary timescale for the family of mammalian herpesviruses. *J Mol Biol* 247, 443-58 (1995)
144. Davison, A.J. et al. New genes from old: redeployment of dUTPase by herpesviruses. *J Virol* 79, 12880-92 (2005)
145. McGeoch, D.J. et al. Topics in herpesvirus genomics and evolution. *Virus Res* 117, 90-104 (2006)
146. Davison, A.J. et al. The order Herpesvirales. *Arch Virol* 154, 171-7 (2009)
147. Arvin, A. et al. *Human Herpesviruses: Biology, Therapy, and Immunoprophylaxis* Cambridge University Press, Cambridge (2007)
148. Connolly, S.A. et al. Fusing structure and function: a structural view of the herpesvirus entry machinery. *Nat Rev Microbiol* 9, 369-81 (2011)
149. Martin, R. *International Journal of Primatology* (Chapman and Hall London, Princeton NJ, 1990)
150. Ablashi, D.V. et al. Herpesviruses and cancer in man and subhuman primates. *Biomedicine* 24, 286-305 (1976)
151. Barahona, H. et al. A compendium of herpesviruses isolated from non-human primates. *Intervirology* 3, 175-92 (1974)
152. Ehlers, B. et al. Novel simian homologues of Epstein-Barr virus. *J Virol* 77, 10695-9 (2003)

153. Ramer, J.C. et al. Fatal lymphoproliferative disease associated with a novel gamma-herpesvirus in a captive population of common marmosets. *Comp Med* 50, 59-68 (2000)
154. Rivaille, P. et al. Complete genomic sequence of an Epstein-Barr virus-related herpesvirus naturally infecting a new world primate: a defining point in the evolution of oncogenic lymphocryptoviruses. *J Virol* 76, 12055-68 (2002)
155. Fotheringham, J. et al. Human herpesvirus 6 and multiple sclerosis: potential mechanisms for virus-induced disease. *Herpes* 12, 4-9 (2005)
156. Lünemann, J.D. et al. Cerebrospinal fluid-infiltrating CD4+ T cells recognize *Borrelia burgdorferi* lysine-enriched protein domains and central nervous system autoantigens in early Lyme encephalitis. *Infect Immun* 75, 243-51 (2007)
157. Kanzaki, A. et al. Acute disseminated encephalomyelitis (ADEM) associated with cytomegalovirus infection--a case report. *Rinsho Shinkeigaku* 34, 511-3 (1994)
158. Cohen, P.A. et al. CD4+ T cells in adoptive immunotherapy and the indirect mechanism of tumor rejection. *Crit Rev Immunol* 20, 17-56 (2000)
159. Sumaya, C.V. et al. Epstein-Barr virus antibodies in multiple sclerosis. *Arch Neurol* 37, 94-6 (1980)
160. Levin, L.I. et al. Temporal relationship between elevation of Epstein-Barr virus antibody titers and initial onset of neurological symptoms in multiple sclerosis. *JAMA* 293, 2496-500 (2005)
161. Ascherio, A. et al. Environmental risk factors for multiple sclerosis. Part I: the role of infection. *Ann Neurol* 61, 288-99 (2007)
162. Pohl, D. et al. High seroprevalence of Epstein-Barr virus in children with multiple sclerosis. *Neurology* 67, 2063-5 (2006)
163. Lünemann, J.D. et al. Increased frequency and broadened specificity of latent EBV nuclear antigen-1-specific T cells in multiple sclerosis. *Brain* 129, 1493-506 (2006)
164. Lünemann, J.D. et al. EBNA1-specific T cells from patients with multiple sclerosis cross react with myelin antigens and co-produce IFN- γ and IL-2. *J Exp Med* 205, 1763-73 (2008)
165. Pender, M.P. Infection of autoreactive B lymphocytes with EBV, causing chronic autoimmune diseases. *Trends Immunol* 24, 584-8 (2003)
166. Braun, D.K. et al. Human herpesvirus 6. *Clin Microbiol Rev* 10, 521-67 (1997)
167. Berthold, F. et al. Monoclonal B cell proliferation in lymphoproliferative disease associated with herpes virus type 6 infection. *Anticancer Res* 9, 1511-8 (1989)
168. Dolcetti, R. et al. Human herpesvirus 6 in human immunodeficiency virus-infected individuals: association with early histologic phases of lymphadenopathy syndrome but not with malignant lymphoproliferative disorders. *J Med Virol* 48, 344-53 (1996)
169. Cameron, B. et al. Serological and virological investigation of the role of the herpesviruses EBV, CMV and HHV-6 in post-infective fatigue syndrome. *J Med Virol* 82, 1684-8 (2010)
170. Behzad-Behbahani, A. et al. Human herpesvirus-6 viral load and antibody titer in serum samples of patients with multiple sclerosis. *J Microbiol Immunol Infect* 44, 247-51 (2011)
171. Voumvourakis, K.I. et al. Human herpesvirus 6 infection as a trigger of multiple sclerosis. *Mayo Clin Proc* 85, 1023-30 (2010)
172. Challoner, P.B. et al. Plaque-associated expression of human herpesvirus 6 in multiple sclerosis. *Proc Natl Acad Sci USA* 92, 7440-4 (1995)
173. Cermelli, C. et al. Viruses and multiple sclerosis. *Viral Immunol* 13, 255-67 (2000)
174. Alvarez-Lafuente, R. et al. Relapsing-remitting multiple sclerosis and human herpesvirus 6 active infection. *Arch Neurol* 61, 1523-7 (2004)
175. Alvarez-Lafuente, R. et al. Human herpesvirus-6 and multiple sclerosis: relapsing-remitting versus secondary progressive. *Mult Scler* 13, 578-83 (2007)
176. Cirone, M. et al. Human herpesvirus 6 and multiple sclerosis: a study of T cell cross-reactivity to viral and myelin basic protein antigens. *J Med Virol* 68, 268-72 (2002)
177. Tejada-Simon, M.V. et al. Cross-reactivity with myelin basic protein and human herpesvirus-6 in multiple sclerosis. *Ann Neurol* 53, 189-97 (2003)
178. Staras, S.A. et al. Seroprevalence of cytomegalovirus infection in the United States, 1988-1994. *Clin Infect Dis* 43, 1143-51 (2006)
179. Sekigawa, I. et al. Cytomegalovirus infection in patients with systemic lupus erythematosus. *Clin Exp Rheumatol* 20, 559-64 (2002)
180. Filippi, C. et al. How viral infections affect the autoimmune process leading to type 1 diabetes. *Cell Immunol* 233, 125-32 (2005)
181. Roberts, B.W. et al. Association of type 2 diabetes mellitus and seroprevalence for cytomegalovirus. *South Med J* 98, 686-92 (2005)
182. Yuki, N. et al. Overlapping Guillain-Barré syndrome and Bickerstaff's brainstem encephalitis associated with anti-GQ1b IgG antibody after herpes simplex virus infection. *Acta Neurol Scand* 104, 57-60 (2001)

183. Zaguri, R. et al. Fatal acute disseminated encephalomyelitis associated with cytomegalovirus infection. *BMJ Case Rep* 2009 (2009)
184. Wender, M. Acute disseminated encephalomyelitis (ADEM). *J Neuroimmunol* 231, 92-9 (2011)
185. Devetag, F.C. et al. Cytomegalovirus meningoencephalitis with paroxysmal course in immunocompetent adults: a new nosographical entity. Clinical, diagnostic and therapeutic correlations, and pathogenetic hypothesis. *Eur Neurol* 44, 242-7 (2000)
186. Mowry, E.M. et al. Vitamin D status is associated with relapse rate in pediatric-onset multiple sclerosis. *Ann Neurol* 67, 618-24 (2010)
187. Scotet, E. et al. Frequent enrichment for CD8 T cells reactive against common herpes viruses in chronic inflammatory lesions: towards a reassessment of the physiopathological significance of T cell clonal expansions found in autoimmune inflammatory processes. *Eur J Immunol* 29, 973-85 (1999)
188. Sylwester, A.W. et al. Broadly targeted human cytomegalovirus-specific CD4+ and CD8+ T cells dominate the memory compartments of exposed subjects. *J Exp Med* 202, 673-85 (2005)
189. Brok, H.P. et al. The human CMV-UL86 peptide 981-1003 shares a crossreactive T-cell epitope with the encephalitogenic MOG peptide 34-56, but lacks the capacity to induce EAE in rhesus monkeys. *J Neuroimmunol* 182, 135-52 (2007)
190. Kap, Y.S. et al. Fast progression of recombinant human myelin/oligodendrocyte glycoprotein (MOG)-induced experimental autoimmune encephalomyelitis in marmosets is associated with the activation of MOG34-56-specific cytotoxic T cells. *J Immunol* 180, 1326-37 (2008)
191. Layne, D.G. et al. Husbandry, handling, and nutrition for marmosets. *Comp Med* 53, 351-9 (2003)
192. Haig, D. What is a marmoset? *Am J Primatol* 49, 285-96 (1999)
193. Mansfield, K. Marmoset models commonly used in biomedical research. *Comp Med* 53, 383-92 (2003)
194. Abbott, D.H. et al. Aspects of common marmoset basic biology and life history important for biomedical research. *Comp Med* 53, 339-50 (2003)
195. Cadavid, L.F. et al. Evolutionary instability of the major histocompatibility complex class I loci in New World primates. *Proc Natl Acad Sci USA* 94, 14536-41 (1997)
196. Shiina, T. et al. Comparative genome analysis of the major histocompatibility complex (MHC) class I B/C segments in primates elucidated by genomic sequencing in common marmoset (*Callithrix jacchus*). *Immunogenetics* 63, 485-99 (2011)
197. Watkins, D.I. et al. Genetically distinct cell populations in naturally occurring bone marrow-chimeric primates express similar MHC class I gene products. *J Immunol* 144, 3726-35 (1990)
198. Adams, E.J. et al. Species-specific evolution of MHC class I genes in the higher primates. *Immunol Rev* 183, 41-64 (2001)
199. Klein, J. et al. The molecular descent of the major histocompatibility complex. *Annu Rev Immunol* 11, 269-95 (1993)
200. Antunes, S.G. et al. The common marmoset: a new world primate species with limited MHC class II variability. *Proc Natl Acad Sci USA* 95, 11745-50 (1998)
201. Wu, M.S. et al. MHC (major histocompatibility complex)-DRB genes and polymorphisms in common marmoset. *J Mol Evol* 51, 214-22 (2000)
202. Otting, N. et al. Extensive Mhc-DQB variation in humans and non-human primate species. *Immunogenetics* 54, 230-9 (2002)
203. Middleton, S.A. et al. Identification of New World monkey MHC-DRB alleles using PCR, DGGE and direct sequencing. *Immunogenetics* 55, 785-90 (2004)
204. Prasad, S. et al. MHC Class II DRB genotyping is highly predictive of in-vitro alloreactivity in the common marmoset. *J Immunol Methods* 314, 153-63 (2006)
205. Prasad, S. et al. The common marmoset as a novel preclinical transplant model: identification of new MHC class II DRB alleles and prediction of *in vitro* alloreactivity. *Tissue Antigens* 69 Suppl 1, 72-5 (2007)
206. Doxiadis, G.G. et al. Reactivation by exon shuffling of a conserved HLA-DR3-like pseudogene segment in a New World primate species. *Proc Natl Acad Sci USA* 103, 5864-8 (2006)
207. Wilson, R.K. et al. Structure, organization and polymorphism of murine and human T-cell receptor alpha and beta chain gene families. *Immunol Rev* 101, 149-72 (1988)
208. Uccelli, A. et al. Characterization of the TCRB chain repertoire in the New World monkey *Callithrix jacchus*. *J Immunol* 158, 1201-7 (1997)
209. Matsutani, T. et al. Increased positive selection pressure within the complementarity determining regions of the T-cell receptor beta gene in New World monkeys. *Am J Primatol* 73, 1082-92 (2011)
210. Fujii, Y. et al. Comprehensive analysis and characterization of the TCR alpha chain sequences in the common marmoset. *Immunogenetics* 62, 383-95 (2010)

211. von Büdingen, H.C. et al. Characterization of the expressed immunoglobulin IGHV repertoire in the New World marmoset *Callithrix jacchus*. *Immunogenetics* 53, 557-63 (2001)
212. Schmidt, S. et al. Studies on the immunoglobulin-E system of the common marmoset in comparison with human data. *Life Sci* 59, 719-30 (1996)
213. Ohtani, H. et al. Molecular evolution of immunoglobulin superfamily genes in primates. *Immunogenetics* 63, 417-28 (2011)
214. Averdam, A. et al. Genomics and diversity of the common marmoset monkey NK complex. *J Immunol* 178, 7151-61 (2007)
215. Kap, Y.S. et al. Late B cell depletion with a human anti-human CD20 IgG1kappa monoclonal antibody halts the development of experimental autoimmune encephalomyelitis in marmosets. *J Immunol* 185, 3990-4003 (2010)
216. Brok, H.P. et al. An extensive monoclonal antibody panel for the phenotyping of leukocyte subsets in the common marmoset and the cotton-top tamarin. *Cytometry* 45, 294-303 (2001)
217. Ito, R. et al. Novel monoclonal antibodies recognizing different subsets of lymphocytes from the common marmoset (*Callithrix jacchus*). *Immunol Lett* 121, 116-22 (2008)
218. Kametani, Y. et al. Development of monoclonal antibodies for analyzing immune and hematopoietic systems of common marmoset. *Exp Hematol* 37, 1318-29 (2009)
219. Brady, J.L. et al. Monoclonal antibodies generated by DNA immunization recognize CD2 from a broad range of primates. *Immunol Cell Biol* 87, 413-8 (2009)
220. Kap, Y.S. et al. A monoclonal antibody selection for immunohistochemical examination of lymphoid tissues from non-human primates. *J Histochem Cytochem* 57, 1159-67 (2009)
221. Lyons, A.B. Analysing cell division *in vivo* and *in vitro* using flow cytometric measurement of CFSE dye dilution. *J Immunol Methods* 243, 147-54 (2000)
222. 't Hart, B.A. et al. MRI-guided immunotherapy development for multiple sclerosis in a primate. *Drug Discov Today* 11, 58-66 (2006)
223. 't Hart, B.A. et al. Non-invasive measurement of brain damage in a primate model of multiple sclerosis. *Trends Mol Med* 10, 85-91 (2004)
224. Kap, Y.S. et al. Experimental autoimmune encephalomyelitis in the common marmoset, a bridge between rodent EAE and multiple sclerosis for immunotherapy development. *J Neuroimmune Pharmacol* 5, 220-30 (2010)
225. 't Hart, B.A. et al. The use of animal models to investigate the pathogenesis of neuroinflammatory disorders of the central nervous system. *Current opinion in neurology* 16, 375-83 (2003)
226. 't Hart, B.A. et al. Non-human primate models of experimental autoimmune encephalomyelitis: Variations on a theme. *J Neuroimmunol* 168, 1-12 (2005)
227. Delarasse, C. et al. Myelin/oligodendrocyte glycoprotein-deficient (MOG-deficient) mice reveal lack of immune tolerance to MOG in wild-type mice. *J Clin Invest* 112, 544-53 (2003)
228. 't Hart, B.A. et al. Modelling of multiple sclerosis: lessons learned in a non-human primate. *Lancet Neurol* 3, 588-97 (2004)
229. Brunner, C. et al. Differential ultrastructural localization of myelin basic protein, myelin/oligodendroglial glycoprotein, and 2',3'-cyclic nucleotide 3'-phosphodiesterase in the CNS of adult rats. *J Neurochem* 52, 296-304 (1989)
230. Slavin, A.J. et al. Regulation of myelin oligodendrocyte glycoprotein in different species throughout development. *Dev Neurosci* 19, 69-78 (1997)
231. Scolding, N. et al. Immune mechanisms in the pathogenesis of demyelinating diseases. *Autoimmunity* 4, 131-42 (1989)
232. Iglesias, A. et al. T- and B-cell responses to myelin oligodendrocyte glycoprotein in experimental autoimmune encephalomyelitis and multiple sclerosis. *Glia* 36, 220-34 (2001)
233. Villoslada, P. et al. Frequency, heterogeneity and encephalitogenicity of T cells specific for myelin oligodendrocyte glycoprotein in naive outbred primates. *Eur J Immunol* 31, 2942-50 (2001)
234. Adelman, M. et al. The N-terminal domain of the myelin oligodendrocyte glycoprotein (MOG) induces acute demyelinating experimental autoimmune encephalomyelitis in the Lewis rat. *Journal of neuroimmunology* 63, 17-27 (1995)
235. Lyons, J.A. et al. B cells are critical to induction of experimental allergic encephalomyelitis by protein but not by a short encephalitogenic peptide. *European journal of immunology* 29, 3432-9 (1999)
236. Abdul-Majid, K.B. et al. Screening of several H-2 congenic mouse strains identified H-2(q) mice as highly susceptible to MOG-induced EAE with minimal adjuvant requirement. *J Neuroimmunol* 111, 23-33 (2000)
237. Genain, C.P. et al. Creation of a model for multiple sclerosis in *Callithrix jacchus* marmosets. *J Mol Med* 75, 187-97 (1997)
238. Bradford, M.M. A rapid and sensitive method for the quantitation of microgram quantities of protein utilizing the principle of protein-dye binding. *Anal Biochem* 72, 248-54 (1976)

239. Hughes, L.E. et al. Cross-reactivity between related sequences found in *Acinetobacter* sp., *Pseudomonas aeruginosa*, myelin basic protein and myelin oligodendrocyte glycoprotein in multiple sclerosis. *J Neuroimmunol* 144, 105-15 (2003)
240. 't Hart, B.A. et al. *The Laboratory Primate* (ed. Wolfe-Coote, S.P.) 417-433 (Elsevier Academic Press, London, UK, 2005)
241. Blezer, E.L. et al. Quantitative MRI-pathology correlations of brain white matter lesions developing in a non-human primate model of multiple sclerosis. *NMR Biomed* 20, 90-103 (2007)
242. Laman, J.D. et al. Expression of accessory molecules and cytokines in acute EAE in marmoset monkeys (*Callithrix jacchus*). *J Neuroimmunol* 86, 30-45 (1998)
243. Laman, J.D. et al. Protection of marmoset monkeys against EAE by treatment with a murine antibody blocking CD40 (mu5D12). *Eur J Immunol* 32, 2218-28 (2002)
244. Brok, H.P. et al. Prevention of experimental autoimmune encephalomyelitis in common marmosets using an anti-IL-12p40 monoclonal antibody. *J Immunol* 169, 6554-63 (2002)
245. Morris-Downes, M.M. et al. Pathological and regulatory effects of anti-myelin antibodies in experimental allergic encephalomyelitis in mice. *J Neuroimmunol* 125, 114-24 (2002)
246. de Vos, A.F. et al. Transfer of central nervous system autoantigens and presentation in secondary lymphoid organs. *J Immunol* 169, 5415-23 (2002)
247. Villinger, F. et al. Cloning, sequencing, and homology analysis of nonhuman primate Fas/Fas-ligand and co-stimulatory molecules. *Immunogenetics* 53, 315-28 (2001)
248. Berger, T. et al. Antimyelin antibodies as a predictor of clinically definite multiple sclerosis after a first demyelinating event. *N Engl J Med* 349, 139-45 (2003)
249. Lim, E.T. et al. Anti-myelin antibodies do not allow earlier diagnosis of multiple sclerosis. *Multiple sclerosis* 11, 492-4 (2005)
250. Rauer, S. et al. Antimyelin antibodies and the risk of relapse in patients with a primary demyelinating event. *J Neurol Neurosurg Psychiatry* 77, 739-42 (2006)
251. 't Hart, B.A. et al. Yin-Yang regulation of autoimmunity by DCs. *Trends Immunol* 25, 353-9 (2004)
252. Hawiger, D. et al. Dendritic cells induce peripheral T cell unresponsiveness under steady state conditions *in vivo*. *The Journal of experimental medicine* 194, 769-79 (2001)
253. Geijtenbeek, T.B. et al. Mycobacteria target DC-SIGN to suppress dendritic cell function. *The Journal of experimental medicine* 197, 7-17 (2003)
254. Gavin, A.L. et al. Adjuvant-enhanced antibody responses in the absence of toll-like receptor signaling. *Science* 314, 1936-8 (2006)
255. McFarland, H.I. et al. Determinant spreading associated with demyelination in a nonhuman primate model of multiple sclerosis. *J Immunol* 162, 2384-90 (1999)
256. Gaertner, S. et al. Antibodies against glycosylated native MOG are elevated in patients with multiple sclerosis. *Neurology* 63, 2381-3 (2004)
257. Sospedra, M. et al. Immunology of multiple sclerosis. *Annu Rev Immunol* 23, 683-747 (2005)
258. Sospedra, M. et al. Molecular mimicry in multiple sclerosis. *Autoimmunity* 39, 3-8 (2006)
259. 't Hart, B.A. et al. A new primate model for multiple sclerosis in the common marmoset. *Immunol Today* 21, 290-7 (2000)
260. Pomeroy, I.M. et al. Demyelinated neocortical lesions in marmoset autoimmune encephalomyelitis mimic those in multiple sclerosis. *Brain* 128, 2713-21 (2005)
261. Merkler, D. et al. Differential Macrophage/Microglia Activation in Neocortical EAE Lesions in the Marmoset Monkey. *Brain Pathol* 16, 117-23 (2006)
262. 't Hart, B.A. et al. Broad spectrum immune monitoring in immune-mediated inflammatory disorders. *Drug Discov Today* 10, 1348-1351 (2005)
263. Jagessar, S.A. et al. Autoimmunity against myelin oligodendrocyte glycoprotein is dispensable for the initiation although essential for the progression of chronic encephalomyelitis in common marmosets. *J Neuropathol Exp Neurol* 67, 326-40 (2008)
264. Boon, L. et al. Prevention of experimental autoimmune encephalomyelitis in the common marmoset (*Callithrix jacchus*) using a chimeric antagonist monoclonal antibody against human CD40 is associated with altered B cell responses. *J Immunol* 167, 2942-9 (2001)
265. Brehm, U. et al. Epitope specificity of demyelinating monoclonal autoantibodies directed against the human myelin oligodendrocyte glycoprotein (MOG). *J Neuroimmunol* 97, 9-15 (1999)
266. 't Hart, B.A. et al. Suppression of ongoing disease in a nonhuman primate model of multiple sclerosis by a human-anti-human IL-12p40 antibody. *J Immunol* 175, 4761-8 (2005)
267. Heijmans, N. et al. Antibodies to native myelin oligodendrocyte glycoprotein are critical for severe chronic experimental autoimmune encephalomyelitis and demyelination in mice

- and marmosets. *J Neuroimmunol* 178, 52 (Abstract) (2006)
268. von Büdingen, H.C. et al. Frontline: Epitope recognition on the myelin/oligodendrocyte glycoprotein differentially influences disease phenotype and antibody effector functions in autoimmune demyelination. *Eur J Immunol* 34, 2072-83 (2004)
269. Vergelli, M. et al. A novel population of CD4+CD56+ myelin-reactive T cells lyses target cells expressing CD56/neural cell adhesion molecule. *J Immunol* 157, 679-88 (1996)
270. Antel, J.P. et al. Non-MHC-restricted cell-mediated lysis of human oligodendrocytes *in vitro*: relation with CD56 expression. *J Immunol* 160, 1606-11 (1998)
271. Lopez-Diego, R.S. et al. Novel therapeutic strategies for multiple sclerosis--a multifaceted adversary. *Nat Rev Drug Discov* 7, 909-25 (2008)
272. 't Hart, B.A. et al. Evaluating the validity of animal models for research into therapies for immune-based disorders. *Drug Discov Today* 9, 517-24 (2004)
273. Adams, A.B. et al. Heterologous immunity: an overlooked barrier to tolerance. *Immunol Rev* 196, 147-60 (2003)
274. Koch, S. et al. Cytomegalovirus infection: a driving force in human T cell immunosenescence. *Ann NY Acad Sci* 1114, 23-35 (2007)
275. Feldmann, M. et al. Design of effective immunotherapy for human autoimmunity. *Nature* 435, 612-9 (2005)
276. Darabi, K. et al. The third signal in T cell-mediated autoimmune disease? *J Immunol* 173, 92-9 (2004)
277. Visser, L. et al. Proinflammatory bacterial peptidoglycan as a cofactor for the development of central nervous system autoimmune disease. *J Immunol* 174, 808-16 (2005)
278. Kataoka, T. et al. Concanamycin A, a powerful tool for characterization and estimation of contribution of perforin- and Fas-based lytic pathways in cell-mediated cytotoxicity. *J Immunol* 156, 3678-86 (1996)
279. Billiau, A. et al. Modes of action of Freund's adjuvants in experimental models of autoimmune diseases. *J Leukoc Biol* 70, 849-60 (2001)
280. de Vos, A.F. et al. Severe T-cell depletion from the PALS leads to altered spleen composition in common marmosets with experimental autoimmune encephalomyelitis (EAE). *J Neuroimmunol* 161, 29-39 (2005)
281. von Büdingen, H.C. et al. Immune responses against the myelin/oligodendrocyte glycoprotein in experimental autoimmune demyelination. *J Clin Immunol* 21, 155-70 (2001)
282. Saikali, P. et al. NKG2D-mediated cytotoxicity toward oligodendrocytes suggests a mechanism for tissue injury in multiple sclerosis. *J Neurosci* 27, 1220-8 (2007)
283. Hoftberger, R. et al. Expression of major histocompatibility complex class I molecules on the different cell types in multiple sclerosis lesions. *Brain Pathol* 14, 43-50 (2004)
284. Chapman, K. et al. Preclinical safety testing of monoclonal antibodies: the significance of species relevance. *Nat Rev Drug Discov* 6, 120-6 (2007)
285. Segal, B.M. et al. Repeated subcutaneous injections of IL12/23 p40 neutralising antibody, ustekinumab, in patients with relapsing-remitting multiple sclerosis: a phase II, double-blind, placebo-controlled, randomised, dose-ranging study. *Lancet Neurol* 7, 796-804 (2008)
286. Munz, C. et al. Antiviral immune responses: triggers of or triggered by autoimmunity? *Nat Rev Immunol* 9, 246-58 (2009)
287. 't Hart, B.A. et al. Multiple sclerosis - a response-to-damage model. *Trends Mol Med* 15, 235-44 (2009)
288. Jagessar, S.A. et al. Induction of progressive demyelinating autoimmune encephalomyelitis in common marmoset monkeys using MOG34-56 peptide in incomplete Freund adjuvant. *J Neuropathol Exp Neurol* 69, 372-85 (2010)
289. Bielekova, B. et al. Expansion and functional relevance of high-avidity myelin-specific CD4+ T cells in multiple sclerosis. *J Immunol* 172, 3893-904 (2004)
290. Knapp, L.A. et al. The MHC-E locus is the most well conserved of all known primate class I histocompatibility genes. *J Immunol* 160, 189-96 (1998)
291. de Groot, N.G. et al. The chimpanzee Mhc-DRB region revisited: gene content, polymorphism, pseudogenes, and transcripts. *Mol Immunol* 47, 381-9 (2009)
292. Miller, J.D. et al. Analysis of HLA-E peptide-binding specificity and contact residues in bound peptide required for recognition by CD94/NKG2. *J Immunol* 171, 1369-75 (2003)
293. Nattermann, J. et al. The HLA-A2 restricted T cell epitope HCV core 35-44 stabilizes HLA-E expression and inhibits cytolysis mediated by natural killer cells. *Am J Pathol* 166, 443-53 (2005)
294. Rolleke, U. et al. Differential expression of major histocompatibility complex class I molecules in the brain of a New World monkey, the common marmoset (*Callithrix jacchus*). *J Neuroimmunol* 176, 39-50 (2006)
295. Klein, J. et al. Nomenclature for the major histocompatibility complexes of different

- species: a proposal. *Immunogenetics* 31, 217-9 (1990)
296. Stevens, J. et al. Peptide binding characteristics of the non-classical class Ib MHC molecule HLA-E assessed by a recombinant random peptide approach. *BMC Immunol* 2:5 (2001)
 297. Strong, R.K. et al. HLA-E allelic variants. Correlating differential expression, peptide affinities, crystal structures, and thermal stabilities. *J Biol Chem* 278, 5082-90 (2003)
 298. Schulte, D. et al. The HLA-E(R)/HLA-E(R) genotype affects the natural course of hepatitis C virus (HCV) infection and is associated with HLA-E-restricted recognition of an HCV-derived peptide by interferon-gamma-secreting human CD8(+) T cells. *J Infect Dis* 200, 1397-401 (2009)
 299. Ruijs, T.C. et al. Human oligodendrocytes are susceptible to cytolysis by major histocompatibility complex class I-restricted lymphocytes. *J Neuroimmunol* 27, 89-97 (1990)
 300. Mazarino, P. et al. Identification of effector-memory CMV-specific T lymphocytes that kill CMV-infected target cells in an HLA-E-restricted fashion. *Eur J Immunol* 35, 3240-7 (2005)
 301. Mendel Kerlero de Rosbo, N. et al. Delineation of the minimal encephalitogenic epitope within the immunodominant region of myelin oligodendrocyte glycoprotein: diverse V beta gene usage by T cells recognizing the core epitope encephalitogenic for T cell receptor V beta b and T cell receptor V beta a H-2b mice. *Eur J Immunol* 26, 2470-9 (1996)
 302. Reboldi, A. et al. C-C chemokine receptor 6-regulated entry of TH-17 cells into the CNS through the choroid plexus is required for the initiation of EAE. *Nature immunology* 10, 514-23 (2009)
 303. Gobin, S.J. et al. Upregulation of transcription factors controlling MHC expression in multiple sclerosis lesions. *Glia* 36, 68-77 (2001)
 304. Ulbrecht, M. et al. Cutting edge: the human cytomegalovirus UL40 gene product contains a ligand for HLA-E and prevents NK cell-mediated lysis. *J Immunol* 164, 5019-22 (2000)
 305. Nigida, S.M. et al. Isolation of a cytomegalovirus from salivary glands of white-lipped marmosets (*Saguinus fuscicollis*). *Lab Anim Sci* 29, 53-60 (1979)
 306. Romagnani, C. et al. HLA-E-restricted recognition of human cytomegalovirus by a subset of cytolytic T lymphocytes. *Hum Immunol* 65, 437-45 (2004)
 307. Jagessar, S.A. et al. Unravelling the T-cell-mediated autoimmune attack on CNS myelin in a new primate EAE model induced with MOG(34-56) peptide in incomplete adjuvant. *Eur J Immunol* 42, 217-27 (2012)
 308. Menge, T. et al. Relevant antibody subsets against MOG recognize conformational epitopes exclusively exposed in solid-phase ELISA. *Eur J Immunol* 37, 3229-3239 (2007)
 309. Barun, B. et al. Treatment of multiple sclerosis with Anti-CD20 antibodies. *Clin Immunol* 142, 31-7 (2012)
 310. Teeling, J.L. et al. Characterization of new human CD20 monoclonal antibodies with potent cytolytic activity against non-Hodgkin lymphomas. *Blood* 104, 1793-800 (2004)
 311. Kap, Y.S. et al. B-cell depletion attenuates white and gray matter pathology in marmoset experimental autoimmune encephalomyelitis. *J Neuropathol Exp Neurol* 70, 992-1005 (2011)
 312. Schmierer, K. et al. Quantitative magnetic resonance of postmortem multiple sclerosis brain before and after fixation. *Magn Reson Med* 59, 268-77 (2008)
 313. Nam, K. et al. Peripheral blood extrathymic CD4(+)CD8(+) T cells with high cytotoxic activity are from the same lineage as CD4(+)CD8(-) T cells in cynomolgus monkeys. *Int Immunol* 12, 1095-103 (2000)
 314. Kiyotaki, M. et al. Herpesvirus atele immortalizes *in vitro* a CD3+CD4+CD8+ marmoset lymphocyte with NK function. *J Immunol* 140, 730-6 (1988)
 315. Serafini, B. et al. Dysregulated Epstein-Barr virus infection in the multiple sclerosis brain. *J Exp Med* 204, 2899-912 (2007)
 316. Lassmann, H. et al. Epstein-Barr virus in the multiple sclerosis brain: a controversial issue-report on a focused workshop held in the Centre for Brain Research of the Medical University of Vienna, Austria. *Brain* 134, 2772-86 (2011)
 317. Bielekova, B. et al. Preferential expansion of autoreactive T lymphocytes from the memory T-cell pool by IL-7. *J Neuroimmunol* 100, 115-23 (1999)
 318. Pender, M.P. The essential role of Epstein-Barr virus in the pathogenesis of multiple sclerosis. *Neuroscientist* 17, 351-67 (2011)
 319. Jiang, W. et al. Presentation of Soluble Antigens to CD8+ T Cells by CpG Oligodeoxynucleotide-Primed Human Naive B Cells. *J Immunol* 186, 2080-6 (2011)
 320. Lünemann, J.D. et al. EBV in MS: guilty by association? *Trends Immunol* 30, 243-8 (2009)
 321. Lassmann, H. et al. The immunopathology of multiple sclerosis: an overview. *Brain Pathol* 17, 210-8 (2007)
 322. Laws, P.M. et al. Ustekinumab for the treatment of psoriasis. *Expert Rev Clin Immunol* 7, 155-64 (2011)

323. Pers, J.O. et al. B-cell depletion and repopulation in autoimmune diseases. *Clin Rev Allergy Immunol* 34, 50-5 (2008)
324. Carson, K.R. et al. Monoclonal antibody-associated progressive multifocal leukoencephalopathy in patients treated with rituximab, natalizumab, and efalizumab: a Review from the Research on Adverse Drug Events and Reports (RADAR) Project. *Lancet Oncol* 10, 816-24 (2009)
325. Daridon, C. et al. BAFF, APRIL, TWE-PRIL: who's who? *Autoimmun Rev* 7, 267-71 (2008)
326. 't Hart, B.A. et al. EAE: imperfect but useful models of multiple sclerosis. *Trends Mol Med* 17, 119-25 (2011)
327. Bacchetti, P. et al. Breaking free of sample size dogma to perform innovative translational research. *Sci Transl Med* 3, 87ps24 (2011)
328. Jagessar, S.A. et al. Discrepant Effects of Human Interferon-gamma on Clinical and Immunological Disease Parameters in a Novel Marmoset Model for Multiple Sclerosis. *J Neuroimmune Pharmacol* 7, 253-65 (2012)
329. Moisini, I. et al. BAFF: a local and systemic target in autoimmune diseases. *Clin Exp Immunol* 158, 155-63 (2009)
330. Miller, J.P. et al. Space, selection, and surveillance: setting boundaries with BLYS. *J Immunol* 176, 6405-10 (2006)
331. Zhang, L. et al. Identification of BLYS (B lymphocyte stimulator), a non-myelin-associated protein, as a functional ligand for Nogo-66 receptor. *J Neurosci* 29, 6348-52 (2009)
332. 't Hart, B.A. et al. Treatment with chimeric anti-human CD40 antibody suppresses MRI-detectable inflammation and enlargement of pre-existing brain lesions in common marmosets affected by MOG-induced EAE. *J Neuroimmunol* 163, 31-9 (2005)
333. Willenborg, D.O. et al. IFN- γ is critical to the control of murine autoimmune encephalomyelitis and regulates both in the periphery and in the target tissue: a possible role for nitric oxide. *J Immunol* 163, 5278-86 (1999)
334. Gran, B. et al. Early administration of IL-12 suppresses EAE through induction of interferon-gamma. *J Neuroimmunol* 156, 123-31 (2004)
335. Sanvito, L. et al. The multifaceted role of interferon-g in central nervous system autoimmune demyelination. *The Open Autoimmunity Journal* 2, 151-159 (2010)
336. Constantinescu, C.S. et al. IL-12 reverses the suppressive effect of the CD40 ligand blockade on experimental autoimmune encephalomyelitis (EAE). *J Neurol Sci* 171, 60-4 (1999)
337. Mauritz, N.J. et al. Treatment with gamma-interferon triggers the onset of collagen arthritis in mice. *Arthritis Rheum* 31, 1297-304 (1988)
338. Brok, H.P. et al. Interferon-gamma prevents graft-versus-host disease after allogeneic bone marrow transplantation in mice. *J Immunol* 151, 6451-9 (1993)
339. Panitch, H.S. et al. Exacerbations of multiple sclerosis in patients treated with gamma interferon. *Lancet* 1, 893-5 (1987)
340. Cahlin, C. et al. Experimental cancer cachexia: the role of host-derived cytokines interleukin (IL)-6, IL-12, interferon-gamma, and tumor necrosis factor alpha evaluated in gene knockout, tumor-bearing mice on C57 Bl background and eicosanoid-dependent cachexia. *Cancer Res* 60, 5488-93 (2000)
341. Axtell, R.C. et al. T helper type 1 and 17 cells determine efficacy of interferon-beta in multiple sclerosis and experimental encephalomyelitis. *Nat Med* 16, 406-12 (2010)
342. Mancardi, G. et al. Demyelination and axonal damage in a non-human primate model of multiple sclerosis. *J Neurol Sci* 184, 41-9 (2001)
343. Genain, C.P. et al. Identification of autoantibodies associated with myelin damage in multiple sclerosis. *Nat Med* 5, 170-5 (1999)
344. Kap, Y.S. et al. Effects of early IL-17A neutralization on disease induction in a primate model of experimental autoimmune encephalomyelitis. *J Neuroimmune Pharmacol* 6, 341-53 (2011)
345. Moretta, L. et al. NK-CTLs, a novel HLA-E-restricted T-cell subset. *Trends Immunol* 24, 136-43 (2003)
346. Kaiser, B.K. et al. Structural basis for NKG2A/CD94 recognition of HLA-E. *Proc Natl Acad Sci USA* 105, 6696-701 (2008)
347. Weber, M.S. et al. B-cell activation influences T-cell polarization and outcome of anti-CD20 B-cell depletion in central nervous system autoimmunity. *Ann Neurol* 68, 369-83 (2010)
348. Lehmann-Horn, K. et al. Anti-CD20 B-cell depletion enhances monocyte reactivity in neuroimmunological disorders. *J Neuroinflammation* 8, 146-54 (2011)
349. Major, E.O. Progressive multifocal leukoencephalopathy in patients on immunomodulatory therapies. *Ann Rev Med* 61, 35-47 (2010)
350. Kalled, S.L. The role of BAFF in immune function and implications for autoimmunity. *Immunol Rev* 204, 43-54 (2005)

351. Munafo, A. et al. Safety, pharmacokinetics and pharmacodynamics of atacept in healthy volunteers. *Eur J Clin Pharmacol* 63, 647-56 (2007)
352. Nestorov, I. et al. Pharmacokinetics and biological activity of atacept in patients with rheumatoid arthritis. *J Clin Pharmacol* 48, 406-17 (2008)
353. Hartung, H.P. et al. Atacept: targeting B cells in multiple sclerosis. *Ther Adv Neurol Disord* 3, 205-16 (2010)
354. Cancro, M.P. et al. The role of B lymphocyte stimulator (BLyS) in systemic lupus erythematosus. *J Clin Invest* 119, 1066-73 (2009)
355. Edwards, J.C. et al. B-cell targeting in rheumatoid arthritis and other autoimmune diseases. *Nat Rev Immunol* 6, 394-403 (2006)
356. Chapman, K. et al. Preclinical development of monoclonal antibodies: considerations for the use of non-human primates. *mAbs* 1, 505-16 (2009)
357. Balls, M. et al. The three Rs of Russell & Burch and the testing of biological products. *Developments in biological standardization* 86, 11-8 (1996)
358. Bacchetti, P. et al. Ethics and sample size. *Am J Epidemiol* 161, 105-10 (2005)
359. Vitale, A. et al. Refinement techniques in experimental protocols involving Callitrichids. *Ann Ist Super Sanita* 40, 237-40 (2004)
360. Schapiro, S.J. et al. A comparison of cell-mediated immune responses in rhesus macaques housed singly, in pairs, or in groups. *Appl Anim Behav Sci* 68, 67-84 (2000)
361. Vitale, A. et al. Environmental enrichment techniques in non-human primates. The case of Callitrichids. *Ann Ist Super Sanita* 40, 181-6 (2004)
362. Buchanan-Smith, H.M. Environmental enrichment for primates in laboratories. *Adv Sci Res* 5, 41-56 (2010)
363. Banks, R.E. The 4th R of research. *Contemp Top Lab Anim Sci* 34, 50-1 (1995)
364. Albrecht, J.C. et al. Herpesvirus ateles Tio can replace herpesvirus saimiri StpC and Tip oncoproteins in growth transformation of monkey and human T cells. *J Virol* 78, 9814-9 (2004)
365. Meinel, E. et al. Growth transformation of antigen-specific T cell lines from rhesus monkeys by herpesvirus saimiri. *Virology* 229, 175-82 (1997)
366. Fickenscher, H. et al. Herpesvirus saimiri. *Philosophical transactions of the Royal Society of London. Series B, Biological Sciences* 356, 545-67 (2001)

**ENGLISH SUMMARY
NEDERLANDSE SAMENVATTING**

12

SUMMARY

Multiple sclerosis (MS) is a neurological disease characterized by inflammation and demyelination of the white and grey matter of the central nervous system (CNS). The cause and the exact immunopathogenic mechanisms underlying MS are still unknown and therapies without adverse effects are not available. To unravel the immunopathogenic mechanisms and to develop novel therapeutics, the common marmoset is used as a relevant animal model with a close genetic and immunological proximity to humans. The animal model for MS, experimental autoimmune encephalomyelitis (EAE), resembles the clinical and pathological features of the disease.

At the start of the study, which is described in this thesis, little was known about the critical immunological pathways in the common marmoset EAE model. The then available common marmoset EAE model, namely active induction with recombinant human myelin oligodendrocyte glycoprotein (rhMOG) or myelin basic protein (MBP) in complete Freund's adjuvant (CFA) supported with intravenous *Bordetella* particles, gave an acute disease which resembled another immune mediated disease of the brain, acute disseminated encephalomyelitis (ADEM). The characteristic clinical presentation of MS such as a chronic progressive disease course was not observed.

The main objective of the research described in this thesis was to model the clinical and immunological features of MS in the common marmoset, while minimizing artificial requirements that cause discomfort to the animals but are not strictly needed for disease induction. In parallel we assessed the function of autoreactive T-cells and B-cells during disease progression, and examined new targets for MS therapy using novel immunotherapeutics for elucidating mechanistic pathways.

Previous studies in MS patients and animal models indicated that myelin proteins have a central role in the immunopathogenic mechanisms. In **chapter 2** we investigated the pathogenic significance of MOG, a quantitatively minor protein of CNS myelin exposed on the surface of the myelin sheath. We demonstrated that marmoset monkeys immunized with myelin derived from wild type C57BL/6 mice developed EAE symptoms, while common marmosets immunized with myelin from MOG-deficient C57BL/6 mice developed only mild clinical symptoms and mild CNS pathology. These results led to the conclusion that MOG is dispensable for EAE induction, but plays a crucial role in disease progression.

To examine the pathogenic role of MOG, we report in **chapter 3** that common marmosets were immunized with rhMOG in CFA. This leads to a 100% disease incidence with a heterogeneous disease course. An extended analysis revealed that fast disease progression was associated with a broader range of T-cell reactivity with a panel of 23-mer MOG peptides, in particular to MOG34-56 and the overlapping MOG peptides 64-86 and 74-96. Immunization with MOG34-56 in CFA led to a chronic disease, which was characterized by CNS inflammation and demyelination. MOG34-56 autoreactive T-cells in the MOG34-56/CFA EAE model were identified as critical encephalitogenic cells. The phenotype and cytolytic activity of these T-cells were compatible with natural killer–cytotoxic T-lymphocytes (NK-CTL). Immunization with MOG74-96 in CFA did not lead to clinical symptoms, but a single booster with MOG34-56 in IFA induced neurological deficit and CNS pathology within a few weeks. From these results we hypothesized that MOG34-56 in IFA might be sufficient for EAE induction.

We indeed demonstrate in **chapter 4** that MOG34-56 in IFA immunization induced chronic EAE in the common marmosets, and that disease features such as CNS pathology and activation of autoreactive T-cells were comparable with the rhMOG/CFA and MOG34-56/CFA models. Interestingly, IgG antibody formation in the MOG34-56/IFA model was only directed to the MOG peptides 24-46 and 34-56, but not to rhMOG. This led to the interpretation that the disease is most likely caused by the MOG34-56 autoreactive T-cells, and that disease developed in the absence of microbial immune receptor antigens in the inoculum. Moreover, replacement of CFA by IFA was a major refinement for the animal itself, because granuloma formation at the injection sites was not observed. It was also a mechanistical refinement of the animal model since cytokine production against Mycobacteria in CFA was disrupted.

In **chapter 5** we used several immunological assays to unravel the mechanism and nature of the anti-MOG34-56 autoreactive T-cells. Proliferation assays disclosed that the main T-cell proliferation was located in the secondary lymph nodes. These cells were phenotyped as CD3+CD4+CD56+ and CD3+CD4+C8+CD56+, co-expressing CD45RO and CD27 but not CD28 and CCR7. Functional characterization revealed that these T-cells produced high Th17 related cytokines such as IL-17A along with specific cytotoxic activity. In the cytolytic assay T-cells recognized a 9-mer MOG peptide within the MOG34-56 sequence, namely MOG40-48. The MOG40-48 peptide was presented by the MHC class I molecule Caja-E, which is the equivalent of HLA-E in human. All these immunological features supported the characterizations of the T-cells as NK-CTL.

In a final experiment of the refinement process of the common marmoset EAE model, reported in **chapter 6**, animals were immunized with rhMOG in IFA. All immunized common marmosets developed clinical EAE with grey and white matter lesions in the brain. IgG antibodies were formed against rhMOG and the MOG peptides 14-36, 24-46, 54-76, but not to 34-56. Further analyses of the immunological parameters will demonstrate whether this model is comparable with the other common marmoset EAE models or whether it can be used as a valid pre-clinical model for therapeutics aiming at B-cells and/or T-cells.

In **chapter 7** we examined how B-cells contribute to the disease development in the MOG34-56/IFA model. One sibling of five marmoset twins was treated with the B-cell depleting anti-human CD20 HuMab7D8 antibody. The treatment resulted in 100% depletion of mature B-cells in secondary lymphoid organs and blood, and suppression of clinical and pathological EAE symptoms. This led to the hypothesis that B-cells are associated with the activation of pathogenic autoreactive T-cells.

Recently anti-CD20 antibody trials proved to be effective in MS patients. However, it appeared that long-lasting depletion of B-cells in humans with other autoimmune diseases is linked with serious side effects such as cause of another neurological disease, namely progressive multifocal leukoencephalopathy. Therefore, we used in **chapter 8** an alternative approach for B-cell depletion, namely antibodies against B Lymphocyte Stimulator (BLyS) and A Proliferation-Inducing Ligand (APRIL) to block B-cell survival molecules. Treatment with anti-BLyS and anti-APRIL in the rhMOG/CFA model significantly delayed onset of the disease, and reduced pathology in the spinal cord. Immunological analysis showed that anti-BLyS reduced antibody levels against rhMOG and MOG peptides, along with a reduced production of Th1 and Th17 related cytokines, IFN- γ and IL-17A, respectively. This was not the case with the anti-APRIL treatment. Anti-APRIL reduced mRNA transcripts levels of Th1 and Th17 related

cytokines, but it increased IL-10 mRNA, suggesting that anti-APRIL adjusted the T-cell profile from a pro- to an anti-inflammatory response.

We already indicated that the core pathogenic process in the MOG34-56/IFA model in the common marmoset is attributed to the activation of NK-CTL like cells together with activation of Th17 cells. In **chapter 9** we elucidate a possible role of Th1 cells in this Th17 mediated disease by treating MOG34-56/IFA immunized monkeys in a prophylactic and therapeutic fashion with recombinant human IFN- γ . Treatment had no influence on clinical symptoms, but it altered humoral and cellular autoimmune parameters. These data feed the speculation that IL-17A producing effector T-cells are not affected and that a pathogenic role of Th1 cells seems unlikely in the MOG34-56/IFA model.

Finally, in **chapter 10** we discuss our main findings and their contribution to understand the immunopathogenic mechanisms underlying EAE activity in the common marmoset. In conclusion, the common marmoset EAE model has been further refined in a way that it resembles MS more closely, and that the model can be used as a valid model for fundamental and applied research. Nevertheless, more research is needed to unravel the exact immunopathogenic mechanisms to improve therapies for MS.

SAMENVATTING

Multiple sclerose (MS) is een neurologische aandoening die zich kenmerkt door onder andere slecht zien, coördinatieverlies en verlammingen van ledematen. Deze symptomen worden hoogst waarschijnlijk veroorzaakt door ontstekingen en demyelinisatie van de witte en grijze stof in de hersenen en het ruggenmerg. Men denkt dat MS een autoimmuunziekte is, waarbij het immuunsysteem reageert op het eigen lichaam, in dit geval tegen componenten van de myelineschede rondom de zenuwcellen. Om de oorzaak en het verloop van MS in detail te bestuderen, wordt de ziekte in diermodellen nagebootst, ook wel experimentele autoimmuun encefalomyelitis (EAE) genoemd. Vaak gebeurt dit in knaagdieren. Echter, voor dit onderzoek is de common marmoset, ofwel de penseelaap, gebruikt. De penseelaap is een niet-humane primate en lijkt immunologisch en genetisch gezien veel op de mens. Bovendien komen het ziekteverloop en andere karakteristieke symptomen van EAE bij de penseelaap sterk overeen met MS, en maakt het model geschikt voor validatie van nieuwe therapieën.

Aan het begin van in dit proefschrift beschreven onderzoek was er weinig bekend over de kritische immunologische factoren in het EAE model in de penseelaap. De toen beschikbare EAE modellen in de penseelaap, namelijk actieve inductie met recombinant humaan myeline oligodendrocyet glycoproteïne (rhMOG) of myeline basaal eiwit (MBP) gemengd met compleet Freund's adjuvant (CFA), met wel of zonder toediening van *Bordetella* bacterie deeltjes, gaf een acute reactie die nauwelijks vergelijkbaar was met MS.

Het belangrijkste doel van dit proefschrift was om de klinische en immunologische kenmerken van MS in de penseelaap na te bootsen door kunstmatige benodigdheden te minimaliseren, zoals mycobacteriën die verantwoordelijk zijn voor ernstige ongemakken voor het dier. Tegelijkertijd is de rol van witte bloedcellen, namelijk van autoreactieve T- en B-cellen onderzocht tijdens de ziekte, en werden nieuwe therapieën voor MS bestudeerd om meer inzicht te verkrijgen in de mechanistische routes.

Uit eerdere studies in MS patiënten en diermodellen is gebleken dat myeline eiwitten een centrale rol spelen in het ziekteproces. In **hoofdstuk 2** hebben we het vermogen om ziekte te induceren van een enkel myeline eiwit, namelijk MOG onderzocht. Het interessante van MOG is dat het maar een klein deel uitmaakt van de myeline samenstelling en dat het tot expressie komt aan het oppervlak van de myelineschede. Penseelapen geïmmuniseerd met myeline afkomstig van wild-type C57BL/6 muizen ontwikkelden EAE symptomen, terwijl penseelapen die met myeline van MOG-deficiënte C57BL/6 muizen werden ingespoten slechts milde klinische symptomen en milde hersen- en ruggenmergschade ontwikkelden. Deze resultaten leidden tot de conclusie dat MOG overbodig is voor ziekte-inductie, maar een cruciale rol speelt in het verdere beloop van de ziekte.

Om de pathogene rol van MOG in meer detail te besturen, zijn in **hoofdstuk 3** penseelapen met recombinant humaan MOG in CFA geïmmuniseerd. Dit resulteerde in 100% ziekte-incidentie met een heterogeen ziekteverloop. De heterogeniteit kon toegeschreven worden aan het feit dat elk dier genetisch verschillend is, net als de mens. Dieren die relatief snel ziekte ontwikkelden toonden een brede T-cel reactie gericht tegen epitopen van MOG, met name tegen 34-56 en de overlappende peptiden 64-86 en 74-96. Immunisatie met MOG34-56 in CFA leidde tot een chronisch ziektebeeld dat zich kenmerkte door ontstekingen en demyelinisatie. Bovendien werden activatie van MOG34-56 autoreactieve T-cellen gezien als de boosdoeners

in dit model. Deze MOG34-56 autoreactieve T-cellen konden op basis van hun fenotype en cytotoxiciteit toegewezen worden als mogelijke natural killer – cytotoxische T-cellen (NK-CTL).

In tegenstelling tot MOG34-56 in CFA immunisatie, bleven ziekteverschijnselen in penseelapen geïmmuniseerd met MOG74-96 in CFA uit. Echter, een enkele booster-immunisatie met MOG34-56 in incomplete Freund's adjuvant (IFA) leidde tot neurologische symptomen binnen een paar weken. Op basis van deze resultaten veronderstelden wij dat immunisatie met MOG34-56 in IFA voldoende zou moeten zijn voor ziekte-inductie. IFA bevat alleen minerale olie en geen mycobacteriën en onderscheidt zich hiermee van CFA.

In **hoofdstuk 4** hebben we aangetoond dat immunisatie met MOG34-56 in IFA daadwerkelijk leidde tot chronische EAE in de geïmmuniseerde dieren. Daarnaast was de pathologie en activatie van de autoreactieve T-cellen vergelijkbaar met de rhMOG in CFA en MOG34-56 in CFA EAE modellen. Interessant genoeg werd in de MOG34 in IFA model alleen antilichamen gevormd tegen de MOG epitopen 24-46 en 34-56, maar niet tegen rhMOG. Hieruit concludeerden wij dat de ziekteactiviteit door MOG34-56 autoreactieve T-cellen wordt veroorzaakt. Bovendien is dit model zonder CFA een belangrijke verfijning voor zowel het dier, door het ontbreken van granulomavorming op de injectieplaatsen, als op conceptueel gebied.

In **hoofdstuk 5** hebben we gebruik gemaakt van verschillende immunologische testen om het mechanisme en de aard van de MOG34-56 autoreactieve T-cellen te ontrafelen. Hier kwam uit voort dat de meeste delende T-cellen zich in de secundaire lymfeklieren bevinden, zoals de milt, en niet in het bloed. Deze cellen maakten veel van de cytokine IL-17A aan en werden gekarakteriseerd door specifieke cytotoxische capaciteit. In de cytotoxiciteit proeven bleek dat deze T-cellen een peptide van 9 aminozuren lang herkennen binnen de MOG34-56 sequentie, te weten MOG40-48. Het MOG40-48 peptide werd gepresenteerd door het MHC klasse I molecuul Cja-E, dat equivalent is aan HLA-E in de mens. Al deze eigenschappen duiden erop dat deze MOG34-56 autoreactieve T-cellen NK-CTL-achtige zijn.

In een laatste experiment van het verfijningsproces van het EAE model in de penseelaap, zijn in **hoofdstuk 6** de dieren met rhMOG in IFA geïmmuniseerd. Alle dieren ontwikkelden klinische verschijnselen, grijze en witte stof laesies in de hersenen, en antilichamen tegen rhMOG en de MOG peptiden 14-36, 24-46, 54-76, maar niet tegen 34-56. Aangezien de immunologische analyse op het moment van schrijven incompleet was, kan nog niet worden vastgesteld in welke mate het model vergelijkbaar is met de andere EAE modellen in de penseelaap, en of het gebruikt kan worden als een preklinisch model voor therapieën die gericht zijn tegen B- en/of T-cellen.

In **hoofdstuk 7** hebben we onderzocht in welke opzichten B-cellen bijdragen aan de ziekte in het T-cel gemedieerde MOG34-56 in IFA model. Hier werd één helft van vijf tweelingen behandeld met een anti-CD20 antistof dat B-cellen verwijdert, en de ander helft werd behandeld met fysiologisch zout. De anti-CD20 behandeling resulteerde in 100% verwijdering van B-cellen uit bloed en de milt, en onderdrukking van klinische en pathologische EAE symptomen. Dit leidde tot de veronderstelling dat B-cellen direct betrokken zijn bij de activatie van de pathogene autoreactieve T-cellen.

Onlangs hebben anti-CD20 studies bewezen effectief te zijn in MS patiënten, maar het bleek dat langdurige verwijdering van de B-cellen in andere autoimmuunziekten kan leiden tot ernstige bijwerkingen, zoals het ontwikkelen van meerdere laesies in de hersenen. In **hoofdstuk 8** hebben we daarom gekozen voor een alternatieve benadering van B-cel verwijdering, te

weten met antistoffen tegen B-Lymfocyten Stimulator (BLyS) en Een Proliferatie-Inducerende Ligand (APRIL). Deze twee antistoffen zijn in staat moleculen te inactiveren die betrokken zijn bij B-cel overleving. Behandeling met anti-BLyS en anti-APRIL hebben het begin van de ziekte aanzienlijk vertraagd en hadden ook een positief effect op de pathologie in het ruggenmerg. Immunologische parameters gaven aan dat antistoffen tegen rhMOG en MOG peptiden gereduceerd waren, en er was een verminderde activiteit van Th1 (IFN- γ) en Th17 (IL-17A) gerelateerde cytokinen na de anti-BLyS behandeling. De anti-APRIL behandeling leidde tot een afname van de mRNA transcripten van Th1 en Th17 gerelateerde cytokinen, en tot een verhoogd mRNA transcript niveau van de regulerende cytokine IL-10. Deze waarnemingen suggereren dat het T-cel activiteitsprofiel door de behandeling met anti-APRIL is verschoven van een pro-naar een anti-ontstekingsreactie.

Zoals eerder is aangegeven, wordt de kern van de ziekte in de MOG34-56 in IFA model toegewezen aan de activatie van NK-CTL en Th17 cellen. In **hoofdstuk 9** hebben we een mogelijke rol van Th1 cellen onderzocht in het Th17 gemedieerde ziektemodel. Penseelapen die met MOG34-56 in IFA waren geïmmuniseerd, hebben een profylactische en therapeutische behandeling ondergaan met recombinant humaan IFN- γ . Hieruit bleek dat de behandeling geen positief effect had op de klinische symptomen, maar er was verandering opgetreden in B- en T-cel reacties. Deze resultaten droegen bij aan de speculatie dat productie van IL-17A door cytotoxische T-cellen niet wordt beïnvloed en dat Th1 cellen een ondergeschikte rol spelen in het MOG34-56/IFA model.

Tenslotte worden in **hoofdstuk 10** de belangrijkste bevindingen bediscussieerd, met name hoe deze resultaten kunnen bijdragen aan een beter begrip van het immuunpathogene mechanisme van EAE in de penseelaap. Afsluitend kunnen we zeggen dat het diermodel voor MS in de penseelaap zodanig is verfijnd dat het vergelijkbaar is met MS, en kan worden gebruikt als een relevant model voor fundamenteel en toegepast onderzoek. Echter, verder onderzoek is vereist om de exacte mechanismen te ontrafelen en verbeterde MS therapieën te ontwikkelen.

**ABBREVIATIONS
DANKWOORD
CURRICULUM VITAE
LIST OF PUBLICATIONS
PhD PORTFOLIO**



ABBREVIATIONS

Ab	antibody
ADEM	acute disseminated encephalomyelitis
ALN	axillary lymph node
APC	antigen presenting cell
BBB	blood-brain barrier
B-LCL	EBV-transformed B-lymphoblastoid cell line
BlyS	B lymphocyte stimulator
CalHV-3	callithrine herpesvirus 3
CD	cluster of differentiation
CFA	complete Freund's adjuvant
CLN	cervical lymph node
CMV	cytomegalovirus
CNS	central nervous system
cpm	counts per minute
CTL	cytotoxic T-lymphocyte
CSF	cerebrospinal fluid
EAE	experimental autoimmune encephalomyelitis
EBNA	Epstein-Barr virus nuclear antigen
EBV	Epstein-Barr virus
GA	glatiramer acetate
HIV	human immunodeficiency virus
HLA	human leukocyte antigen
HHV	human herpesvirus
ICAM-1	intercellular adhesion molecule 1
IFA	incomplete Freund's adjuvant
IFN	interferon
Ig	immunoglobulin
IgSF	immunoglobulin superfamily
IL	interleukin
ILN	inguinal lymph node
LCV	lymphocryptovirus
LLN	lumbar lymph node
mAb	monoclonal antibody
MAG	myelin associated glycoprotein
MBP	myelin basic protein
MHC	major histocompatibility complex
MMP	matrix metalloproteinase
MNC	mononuclear cells
MOG	myelin oligodendrocyte glycoprotein
MRI	magnetic resonance imaging
MS	multiple sclerosis
NK	natural killer



APPENDICES

NK-CTL	natural killer–cytotoxic T-lymphocyte
ODC	oligodendrocyte
ORF	open reading frame
PBMC	peripheral blood mononuclear cells
PLP	proteolipid protein
PML	progressive multifocal leukoencephalopathy
PPMS	primary progressive MS
PRMS	progressive relapsing MS
psd	post sensitization day
rhMOG	recombinant human MOG
RRMS	relapsing-remitting MS
SaHV-3	saimirine herpesvirus 3
SI	stimulation index
SPMS	secondary progressive MS
TCL	T-cell line
TCR	T-cell receptor
TLR	Toll-like receptor
TMEV	Theiler’s murine encephalomyelitis virus
TNF	tumour necrosis factor
VCAM-1	vascular adhesion molecule 1
VLA-4	$\alpha 4\beta 1$ integrin

DANKWOORD

Het is zover, ik mag eindelijk het laatste stukje van mijn boekje schrijven, misschien ook wel het leukste en het meest gelezen deel. Langs deze weg wil ik iedereen bedanken die op welke wijze dan ook heeft bijgedragen bij de totstandkoming van mijn proefschrift. Hoewel ik niet iedereen persoonlijk kan bedanken, wil ik toch paar mensen bij naam noemen.

Bert, bedankt dat je mij de kans hebt gegeven om aan mijn promotieonderzoek te beginnen en ook het volste vertrouwen in mij had. Ik waardeer je enthousiasme en passie voor het vak, vooral als je weer een nieuwe hypothese had bedacht. Dit motiveerde mij elke keer weer om in de nieuwe materie te verdiepen en er 100% voor te gaan. Daarnaast ben ik blij dat ik altijd bij je terecht kon om wat te bespreken. Ik hoop dat we onze prettige samenwerking lang kunnen voortzetten en snel het mechanisme van MS kunnen oplossen, vooral nu je professor bent geworden.

Jon, jij bent vanaf het begin van mijn promotietraject nauw betrokken geweest. Jij hebt me tijdens de vele discussies op het BPRC geleerd kritisch na te denken over de experimenten en nog dieper de literatuur in te duiken. Ik heb ook veel opgestoken van alle artikelen die je doorstuurde. Daarnaast heb ik waardering voor het geduld dat je opbracht om mij soms stapvoets door bepaalde materie te leiden en dat je altijd bereid was mijn manuscripten heel grondig door te nemen. Hopelijk kunnen we de banden tussen ErasMS en BPRC in de toekomst verder verstevigen.

Ik wil ook alle afdelingen van het BPRC bedanken, met name Immunobiologie, CG&R en Alternatieven voor de leuke uitjes en gezellige momenten. Ondanks de gesprekken over huishoudelijke artikelen tot aan luiers aan de lunchtafel, hebben we veel gelachen. Met Sam als mannelijke aanwinst op de afdeling kon ik me hiervan een beetje afzonderen. Sam, we hadden altijd wat te bespreken op de fiets en ik kon het zeker waarderen dat je op de dagen dat ik tot laat doorwerkte, op het eind van de dag even langs kwam om een praatje te maken. Alle collega's bedankt voor de fijne samenwerking op het lab en CG&R voor de assistentie tijdens de moleculair genetische experimenten. Bart, jij en je analisten hebben mij op weg geholpen met de FPLC, zonder dit had ik geen MOG kunnen opzuiveren en geen EAE experimenten kunnen inzetten.

Mijn oude kamergenoten van gebouw 139 bedankt. Paul, Ruth en Nicole jullie hebben mij ingewijd in het MS-werk, vooral bij het aanleren van verschillende technieken en in het muizenwerk. Jeffrey, jij voor de leuke tijd en gesprekken op congressen. Celine, jij bent geen kamergenoot geweest maar met jou op congres konden we altijd een feestje bouwen. Yolanda, wij delen nu al een tijdje samen een kamer. Ik had het voordeel dat jij niet zo lang geleden dezelfde weg hebt afgelegd en kon bij jou terecht voor alle ins en outs van het AIO-schap. We hebben vaak gediscussieerd over wetenschap en onze frustraties gedeeld over van alles en nog wat. Hopelijk kunnen we het marmoset EAE werk naar een nog een hoger niveau tillen.

Nicole, jou ben ik ook veel dank verschuldigd. Je hebt me vanaf de eerste dag van mijn promotieonderzoek bijgestaan. Ik heb enorme bewondering voor je inzet. En ook schroomde je nooit om het in het weekend of tijdens de feestdagen terug te komen voor een sectie of experiment. Jij bent soms anders dan anderen en dat maakt jou daarom ook zo bijzonder. Ik hoop dat we onze fijne samenwerking verder kunnen voortzetten en nog meer papers bij elkaar kunnen pipetteren. Leuk dat je tijdens mijn verdediging mij weer zal bijstaan, maar dan als paranimf.



ASD, het ging niet altijd even soepel, maar uiteindelijk kwam alles toch weer goed. Ik wil iedereen bedanken die betrokken is geweest bij mijn experimenten, met name Annet, Herbert, projectbureau en het marmoset-groepje, Fred, Jeroen en Mariska. Jaco, jou kon ik altijd bellen om wat te vragen of te regelen. Tom, jouw passie voor het werk en bereidheid, ongeacht het tijdstip van dag of de week een sectie te doen, heeft veel indruk op me gemaakt.

Henk, zonder jou waren de figuren in mijn boekje, artikelen en presentaties niet zo mooi geworden. Bedankt dat ik altijd bij je binnen kon lopen en dat je open stond voor suggesties.

PersoneelsVereniging, bedankt voor de leuke uitjes en workshops. Ik vind het nog steeds leuk om deel uit te maken van het bestuur.

Erwin, bedankt voor de MRI figuren en Jan, voor de histologie en immunohistochemie plaatjes. Jullie hebben een substantiële bijdrage geleverd aan onze papers. Zonder deze goede analyses en figuren waren we niet zover gekomen en hadden we niet zulke mooie papers gehad.

Kirsten, Ruud en Abdel het was leuk om jullie als stagiaires te hebben. Jullie hebben mooi werk afgeleverd en veel succes met jullie loopbaan.

Hasna, bedankt dat je ook mijn paranimf wilt zijn. Wij kennen elkaar al vanaf het begin van onze studie. Uiteindelijk bleken we ongeveer dezelfde interesses te hebben en zijn ook bijna altijd elkaars werkpartner geweest. Yasemin, met jou erbij was het altijd lachen en met ons drieën was niets onbespreekbaar.

Als laatste wil ik mijn familie bedanken voor de vertrouwde omgeving. Jullie hebben mij altijd gestimuleerd. Pa, ik weet dat je al trots op me bent, maar nu nog trotser zult zijn. Dit geldt ook voor mijn zussen Sharmila en Sharita. Roshini, de laatste paar regels zijn speciaal voor jou gereserveerd. Bedankt voor je steun, je begrip als ik in de weekenden uit bed werd gebeld en dat je mij de laatste periode de ruimte hebt gegeven om mijn onderzoek succesvol af te ronden. Ik hoop dat we ons leuk leventje voor altijd kunnen voortzetten.

CURRICULUM VITAE

Sunil Anwar Jagessar was born on July the 19th of 1982 in Paramaribo, Surinam. He started his high general secondary education in 1994 at CSG Johannes Calvijn in Rotterdam and graduated in June 1999. Then, he studied Biochemistry at the Higher Laboratory education (HLO) at Hogeschool Rotterdam. During this study, he did two internships. At the Erasmus MC Rotterdam, Department Clinical Genetics, he performed mutation analyses for patients with the Pompe's disease under supervision of Dr. Arnold Reuser. Thereafter at TNO Prevention and Health in Leiden, he developed an ELISA to measure the effect of statins in relation to phosphorylation in human umbilical endothelial cells under supervision of Dr. Louis Cohen. In June of 2003, he obtained his Bachelor degree in Applied Science. From December 2003 till September 2007 he worked as a research technician at the Biomedical Primate Research Centre (BPRC) at the Department Virology, and subsequently at the Department Immunobiology under supervision of Prof. Dr. Bert 't Hart. Then, he started his PhD project within the Department Immunobiology in October 2007 under supervision of Prof. Dr. Jon Laman and Prof. Dr. Bert 't Hart. From May 2012 he will continue his research on multiple sclerosis in the common marmoset as a postdoc at the BPRC.

Sunil Anwar Jagessar werd geboren op 19 juli 1982 in Paramaribo, Suriname. Vanaf 1994 volgde hij middelbaar onderwijs aan de christelijke scholengemeenschap Johannes Calvijn in Rotterdam, en behaalde zijn HAVO-diploma in juni 1999. In september van hetzelfde jaar is hij begonnen aan de opleiding Biologie en Medisch Laboratorium onderzoek aan de Hogeschool Rotterdam met als specialisatie Biochemie. Tijdens de opleiding heeft hij twee onderzoeksstages doorlopen. Op het Erasmus MC Rotterdam op de afdeling Klinische Genetica voerde hij mutatie-analyses uit voor patiënten met de ziekte van Pompe onder supervisie van dr. Arnold Reuser. Daarna heeft hij bij TNO Preventie en Gezondheid in Leiden een ELISA ontwikkeld om de rol van statines in relatie tot fosforylering in humane navelstreng endotheelcellen te meten, onder supervisie van dr. Louis Cohen. In 2003 behaalde hij zijn Bachelor in de toegepaste wetenschap. Vanaf december 2003 tot en met september 2007 werkte hij als research analist op het Biomedisch Primaten Onderzoekscentrum (BPRC) in Rijswijk op de afdeling Virologie en vervolgens op de afdeling Immunobiologie onder supervisie van prof. dr. Bert 't Hart. Aansluitend hieraan is hij in oktober 2007 begonnen aan zijn promotieonderzoek binnen de afdeling Immunobiologie onder begeleiding van prof. dr. Jon Laman en prof. dr. Bert 't Hart. Vanaf mei 2012 zal hij als postdoc zijn onderzoek in multiple sclerose in de penseelaap voorzetten op het BPRC.



LIST OF PUBLICATIONS

Jagessar SA, Heijmans N, Blezer ELA, Bauer J, Laman JD, and 't Hart BA. Recombinant human MOG in incomplete Freund's adjuvant induces a multiple sclerosis-like disease in the common marmoset. *Manuscript in preparation*

Jagessar SA, Heijmans N, Bauer J, Blezer ELA, Laman JD, Thi-Sau Migone, Devalaraja MN, and 't Hart BA. Antibodies against human BLYS and APRIL attenuate EAE development in marmoset monkeys. *Submitted*

Jagessar SA, Heijmans N, Bauer J, Blezer ELA, Laman JD, Hellings N, and 't Hart BA. B-cell depletion abrogates T-cell mediated demyelination in an antibody non-dependent common marmoset EAE model. *Submitted*

Jagessar SA, Gran B, Heijmans N, Bauer J, Laman JD, 't Hart BA, and Constantinescu CS. Discrepant effects of human interferon-gamma on clinical and immunological disease parameters in a novel marmoset model for multiple sclerosis. *J Neuroimmune Pharmacol* 7, 253-65 (2012)

Jagessar SA, Heijmans N, Blezer ELA, Bauer J, Blokhuis JH, Wubben JAM, Drijfhout JW, van den Elsen PJ, Laman JD, and 't Hart BA. Unravelling the T-cell mediated autoimmune attack on CNS myelin in a new primate EAE model induced with MOG34-56 peptide in incomplete adjuvant. *Eur J Immunol* 42, 217-27 (2012)

Jagessar SA, Heijmans N, van Driel N, 't Hart BA, and Kap YS. Modelling of autoimmune encephalomyelitis in a non-human primate. Book Chapter in Pathogenesis of encephalitis. Ed. Daisuke Hayasaka, InTech, Rijeka, Croatia. 323-40 (2011).

Kap YS, **Jagessar SA**, van Driel N, Blezer E, Bauer J, van Meurs M, Smith P, Laman JD, and 't Hart BA. Effects of early IL-17A neutralization on disease induction in a primate model of experimental autoimmune encephalomyelitis. *J Neuroimmune Pharmacol* 6, 341-53 (2011)

Jagessar SA*, Kap YS*, Heijmans N, van Driel N, van Straalen L, Bajramovic JJ, Brok HPM, Blezer LA, Bauer J, Laman JD, and 't Hart BA. Induction of progressive demyelinating autoimmune encephalomyelitis in common marmoset monkeys using MOG₃₄₋₅₆ peptide in incomplete Freund's adjuvant. *J Neuropathol Exp Neurol* 69, 372-85 (2010)

* shared first authorship

Kap YS*, Smith P*, **Jagessar SA***, Remarque E, Blezer E, Strijkers GJ, Laman JD, Hintzen RQ, Bauer J, Brok HP, and 't Hart BA. Fast progression of recombinant human myelin/oligodendrocyte glycoprotein (MOG)-induced experimental autoimmune encephalomyelitis in marmosets is associated with the activation of MOG34-56-specific cytotoxic T cells. *J Immunol* 180, 1326-37 (2008)

* shared first authorship

Jagessar SA*, Smith PA*, Blezer E, Delarasse C, Pham-Dinh D, Laman JD, Bauer J, Amor S, and 't Hart B. Autoimmunity against myelin oligodendrocyte glycoprotein is dispensable for the initiation although essential for the progression of chronic encephalomyelitis in common marmosets. *J Neuropathol Exp Neurol* 67, 326-40 (2008)

* shared first authorship

Bajramovic JJ, Brok HP, Ouwerling B, **Jagessar SA**, van Straalen L, Kondova I, Bauer J, Amor S, 't Hart BA, and Ben-Nun A. Oligodendrocyte-specific protein is encephalitogenic in rhesus macaques and induces specific demyelination of the optic nerve. *Eur J Immunol* 38, 1452-64 (2008)

Brok HP, Boven L, van Meurs M, Kerlero de Rosbo N, Celebi-Paul L, Kap YS, **Jagessar A**, Hintzen RQ, Keir G, Bajramovic J, Ben-Nun A, Bauer J, Laman JD, Amor S, and 't Hart BA. The human CMV-UL86 peptide 981-1003 shares a crossreactive T-cell epitope with the encephalitogenic MOG peptide 34-56, but lacks the capacity to induce EAE in rhesus monkeys. *J Neuroimmunol* 182, 135-52 (2007)

't Hart BA, **Jagessar SA**, Kap YS, and Brok HPM, 2007. Preclinical models of multiple sclerosis in nonhuman primates. *Expert Rev Clin Immunol* 3, 749-61 (2007)

't Hart BA, Kap YS, **Jagessar SA**, Amor S, and Brok HPM. Neuroimmunology research in non-human primates. Book chapter in: *Neuroimmunology Research Perspectives*. Ed. Johansson LM, Nova Science Publisher, Hauppauge, NY. 191-205 2007



PhD PORTFOLIO

General academic and research skills	Year	ECTS
Laboratory Animals Science (Article 9), Rotterdam, NL	2008	3.0
Management for PhD students and postdocs, Utrecht, NL	2009	1.0
Introduction to data-analysis, Rotterdam, NL	2009	2.0
Molecular Immunology, Rotterdam, NL	2009	3.0
Bio-ethics, Rijswijk, NL	2010	1.0
Biomedical English Writing Course for PhD students, Rotterdam, NL	2011	2.0
In-depth course		
Neuro-Immunology: MS as a model, Rotterdam, NL	2005	1.1
7 th European School of Neuroimmunology, Oxford, UK	2007	1.1
8 th European School of Neuroimmunology, Fort Worth, TX, USA	2008	0.3
Bioinformatics: Browsing Genes and Genomes with Ensembl, Rotterdam, NL	2010	0.6
Seminars and workshops		
Integrating proteomics in biology, Utrecht, NL	2004	0.3
Luminex, Amsterdam, NL	2006	0.6
LIFI Symposium on NK cells, Leiden, NL	2008	0.3
CD8 workshop in MS/EAE, Rome, Italy, NL	2009	0.6
From Genes to Pathogenesis of MS, Lofoten, Norway	2010	1.1
MS Immunology seminar, Nottingham, UK	2010	0.6
(Inter)national conferences		
8x Annual MS meeting of the Dutch MS Research Foundation, Amsterdam (2x), Rotterdam, Hasselt (Belgium), Oegstgeest (2x), Groningen, Alphen a/d Rijn, NL	2004-2011	4.8
5x Annual Immunology spring meeting of the Dutch Society for Immunology, Lunteren, NL	2005-2011	3.0
European Marmoset Research Group, Milan, Italy	2006	1.0
9 th International Society of Neuroimmunology, Fort Worth, TX, USA	2008	1.1
2x Annual Immunology autumn meeting of the Dutch Society for Immunology, Noordwijkerhout, NL	2008-2009	1.2
10 th International Society of Neuroimmunology, Barcelona, Spain	2010	1.1
Keystone; Genetics, Immunology and Repair in MS, Taos, NM, USA	2011	1.4
International Marmoset Research Group, Göttingen, Germany	2011	0.6
Oral presentations		
Induction of EAE in a non-human primate without bacterial adjuvant, BPRC, Rijswijk, NL	2008	0.5
EAE induction in a non-humane primate without bacterial adjuvant, Annual MS research meeting, Oegstgeest, NL	2008	0.5
EAE induction in a non-humane primate without bacterial adjuvant, ErasMS Audit, Rotterdam, NL	2008	0.5
Induction of EAE in a non-humane primate without innate immune activation, BPRC Retreat, Rijswijk, NL	2009	0.5

Refinement of the marmoset EAE model, BPRC, Rijswijk, NL	2009	0.5
Modelling of multiple sclerosis in the common marmoset, Department Immunology, Erasmus MC, Rotterdam, NL	2009	0.5
Induction of EAE in a non-humane primate without innate immune activation, Annual MS research meeting, Groningen, NL	2009	0.5
Unravelling the MHC restriction elements of auto-reactive T-cells in the MOG34-56/IFA marmoset EAE model, MS Workshop, Lofoten, Norway	2010	0.5
Effect of interferon-gamma in the marmoset MOG34-56/IFA EAE model, BPRC, Rijswijk, NL	2010	0.5
Effect of Interferon-gamma in the marmoset EAE model, MS Immunology Seminar, Nottingham, UK	2010	0.5
Effect of Interferon-gamma in the marmoset EAE model, Annual MS research meeting, Alphen a/d Rijn, NL	2010	0.5
Modelling of multiple sclerosis in the common marmoset, NIH, MD, USA	2011	0.5
Targeting B cell using anti-B cell molecules in the marmoset EAE model, BPRC Retreat, Rijswijk, NL	2011	0.5
Antagonism of BLYS / APRIL / TACI: in the marmoset EAE model, BPRC, Rijswijk, NL	2011	0.5
T-cell mediated grey matter demyelination in a new marmoset EAE model, ECTRIMS, Amsterdam, NL	2011	0.5
Targeting B-cell survival molecules in the common marmoset EAE model with anti-BLYS and anti-APRIL, Annual MS research meeting, Alphen a/d Rijn, NL	2011	0.5
T-cell mediated grey matter demyelination in the MOG34-56/IFA marmoset EAE model, ErasMS, ErasmusMC, Rotterdam, NL	2012	0.5
B-cells as APC for activation of autoreactive T-cells, BPRC Retreat, Rijswijk, NL	2012	0.5
Poster presentations		
Accelerated expression of experimental autoimmune encephalomyelitis in marmosets by activation of MOG34-56-specific cytotoxic T-cells, Annual MS research meeting, Hasselt, Belgium	2007	0.2
EAE induction in a non-humane primate without bacterial adjuvant, 9 th International Society congress of Neuroimmunology, Fort Worth, TX, USA	2008	0.2
EAE induction in a non-human primate without bacterial adjuvant, Annual Immunology meeting, Noordwijkerhout, NL	2008	0.2
Induction of EAE in a non-humane primate without innate immune activation, CD8 CNS workshop, Rome, Italy	2009	0.2
Unraveling the MHC restriction elements of auto-reactive T-cells in the MOG34-56/IFA marmoset EAE model, Annual Immunology meeting, Noordwijkerhout, NL	2009	0.2
Fine specificity and MHC restriction elements of auto-reactive T-cells in the marmoset EAE model, 10 th International Society congress of Neuroimmunology, Barcelona, Spain	2010	0.2
Fine specificity and MHC restriction elements of auto-reactive T-cells in the marmoset EAE model, Keystone meeting, Taos, NM, USA	2010	0.2



APPENDICES

Teaching	
Supervising one trainee from the middle laboratory education (MLO)	2008-2007
Supervising two master students in Biomedical Sciences	2009-2010
Supervising one research technician of high laboratory education (HLO)	2007-present
Other	
Working visit of one week to NIH, Prof. Dr. Steven Jacobson, Bethesda, MD, USA	2011
Translation of scientific papers on MS for laymen (www.msweb.nl)	